



LIGANDS AND COMPLEXES FOR NON-COVALENT BINDING TO
G-QUADRUPLEX DNA STRUCTURES

by

LOIS ELEANOR BRIGHT

A thesis submitted to
The University of Birmingham
for the degree of
DOCTOR OF PHILOSOPHY

PSIBS Doctoral Training Centre
School of Chemistry
College of Engineering and Physical Sciences
University of Birmingham
September 2016

UNIVERSITY OF
BIRMINGHAM

University of Birmingham Research Archive

e-theses repository

This unpublished thesis/dissertation is copyright of the author and/or third parties. The intellectual property rights of the author or third parties in respect of this work are as defined by The Copyright Designs and Patents Act 1988 or as modified by any successor legislation.

Any use made of information contained in this thesis/dissertation must be in accordance with that legislation and must be properly acknowledged. Further distribution or reproduction in any format is prohibited without the permission of the copyright holder.

ABSTRACT

The structure, occurrence and biological relevance of G-quadruplex DNA structures has been reviewed, along with a review of several notable G-quadruplex binding compounds published in the literature to date.

The synthetic route towards two G-quadruplex DNA binders previously developed within the Hannon group has been modified and improved. Electrospray ionisation mass spectrometry studies have been carried out to evaluate nucleotide binding. The *in vitro* biological activities of these compounds have been validated against the human ovarian carcinoma cell line A2780 *via* MTT and comet assays, flow cytometry and inductively coupled plasma mass spectrometry. Both compounds and the corresponding metal-free ligand exhibited higher drug efficiencies than cisplatin against A2780 cells. Both compounds display mild genotoxicity and induce G₂/M phase cell cycle arrest. The overall cellular uptake and nuclear localisation demonstrated by both complexes exceeds that of cisplatin.

A new class of palladium and platinum(II) complexes have been synthesised from methylthio-substituted terpyridine ligands. In addition to assessing their stability in solution *via* UV-Vis spectroscopy, initial DNA binding studies with both duplex and quadruplex-forming sequences of DNA have been carried out *via* circular dichroism and gel electrophoresis.

The design and synthesis of alternative ligand systems proffering a range of desirable characteristics to aid future ligand and complex development has been investigated.

ACKNOWLEDGEMENTS

I would like to thank my supervisor, Professor Mike Hannon for inviting me to join his research group and supporting my research over the past four years. I have learnt a great amount under his supervision and developed many new skills. I also wish to thank my co-supervisor Dr Nik Hodges for his guidance, helpful discussions and willingness to train me in cell culture techniques.

I am grateful to the EPSRC for funding this research through the PSIBS (Physical Sciences of Imaging in the Biomedical Sciences) Doctoral Training Centre and COST for funding a very enjoyable week-long training school at the University of Strasbourg. I am extremely thankful for my time spent studying at both the University of Leicester and Colorado State University, both of which enabled me to experience research and have played a large part in getting me to where I am today.

I am very appreciative of the help and assistance of the University of Birmingham School of Chemistry analytical facility. In particular Chi Tsang and Peter Ashton, who have always gone above and beyond to assist with my experiments.

Many thanks to the members of the Hannon group, both past and present, for their support, encouragement and copious amounts of cake. Special thanks to Ashleigh for being the perfect partner-in-crime. Thanks also to the members of the Hodges group in Biosciences for their helpful advice.

Special thanks go to the members of the PSIBS 2011 cohort, in particular Ashleigh, Chris, David, Rachel and Vicky, for their humour, friendship, support and encouragement over the past five years. You have made my time in Birmingham unforgettable.

I wish to acknowledge my wonderful and ever-expanding family; my parents Cliff and Sarah for their love, prayers, encouragement and guidance (not forgetting you forced

me to take triple sciences all those years ago) and my siblings Beth, Hannah, Ben, Sam, Phil, Jo and Tom for their continued interest and encouragement, particularly throughout the writing-up process. Thank you all for the long chats, guaranteed laughter, open homes and reminding me of the important things in life. You are the best advertisement for big families. Finally, to Guy, you have made the journey so much more enjoyable. Thank you for always being there. It's difficult not to believe in yourself when somebody else is so certain you can do it.

Proverbs 3 v 5-6: Trust in the Lord with all your heart and lean not on your own understanding. In all your ways acknowledge Him and He shall direct your paths.

TABLE OF CONTENTS

Abstract	i
Acknowledgements	ii
Table of Contents	iv
Abbreviations	ix
 CHAPTER I: INTRODUCTION	 1
1.1 Deoxyribonucleic acid (DNA)	2
1.1.1 Structure	2
1.1.2 Function	4
1.2 Alternative DNA structures	4
1.2.1 Holliday junctions	4
1.2.2 Three-way helical junctions	5
1.2.3 Replication forks	6
1.2.4 Bulges	7
1.2.5 The importance of alternative DNA structures	7
1.3 G-quadruplex DNA	9
1.3.1 Structure	9
1.3.2 Prediction of G-quadruplex structures and stability	12
1.4 Biological relevance of G-quadruplex structures	13
1.4.1 Telomeres	13
1.4.2 Oncogene promoter regions	17
1.5 G-quadruplex DNA-ligand binding	19
1.5.1 Modes of binding	19
1.5.2 π -stacking compounds	20
1.5.3 Loop/groove binding compounds	21
1.5.4 Central channel binding compounds	22
1.6 Methods for investigating G-quadruplex DNA-ligand interactions	22
1.7 G-quadruplex binders	24
1.7.1 Organic neutral macrocyclic ligands	25
1.7.2 Organic <i>in situ</i> protonated G-quadruplex ligands	26
1.7.3 Organic N-methylated aromatic ligands	27
1.7.4 Metallo-organic complexes	30
1.8 Summary	36
1.9 Thesis aims	36
1.10 References	38
 CHAPTER II	 46
2.1 Introduction	47
2.1.1 Summary of previous group research into G-quadruplex binding	49

PART I: SYNTHESIS AND CHARACTERISATION OF 3,3-BIISOQUINOLINE METAL COMPLEXES	51
2.2 Overview of synthetic methodology	51
2.2.1 Isoquinoline building blocks	51
2.2.2 Metal-catalysed homocoupling	55
2.3 3-chloroisoquinoline precursor synthesis and characterisation	58
2.3.1 Isoquinoline-1,3-dione (1)	58
2.3.2 1,3-dichloroisoquinoline (2)	59
2.3.3 3-chloroisoquinoline (3)	60
2.3.4 An alternative route to 3-chloroisoquinoline (3)	61
2.4 3,3-biisoquinoline synthesis and characterisation	62
2.4.1 Nickel-catalysed homocoupling of aryl chlorides	62
2.4.2 3,3-biisoquinoline (4)	63
2.4.3 An alternative route to 3,3-biisoquinoline: aryl-bromide vs. aryl chloride	66
2.4.4 3-bromoisoquinoline precursor synthesis and characterisation	67
2.4.5 1,3-dibromoisoquinoline (5)	67
2.4.6 3-bromoisoquinoline (6)	68
2.4.7 Nickel-catalysed Colom-coupling of aryl bromides	71
2.5 Synthesis and characterisation of palladium, platinum and gold 3,3-biisoquinoline complexes	71
2.5.1 [Pd(<i>i</i> -biq) ₂](BF ₄) ₂ (7)	71
2.5.2 [Pt(<i>i</i> -biq) ₂](PF ₆) ₂ (8)	73
2.5.3 Gold(III) complexes: an emerging new class of anticancer drugs	76
2.5.4 [Au(<i>i</i> -biq) ₂](3Cl) (9)	77
2.6 Binding of Pd(II) and Pt(II) complexes toward model nucleobases	79
2.6.1 ESI-MS binding studies	79
2.6.2 Preliminary ESI-MS studies with 9-ethylguanine	80
2.6.3 Further ESI-MS studies with 1-methylthymine, 9-methylguanine, 1-methylcytosine and 9-methyladenine	83
2.7 Part I: Conclusions	88
 PART II: <i>IN VITRO</i> BIOLOGICAL ACTIVITY OF PALLADIUM AND PLATINUM 3,3-BIISOQUINOLINE COMPLEXES	 90
2.8 Introduction	90
2.8.1 Choice of cell line	91
2.9 Cell viability	92
2.9.1 MTT assay	92
2.9.2 IC ₅₀ results	93
2.10 Genotoxicity	100
2.10.1 Comet assay for DNA double strand breaks	100
2.10.2 DNA strand break results	102
2.11 Cell cycle analysis	107
2.11.1 Cell cycle	107
2.11.2 Flow cytometry with propidium iodide staining	108

2.11.3	Cell cycle arrest results	109
2.12	Cell uptake and localisation	114
2.12.1	Inductively coupled plasma mass spectrometry	114
2.12.2	Cell uptake results	115
2.13	Part II: Conclusions	119
2.14	Experimental materials and methods	120
2.14.1	General chemistry	120
2.14.2	Analytical characterisation techniques	120
2.14.3	Chemical synthesis	120
2.14.4	ESI-MS nucleotide binding studies	128
2.14.5	General cell culture	128
2.14.6	MTT assay for cell viability	131
2.14.7	Neutral comet assay for DNA double strand breaks	132
2.14.8	Flow cytometry (inc. PI staining) for cell cycle analysis	133
2.14.9	Inductively coupled plasma mass spectrometry for cell uptake	134
2.14.10	Statistical analysis of data	136
2.15	References	137
 CHAPTER III: DEVELOPING A TERPYRIDINE PLATFORM FOR METAL-TERPYRIDINE G-QUADRUPLEX BINDING COMPLEXES		 142
3.1	Introduction	143
3.2	Overview of synthetic methodology	144
3.2.1	Molecular design of G-quadruplex end-stacking terpyridine complexes	144
3.2.2	Routes towards 2,2':6',2''-terpyridines	146
3.2.3	Preparation of methylsulphonyl-substituted terpyridines	148
3.3	4'-(methylsulphonyl)-2,2':6',2''-terpyridine synthesis and characterisation	151
3.3.1	3,3-bis(methylthio)-1-(pyridine-2-yl)prop-2-en-1-one (10)	151
3.3.2	4'-(methylthio)-2,2':6',2''-terpyridine (11)	154
3.3.3	4'-(methylsulphonyl)-2,2':6',2''-terpyridine (12)	154
3.3.4	Synthesis and characterisation of palladium and platinum complexes incorporating 4'-(methylsulphonyl)-2,2':6',2''-terpyridine (12)	156
3.3.5	[Pd(12)(CH ₃ CN)](BF ₄) ₂ (13)	156
3.3.6	[Pt(12)Cl](PF ₆) (14)	158
3.4	UV-Visible spectroscopy studies	160
3.4.1	Absorbance characteristics	160
3.4.2	Stability in solution	163
3.5	Circular dichroism DNA Binding Studies	165
3.5.1	Circular dichroism (CD)	165
3.5.2	Types of DNA investigated	166
3.5.3	Circular dichroism binding results	171
3.6	Gel electrophoresis DNA Binding Studies	178
3.6.1	Polyacrylamide gel electrophoresis (PAGE)	178
3.6.2	PAGE results	179
3.7	Conclusions	183

3.8	Experimental materials and methods	183
3.8.1	General chemistry	183
3.8.2	Analytical characterisation techniques	184
3.8.3	Chemical synthesis	184
3.8.4	Circular dichroism (CD)	190
3.8.5	Polyacrylamide gel electrophoresis (PAGE)	191
3.9	References	193
 CHAPTER IV: EXPLORING ROUTES TO ALTERNATIVE LIGANDS		196
4.1	Introduction	197
4.2	Incorporating isoquinoline into an unsymmetrical ligand	197
4.2.1	Target compound 1: 3-(pyridine-2-yl)isoquinoline	197
4.2.2	Palladium-catalysed α -arylation of ketones with aryl halides	198
4.2.3	3-(pyridine-2-yl)isoquinoline (15)	199
4.3	Incorporating isoquinoline into an unsymmetrical N[^]C-coordinating ligand with “click” capable functionality	200
4.3.1	Target compound 2: 3-(4-ethynylphenyl)isoquinoline	200
4.3.2	“Click chemistry”	201
4.3.3	N [^] C coordination	202
4.3.4	Palladium-catalysed Suzuki-coupling of organoboranes with organohalides	203
4.3.5	3-(4-ethynylphenyl)isoquinoline (17)	205
4.4	An alternative route to an unsymmetrical N[^]C-coordinating isoquinoline ligand: coupling in the absence of an alkyne	208
4.4.1	Target ligand 3: 3-(4-chlorophenyl)isoquinoline	208
4.4.2	Palladium-catalysed Stille-coupling of organostannanes with halides	208
4.4.3	3-(4-chlorophenyl)isoquinoline (19)	210
4.5	Incorporating N[^]C-coordination into a terdentate ligand system	211
4.5.1	Target ligand 4: 5-chloro-1,3-di(2-pyridyl)benzene	211
4.5.2	5-chloro-1,3-di(2-pyridyl)benzene (20)	213
4.6	Exploring an alternative coupling route towards 3,3-biisoquinoline	214
4.6.1	Grignard-mediated homocoupling of sulphoxide ligands	214
4.6.2	Method trial: 5,5'-dibromo-2,2'-bipyridine synthesis	214
4.6.3	Synthesis of 3,3-biisoquinoline <i>via</i> Grignard-mediated homocoupling	218
4.7	Incorporating alkyne functionality	222
4.7.1	Palladium- and copper-catalysed Sonogashira-coupling of terminal alkynes with halides	222
4.7.2	6-(2-trimethylsilyl)ethynyl-3-chloroisoquinoline (27)	224
4.8	Conclusions	226
4.9	Experimental materials and methods	226
4.9.1	General chemistry	226
4.9.2	Analytical characterisation techniques	227
4.9.3	Chemical synthesis	227
4.10	References	238

CHAPTER V: CONCLUSIONS AND FUTURE WORK	241
APPENDIX	246
A BioVision cell fractionation procedure	247
B ICP-MS calculations	248

ABBREVIATIONS

1MC	1-methylcytosine
1MT	1-methylthymine
9EG	9-ethylguanine
9MA	9-methyladenine
9MG	9-methylguanine
CD ₃ CN	deuterated acetonitrile
CDCl ₃	deuterated chloroform
CH ₃ CN	acetonitrile
CHCl ₃	chloroform
d ₆ -DMSO	deuterated dimethylsulphoxide
DCM	dichloromethane
DMF	dimethylformamide
DMSO	dimethylsulphoxide
ESI-MS	electrospray ionisation mass spectrometry
Et ₂ O	diethyl ether
EtOAc	ethyl acetate
EtOH	ethanol
FBS	foetal bovine serum
H ₂ O	water
H ₂ O ₂	hydrogen peroxide
HCl	hydrochloric acid
HNO ₃	nitric acid
HOAc	acetic acid
LMPA	low melting point agarose
MeOD	deuterated methanol
MeOH	methanol
MgSO ₄	magnesium sulphate
MTT	(3-(4,5-dimethylthiazol-2-yl)-2,5-diphenyltetrazolium bromide)
NaH	sodium hydride
NaOH	sodium hydroxide
NH ₃	ammonia
NH ₄ OAc	ammonium acetate
NH ₄ OH	ammonium hydroxide
NH ₄ PF ₆	ammonium hexafluorophosphate
NMPA	normal melting point agarose
NMR	nuclear magnetic resonance
PBS	phosphate buffered saline
THF	tetrahydrofuran

Chapter I

I. INTRODUCTION

1.1 Deoxyribonucleic acid (DNA)

1.1.1 Structure

Deoxyribonucleic acid is the molecule that carries the genetic information in all cellular forms of life. Classified as a nucleic acid, this fundamental molecule consists of a long chain of nucleotides. Each nucleotide itself consists of three components; a pentose sugar, phosphate molecule and nitrogenous base: cytosine (C), adenine (A), guanine (G) and thymine (T). Phosphodiester covalent bonds between nucleotides form an alternating sugar-phosphate backbone of a polynucleotide strand.

First elucidated in 1953 by Watson and Crick, hydrogen bonds form between complementary bases of two polynucleotide strands aligned anti-parallel to one another, resulting in the formation of a double helix structure resembling a spiral staircase.^{1,2} The spatial arrangement of the base pairs creates two recurring cavities of different magnitude, termed the major and minor groove,³ shown in Figure 1.1.1-1.

Three common types of duplex DNA have been discovered, each distinguished by its characteristic direction of winding and the number of bases in one helical turn. The most common form encountered in biological systems is B-DNA,³ which exists as a right-handed helix, with 10-10.5 bases per helical turn.⁴ A-DNA is similarly right-handed,⁵ but exists as a shorter, wider helix, whilst Z-DNA is left-handed and also found in biological systems.⁶

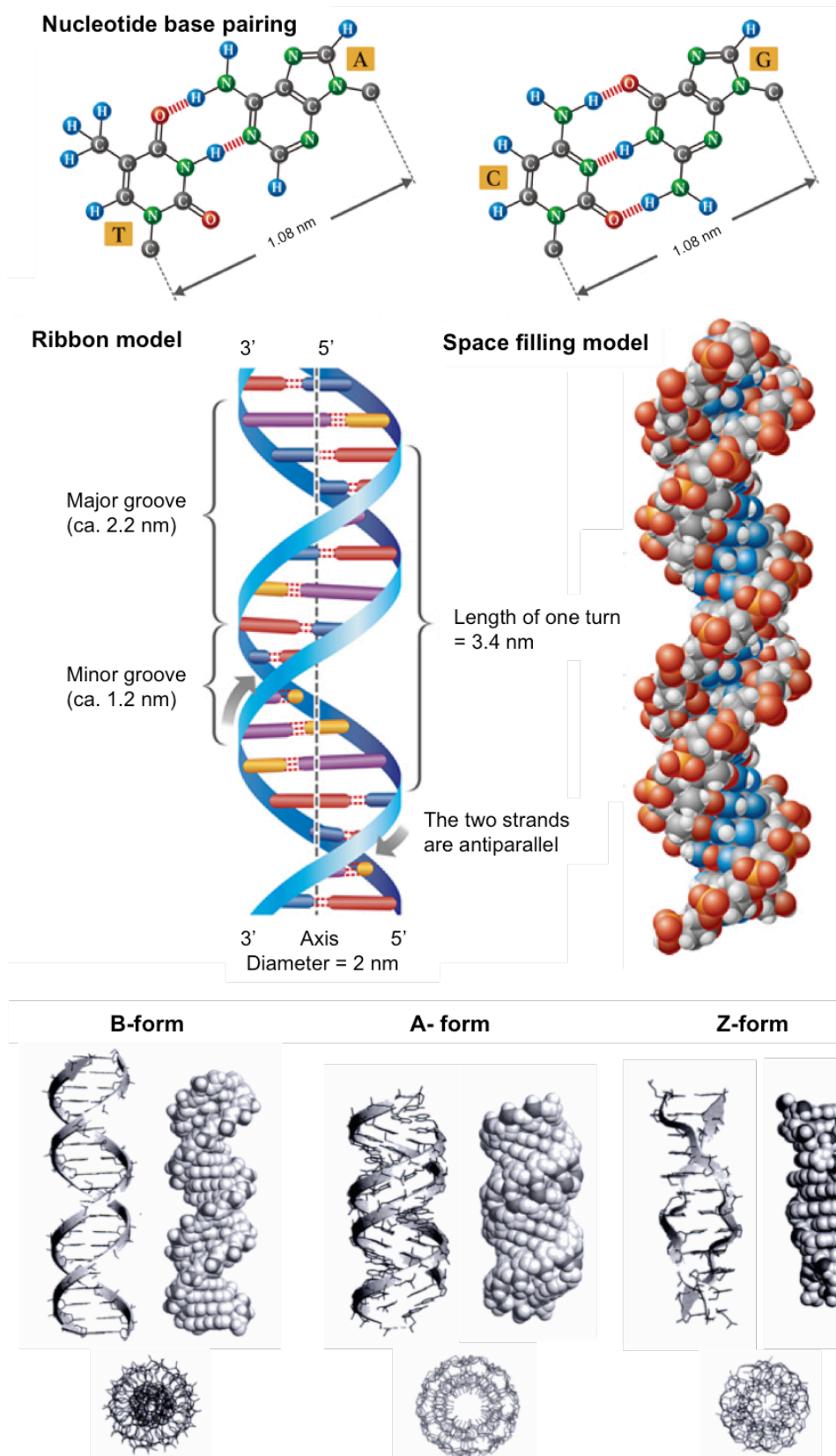


Figure 1.1.1-1 DNA structure: complementary nucleotide base pairing, structure of double-stranded helix,⁷ comparison of the B-, A- and Z-forms of DNA.⁸

1.1.2 Function

DNA is a fundamental molecule, the ability of which to store and transmit information lies in its structure. Information is stored in the linear sequence of the nucleotides, specifically the order of the bases along a single strand, which constitutes the universal and degenerate genetic code. Crucially, the molecule can be replicated, whereby each strand acts as a template for the generation of a new complementary strand.

1.2 Alternative DNA structures

Nucleic acids may also adopt alternative, less familiar non-canonical structural conformations that are proving to be no less biologically relevant, such as Holliday junctions, three-way junctions, replication forks, bulges and G-quadruplexes. Formed during active processes such as replication, transcription and recombination,^{9,10} these emerging structures may prove to be effective targets for anticancer agents, since the loss of control over such processes is often the cause for cancer proliferation.^{11,12}

1.2.1 Holliday junctions

Junctions formed between DNA helices play an important role as intermediates in DNA rearrangements.¹³ Undoubtedly the most important of these structures, is the four-way junction, termed the Holliday junction after the geneticist Robin Holliday who proposed its existence in 1964.¹⁴ During homologous recombination, two helices

(four strands) stack pairwise to generate two coaxial, quasi-continuous helices that form an X-shaped structure (Figure 1.2.1-1).¹⁵



Figure 1.2.1-1 Representative structure of four-stranded Holliday junction (4WJ).¹⁶

1.2.2 Three-way helical junctions

Three-way junctions are the simplest and most commonly occurring branched nucleic acids.¹⁷ Consisting of three double helical arms connected at a junction point, the Y-shaped structure also features a hydrophobic cavity at the branch point^{18,19} (Figure 1.2.2-1). The formation of these structures within genetically unstable genomic DNA has been linked to neurodegenerative disorders such as Huntington's disease. Unstable DNA can accommodate looped out triplet-repeat expansions,¹⁸ the formation of which results in three-way junctions also being formed (at the loop-out) in the process, introducing considerable kinks and bends into the DNA. Sinden *et al.* have reported the occurrence of mutated DNA triplet-repeat expansions in fourteen genetic neurodegenerative disorders.²⁰



Figure 1.2.2-1 Representative structure of three-way junction (3WJ).¹⁶

1.2.3 Replication forks

Replication forks form during DNA replication, when DNA helicases unwind the double stranded DNA helix to expose the nucleotides of a single strand in preparation for transcription. A Y-shaped junction emerges, with the separated single strands serving as templates for nascent leading and lagging strands, formed from complementary nucleotides joined together by DNA polymerase (Figure 1.2.3-1). The branch point consists of one base-pair and two unpaired bases, resulting in a cavity which represents a significant therapeutic target for synthetic agents intending to halt the replication process.²¹

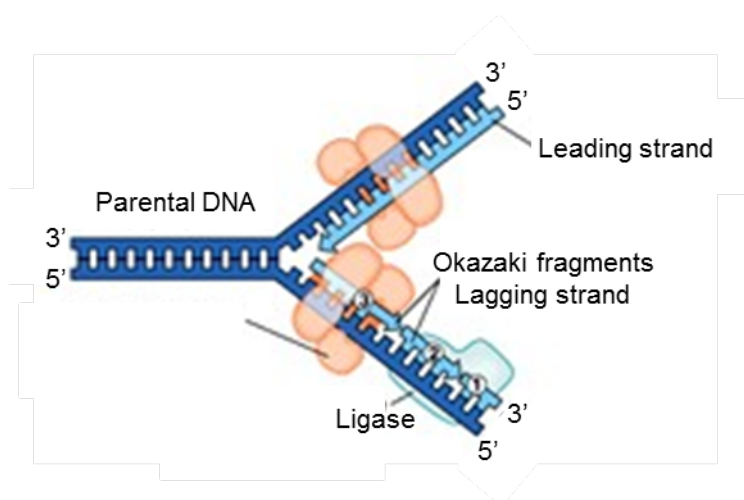


Figure 1.2.3-1 Representation of the Y-shaped junction formed during DNA replication.²²

1.2.4 Bulges

Base bulges form where a duplex section of DNA is interrupted by one or more single-stranded bases on one strand that are unopposed by bases on the other strand (Figure 1.2.4-1).²³ Such bulges may arise as a consequence of DNA mismatches,²⁴ which if left uncorrected by a mismatch repair pathway would result in recombination between imperfectly homologous DNA sequences, causing a bulge to emerge. Bulges bring about substantial destabilisation of DNA²⁵⁻²⁷ and are an important feature that can be exploited for specific recognition.

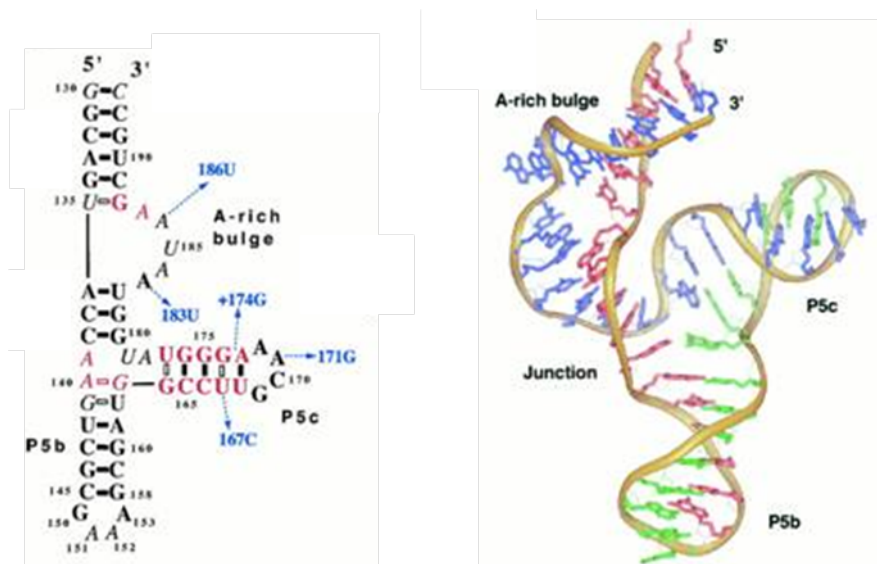


Figure 1.2.4-1 The extended structure of Tp5abc showing the effect of the A-rich bulge on 3D conformation.²⁸

1.2.5 The importance of alternative DNA structures

An understanding of the processes that occur during replication and gene expression, when DNA is often described as being in its 'active' state, is vital in the diagnosis and subsequent treatment of diseases such as cancer. This is because the rate of such processes is elevated in rapidly-proliferating cancer cells,²⁹ thereby

implicating these processes in the development of the disease and prompting the investigation of their particular role as a potential therapeutic target.

Currently, there exists a wide selection of metallo-anticancer agents, shown to interact with duplex DNA in order to alter its function. Most notably cisplatin (Figure 1.2.5-1), which remains the most effective anticancer agent to date, effecting apoptosis in cells following its irreversible interaction with duplex DNA.

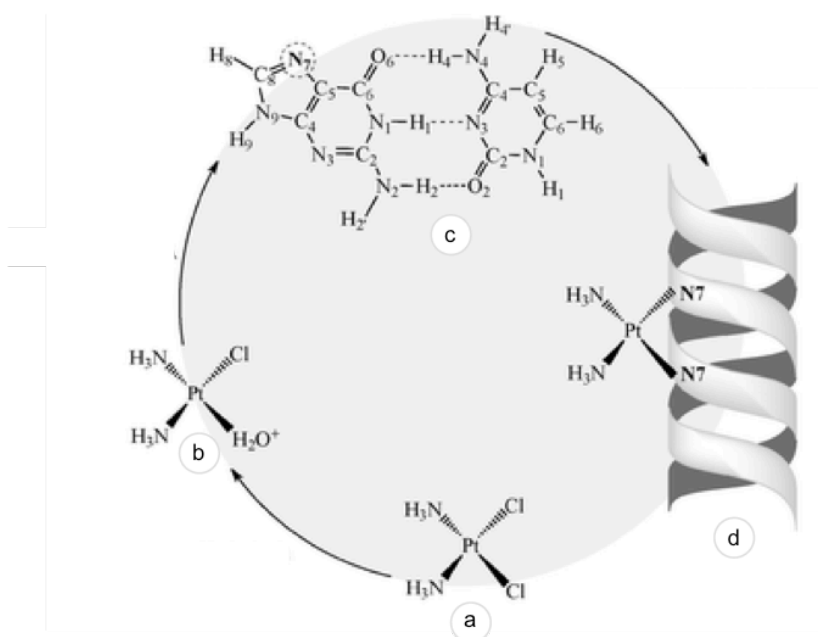


Figure 1.2.5-1 Main reactions involved in the biochemical activity of cisplatin. Once cisplatin (a) has entered the cell, one water molecule is incorporated into the complex with displacement of one chlorine. The resulting activated aqua platinum complex (b) attacks the N7 positions of two adjacent GC base pairs (c) to form the Pt–DNA intrastrand cross-link adduct (d).³⁰

The discovery of alternative, more unusual DNA structures has prompted the development of complexes that display specificity and selectivity for a particular DNA structure. The advantage of such compounds lies in their ability to minimise the damage incurred by healthy cells, in that their cytotoxicity is targeted towards cells containing a particular DNA structure implicated in cancer progression.

1.3 G-quadruplex DNA

1.3.1 Structure

Of particular interest herein, and the subject of an ever-expanding area of research exploring non-duplex DNA, are G-quadruplex structures. These structures have been characterised as multiple-stranded assemblies, formed *via* folding of guanine-rich single stranded sequences into tetraplex structures. Whilst the N(1), N(2) and O(6) atoms of guanine are key atoms in establishing Watson-Crick hydrogen bonding in duplex DNA, alternative hydrogen bonding atoms are possible. Utilising the N(2) and N(3) atoms along the Hoogsteen face, hydrogen bonding can lead to triple or four-stranded structures³¹ (Figure 1.3.1-1).

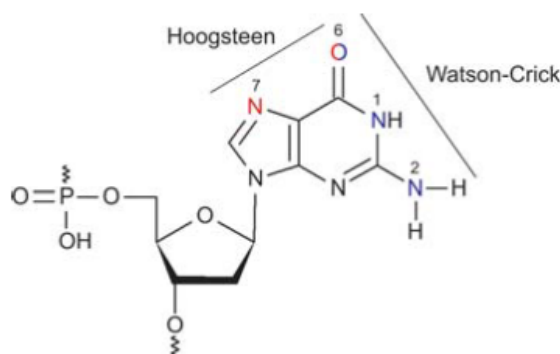


Figure 1.3.1-1 Molecular structure of a G nucleotide unit showing the Hoogsteen and Watson-Crick faces.³¹

Formed from four guanine bases hydrogen-bonded to each other (involving both the Hoogsteen and Watson-Crick faces), the G-quartet (also referred to as G-tetrad) structure exhibits a large π -surface, with π -stacking interactions highly favoured in order to aid stability (Figure 1.3.1-2). Crystallographic evidence for G-quartets was first provided by Gellert *et al.* in 1962.³² G-quadruplexes are formed when the G-quartets π -stack on top of one another.

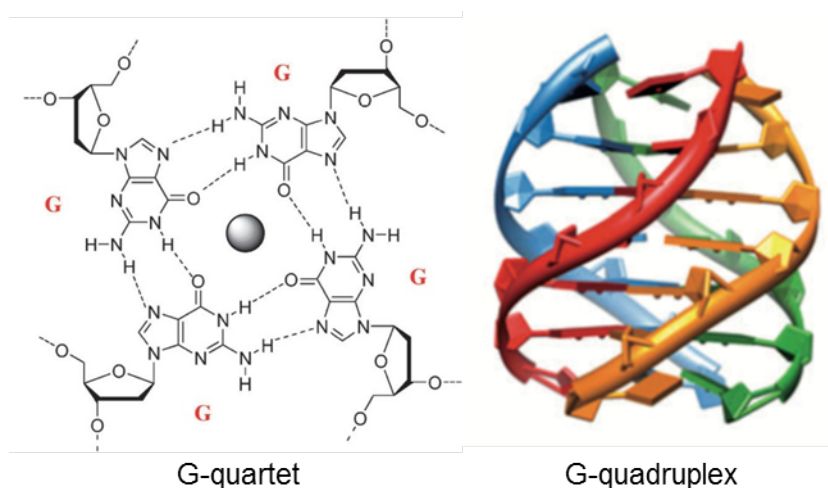


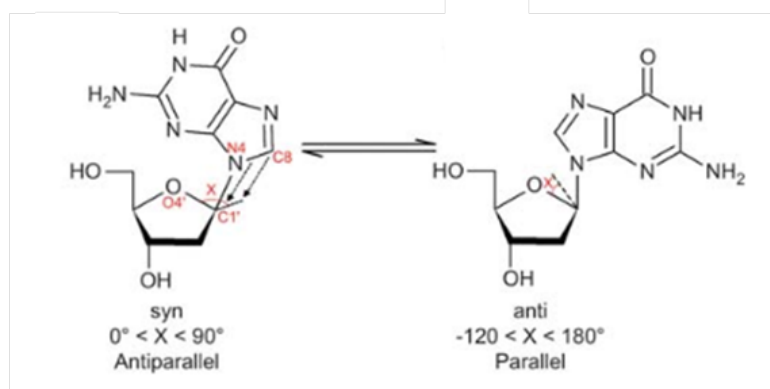
Figure 1.3.1-2 The structure of a G-quartet,³³ showing hydrogen bonds involving both faces of the guanine base, alongside the structure of a G-quadruplex formed from several G-quartets stacked together.¹⁶

The presence of a monovalent cation which can coordinate within the quadruplex core and engage in electrostatic interactions with the O(6) atoms strongly stabilises the G-quadruplex structure.³⁴ The ability of the cation to undertake coordination to the guanine bases and thus facilitate stabilisation of the quadruplex is dependent upon the amount of energy released upon coordination and the energy required to dehydrate the solvated cation.^{35,36} Stabilisation using Na^+ and K^+ is well precededented, with K^+ the strongest known coordinating cation for G-quadruplexes.^{35–40}

G-quadruplexes can form from both intermolecular and intramolecular interactions of guanine bases. Unimolecular, bimolecular, and tetramolecular forms have all been observed (Figure 1.3.1-3, b). Owing to the directionality possessed by nucleic acids (5' end to 3' end), both parallel and antiparallel conformations exist depending on the direction of the four strands relative to one another. The position of the guanine base relative to the phosphodiester backbone is determined by the

glycosidic angle χ , which is therefore related to the directionality of the strands (and the adopted conformation) (Figure 1.3.1-3, a).³¹

(a)



(b)

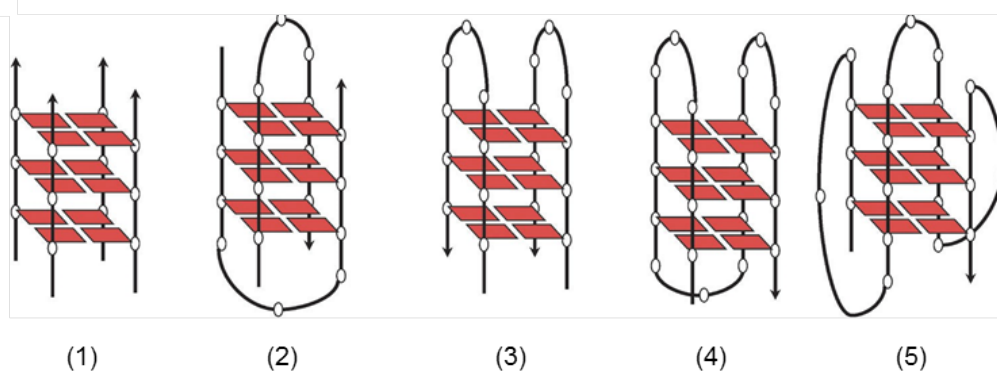


Figure 1.3.1-3 (a) Preferred base geometries. Rotation around the glycosidic bond (χ defined as the angle $O4' C1', N4-C8$) causes interconversion between the syn and anti conformation.³¹ (b) Structure and topology of G-quadruplexes: (1) tetramolecular with parallel strands; (2) bimolecular with diagonal loops; (3) bimolecular with lateral loops; (4) unimolecular/intramolecular with lateral loops; and (5) unimolecular/intramolecular with one diagonal and two external (propeller) loops.³³

In contrast to intermolecular G-quadruplexes consisting of neighbouring strands that are independently aligned in the absence of covalent bonding, intramolecular G-quadruplexes contain covalently linked loops that connect the guanine bases constituting the quadruplex structure. These loops may adopt several distinct conformations, imparting further diversity to G-quadruplex topology. In addition to

loops, all G-quadruplex structures contain grooves (defined as the cavities between two adjacent guanine bases bounded by the phosphodiester backbones),³¹ varying in size depending on the nature of the loops.⁴¹

1.3.2 Prediction of G-quadruplex structure and stability

Data obtained from biophysical analytical methods used to study G-quadruplex formation and topology (X-ray diffraction, NMR spectroscopy, UV-spectroscopy, circular dichroism and fluorescence resonance energy transfer) demonstrates that it is possible to predict the likelihood of *in vitro* G-quadruplex formation by a particular sequence using the ‘folding rule’:⁴² This states that any sequence $G_nX_{1-7}G_nX_{1-7}G_nX_{1-7}G_n$ where G = guanine, X = any base, $3 < n < 5$, will form a G-quadruplex.

This rule can be implemented algorithmically to scan a sequence of putative G-quadruplex sequences (PQS) for possible G-quadruplex formation. A scan of the human genome predicted the existence of 376,000 G-quadruplex forming sequences.⁴² Whilst potentially very informative, care must be taken when interpreting these predictive data, which neither prove *in vitro* or *in vivo* formation, nor take into account the numerous factors affecting the stability of any particular G-quadruplex structure. For example, thermodynamic G-quadruplex stability is known to increase with increasing G-quartets involved due to additional π - π stacking.⁴³ Furthermore, short loops adopt the thermodynamically more favourable parallel conformation, in contrast to long loops which induce antiparallel G-quadruplexes.^{44–46} Intermediate loop lengths thus exhibit structural polymorphism.⁴⁷

The accurate prediction of G-quadruplex stability from its sequence is vital in determining PQSs with a low error rate. A promising machine-learning approach to

predict the stability of an unknown G-quadruplex, based on an existing dataset of experimental values has been proposed by Stegle *et al.* and looks to offer an improved prediction tool.⁴⁸

1.4 Biological relevance of G-quadruplex structures

Within the human genome, approximately 376,000 PQSs have been identified, often correlating with functional genomic regions.⁴⁹ Of particular interest, is their abundance in both eukaryotic gene promotor regions and G-rich telomere sequences located at the end of chromosomes.^{50–53}

1.4.1 Telomeres

Telomeres are single-stranded repeats of TTAGGG located at the ends of chromosomes. Containing no genetic information, telomeres act as a 'cap', protecting the chromosome from deterioration and genetic instability. Two opposing processes occur within telomeres, summarised in Figure 1.4.1-1. The first is telomere shortening, which occurs with each cell replication. The characteristic shortening of the telomeric sequence is due to the absence of hydroxyl groups at the 5' end of the newly replicated strands, which prevents the replacement of RNA primers with DNA, and thus produces two daughter strands marginally shorter than the parent strands from which they were synthesised.

The second process is telomere lengthening; the result of an enzyme called telomerase which is known to add telomeric repeats of TTAGGG to the 3'-end of the chromosome, causing elongation of the telomere.⁵⁴ This process occurs in order to

maintain the genetic integrity of the chromosome and protect it from deterioration over time.

The net effect of these two processes is that of a gradual shortening of the telomere length in normal cells with each successive cell replication. Following a certain number of divisions, termed the Hayflick limit, the telomere reaches a critical length and causes the cell to enter senescence, inducing apoptosis.^{55,56} This sequence of events prevents genomic instability in aged cells by limiting the number of cell divisions.

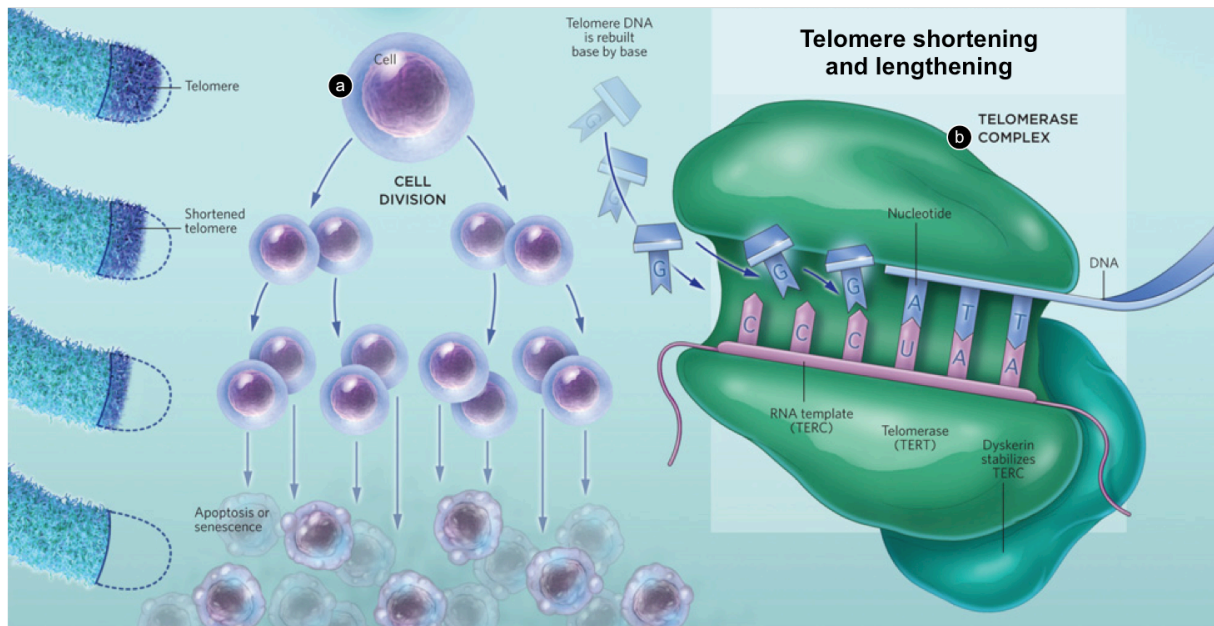


Figure 1.4.1-1 Overview of the two processes occurring within telomeres (a) telomere shortening; (b) telomere lengthening⁵⁷

Telomere sequences were found to account for approximately 20,000 of the PQSSs identified during algorithmic analysis of the whole genome.⁴² Of special interest, and thus the focus of research efforts, is the 12-200 base 3'-overhang sequence.⁵⁸ Containing repeats of guanine-rich motifs, these single-stranded sequences are

capable of adopting G-quadruplex structures under physiological conditions (Figure 1.4.1-2).

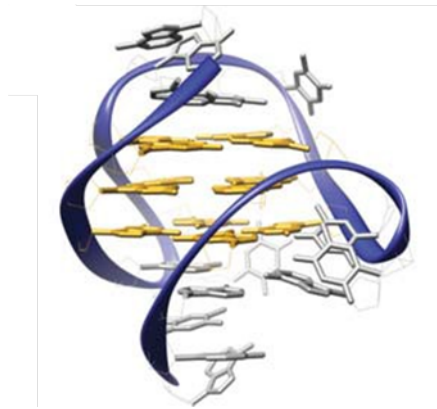


Figure 1.4.1-2 NMR structure of a human telomeric G-quadruplex.⁵⁹

G-quadruplex structures have been successfully visualised at the telomeres of ciliate macronuclei (selected as a model organism due to the higher concentration of telomeres found in their cells compared to other genomes) using fluorescent imaging of an antibody.⁴⁷ Support for the presence of G-quadruplexes in human telomeres has been reported by Tang *et al.* following the use of a fluorescent cyanine dye that specifically binds to G-quadruplexes, allowing *in vitro* visualisation.⁶⁰

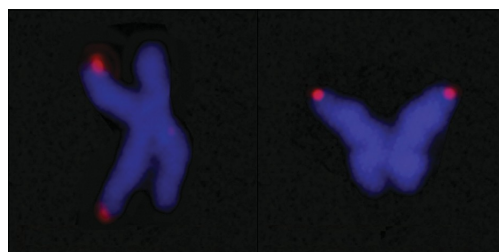


Figure 1.4.1-3 Localization of G-quadruplex structures in chromosomes: Immunofluorescence for BG4 on metaphase chromosomes. Discrete BG4 foci (red) DAPI counterstaining (blue).⁶¹

Confirmation of G-quadruplex formation in human telomeres has been subsequently reported by Balasubramanian *et al.*, whose use of an engineered, structure-specific antibody has enabled quantitative visualisation of these structures in human cells (Figure 1.4.1-3).⁶¹ This approach utilises the single chain antibody clone BG4, selected from a library of over 10^{10} antibodies due to its high affinity for G-quadruplexes. Treatment of BG4 with a second antibody to amplify the fluorescent signal, followed by a tertiary fluorochrome-labelled antibody yields a highly specific probe for G-quadruplex structures in the DNA of human cells.

The enormous significance of the formation of G-quadruplex structures in telomeric regions is due to their ability to inhibit the activity of telomerase *in vitro*.⁶² Whilst essential in maintaining the lifespan of frequently replicated cells such as white blood cells, telomerase is overexpressed and upregulated in 85-90% of cancer cells.^{63,64} Consequently, these cells evade the usual process of telomere shortening leading to the induced death of aged cells that is crucial for genomic stability. Rather, they replicate indefinitely, enabling cancer proliferation. The ability of G-quadruplex structures to inhibit telomerase renders them an important new therapeutic target, whereby G-quadruplex stabilisation has the potential to regulate telomerase activity, thereby inhibiting immortality in cancer cells (Figure 1.4.1-4).

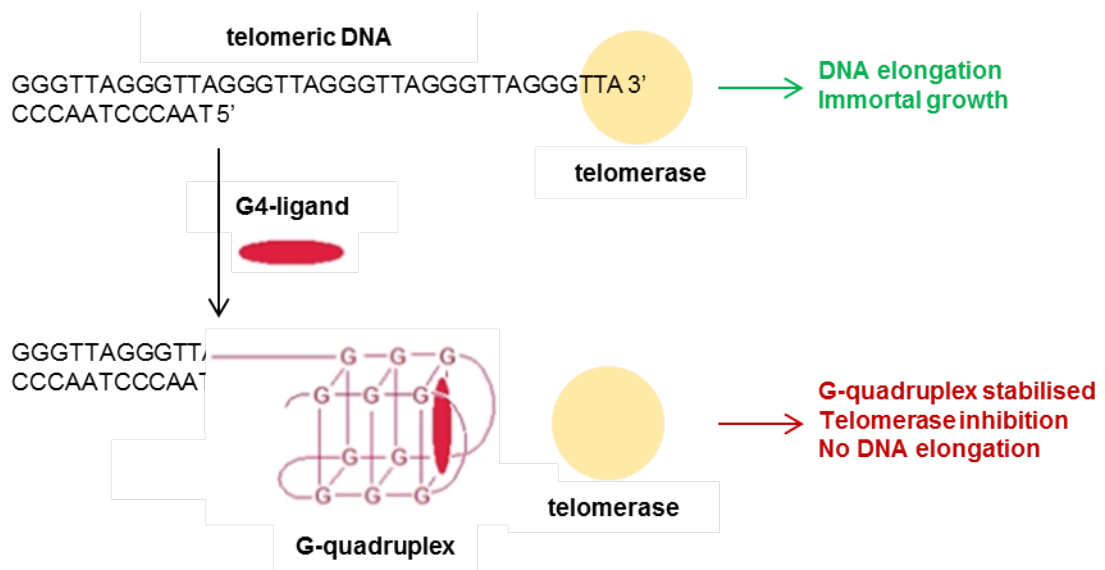


Figure 1.4.1-4 Representation of the therapeutic strategy involving ligand binding to telomeric G-quadruplex structures in order to inhibit telomerase activity.

1.4.2 Oncogene promoter regions

Promoter regions have a regulatory role, controlling the transcription of a particular gene. Located upstream of an oncogene (5' end) which has the potential to cause cancer, the promoter region often serves as the binding site for transcription factors that further regulate transcriptional activity.³¹ Activation of RNA polymerase initiates RNA synthesis from the coding part of the gene.⁶⁵

Mutation or transformation of an oncogene may lead to the abnormal regulation of processes, resulting in unfavourable cellular outcomes including evasion of apoptosis, insensitivity to anti-growth signals, continuous angiogenesis, infinite replicative potential and metastasis.⁶⁵

Computational studies have shown that promoter-associated G-quadruplex structures are frequently found proximal to or overlapping with transcription factor binding sites within promoter regions, suggesting that they could play some

regulatory role in gene expression.^{49,66,67} The presence of G-quadruplex forming sequences in promoter regions has been confirmed for a number of oncogenes *in vitro*, including c-Myc (Figure 1.4.2-1), c-kit, bcl-2, k-ras and VEGF.^{68–73}



Figure 1.4.2-1 NMR structure of cMyc G-quadruplex.⁵⁹

The effect of G-quadruplex formation within a promoter region, on transcriptional activity of a gene has been extensively studied for the c-Myc oncogene and its corresponding NHEIII-promoter region, which has been shown to regulate 90% of c-Myc oncogene transcription *in vitro*.⁷⁴ The c-Myc oncogene is overexpressed in the majority of human cancers and contributes to the cause of at least 40% of tumours,⁷⁵ including colon, breast, cervix, small cell lung, osteosarcomas and myeloid leukaemias.^{76,77} Termed a “master regulator”,⁷⁸ c-Myc stimulates genes involved in protein biosynthesis, cancer metabolism, transcription factors and the cell cycle, while inhibiting the expression of some tumour suppressor genes.^{78,79} Owing to its ubiquitous regulatory role in human tumour initiation and progression, efforts to utilize c-Myc as a therapeutic target remain an attractive prospect.

The region of most interest remains the nuclease hypersensitive element, NHEIII, due to the ability of G-quadruplex structures to form in Pu27 sequence of this region (Figure 1.4.2-2). G-quadruplex-stabilising compounds have been shown to

downregulate c-Myc expression levels⁸⁰ and cause selective leukaemic cell death.⁸¹ The ability to selectively target and stabilise G-quadruplex structures within the Pu27 sequence has potentially widespread downstream effects regarding transcription and subsequent gene expression.

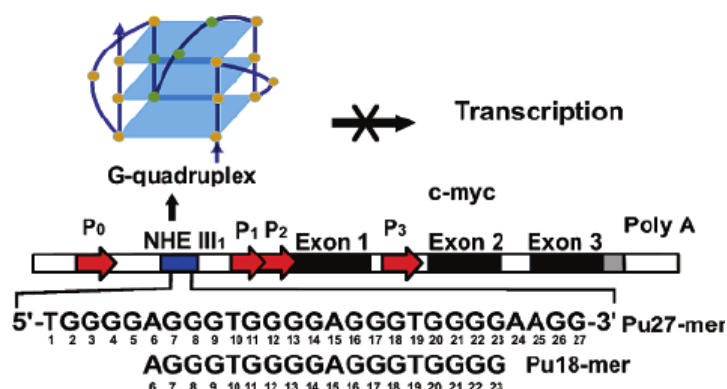


Figure 1.4.2-2 Location of the NHE III 1 in the c-Myc gene and proposed biological function of G-quadruplex in this region.⁸²

1.5 G-quadruplex DNA-ligand binding

1.5.1 Modes of binding

The significant enrichment of PQSs in the functional parts of the genome suggest that G-quadruplexes very likely possess key biological regulatory function within the telomeric and promoter regions of the genome. Consequently, the development of compounds capable of interacting with and stabilising G-quadruplex structures remains the principal aim of the G-quadruplex nucleic acids research community.

Generally, compounds consisting of planar aromatic systems containing delocalised electrons will undergo π -stacking onto the G-quartet face, whereas compounds containing cationic moieties will typically interact with the loops, grooves and anionic phosphate backbone of G-quadruplexes (Figure 1.5.1-1).

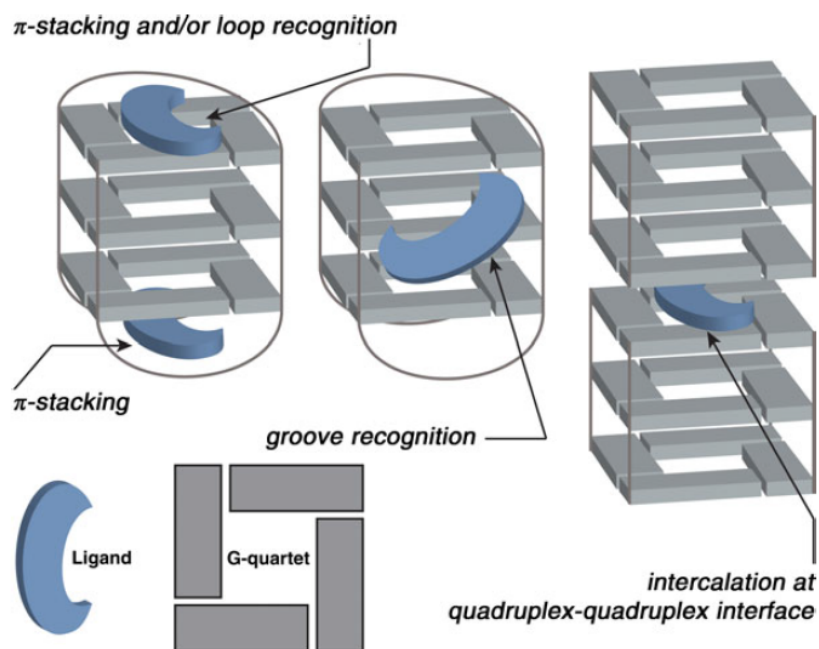


Figure 1.5.1-1 Binding modes of ligands to G-quadruplex.⁸³

1.5.2 π -stacking compounds

π -stacking refers to the stacked arrangement of aromatic systems, predominantly controlled by hydrophobic and Van der Waal interactions.³³ Ligands capable of efficiently engaging in this mode of binding should possess a large aromatic surface for aromatic-aromatic overlap, sufficiently large to prohibit duplex binding, thus providing selectivity for G-quadruplex structures. The incorporation of protonable side-chains around the aromatic core assists water solubility. Such side-chains may also establish electrostatic interactions with atoms in the grooves and central G-quadruplex channel, further stabilising the structure. Ma *et al.* have reported a series of pyridyl-substituted corrole isomers (Figure 1.5.2-1) which show high selectivity for G-quadruplex structures over duplex DNA, all of which demonstrate π -stacking as their mode of G-quadruplex interaction.⁸⁴

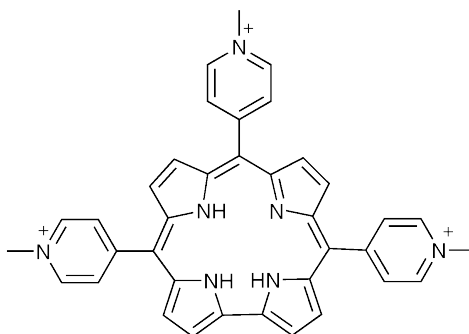


Figure 1.5.2-1 π -stacking ligand pyridyl-substituted corrole, reported by Ma *et al.*⁸⁴

1.5.3 Loop/groove binding compounds

Groove recognition is expected to impart higher G-quadruplex versus duplex selectivity due to the significant chemical and conformational differences between the grooves encountered in these two regions. The first compound proven to interact with G-quadruplex DNA using this binding mode was Distamycin A (Figure 1.5.3-1). Martino *et al.* discovered that Distamycin A adopts a crescent shape and lies side-by-side (as a head-to-tail dimer) in the groove, binding with a 4:1 ratio (ligand:G4-d[TGGGGT]₄). Four hydrogen bonds are made with guanine, in addition to strong electrostatic interactions between the positively charged amidinium moiety of the ligand and the negatively charged G-quadruplex backbone.⁸⁵

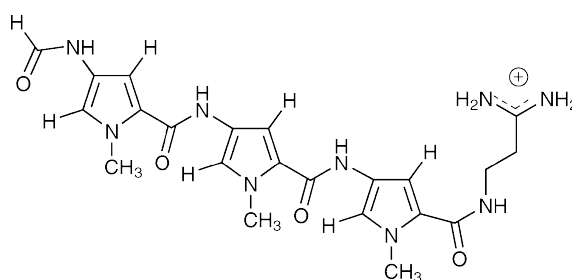


Figure 1.5.3-1 Groove binder ligand Distamycin A, reported by Martino *et al.*⁸⁵

It is worth noting that the implementation of octahedral metal complexes with planar ligands has been investigated by Vilar *et al.* with the intention of promoting groove/loop binding.⁸⁶ Octahedral geometry prevents the metal centre from engaging in stacking interactions with the G-quartet, therefore promoting groove and loop recognition as an alternative binding mode.

1.5.4 Central channel binding compounds

The ability to mimic the cations that usually reside within the central channel of the G-quadruplex stack may induce G-quadruplex formation. Rodriguez *et al.* developed an anthracene-based ligand containing ammonium centres that was shown to induce parallel G-quadruplex formation in a human telomeric sequence, in the absence of cations (Figure 1.5.4-1).⁸⁷ With the aid of NMR studies, the binding mode was proposed to be a combination of threading and stacking.

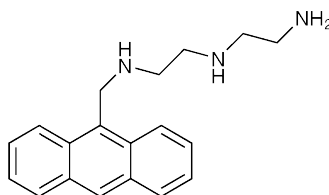


Figure 1.5.4-1 Central channel binding ligand, reported by Rodriguez *et al.*⁸⁷

1.6 Methods for investigating G-quadruplex DNA-ligand interactions

The following is by no means an exhaustive list of the techniques currently available for investigating G-quadruplex DNA-ligand interactions, rather it is intended to give an overview of the most commonly employed methods.

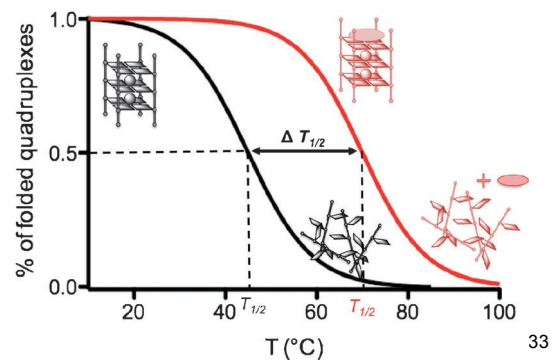
Biophysical

Thermal melting temperature (UV or CD)

Demonstrates the **stabilisation or destabilisation** of a nucleic acid structure by a ligand. Characteristic signals of G4 DNA at 295 nm are reduced upon denaturation by heating.³³

Output: Melting temperature $T_{1/2}$

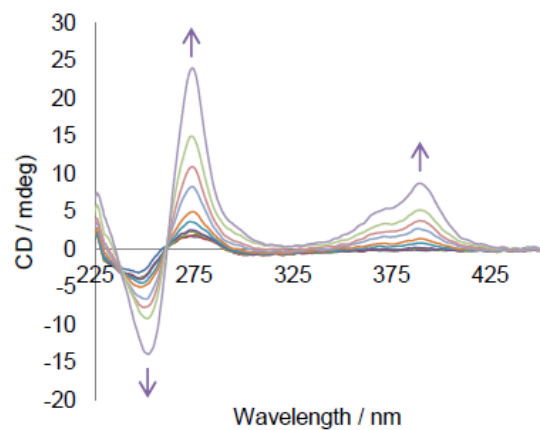
An increase in $T_{1/2}$ indicates preferential binding to the folded form corresponding to a stabilising ligand.



Circular dichroism spectroscopy (CD)

Demonstrates the **conformational changes** of a nucleic acid structure. Characteristic signals of G4 DNA can be monitored during ligand titration.

Output: Increase or decrease in characteristic signal intensity. Emergence of induced peaks (ICD).



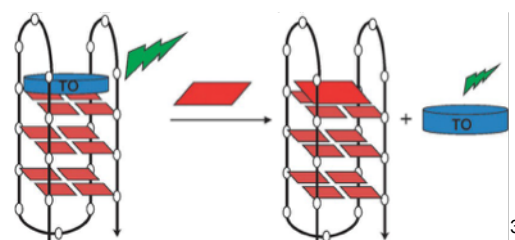
Fluorescent intercalator displacement

Demonstrates G-quadruplex over duplex DNA **selectivity**.

Displacement of thiazole orange (TO) from DNA causes a 1000-fold decrease in its fluorescence intensity.

Output: Fluorescence intensity.

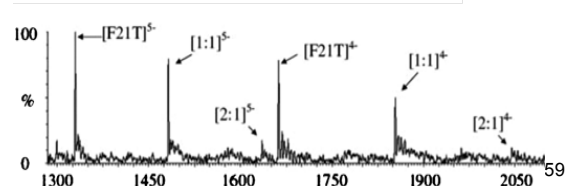
Ligand binding induces TO displacement causing a decrease in intensity.



Mass spectroscopy

Demonstrates non-covalent interactions between small molecules and G4 DNA/nucleobases.

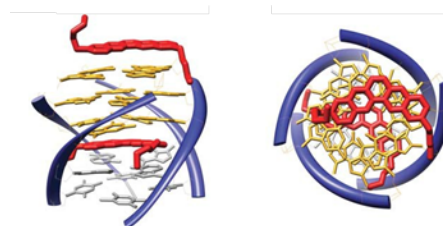
Output: Novel peaks in spectrum due to G4-ligand species.



NMR spectroscopy

Demonstrates the process involved in small-molecule G4 recognition, providing **structural** information at an atomic level.

Output: Structures of G4-ligand complexes



59

Biological

Telomere Repeat Amplification Protocol (TRAP-G4) assay

Demonstrates the ability of a ligand to induce **telomerase inhibition** through stabilisation of a G4 structure (human telomeric sequence).

Output: **IC₅₀-TRAP**. Ligand concentration required to inhibit telomerase activity by 50%.

Mitochondrial reductase (MTT) assay

Demonstrates the cytotoxicity of a ligand.

Output: Half maximal inhibitory concentration, **IC₅₀**. Ligand concentration required to inhibit mitochondrial reductase activity by 50%.

1.7 G-quadruplex binders

The past twenty years has seen a spectacular emergence of molecules designed to selectively interact with G-quadruplex DNA structures. Such compounds can be classified into four different categories on the basis of their cationic structure; (1) non-cationic (2) cationic upon *in situ* protonation of an amine appendage, (3) cationic *via* N-methylation of an aza-aromatic moiety, (4) cationic due to metal coordination.⁵⁹ An overview of the structural design and molecular interaction with G-quadruplex of some of the key examples from each category will now be included.

1.7.1 Organic neutral macrocyclic ligands

Telomestatin

Isolated from *Streptomyces annulatus* by Shinya,⁸⁹ telomestatin is a natural macrocyclic compound that has been shown to induce and stabilise G-quadruplex structures ($\Delta T_{1/2} = 24\text{ }^{\circ}\text{C}$), in addition to inhibiting the proliferation of telomerase-positive cells ($\text{IC}_{50}\text{-TRAP} = 5\text{ nM}$).⁹⁰ Initially studied due to its known absence of affinity for canonical duplex-DNA (on account of its neutrality and cyclic structure), extensive studying of telomestatin has shown it to be one of the most selective G-quadruplex ligands, exhibiting 70-fold selectivity for intramolecular G-quadruplex DNA structures over that of duplex DNA.⁹¹ Telomestatin binding is driven by stacking forces, with the macrocycle able to coordinate a monovalent cation such as K^+ , which sits between the ligand and G-quartet (Figure 1.7.1-1).⁹² The apparent drawback in the use of telomestatin for therapeutic purposes is its availability. Total synthesis of telomestatin is currently a sophisticated and small-scale process.⁹³

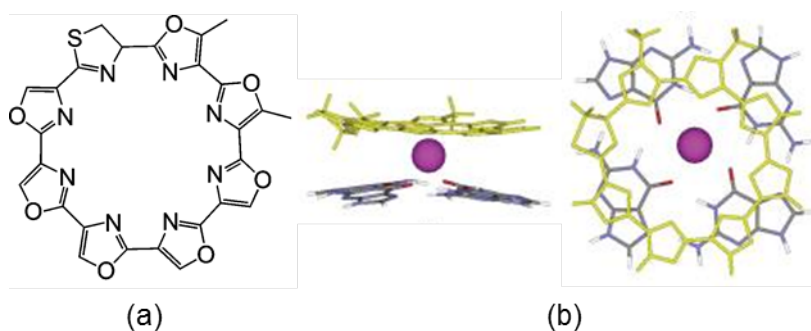


Figure 1.7.1-1 (a) Structure of telomestatin (b) Overlaid side- and top-view structures of telomestatin (yellow) over a G-quartet (blue) with a potassium ion in the central cavity (purple). The potassium ion sits directly between the two units.⁹²

1.7.2 Organic *in situ* protonated G-quadruplex ligands

BRACO-19

BRACO-19 represents an optimized prototype, designed to incorporate binding mode duality into a well-studied and promising family of compounds. Initially based on the bisamidoanthraquinone family,^{94,95} modifications to the core and sidearms of early ligands resulted in a structure capable of both π -stacking onto the G-tetrad surface, coupled with electrostatic interactions between the three protonable sidechains and quadruplex grooves (Figure 1.7.2-1).^{96,97} Demonstrating a 31-fold binding preference for G-quadruplex over duplex DNA structures, in addition to inhibition of both telomerase (IC₅₀-TRAP = 115 nM)^{98,99} and cancer cell proliferation,^{100,101} the acridine-based ligand has proved to be an efficient G-quadruplex binder. Further modification of BRACO-19 is ongoing. Recent developments include the incorporation of a monomethine cyanine dye to create a pH-sensitive, fluorescent and colorimetric G-quadruplex binder¹⁰² and the synthesis of a series of bifunctional hybrid acridine-HSP90 ligands demonstrating significant toxicity in the sub- μ M range.¹⁰³

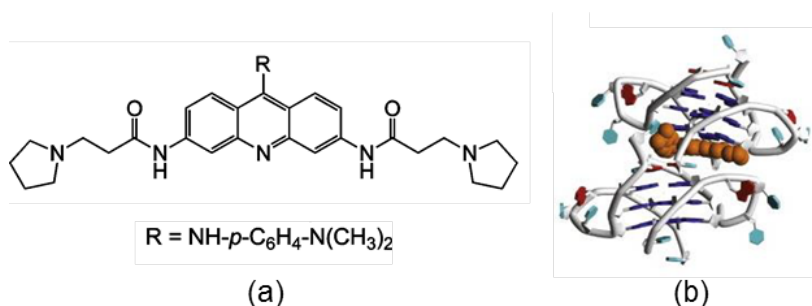


Figure 1.7.2-1 (a) Structure of BRACO-19 (b) Structure of BRACO-19 (orange) stacked between two G-quadruplex structures.¹⁰⁴

MMQ₃

MMQ₃ incorporates a feature introduced into G-quadruplex ligand design by Teulade-Fichou, Mergny and coworkers. The use of pentacyclic quinacridines that contain a crescent shape was introduced as a means to maximise the overlap between the aromatic ligand surface and G-quartet (Figure 1.7.2-2). MMQ₃ demonstrates excellent G-quadruplex stabilisation ($\Delta T_{1/2} = 20\text{ }^{\circ}\text{C}$) and high telomerase inhibition ($\text{IC}_{50}\text{-TRAP} = 28\text{ nM}$).¹⁰⁵ The quinacridine unit is able to overlap three of the G-quartet guanines, whilst participating in further G-quadruplex recognition *via* protonated sidearms that can interact with grooves.¹⁰⁶

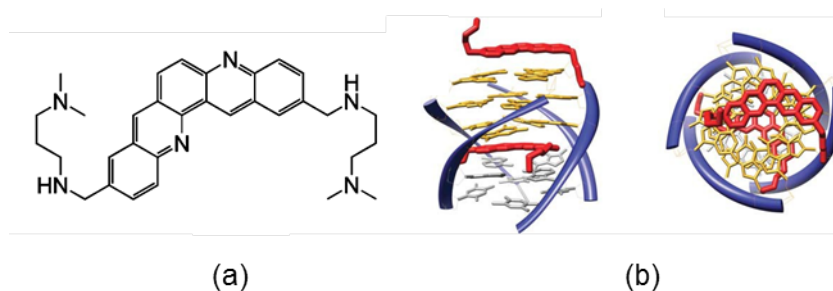


Figure 1.7.2-2 (a) Structure of MMQ (b) Side- and top-view NMR structures of MMQ (red) stacked on top of and between two G-quadruplex structures.⁵⁹

1.7.3 Organic N-methylated aromatic ligands

TMPyP4

TMPyP4 is a tetracationic porphyrin, representative of a family of ligands that are quaternized on the aromatic ring nitrogens, thus affording water solubility in the absence of cationic side-chains. Reduction of electron density of the aromatic core results in increased π -stacking availability of the ligand, enhancing its G-quadruplex

binding potential. Extensive studies of TMPyP4 by Hurley *et al.* have demonstrated high affinity for G-quadruplex structures ($\Delta T_{1/2} = 17\text{ }^{\circ}\text{C}$), in addition to an ability to inhibit telomerase ($\text{IC}_{50}\text{-TRAP} = 6\text{ }\mu\text{M}$) and downregulate oncogenic expression. Despite this, TMPyP4 displays poor selectivity for these structures.^{107,108}

TMPyP4 exhibits diverse binding modes including intercalation between adjacent G-tetrads, π -stacking onto the external G-quartet surface (Figure 1.7.3-1)¹⁰⁹ and external stacking onto the TTA nucleotides with no direct contact with the G-quartet itself.¹¹⁰ Consequently, there remains a great deal of interest in these fascinating molecules, with several structurally similar ligands being subsequently reported in the literature. Worth mentioning is the development of a porphyrazine derivative, 3,4-TMPyPz, which has shown a 100-fold increase in affinity, coupled with improved specificity (>30-fold preference) for G-quadruplex DNA over duplex DNA.¹¹¹

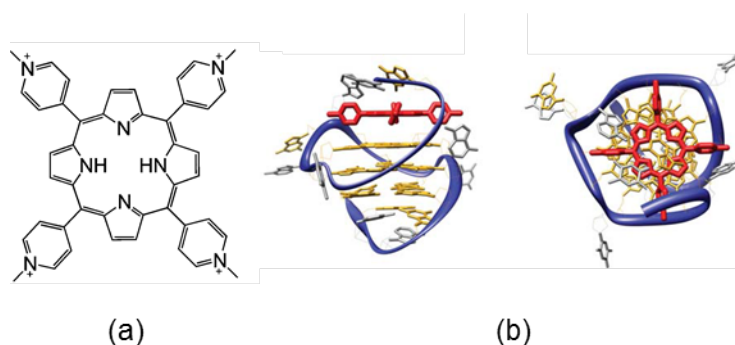


Figure 1.7.3-1 (a) Structure of TMPyP4 (b) Side- and top-view NMR structures of TMPyP4 (red) stacked on top of a G-quadruplex.⁵⁹

RHPS4

Reported by Stevens and coworkers,^{112,113} RHPS4 is an N-methylated pentacyclic acridinium that has been shown to decrease telomere length, acting as a modulator to the binding of telomere proteins ($\text{IC}_{50}\text{-TRAP} = 330\text{ nM}$).^{114,115} This cationic small molecule, with its condensed aromatic structure, sandwiches the G-quadruplex

structure (Figure 1.7.3-2) and was one of the earliest ligands whose complex structure with G-quadruplex DNA was solved by NMR (Fig).¹¹⁶

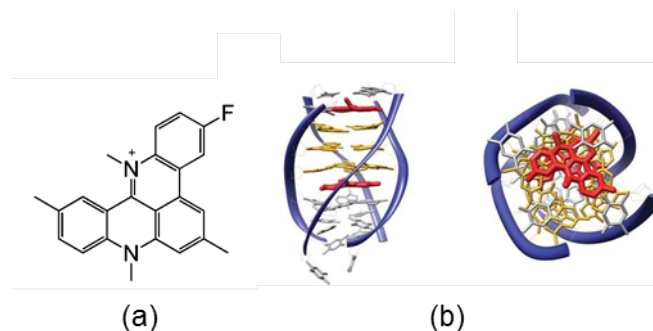


Figure 1.7.3-2 (a) Structure of RHPS4 (b) Side- and top-view NMR structures of RHPS4 (red) stacked on top of a G-quadruplex.⁵⁹

Phen-DC3

Phen-DC3 is a phenanthroline-bisquinolinium compound, developed as part of a series of compounds intended to balance rapid synthetic access and efficient G-quadruplex recognition. Following the earlier success of a series of bisquinolinium compounds that displayed exceptional properties, including a high degree of G-quadruplex stabilisation, excellent G-quadruplex over duplex selectivity, efficient telomerase inhibition, delayed growth arrest and induction of apoptosis in immortalised cells,¹¹⁷ a series of phenanthroline analogues were subsequently developed. The Phen-DC series demonstrated a perfect geometrical match with a G-quartet¹¹⁸ alongside remarkable G-quadruplex selectivity, exceeding that of telomestatin.

Phen-DC3 is a particularly promising compound from the series, specifically targeting G-quadruplexes and demonstrating potent biological effects *in vivo*.^{119,120} Utilising NMR spectroscopy to solve the structure of the complex formed between Phen-DC3 and an intramolecular G-quadruplex (derived from the c-Myc promoter),

Phen-DC3 was revealed to interact through extensive π -stacking with the G-tetrad¹²¹ (Figure 1.7.3-3).

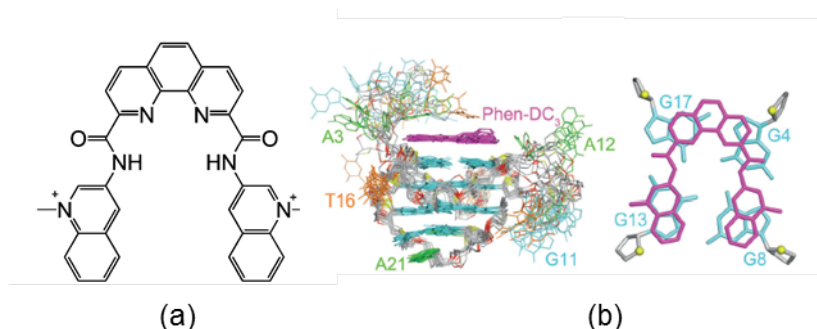


Figure 1.7.3-3 (a) Structure of Phen-DC3 (b) Side- and top-view solution structures of Phen-DC3 (magenta) stacked on top of a G-quadruplex.¹²²

1.7.4 Metallo-organic complexes

The incorporation of a metal centre into a potential G-quadruplex binding compound is extremely advantageous on account of the unique properties metals can confer to these compounds:

- (1) Structural provision: Metals dictate complex geometry based on their electronic configuration. For example, Pt(II) is a d^8 metal centre that will always form square planar complexes upon ligand binding. The ability to use the metal as a template in this way means that small changes in ligand design can be made, whilst retaining the geometry around the metal centre. Alternatively, incorporation of a different metal centre into the same ligand system may cause a change in geometry and optical properties.⁸⁶
- (2) Cationic charge: The presence of a metal centre imparts cationic charge into the complex, which is essential in promoting association with the negatively-charged backbone of the target DNA structure.

- (3) Increasing π -stacking interactions: A positively charged metal ion will withdraw electron density from the coordinated ligand's aromatic π -system. This acts to increase the strength of π -stacking interactions between the now electron-deficient ligand and the G-quartets. Furthermore, the positively charged metal is able to imitate the sodium and potassium cations that usually occupy the central cavity between G-quartet layers, providing further electrostatic stabilisation.⁸⁶
- (4) Direct nucleic acid interaction: Metals may interact directly with nucleic acids through coordinate bonding.
- (5) Detection: The presence of a metal enables complex examination by a variety of techniques including fluorescence, UV-Vis spectroscopy or redox electrochemistry.⁸⁶

Mn(III)-TMPyP4

The first reported examples of metallo-organic G-quadruplex ligands featured the insertion of a metal centre, such as Cu(II)^{123,124} and Ni(II),¹²⁵ into the central cavity of TMPyP4.¹²⁶ Despite displaying modest telomerase inhibition (IC_{50} -TRAP = 26 μ M), Mn(III)-TMPyP4 (Figure 1.7.4-1) showed a 10-fold preference for G-quadruplex DNA over duplex DNA.¹²⁵

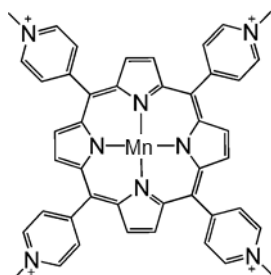


Figure 1.7.4-1 Structure of Mn(III)-TMPyP4.

Ni(II)-salphen

A selection of metal-salphen complexes were first reported by Neidle and Vilar, with Ni(II)-salphens among the most promising compounds due to their excellent stabilisation of a human telomeric intramolecular G-quadruplex structure ($\Delta T_{1/2} = 33\text{ }^{\circ}\text{C}$).¹²⁷ Further studies of the Ni(II)-salphen shown in Figure 1.7.4-2 suggested a >50-fold selectivity for telomeric G-quadruplex over duplex DNA.¹²⁸ Elucidation of the X-ray crystal structure of this complex bound to human telomeric G-quadruplex shows end-stacking as the binding mode, with the Ni(II) ion sitting almost in line with the potassium ions occupying the central cavity. This complex shows significant antiproliferative activity and telomerase inhibition ($\text{IC}_{50}\text{-TRAP} = 120\text{ nM}$).⁵⁹

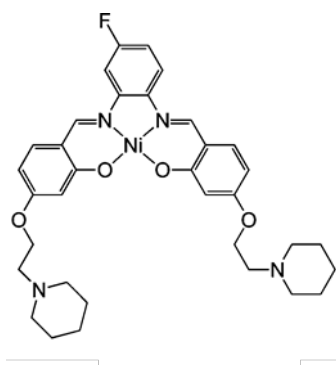


Figure 1.7.4-2 Structure of Ni(II)-salphen.

Mn(III)-porphyrin

A pentacationic manganese(III) porphyrin (Figure 1.7.4-3) was reported by Pratviel and coworkers to exhibit a 10 000-fold selectivity for telomeric G-quadruplex over duplex DNA. Combining a central aromatic core and four flexible cationic arms, the exceptional affinity of this metalloporphyrin for G-quadruplex DNA is associated with a good capacity to inhibit telomerase at submicromolar concentrations ($\text{IC}_{50}\text{-TRAP} = 580\text{ nM}$).¹²⁹ The strong binding affinity arises from the π -stacking interactions

between the aromatic core and G-quartet, coupled with proposed interactions between the cationic sidearms and loops and/or grooves of the G-quadruplex stack.¹²⁹

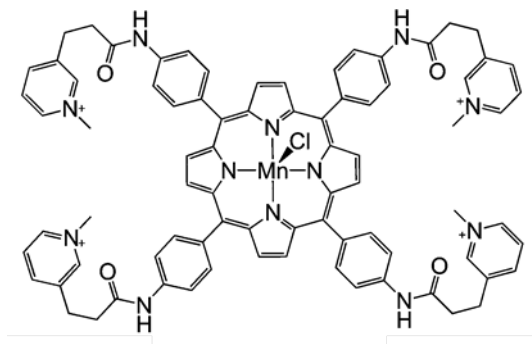


Figure 1.7.4-3 Structure of Mn(III)-porphyrin.

Metal-terpyridines

Cu(tppy)

Metal terpyridine (2,2':6',2''-terpyridine, tpy) complexes are synthetically attractive due to their relatively simple structure and straightforward preparation, often in two-step processes. A range of metals including Cu(II), Pt(II), Zn(II) and Ru(III) can be easily accommodated by the ligand, allowing a series of complexes to be prepared with relative ease.¹³⁰ Modified tpy ligands, such as tolyl-terpyridine (featuring a methylphenyl moiety on the central ring, ttpy) have also been extensively studied. Metal complexes incorporating both the tpy and ttpy ligands have been investigated for their potential as G-quadruplex binders by Teulade-Fichou and coworkers.¹³¹ Such compounds proved to be both high affinity and highly selective G-quadruplex binders, particularly Cu(tppy) (Figure 1.7.4-4) which showed a 22-fold selectivity for telomeric G-quadruplex DNA over duplex DNA (G4-FID assay) and excellent stability ($\Delta T_{1/2} = 15\text{ }^{\circ}\text{C}$).¹³⁰ Highlighting the geometry of the metal centre as a key parameter

governing selectivity, the pseudo-square pyramidal structure of the Cu-ttpy compound was best able to maximise G-quartet interactions (planar aromatic surface engaging in stabilising π -stacking interactions, centrally positioned Cu(II) ion mimicking naturally occurring cations, highly polarised metal-ligand bonds favouring electrostatic interaction with negatively charged DNA), whilst also impeding duplex DNA intercalation (pyramidal shape).¹³⁰

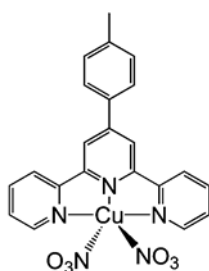


Figure 1.7.4-4 Structure of Cu(ttpy).

Dimetallic Cu(II) and Pt(II)

Dimetallic complexes with terpyridine-based ligands have been investigated by Vilar *et al.*. Dicopper and diplatinum complexes (Figure 1.7.4-5) were shown to bind very strongly to G-quadruplex DNA (Htelo and cMyc) with up to 100-fold selectivity over duplex DNA.¹³² Consisting of a metal-terpyridine unit displaying either square-based pyramidal (Cu(II)) or square planar (Pt(II)) geometry linked by a three-atom spacer to a dipicolyl amine coordinated to the second metal, these complexes possess binding mode duality; (1) π - π stacking of the metal-terpyridine unit onto the external G-quartet (2) electrostatic interactions between the metal-dipicolyl amine fragment and the DNA backbone. Interestingly, the metal-free ligands did not display comparable activity, confirming the necessity of metal coordination in achieving the high binding affinities seen between these polydentate ligands and G-quadruplex DNA.¹³²

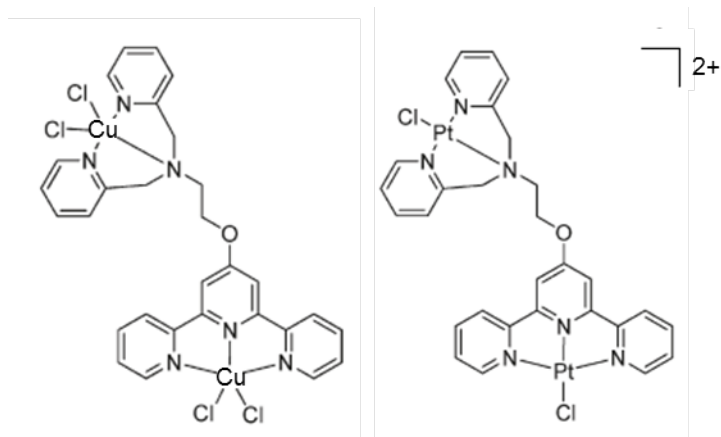


Figure 1.7.4-5 Structure of dimetallic Cu(II) and Pt(II) species.

Pt-MPQ

Pt-MPQ is another example of a dual-modality G-quadruplex binder, this time achieved through a single metal moiety grafted in the periphery of the central metal core. Pt(II) was first exploited for this purpose following the discovery by Bombard and coworkers that terminal G-quartets could be platinated.¹³³ Pt-MPQ (Figure 1.7.4-6) is a platinum-quinacridine hybrid compound that achieves a dual covalent-non-covalent binding mode *via* π -stacking interactions between the aromatic quinacridine unit and the G-quartet alongside covalent interactions with the platinum moiety.¹³⁴

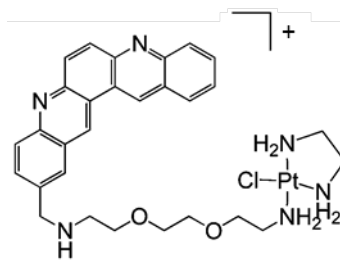


Figure 1.7.4-6 Structure of Pt-MPQ.

1.8 Summary

There exists a key requirement, common among G-quadruplex binding compounds such as those discussed, that must be met in order to facilitate G-quadruplex binding; a large, planar aromatic system prone to π -stacking with a G-tetrad platform (hydrophobic nature), while retaining reasonable water solubility (hydrophilic nature).⁵⁹

The preceding examples of G-quadruplex binding compounds demonstrate the wide scope and ongoing developments in the G-quadruplex nucleic acids research community. Targeting G-quadruplex DNA remains challenging due to the structural polymorphism displayed by G-quadruplexes as a result of differing strand sequences, loop lengths, metal cation stabilisation and folding patterns. The advantage of this polymorphic nature, however, lies in the potential to target a specific G-quadruplex structure implicated in a process of interest. The development of compounds that are capable of discriminating not only G-quadruplex DNA from duplex DNA, but also between different structures of G-quadruplex is therefore vital, and represents a large proportion of recent advances in the field.

1.9 Thesis aims

The work contained within this thesis focuses on the development of ligands and complexes for G-quadruplex nucleic acid binding. It will commence with the further synthetic exploration of two complexes incorporating 3,3-biisoquinoline. These complexes possess large, planar aromatic surfaces suitable for π -stacking, coordinated around a central cationic metal ion capable of engaging in electrostatic

interactions whilst mimicking naturally occurring sodium and potassium cations. By way of extension from previous biophysical studies (reviewed in Chapter II), the first *in vitro* biological studies of these complexes will be carried out. This will include investigating the cytotoxicity, cell uptake, induced DNA damage and cell cycle arrest effects of each complex.

The design, synthesis and characterisation of novel terpyridine-based metal complexes will be carried out and these complexes assessed for their suitability as G-quadruplex binders by UV-Vis spectroscopy, circular dichroism and gel electrophoresis. The key aim is to establish a terpyridine platform. A variety of synthetic strategies towards novel G-quadruplex ligands will be tested, in order to expand our understanding of the suitability and scope of particular routes and aid the future development of novel complexes.

1.10 References

- 1 J. D. Watson and F. H. C. Crick, *Cold Spring Harb. Symp. Quant. Biol.*, 1953, **18**, 123–131.
- 2 J. D. Watson and F. H. C. Crick, *Nature*, 1953, **171**, 737–738.
- 3 M. J. Hannon, *Chem. Soc. Rev.*, 2007, **36**, 280–295.
- 4 M. Levitt, *Proc. Natl. Acad. Sci. U. S. A.*, 1978, **75**, 640–4.
- 5 J. M. Berg, J. L. Tymoczko and L. Stryer, *Biochemistry, 5th Edition*, W H Freeman, 2002.
- 6 A. Rich and S. Zhang, *Nat. Rev. Genet.*, 2003, **4**, 566–72.
- 7 University of Tokyo, *Nucleic Acids*, 2016.
- 8 D. Buck, *Proc. Symp. Appl. Math.*, 2009, **66**, 1–33.
- 9 J. Zlatanova and K. van Holde, *FASEB J.*, 1998, **12**, 421–31.
- 10 P. Gottipati and T. Helleday, *Mutagenesis*, 2009, **24**, 203–210.
- 11 M. Micco, G. W. Collie, A. G. Dale, S. A. Ohnmacht, I. Pazitna, M. Gunaratnam, A. P. Reszka and S. Neidle, *J. Med. Chem.*, 2013, **56**, 2959–2974.
- 12 A. C. G. Hotze, N. J. Hodges, R. E. Hayden, C. Sanchez-Cano, C. Paines, N. Male, M.-K. Tse, C. M. Bunce, J. K. Chipman and M. J. Hannon, *Chem. Biol.*, 2008, **15**, 1258–1267.
- 13 D. R. Duckett and D. M. Lilley, *EMBO J.*, 1990, **9**, 1659–64.
- 14 R. Holliday, *Genet. Res.*, 1964, **5**, 282.
- 15 D. R. Duckett, A. I. H. Murchie, S. Diekmann, E. von Kitzing, B. Kemper and D. M. J. Lilley, *Cell*, 1988, **55**, 79–89.
- 16 L. Stefan, B. Bertrand, P. Richard, P. Le Gendre, F. Denat, M. Picquet and D. Monchaud, *Chembiochem*, 2012, **13**, 1905–12.
- 17 B. Wu, F. Girard, B. van Buuren, J. Schleucher, M. Tessari and S. Wijmenga, *Nucleic Acids Res.*, 2004, **32**, 3228–3239.
- 18 S. Muhuri, K. Mimura, D. Miyoshi and N. Sugimoto, *J. Am. Chem. Soc.*, 2009, **131**, 9268–80.
- 19 S. Vuong, L. Stefan, P. Lejault, Y. Rousselin, F. Denat and D. Monchaud, *Biochimie*, 2012, **94**, 442–50.
- 20 R. R. Sinden, V. N. Potaman, E. A. Oussatcheva, C. E. Pearson, Y. L.

- Lyubchenko and L. S. Shlyakhtenko, *J. Biosci.*, 2002, **27**, 53–65.
- 21 J. Malina, M. J. Hannon and V. Brabec, *Chem. - A Eur. J.*, 2007, **13**, 3871–3877.
 - 22 N. Campbell, J. Reece, L. Urry, M. Cain, S. Wasserman, P. Minorsky and R. Jackson, *Biology (8th edition)*, Pearson Education Inc. Benjamin Cummings, 2008.
 - 23 D. M. J. Lilley, *Proc. Natl. Acad. Sci. U. S. A.*, 1995, **92**, 7140–7142.
 - 24 R. J. Ernst, H. Song and J. K. Barton, *J. Am. Chem. Soc.*, 2009, **131**, 2359–66.
 - 25 D. J. Patel, S. A. Kozlowski, L. A. Marky, C. Broka, J. A. Rice, K. Itakura and K. J. Breslauer, *Biochemistry*, 1982, **21**, 428–36.
 - 26 P. T. Henderson, E. Boone and G. B. Schuster, *Helv. Chim. Acta*, 2002, **85**, 135–151.
 - 27 D. A. LeBlanc and K. M. Morden, *Biochemistry*, 1991, **30**, 4042–4047.
 - 28 M. Zheng, M. Wu and I. Tinoco, *Proc. Natl. Acad. Sci. U. S. A.*, 2001, **98**, 3695–700.
 - 29 G. M. Cooper, *The Cell: A Molecular Approach (2nd Edition)*, Sinauer Associates, 2000.
 - 30 J. P. Cerón-Carrasco, D. Jacquemin and E. Cauët, *Phys. Chem. Chem. Phys.*, 2012, **14**, 12457.
 - 31 S. L. B. König, A. C. Evans and J. L. Huppert, *Biomol. Concepts*, 2010, **1**, 197–213.
 - 32 I. Gellert, M. N. Lipsett and D. R. Davies, *Proc. Natl. Acad. Sci. U. S. A.*, 1962, **48**, 2013–2018.
 - 33 P. Murat, Y. Singh and E. Defrancq, *Chem. Soc. Rev.*, 2011, **40**, 5293–5307.
 - 34 J.-L. Mergny, A. De Cian, A. Ghelab, B. Saccà and L. Lacroix, *Nucleic Acids Res.*, 2005, **33**, 81–94.
 - 35 N. V Hud, F. W. Smith, F. A. L. Anet and J. Feigon, *Biochemistry*, 1996, **35**, 15383–15390.
 - 36 J. Gu and J. Leszczynski, *J. Phys. Chem. A*, 2002, **106**, 529–532.
 - 37 C. C. Hardin, T. Watson, M. Corregan and C. Bailey, *Biochemistry*, 1992, **31**, 833–841.
 - 38 A. Włodarczyk, P. Grzybowski, A. Patkowski and A. Dobek, *J. Phys. Chem. B*,

- 2005, **109**, 3594–3605.
- 39 W. Guschlbauer, J.-F. Chantot and D. Thiele, *J. Biomol. Struct. Dyn.*, 1990, **8**, 491–511.
- 40 E. A. Venczel and D. Sen, *Biochemistry*, 1993, **32**, 6220–6228.
- 41 S. Burge, G. N. Parkinson, P. Hazel, A. K. Todd and S. Neidle, *Nucleic Acids Res.*, 2006, **34**, 5402–15.
- 42 J. L. Huppert and S. Balasubramanian, *Nucleic Acids Res.*, 2005, **33**, 2908–16.
- 43 Y. Wang and D. J. Patel, *Structure*, 1993, **1**, 263–282.
- 44 A. Risitano and K. R. Fox, *Nucleic Acids Res.*, 2004, **32**, 2598–2606.
- 45 Y. Wang and D. J. Patel, *J. Mol. Biol.*, 1993, **234**, 1171–1183.
- 46 M. Vorlíčková, J. Chládková and I. Kejnovská, *Nucleic Acids Res.*, 2005, **33**, 5851–5860.
- 47 C. Schaffitzel, I. Berger, J. Postberg, J. Hanes, H. J. Lipps and A. Pluckthun, *Proc. Natl. Acad. Sci. U. S. A.*, 2001, **98**, 8572–8577.
- 48 O. Stegle, L. Payet, J. Mergny and D. MacKay, *Bioinformatics*, 2009, **25**, 374–382.
- 49 H. Lipps and D. Rhodes, *Trends Cell Biol.*, 2009, **19**, 414–422.
- 50 L. Petraccone, E. Erra, I. Duro, V. Esposito, A. Randazzo, L. Mayol, C. A. Mattia, G. Barone and C. Giancola, *Nucleosides, Nucleotides and Nucleic Acids*, 2005, **24**, 757–760.
- 51 H. M. Wong, O. Stegle, S. Rodgers and J. L. Huppert, *J. Nucleic Acids*, 2010, **2010**, 1–6.
- 52 J. Johnson, J. Smith, M. Kozak and F. Johnson, *Biochimie*, 2008, **90**, 1250–1263.
- 53 N. Maizels, *Nat. Struct. Mol. Biol.*, 2006, **13**, 1055–1059.
- 54 A. G. Bodnar, M. Ouellette, M. Frolkis, S. E. Holt, C. P. Chiu, G. B. Morin, C. B. Harley, J. W. Shay, S. Lichtsteiner and W. E. Wright, *Science*, 1998, **279**, 349–52.
- 55 L. Hayflick and P. S. Moorhead, *Exp. Cell Res.*, 1961, **25**, 585–621.
- 56 L. Hayflick, *Exp. Cell Res.*, 1965, **37**, 614–636.
- 57 R. Calado and N. Young, *Telomeres in disease*, 2012.
- 58 V. L. Makarov, Y. Hirose and J. P. Langmore, *Cell*, 1997, **88**, 657–66.

- 59 D. Monchaud and M.-P. Teulade-Fichou, *Org. Biomol. Chem.*, 2008, **6**, 627–36.
- 60 Q. Yang, J. Xiang, S. Yang, Q. Zhou, Q. Li, Y. Tang and G. Xu, *Chem. Commun.*, 2009, **350**, 1103.
- 61 G. Biffi, D. Tannahill, J. McCafferty and S. Balasubramanian, *Nat. Chem.*, 2013, **5**, 182–186.
- 62 A. Zahler, J. Williamson, T. Cech and D. Prescott, *Nature*, 1991, **350**, 718–720.
- 63 J. E. Reed, A. J. P. White, S. Neidle and R. Vilar, *Dalt. Trans.*, 2009, **14**, 2558–68.
- 64 J. Williamson, *Proc. Natl. Acad. Sci. United States Am.*, 1993, **90**, 3124.
- 65 T. A. Brooks, S. Kendrick and L. Hurley, *FEBS J.*, 2010, **277**, 3459–3469.
- 66 A. K. Todd and S. Neidle, *Nucleic Acids Res.*, 2008, **36**, 2700–2704.
- 67 J. Eddy and N. Maizels, *Nucleic Acids Res.*, 2007, **36**, 1321–1333.
- 68 S. Cogoi and L. E. Xodo, *Nucleic Acids Res.*, 2006, **34**, 2536–2549.
- 69 R. De Armond, S. Wood, D. Sun and L. Hurley, *Biochemistry*, 2005, **44**, 16341–16350.
- 70 T. Simonsson, M. Kubista and P. Pecinka, *Nucleic Acids Res.*, 1998, **26**, 1167–1172.
- 71 S. Rankin, A. P. Reszka, J. Huppert, M. Zloh, G. N. Parkinson, A. K. Todd, S. Ladame, S. Balasubramanian and S. Neidle, *J. Am. Chem. Soc.*, 2005, **127**, 10584–10589.
- 72 J. Dai, T. Dexheimer, D. Chen and M. Carver, *J. Am. Chem. Soc.*, 2006, **128**, 1096–1098.
- 73 D. Sun, K. Guo, J. Rusche and L. Hurley, *Nucleic Acids Res.*, 2005, **33**, 6070–6080.
- 74 A. Siddiqui-Jain and C. Grand, *Proc. Natl. Acad. Sci. U. S. A.*, 2002, **99**, 11593–11598.
- 75 C. V Dang, A. Le and P. Gao, *Clin. Cancer Res.*, 2009, **15**, 6479–83.
- 76 V. González and L. H. Hurley, *Annu. Rev. Pharmacol. Toxicol.*, 2010, **50**, 111–129.
- 77 J. A. Nilsson and J. L. Cleveland, *Oncogene*, 2003, **22**, 9007–9021.
- 78 D. M. Miller, S. D. Thomas, A. Islam, D. Muench and K. Sedoris, *Clin. Cancer*

- Res., 2012, **18**, 5546–53.
- 79 M. Eilers and R. N. Eisenman, *Genes Dev.*, 2008, **22**, 2755–66.
 - 80 R. V Brown, F. L. Danford, V. Gokhale, L. H. Hurley and T. A. Brooks, *J. Biol. Chem.*, 2011, **286**, 41018–27.
 - 81 K. C. Sedoris, S. D. Thomas, C. R. Clarkson, D. Muench, A. Islam, R. Singh and D. M. Miller, *Mol. Cancer Ther.*, 2012, **11**, 66–76.
 - 82 T. Ou, Y. Lu, C. Zhang and Z. Huang, *J. Med. Chem.*, 2007, **50**, 1465–1474.
 - 83 E. Largy, A. Granzhan, F. Hamon, D. Verga and M.-P. Teulade-Fichou, in *Quadruplex Nucleic Acids*, Springer Berlin Heidelberg, 2013.
 - 84 H. Ma, M. Zhang, D. Zhang, R. Huang, Y. Zhao, H. Yang, Y. Liu, X. Weng, Y. Zhou, M. Deng, L. Xu and X. Zhou, *Chem. - An Asian J.*, 2010, **5**, 114–122.
 - 85 L. Martino, A. Virno, B. Pagano, A. Virgilio, S. Di Micco, A. Galeone, C. Giancola, G. Bifulco, L. Mayol and A. Randazzo, *J. Am. Chem. Soc.*, 2007, **129**, 16048–16056.
 - 86 S. N. Georgiades, N. H. Abd Karim, K. Suntharalingam and R. Vilar, *Angew. Chemie Int. Ed.*, 2010, **49**, 4020–4034.
 - 87 R. Rodriguez, G. D. Pantoş, D. P. N. Gonçalves, J. K. M. Sanders and S. Balasubramanian, *Angew. Chemie*, 2007, **119**, 5501–5503.
 - 88 H. L. Pritchard, Thesis, University of Birmingham, 2015.
 - 89 K. Shin-ya, K. Wierzba, K. Matsuo and T. Ohtani, *J. Am. Chem. Soc.*, 2001, **123**, 1262–1263.
 - 90 T. Doi, K. Shibata, M. Yoshida, M. Takagi, M. Tera, K. Nagasawa, K. Shin-ya and T. Takahashi, *Org. Biomol. Chem.*, 2011, **9**, 387–393.
 - 91 H. Tahara, K. Shin-Ya, H. Seimiya, H. Yamada and T. Tsuruo, *Oncogene*, 2006, **25**, 1955–1966.
 - 92 F. Rosu, V. Gabelica, N. Smargiasso, G. Mazzuchelli, K. Shin-ya and E. De Pauw, *J. Nucleic Acids*, 2010, **2010**, 1–7.
 - 93 T. Doi, M. Yoshida, K. Shin-ya and T. Takahashi, *Org. Lett.*, 2006, **8**, 4165–4167.
 - 94 P. Perry, S. M. Gowan, A. P. Reszka, P. Polucci, T. C. Jenkins, L. R. Kelland and S. Neidle, *J. Med. Chem.*, 1998, **41**, 3253–3260.
 - 95 P. Perry, A. Reszka, A. Wood and M. Read, *J. Med. Chem.*, 1998, **41**, 4873–

4883.

- 96 C. Schultes, B. Guyen, J. Cuesta and S. Neidle, *Bioorg. Med. Chem. Lett.*, 2004, **14**, 4347–4351.
- 97 M. J. B. Moore, C. M. Schultes, J. Cuesta, F. Cuenca, M. Gunaratnam, F. A. Tanious, W. D. Wilson and S. Neidle, *J. Med. Chem.*, 2006, **49**, 582–599.
- 98 N. Kim, M. Piatyszek, K. Prowse and C. Harley, *Science*, 1994, **266**, 2011–2015.
- 99 J. Cuesta, M. Read and S. Neidle, *Mini Rev. Med. Chem.*, 2003, **3**, 11–21.
- 100 A. Burger, F. Dai, C. Schultes and A. Reszka, *Cancer Res.*, 2005, **65**, 1489–1496.
- 101 S. Gowan, J. Harrison, L. Patterson and M. Valenti, *Mol. Pharmacol.*, 2002, **61**, 1154–1162.
- 102 C. Percivalle, T. Mahmood and S. Ladame, *Med. Chem. Commun.*, 2013, **4**, 211–215.
- 103 S. Roe, M. Gunaratnam, C. Spiteri, P. Sharma, R. D. Alharthy, S. Neidle and J. E. Moses, *Org. Biomol. Chem.*, 2015, **13**, 8500–8504.
- 104 S. Neidle, *Curr. Opin. Struct. Biol.*, 2009, **19**, 239–250.
- 105 J.-L. Mergny, L. Lacroix, M.-P. Teulade-Fichou, C. Hounsou, L. Guittat, M. Hoarau, P. B. Arimondo, J.-P. Vigneron, J.-M. Lehn, J.-F. Riou, T. Garestier and C. Helene, *Proc. Natl. Acad. Sci. U. S. A.*, 2001, **98**, 3062–3067.
- 106 C. Hounsou, L. Guittat, D. Monchaud, M. Jourdan, N. Saettel, J.-L. Mergny and M.-P. Teulade-Fichou, *ChemMedChem*, 2007, **2**, 655–666.
- 107 J. Ren and J. Chaires, *Biochemistry*, 1999, **38**, 16067–16075.
- 108 A. De Cian, L. Guittat, K. Shin-ya and J. Riou, *Nucleic acids Symp. ser*, 2005, **49**, 235–236.
- 109 I. Haq, J. Trent and B. Chowdhry, *J. Am. Chem. Soc.*, 1999, **121**, 1768–1779.
- 110 G. Parkinson, R. Ghosh and S. Neidle, *Biochemistry*, 2007, **46**, 2390–2397.
- 111 D. P. N. Gonçalves, R. Rodriguez, S. Balasubramanian and J. K. M. Sanders, *Chem. Commun.*, 2006, **266**, 4685–4687.
- 112 J. Stanslas, D. J. Hagan, M. J. Ellis, C. Turner, J. Carmichael, W. Ward, T. R. Hammonds and M. F. G. Stevens, *J. Med. Chem.*, 2000, **43**, 1563–1572.
- 113 J. Cookson and R. Heald, *J. Med. Chem.*, 2005, **48**, 7198–7207.

- 114 P. Phatak, J. C. Cookson, F. Dai, V. Smith, R. B. Gartenhaus, M. F. G. Stevens and A. M. Burger, *Br. J. Cancer*, 2007, **96**, 1223–1233.
- 115 E. Salvati, C. Leonetti, A. Rizzo, M. Scarsella, M. Mottolese, R. Galati, I. Sperduti, M. F. G. Stevens, M. D'Incalci, M. Blasco, G. Chiorino, S. Bauwens, B. Horard, E. Gilson, A. Stoppacciaro, G. Zupi and A. Biroccio, *J. Clin. Invest.*, 2007, **117**, 3236–3247.
- 116 E. Gavathiotis, R. Heald and M. Stevens, *Angew. Chemie*, 2001, **40**, 4749–4751.
- 117 T. Lemarteleur, D. Gomez, R. Paterski and E. Mandine, *Biochem. Biophys. Res. Commun.*, 2004, **323**, 802–808.
- 118 A. De Cian, E. Delemos, J.-L. Mergny, M.-P. Teulade-Fichou and D. Monchaud, *J. Am. Chem. Soc.*, 2007, **129**, 1856–7.
- 119 A. Piazza, J.-B. Boulé, J. Lopes, K. Mingo, E. Largy, M.-P. Teulade-Fichou and A. Nicolas, *Nucleic Acids Res.*, 2010, **38**, 4337–48.
- 120 J. Lopes, A. Piazza, R. Bermejo, B. Kriegsman, A. Colosio, M.-P. Teulade-Fichou, M. Foiani and A. Nicolas, *EMBO J.*, 2011, **30**, 4033–46.
- 121 W. J. Chung, B. Heddi, F. Hamon, M.-P. Teulade-Fichou and A. T. Phan, *Angew. Chemie Int. Ed.*, 2014, **53**, 999–1002.
- 122 W. Chung, B. Heddi and F. Hamon, *Angew. Chemie*, 2014, **53**, 999–1002.
- 123 S. E. Evans, M. A. Mendez, K. B. Turner, L. R. Keating, R. T. Grimes, S. Melchoir and V. A. Szalai, *J. Biol. Inorg. Chem.*, 2007, **12**, 1235–1249.
- 124 L. R. Keating and V. A. Szalai, *Biochemistry*, 2004, **43**, 15891–15900.
- 125 I. M. Dixon, F. Lopez, J.-P. Estève, A. M. Tejera, M. A. Blasco, G. Pratviel and B. Meunier, *ChemBioChem*, 2005, **6**, 123–132.
- 126 E. Izbicka, R. T. Wheelhouse, E. Raymond, K. K. Davidson, R. A. Lawrence, D. Sun, B. E. Windle, L. H. Hurley and D. D. Von Hoff, *Cancer Res.*, 1999, **59**, 639–44.
- 127 A. Arola-Arnal, J. Benet-Buchholz, S. Neidle and R. Vilar, *Inorg. Chem.*, 2008, **47**, 11910–9.
- 128 J. E. Reed, A. A. Arnal, S. Neidle and R. Vilar, *J. Am. Chem. Soc.*, 2006, **128**, 5992–3.
- 129 I. M. Dixon, F. Lopez, A. M. Tejera, J.-P. Estève, M. A. Blasco, G. Pratviel and

- B. Meunier, *J. Am. Chem. Soc.*, 2007, **129**, 1502–1503.
- 130 H. Bertrand, D. Monchaud, A. De Cian, R. Guillot, J.-L. Mergny and M.-P. Teulade-Fichou, *Org. Biomol. Chem.*, 2007, **5**, 2555.
- 131 E. Largy, F. Hamon, F. Rosu, V. Gabelica, E. De Pauw, A. Guédin, J.-L. Mergny and M.-P. Teulade-Fichou, *Chem. - A Eur. J.*, 2011, **17**, 13274–83.
- 132 K. Suntharalingam, A. J. P. White and R. Vilar, *Inorg. Chem.*, 2010, **49**, 8371–8380.
- 133 H. Bertrand, S. Bombard, D. Monchaud, E. Talbot, A. Guedin, J.-L. Mergny, R. Grunert, P. J. Bednarski and M.-P. Teulade-Fichou, *Org. Biomol. Chem.*, 2009, **7**, 2864–2871.
- 134 H. Bertrand, S. Bombard, D. Monchaud and M.-P. Teulade-Fichou, *J. Biol. Inorg. Chem.*, 2007, **12**, 1003–1014.

Chapter II

2.1 Introduction

Part I of this chapter explores the synthetic methodology that has been employed in recent years within the Hannon group to prepare novel complexes capable of binding G-quadruplex (G4) forming DNA sequences. Improvements to the synthetic routes utilised, in addition to further biophysical analyses are detailed herein.

Organic compounds such as porphyrins and acridine-based structures form the basis of much of the research into G4 binding molecules. Whilst often effective binders, selectivity for G4 structures is not always observed,¹ and synthetic routes towards these products are often complex and low yielding, particularly in the case of porphyrins. The introduction of metals into complexes can significantly improve binding by providing a central ion to mimic cations (e.g. Na^+ , K^+) already present in the centre of the G-quadruplex, as well as strengthening π -stacking interactions. The cationic charge also aids binding to the anionic DNA target. Furthermore, it is possible to synthesise multiple complexes relatively easily, by changing the metal used, resulting in structural diversity between complexes with the same ligand framework. It is evident that an excellent size match between complex and DNA target is essential in maximising the binding affinity.^{2,3} Therefore, the design and synthesis of a G-quadruplex binder which shows a more accurate size match than those observed in salphen and phenanthroline metal complexes^{1,4,5} would maximise the G-quartet coverage, ensuring all possible π -stacking interactions are explored, resulting in maximum binding affinity.

Owing to its demonstrated binding preference for G4-DNA over duplex DNA, as observed for derivatives of the natural alkaloid berberine,⁶ the isoquinoline

structure was selected as the starting point for the molecular design of a new G-quadruplex binder. Found in many medicinal products,⁷ the isoquinoline unit is able to facilitate side by side stacking of the berberine unit onto a G-quartet at the 3' and 5' ends of the G-quadruplex, as observed by X-ray crystallography (Figure 2.1.1-1).⁷

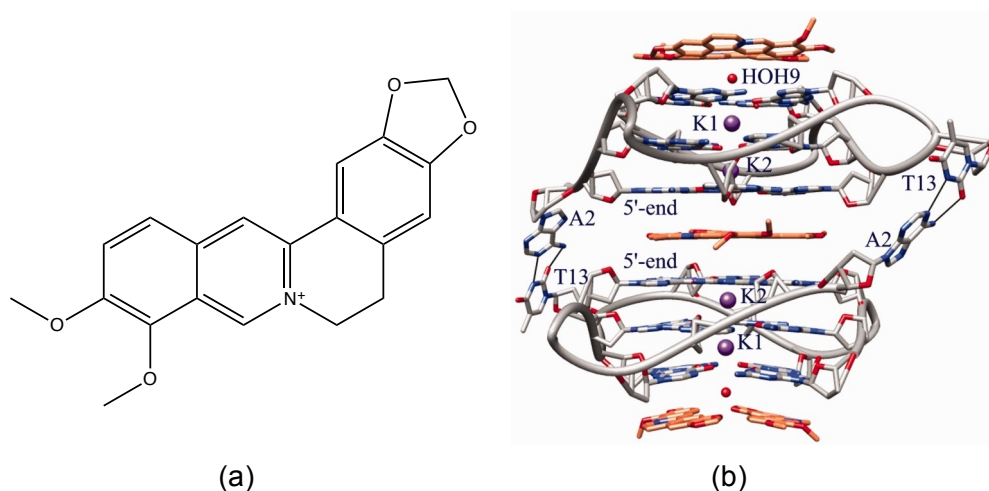


Figure 2.1.1-1 (a) Structure of berberine; (b) DNA topology and binding sites in the Ber/h-Tel23 adduct.⁷

Coupling isoquinoline to itself results in the formation of 3,3-biisoquinoline (*i*-biq). This bidentate ligand can bind to platinum in a 2:1 ratio to furnish a square planar complex, as demonstrated by Kato *et al.*⁸ This complex has great potential as a G-quadruplex binder on account of its excellent size match for a G-quartet, as shown in Figure 2.1.1-2. Furthermore, the complex benefits from a large aromatic surface to maximise π -stacking interactions, along with the central platinum cation, which will enhance electrostatic interactions. Consequently, investigation of this complex and its derivatives formed the basis of the initial research into G-quadruplex recognition, carried out by Hannah Pritchard.⁹ A summary of the notable developments thus far within the Hannon group is now included for the purposes of context.

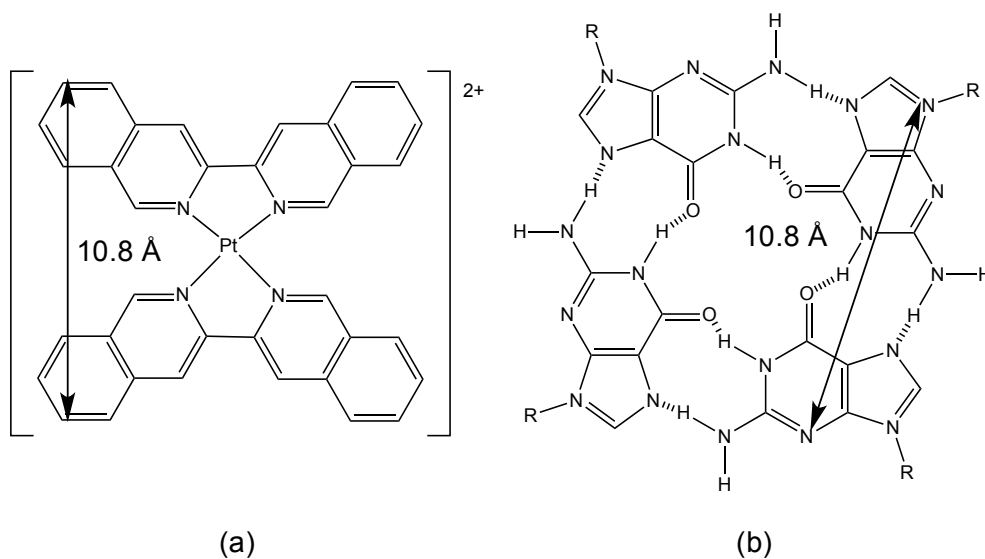


Figure 2.1.1-2 Comparison of the structure and size of (a) $[Pt(i-biq)]^{2+}$; (b) G-quartet

2.1.1 Summary of previous group research into G-quadruplex recognition

The 3,3'-biisoquinoline (*i*-biq) ligand, along with palladium and platinum complexes incorporating the ligand were synthesised in low to moderate yields (ligand: 10%, Pd: 50%, Pt: 27%).⁹ The stability and binding properties of the two complexes with both duplex DNA and G-quadruplex types of DNA were explored using a variety of spectroscopic techniques.

Using circular dichroism (CD) to analyse DNA binding, both complexes were shown to interact well with duplex DNA and Htelo DNA (forms antiparallel hybrid G-quadruplex). Strong ICD (induced CD) peaks were observed with both types of DNA for both complexes. When testing with cMyc DNA (forms parallel G-quadruplex), only the platinum complex showed an interaction. With no interaction observed between the palladium complex and cMyc DNA, this complex clearly demonstrates a degree of selectivity for antiparallel hybrid G-quadruplex conformations (such as Htelo). UV-Vis titration experiments showed a large red shift in the complex absorption

spectrum upon addition of DNA. This observation, along with the strong ICD signals observed in the CD spectra indicated that the mode of binding between the complexes and G4 structures was end-stacking. In the case of the platinum complex, there was also evidence of intercalative binding, resulting in the proposal of dual-modality end-stacking and intercalative binding.

The selectivity of each complex towards G-quadruplex binding over duplex binding was investigated by fluorescence indicator displacement assays. Both complexes were able to displace thiazole orange (fluorescent indicator) at concentrations below the 0.5 μM threshold in both Htelo and cMyc DNA. Furthermore, both complexes were less able to displace the dye from duplex DNA, requiring concentrations above 2 μM . Differences in the binding ability of the two complexes was suggested to be linked to the extent of planarity each complex is able to achieve, and the resultant quality of the 'fit' with the G-quartet surface. The crystal structures of the two complexes showed very subtle differences, with the platinum complex being slightly less planar than the palladium analogue (26° vs. 24° between planes). Since the platinum complex was the better match for G4 binding, the G-quartet was proposed to be slightly distorted itself and it was suggested that this resulted in preferential binding. However, such a small structural difference in the solid state may not be reflected in solution, and so the precise reason for the difference in preference remains to be elucidated.

Whilst both complexes were shown to bind to both duplex and G-quadruplex DNA sequences, their demonstrated preference for G-quadruplex binding coupled with their high affinities for such structures warrants their continued study as promising G4-binding therapeutic drugs. Acting as a direct continuation of the initial

studies, Part I of this chapter details the synthesis of both the palladium and platinum 3,3-biisoquinoline complexes, with particular attention paid to improvements in the routes previously employed, or alternative methodologies utilised. As an extension to previous binding studies carried out, the results of electrospray ionisation mass spectrometry (ESI-MS) model nucleobase binding studies are also discussed.

Part II of this chapter explores the biological activity of the palladium and platinum analogues *in vitro*. Several biological assays have been carried out to assess cell uptake, DNA damage, cell cycle arrest and toxicity effects as a result of complex treatment on cells.

PART I: SYNTHESIS AND CHARACTERISATION OF 3,3-BIISOQUINOLINE METAL COMPLEXES

2.2 Overview of synthetic methodology

2.2.1 Isoquinoline building blocks

The required 3-chloroisoquinoline precursor to enable synthesis of 3,3-biisoquinoline can be synthesised in high yield in a three-step procedure commencing with homophthalic acid (Figure 2.2.1-1).¹⁰ This starting reagent is both readily available and inexpensive, enabling bulk batches of precursor to be prepared.

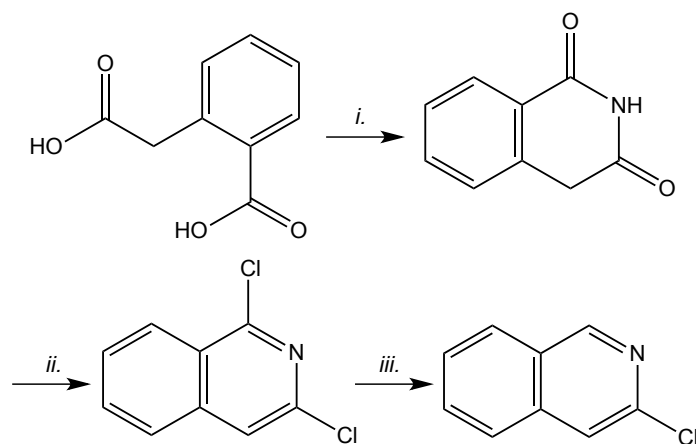


Figure 2.2.1-1 Synthesis of 3-chloroisoquinoline under the following conditions: *i.* NH_4OH , 1,2-dichlorobenzene, 200 °C; *ii.* $\text{PhP}(\text{O})\text{Cl}_2$, 160 °C; *iii.* Method 1: $\text{Sn}(0)$, HOAc/HCl , 60 °C, Method 2: $\text{HI}(\text{aq})\text{-P}_{\text{red}}/\text{HOAc}$, 125 °C.

Step *i.* The first step results in the formation of isoquinoline-1,3-dione following a two-step process. Carboxylic acids do not undergo nucleophilic substitution reactions under basic conditions unless a coupling agent such as dicyclohexylcarbodiimide (DCC) is used. In the absence of DCC, the strong base (NH_4OH) will undergo an acid-base reaction leading to the deprotonation of the carboxylic acid to form an ammonium carboxylate salt (Figure 2.2.1-2-i). Once the carboxylic acid is deprotonated, substitutions are prevented because there are almost no nucleophiles that will attack the carboxylate anion formed.¹¹ In fact, the formation of the resultant amide can only be achieved upon strong heating of the ammonium salt to force its dehydration (Figure 2.2.1-2-ii). The resulting amide can then react intramolecularly in the same manner, with the second carboxylic acid moiety.

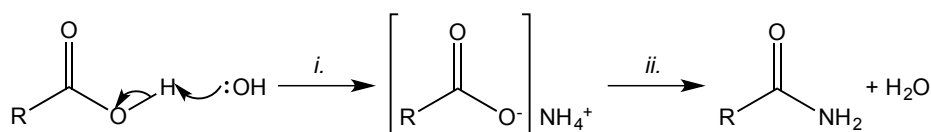


Figure 2.2.1-2 Two step formation of an amide via an ammonium carboxylate salt intermediate: *i.* acid-base reaction with NH_4OH ; *ii.* heat-induced dehydration of intermediate.

Step ii. The cyclic compound generated in step *i*. undergoes chlorodehydroxylation in the second step, using phenylphosphonic dichloride. The participation of the nitrogen lone pair electrons into the six-membered ring leads to the release of chloride ions that are now able to participate in nucleophilic addition reactions at the carbonyl site (Figure 2.2.1-3). Phenylphosphonic acid and its salt are formed as hydrolysis products of the reaction, both of which are water-soluble and thus easily isolated from the desired chlorodehydroxylation product.¹²

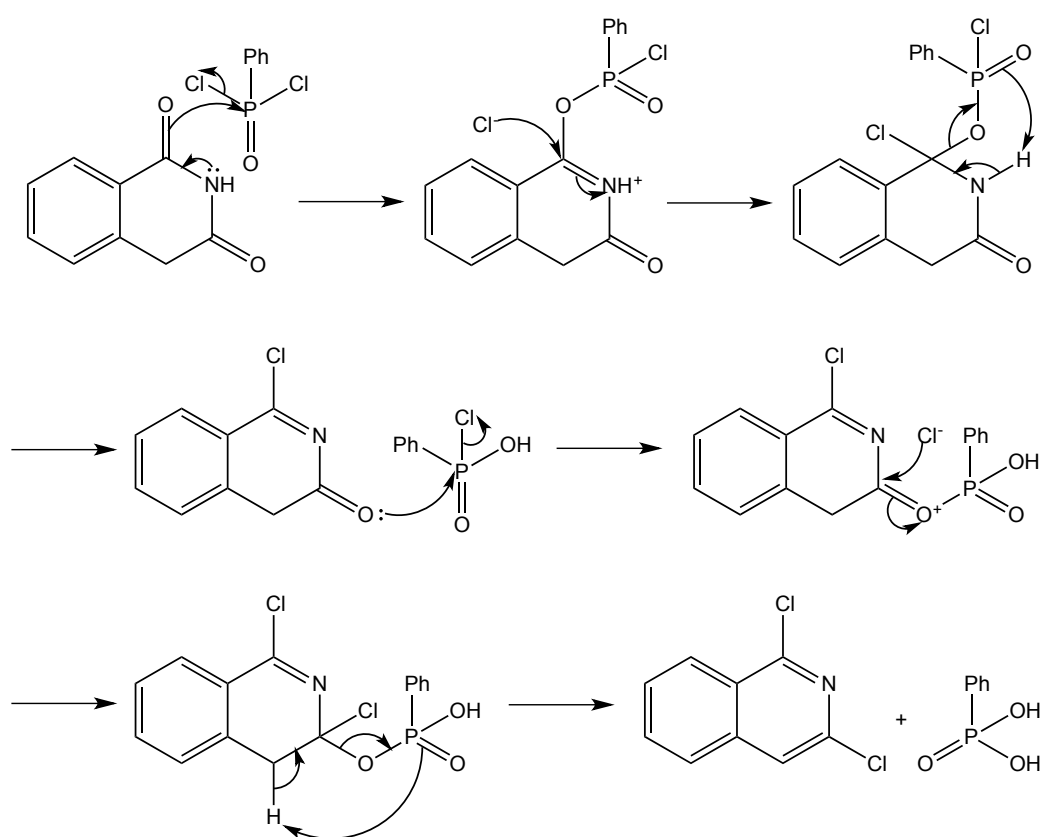


Figure 2.2.1-3 Mechanism of chlorodehydroxylation using phenylphosphonic dichloride.

Step iii. The final step requires the removal of the chloro-substituent in the 1-position, to yield 3-chloroisoquinoline. This was previously achieved within the group using tin powder with hydrochloric acid.⁹ Nucleophilic attack by tin can occur at two

sites around the isoquinoline rings following delocalisation of the charge to either C(1) or C(3) (the two positions capable of undergoing loss of a chloride) (Figure 2.2.1-4). In establishing these charges, it is evident that a positive charge held on C(3) is only achieved following disruption to the aromaticity of the benzene ring. By contrast, the charge can be held on C(1) with very little interruption to the aromaticity of the benzene ring.¹³ Consequently, whilst C(3) is a possible site for nucleophilic attack, in practice it occurs regioselectively at C(1) due to a more readily established electron deficient state.

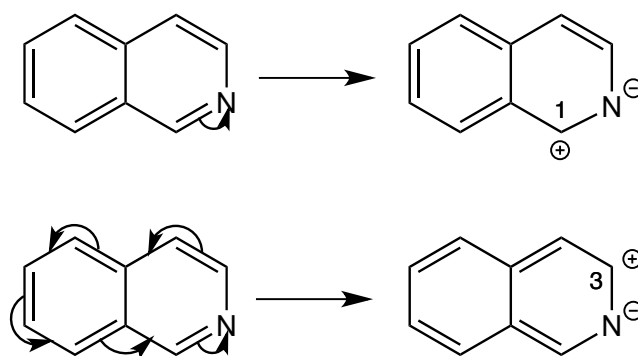


Figure 2.2.1-4 Charged structures of isoquinoline with charge held on C(1) or C(3).

Whilst this method was successful in producing 3-chloroisoquinoline, the yields obtained were consistently poor (averaging 10%), prompting the need to investigate alternative routes to the desired product. The literature reports that it is possible to remove the chloride using a combination of hydriodic acid and red phosphorus.¹⁴ The HI(aq)-P_{red} method has been used to reduce carbonyl groups, nitriles, alcohols and halides.^{15,16}

Exploiting the reversible dissociation of HI at high temperatures (Figure 2.2.1-5-a), this reduction method involves cyclic oxidation of the iodide anion to iodine followed by reduction of the liberated iodine back to the anion by red

phosphorus, which is itself converted to phosphoric acids and phosphorus.^{17,18} Concomittant regeneration of HI occurs, with oxidation of red phosphorus by iodine acting as the driving force. The proposed reaction mechanism (Figure 2.2.1-5-b) displays the regenerative role of the red phosphorous, whereby the presence of this reagent in the couple allows recycling of the HI and enhances its reducing efficiency.¹⁹ Upon implementing this route, which proved to be more successful for this transformation, yields of 30% (following purification) were routinely secured.

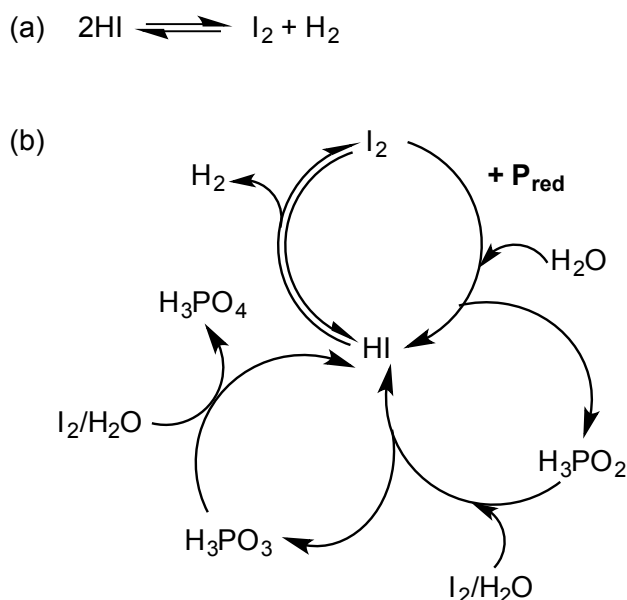


Figure 2.2.1-5 (a) Reversible dissociation of HI at high temperatures; (b) HI(aq)- P_{red} mechanism.

2.2.2 Metal-catalysed homocoupling

The formation of 3,3-biisoquinoline is achieved by the metal-catalysed homocoupling of 3-chloroisoquinoline. A variety of methods exist, including the use of either copper^{20,21} or palladium²² in Ulmann-type coupling reactions. The use of copper is limited in its application due to the harsh reaction conditions required, limited range of substrates upon which it can act, and typically poor yields. By contrast, palladium can

be used in Ullmann-type reactions under relatively mild conditions, and has been shown to successfully couple electron-rich and electron-deficient aromatic bromides and iodides.²² Chlorides, however, couple far less successfully and usually in low yield. The palladium complexes required can also prove to be very expensive, due to the use of equimolar quantities in some cases, or the inability to reuse the palladium despite its use in catalytic quantities.^{23,24} Both copper and palladium catalysed Ullmann-type coupling routes were thus discounted.

An attractive alternative was found in the use of nickel in a Kolbe-type coupling. These reactions require mild conditions to proceed and occur relatively undisturbed in the presence of other functionalities such as aldehydes and ketones. The specific selection of nickel catalyst, along with solvents and additional reagents determines the yield obtained.^{25,26} Furthermore, nickel catalysts are both readily available and relatively cheap, compared to their palladium analogues.²⁷

The reactive nickel(0) reagent, must first be prepared from a mixture of nickel(II) hexahydrate, zinc powder and triphenylphosphine in DMF.²⁷ Due to the air sensitivity of nickel(0), this reaction occurs *in situ* under an argon atmosphere. Upon heating, the activated zinc reduces the nickel(II) to nickel(0), accompanied by a distinctive colour change as the solution changes from teal green to deep red. This confirms the formation of the active nickel(0) reagent. The aryl halide can then be added to the solution (maintaining the inert atmosphere). As the reaction proceeds, the formation of the homocoupled biaryl product results in the oxidation of the nickel(0) back to a nickel(II) species, causing the colour of the solution to turn green again (albeit a different shade). The desired bidentate ligand can be easily removed from the nickel scaffold by the addition of a weak ammonia solution. The proposed

reaction scheme is shown in (Figure 2.2.2-1).²⁸ Oxidative addition of the aryl halide to nickel(0) is followed by its metathesis to a diarylnickel(II) species and corresponding nickel halide. The desired biaryl is generated through reductive elimination of the nickel(II) species,²⁸ regenerating the nickel(0) reagent.

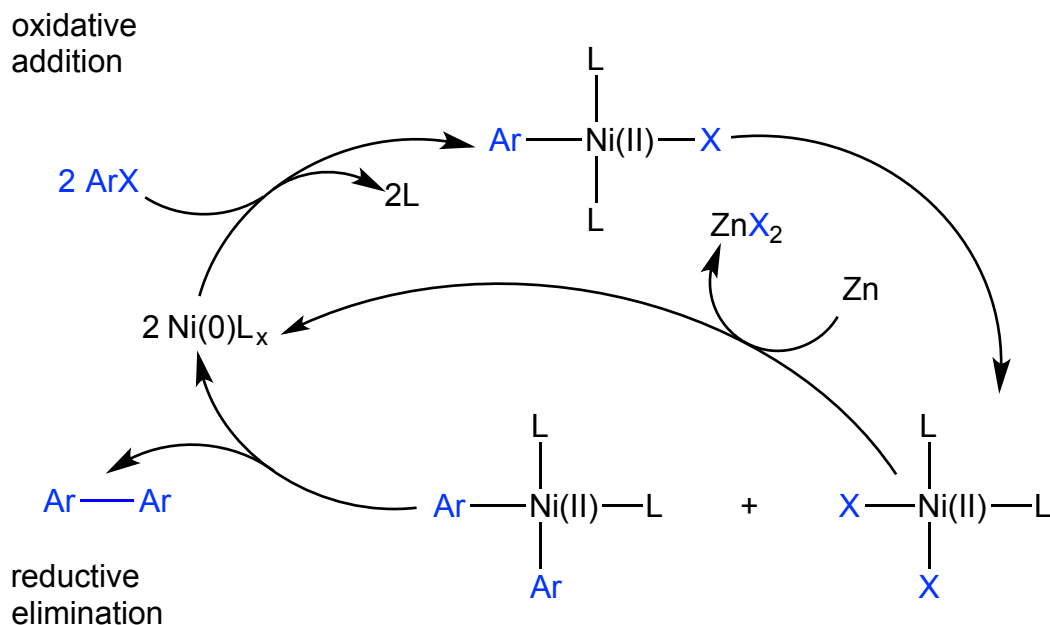


Figure 2.2.2-1 Proposed scheme for nickel-mediated biaryl formation via oxidative addition and reductive elimination. $\text{L} = \text{PPh}_3$

This synthetic procedure was selected to prepare the desired homocoupled product, 3,3-biisoquinoline from 3-chloroisoquinoline (Figure 2.2.2-2). Synthesis of the desired ligand (*i*-biq) was followed by the preparation of pre-existing and novel metal complexes consisting of two ligands bound in a bidentate fashion to form square planar compounds.

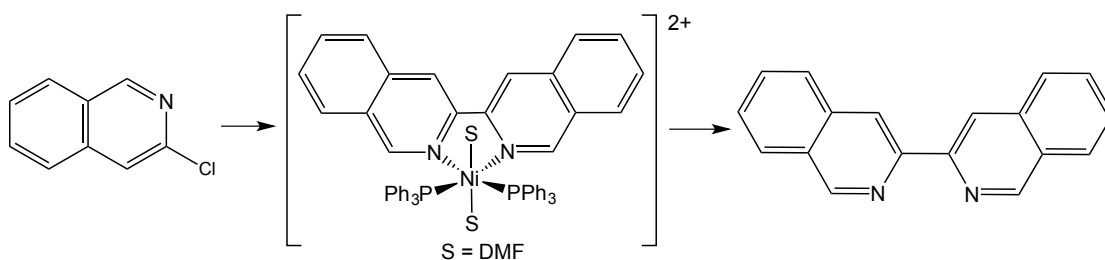


Figure 2.2.2-2 Nickel-mediated 3,3-biisoquinoline formation.

A more detailed consideration of these general routes, including the specifics for preparation of the target compounds will now be discussed.

2.3 3-chloroisoquinoline precursor synthesis and characterisation

2.3.1 Isoquinoline-1,3-dione (1)

In accordance with literature procedure,²⁹ the first step towards the synthesis of 3-chloroisoquinoline involved the conversion of homophthalic acid into isoquinoline-1,3-dione (Figure 2.3.1-1).

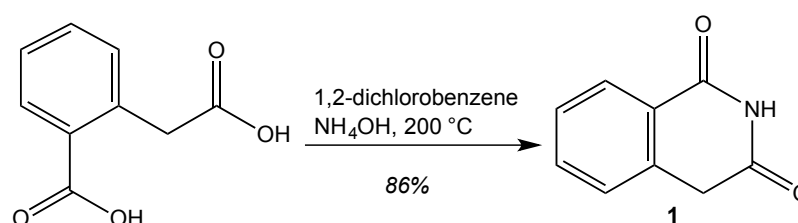


Figure 2.3.1-1 Synthesis of isoquinoline-1,3-dione.

Homophthalic acid was suspended in 1,2-dichlorobenzene and heated to 200 °C to aid dissolution. The dropwise addition of excess ammonium hydroxide solution allowed the ammonium carboxylate salt to be formed *in situ*, followed by a further

period of intense heating to force the dehydration of the amine to the amide. During this time, the constant removal of the dehydration by-product (water) by evaporation drives the reaction to completion. The reaction proceeded well, with the product obtained in very good yield, and requiring no further purification before continuing. Electrospray ionisation mass spectrometry and nuclear magnetic resonance data were in accordance with those reported in the literature.

2.3.2 1,3-dichloroisoquinoline (2)

The second step of precursor synthesis involved the chlorodehydroxylation of isoquinoline-1,3-dione using phenylphosphonic dichloride (Figure 2.3.2-1).

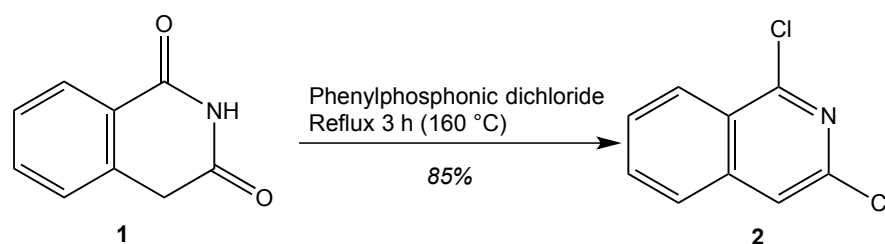


Figure 2.3.2-1 Synthesis of 1,3-dichloroisoquinoline.

In accordance with literature procedure,¹⁰ the two were heated under reflux for 3 hours. Upon cooling to room temperature, the solution solidifies and is subsequently treated with THF and water. This enables the unwanted water-soluble hydrolysis by-products to be easily separated from the desired product, which is extracted into ethyl acetate. Once again, the desired product is isolated in good yield and requires no further purification. Electrospray ionisation mass spectrometry and nuclear magnetic resonance data were in accordance with those reported in the literature. Comparison of the ¹H-NMR spectra obtained for compounds (1) and (2) shows the

loss of two peaks corresponding to the aliphatic CH₂ protons located on C(4) and the NH proton. All remaining peaks now reside in the aromatic region between 7.82 – 8.30 ppm, proving the formation of a fully aromatic system (Figure 2.3.2-2).

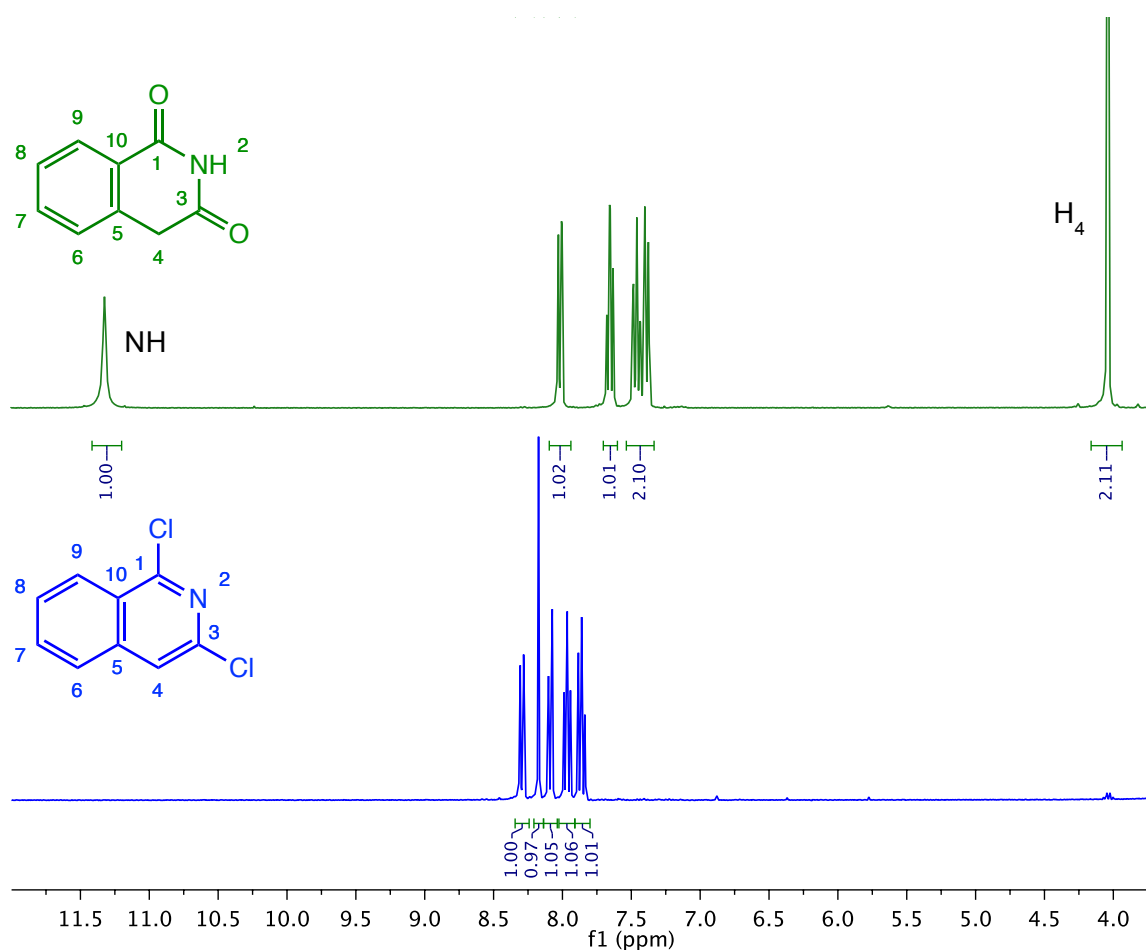


Figure 2.3.2-2 ¹H-NMR spectra overlay of isoquinoline-1,3-dione (1) and 1,3-dichloroisoquinoline (2) (300 MHz, d₆-DMSO, 298 °K).

2.3.3 3-chloroisoquinoline (3)

Selective removal of the 1-chloro substituent was initially achieved using tin powder under acidic conditions (Figure 2.3.3-1, Method a). The tin(II) chloride generated during the nucleophilic attack was isolated by the addition of ammonium hydroxide, resulting in the precipitation of SnO or SnO.H₂O.³⁰ The reaction progress was

monitored by TLC to ensure completion, before isolation and purification of the crude waxy solid by column chromatography. Unfortunately, the yield of product was repeatedly poor (~10%).

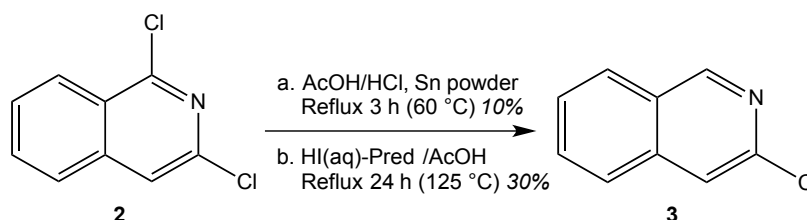


Figure 2.3.3-1 Synthesis of 3-chloroisoquinoline by two alternative methods.

2.3.4 An alternative route to 3-chloroisoquinoline (**3**)

As detailed in 2.2.1, a new synthetic procedure was chosen, avoiding the use of tin powder altogether. This new route utilises a HI(aq)-P_{red} mixture to selectively remove the chloride substituent (Figure 2.3.3-1, Method b). Compound (**2**) was added to a slurry of red phosphorus in hydriodic acid and acetic acid. An excess of P_{red} was used, to drive the regeneration of the HI, allowing the reduction to proceed rapidly. The reaction mixture was heated under reflux for 24 hours before isolation and purification *via* column chromatography produced compound (**3**) in moderate yield (30%). Despite the increased reaction time for this route (24 h vs. 3 h), the reaction proceeded well, resulting in a three-fold increase in yield following a straightforward purification. Consequently, this is the preferred route towards this product on account of its improved yield, which ultimately saves both time and money. Electrospray ionisation mass spectrometry and nuclear magnetic resonance data were in accordance with those reported in the literature. The ¹H-NMR spectrum shows a new peak at 9.23 ppm due to a new proton (H₍₁₎) environment formed following the selective removal of the chloride group on C(1) (Figure 2.3.4-1). This peak appears

downfield compared to the remaining aromatic peaks. This is due to the close proximity of this new proton to the strongly electron-withdrawing nitrogen that sits adjacent in the isoquinoline ring.

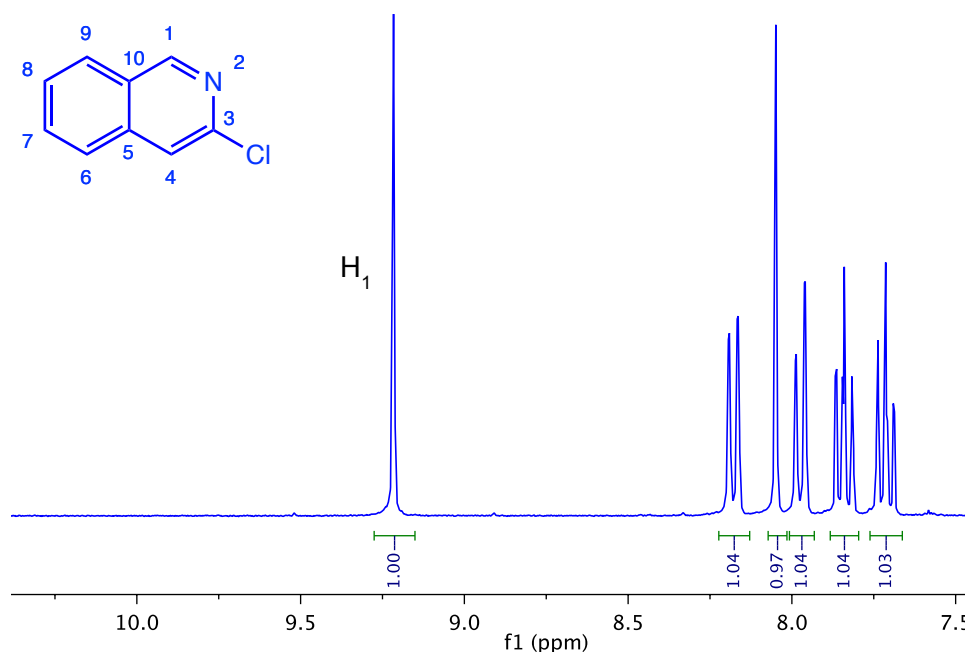


Figure 2.3.4-1 ^1H -NMR spectrum of 3-chloroisoquinoline (**3**) (300 MHz, MeOD, 298 °K).

2.4 3,3-biisoquinoline synthesis and characterisation

2.4.1 Nickel-catalysed homocoupling of aryl chlorides

As described previously in 2.2.2, an activated nickel(0) species created *in situ* is able to mediate the formation of the desired biisoquinoline ligand; acting as a scaffold for homocoupling to occur.

2.4.2 3,3-biisoquinoline (4)

Nickel catalysed homocoupling of the prepared 3-chloroisoquinoline precursor was carried out to furnish the desired bidentate 3,3-biisoquinoline ligand ready for complex formation (Figure 2.4.2-1).

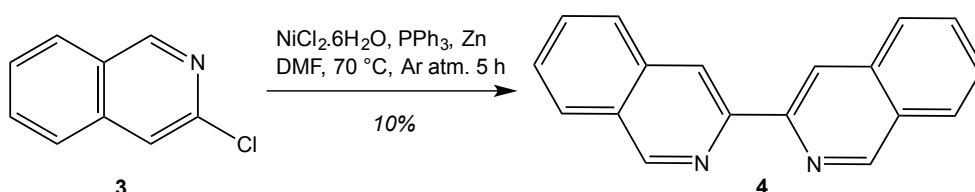


Figure 2.4.2-1 Synthesis of 3,3-biisoquinoline (*i-biq*).

Immediately prior to the reaction, zinc powder was washed with dilute hydrochloric acid, water, acetone and diethyl ether before drying under vacuum.³¹ Washing was carried out to activate the zinc, which acts as the reducing agent for the nickel catalyst. Once dry, it was added to nickel(II)chloride hexahydrate and triphenylphosphine, and the vessel thoroughly degassed before the addition of anhydrous DMF. Upon heating, the activated zinc is able to successfully reduce nickel(II) to nickel(0) *in situ*, as evidenced by the distinct colour change in solution (Figure 2.4.2-2). Only once this colour change is observed can compound (3) be added to the vessel (as a solution in anhydrous DMF) to begin the coupling process. The reaction mixture was heated at 70°C under an argon atmosphere for 4 hours, with the completion of the reaction marked by a return in colour of the mixture to a green complexion. This signals the oxidation of the nickel(0) species back to a nickel(II) species; a result of the oxidative addition of the bidentate ligand to the nickel.

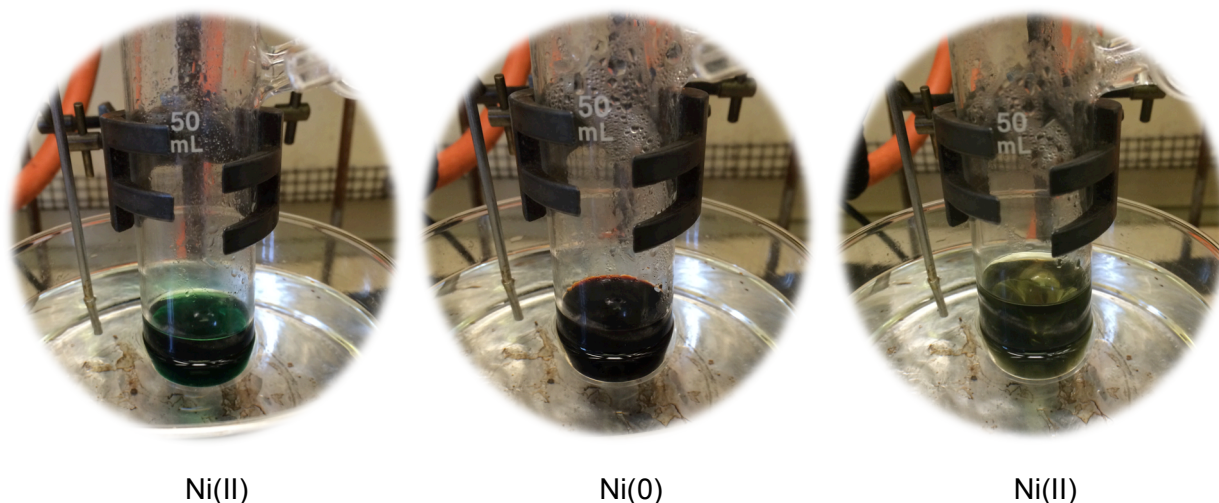


Figure 2.4.2-2 Observable colour changes marking reaction progression; reduction of Ni(II) to Ni(0), followed by oxidation of Ni(0) back to Ni(II).

The newly formed bidentate ligand was removed from the nickel by pouring the cooled solution onto a 7% solution of ammonium hydroxide. This causes dissociation of the ligand, which is replaced by NH_3 ligands. A purple aqueous solution is formed as a result of the formation of this new nickel complex, $[\text{Ni}(\text{NH}_3)_6]^{2+}$. This could be seen in the water layer following extraction of compound **(4)** into 2:1 DCM:Et₂O.

The crude product was heavily contaminated with triphenylphosphine oxide (TPPO, a by-product resulting from the oxidation of triphenylphosphine), which is notoriously difficult to remove. Due to the reported sparing solubility of TPPO in diethyl ether,³² the crude product was dissolved into ether and filtered to remove the insoluble TPPO, however this method proved to be rather ineffective. As an alternative, column chromatography utilising a two-solvent system was carried out cautiously and under gravity alone to remove the TPPO and other impurities (eluting with DCM) before isolating compound **(4)** (eluting with Et₂O). Despite flash column chromatography typically providing better separation of components, gravity alone

proved far more effective at separation in this particular instance. The addition of pumping caused many of the components to merge, making it very difficult to isolate the desired product from the many impurities. Pure product was obtained as a very pale cream solid, in 10% yield.

Electrospray ionisation mass spectrometry analysis was in accordance with that previously reported, with a molecular ion peak at m/z 257.2 $[M + H]^+$ confirming successful synthesis of the product. The ^1H -NMR spectrum of the coupled biaryl product shows a large downfield shift of the C(4) proton peak when compared to its position in the uncoupled ligand (Figure 2.4.2-3). This is due to an increased area of aromaticity resulting from the coupling.

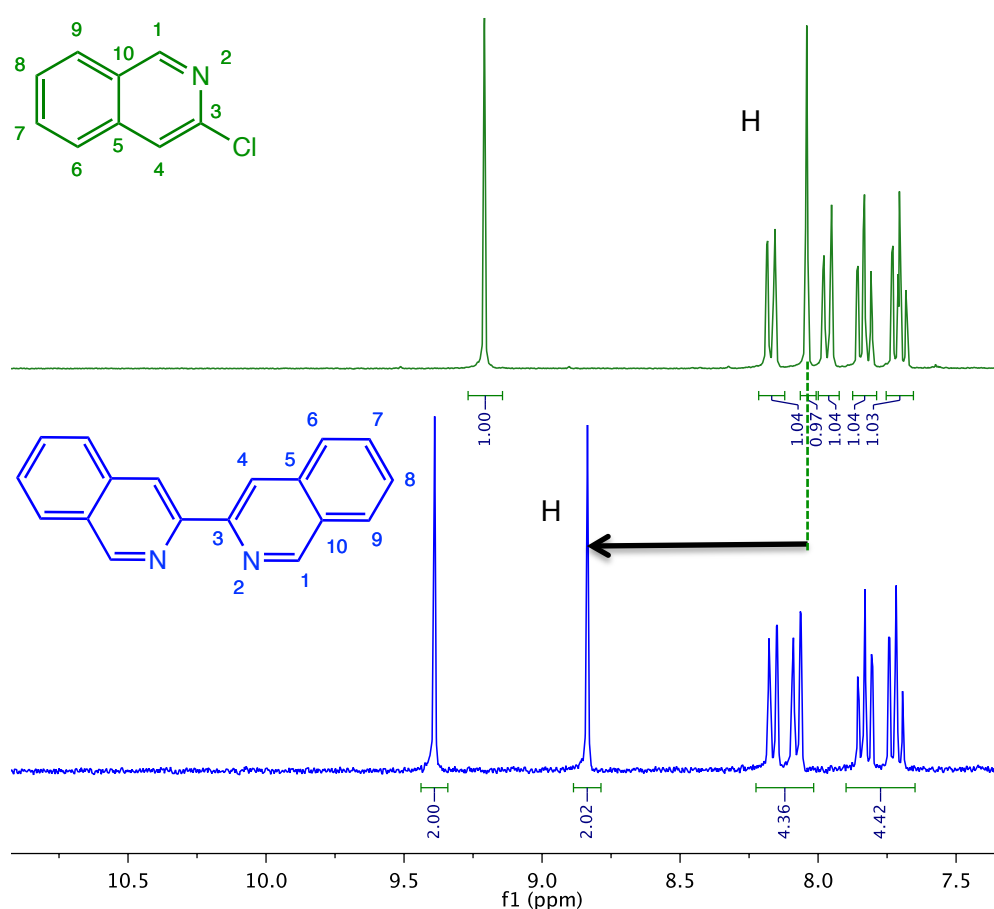


Figure 2.4.2-3 ^1H -NMR spectra overlay of 3-chloroisoquinoline (**3**) and 3,3-biisoquinoline (**4**) (300 MHz, MeOD, 298 °K).

The literature reports alternative methods for the attempted synthesis of this biaryl compound, using bis(triphenylphosphine)palladium chloride, $[\text{Pd}(\text{PPh}_3)_2\text{Cl}_2]$ or bis(triphenylphosphine)nickel bromide, $[\text{Ni}(\text{PPh}_3)_2\text{Br}_2]$. Both routes were unsuccessful, yielding no product.^{28,33} The encountered difficulties in synthesising the homocoupled product emanate from the relative unreactivity of the heteroaryl chlorides when compared to their bromide or iodide counterparts. The bond strength of the C-X bond decreases significantly as the size of the halogen atom increases from F to I (Table 2.4.2-1). The Ar-Cl bond is stronger than the Ar-Br bond. Consequently, the Cl acts as a poorer leaving group, and the ligand is reluctant to engage in oxidative addition to the nickel metal centre.³⁴

Bond	Dissociation energy (kJ mol ⁻¹)
Ph-F	533
Ph-Cl	407
Ph-Br	346
Ph-I	280

Table 2.4.2-1 Bond dissociation energies of aryl halides

Despite this reduced reactivity, aryl chlorides are frequently used since they are the most attainable aryl halides due to low cost and widespread availability.

2.4.3 An alternative route to 3,3-biisoquinoline: aryl-bromide vs. aryl-chloride

Given that the yields obtained for compound (**4**) were reasonably poor, and that the aryl chlorides are known to couple less successfully than other aryl halides, an

alternative route exploring the use of an aryl bromide to obtain 3,3-biisoquinoline was investigated. A bromine analogue can be successfully synthesised with a single alteration to the 3-step procedure used to synthesise 3-chloroisoquinoline (Figure 2.4.3-1).

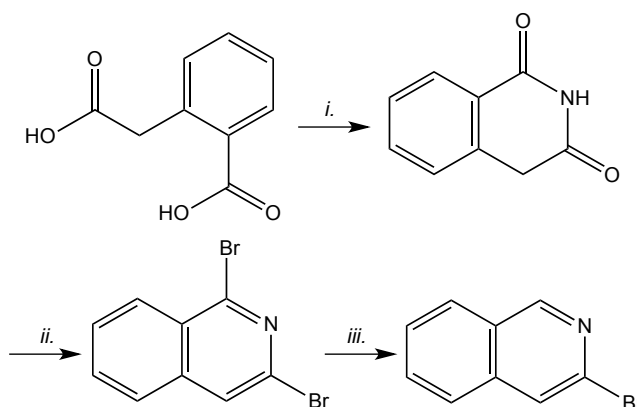


Figure 2.4.3-1 Synthesis of 3-bromoisoquinoline under the following conditions: *i.* NH_4OH , 1,2-dichlorobenzene, $200\text{ }^\circ\text{C}$; *ii.* POBr_3 , $120\text{ }^\circ\text{C}$, 35 m ; *iii.* $\text{HI(aq)}\text{-P}_{\text{red}}/\text{HOAc}$, $125\text{ }^\circ\text{C}$.

During the second step, phosphorus oxybromide is used in place of phenylphosphonic dichloride to facilitate a bromodehydroxylation rather than chlorodehydroxylation. The first and final steps remain identical to those utilised previously. Following the success of the the $\text{HI(aq)}/\text{P}_{\text{red}}$ route, this method was again used to isolate the bromine analogue.

2.4.4 3-bromoisoquinoline precursor synthesis and characterisation

2.4.5 1,3-dibromoisoquinoline (5)

Following its successful synthesis (see 2.3.1), bromodehydroxylation of compound (1) was achieved using phosphorus oxybromide (Figure 2.4.5-1).

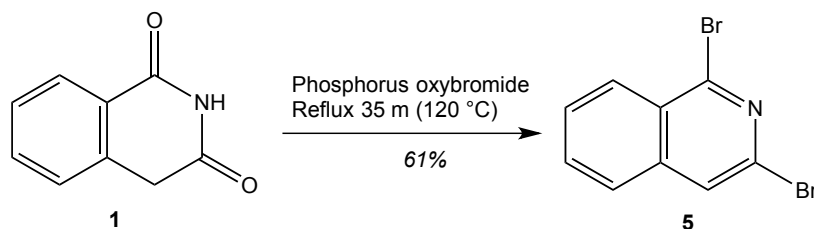


Figure 2.4.5-1 Synthesis of 1,3-dibromoisoquinoline.

POBr₃ reacts violently with water to release toxic fumes so must be handled with extreme caution.³⁵ Consequently, in contrast to chlorodehydroxylation, this procedure was carried out under an inert atmosphere, using anhydrous solvents. Addition of compound (**1**) to the reaction vessel occurred under a strong flow of argon and in small portions. The reaction time is considerably shorter in this instance (35 minutes at reflux *cf.* 3 h when preparing the chlorine analogue) due to the increased reactivity of bromine reagents. The desired product was collected by vacuum filtration and washed thoroughly with propan-2-ol to yield a powdery cream solid in moderate yield (61%). No further purification was required. Electrospray ionisation mass spectrometry and nuclear magnetic resonance data were in accordance with those reported in the literature. The location of all peaks within the aromatic region between 7.70 - 8.28 ppm is once again evidence for the formation of a fully aromatic system, along with the loss of the NH proton peak at 11.18 ppm.

2.4.6 3-bromoisoquinoline (**6**)

1,3-dibromoisoquinoline (**5**) was reduced using the HI(aq)-P_{red} method, following its successful use with the Cl-analogue. The procedure was not amended, however an alternative solvent system was employed during column chromatographic purification

to efficiently elute the desired product (Br: DCM:MeOH (9:1) Cl: EtOAc: Hexane (9:1), Figure 2.4.6-1).

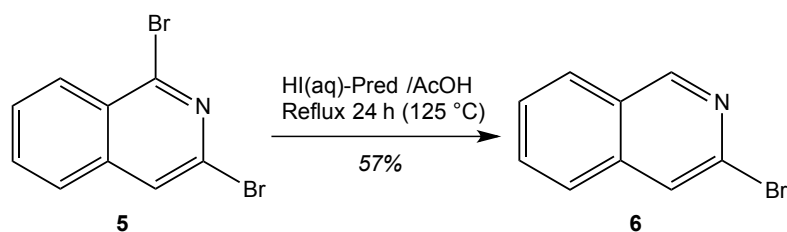


Figure 2.4.6-1 Synthesis of 3-bromoisoquinoline.

Product was obtained as a pale yellow solid in higher yield than the Cl-analogue (57% *cf.* 30%). Electrospray ionisation mass spectrometry and nuclear magnetic resonance data were in accordance with those reported in the literature. The appearance of a new peak at 9.04 ppm confirms that a new proton environment is present as a result of the selective removal of bromine previously substituted at C(1).

Preparation of the aryl bromide analogue is a far more expensive route than preparation of the aryl chloride precursor. This is due to the increased cost of the phosphorus oxybromide, compared with the relatively inexpensive phenylphosphonic dichloride required for the chloride precursor. Despite the increased expense, and the poorer yield experienced in the initial preparation of compound (**5**), the mono-substituted product (**6**) can be prepared in higher overall yield. This is demonstrated in Figure 2.4.6-2, detailing how 82.5 mmol of homophthalic acid will ultimately yield approximately 25.0 mmol of aryl bromide compared to only 18.0 mmol aryl chloride. The cost of preparing the two precursor ligands on this scale is approximately fifteen times higher for the aryl bromide route, which was typically carried out on a much smaller scale (< 5g) due to cost and safety precautions surrounding the use of

POBr₃. Synthesis of 3-bromoisoquinoline is also achieved more quickly than 3-chloroisoquinoline due to a shorter period of heating at reflux during the second step, and yields a far 'cleaner' crude product, which requires less purification by column chromatography.

Ultimately, the trade-off between the increased expense of the bromide route and the increased product yield is only favourable if the aryl bromide proves to be a more reactive species, capable of undergoing more efficient homocoupling to yield the desired ligand 3,3-biisoquinoline in improved yield.

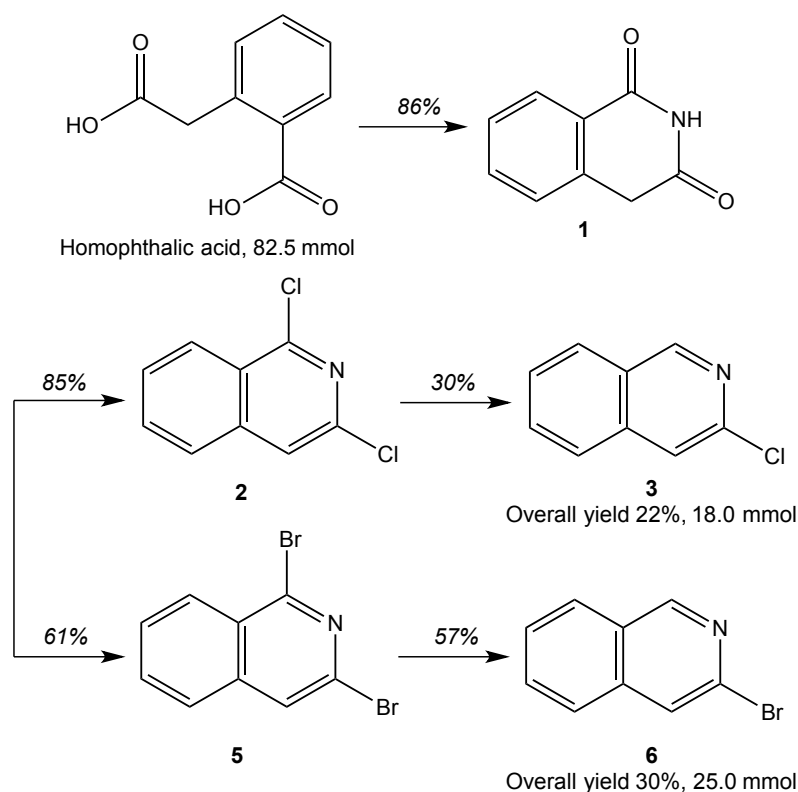


Figure 2.4.6-2 Comparison of the yield of halide-isoquinoline obtained through the chloride or bromide synthetic route.

2.4.7 Nickel-catalysed Colon-coupling of aryl bromides

Nickel-catalysed homocoupling of the newly prepared aryl bromide precursor was carried out under the same conditions used previously (Figure 2.4.7-1).

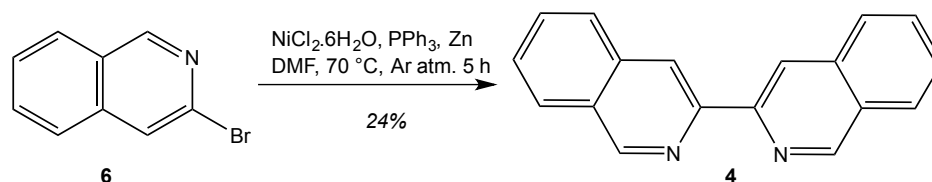


Figure 2.4.7-1 Synthesis of 3,3'-biisoquinoline from 3-bromoisoquinoline.

The crude product was purified by column chromatography eluting with DCM initially to remove some impurities, followed by EtOAc to elute the desired biaryl ligand as pale cream solid. A 24% yield was recorded for this route, which is an improvement upon the 10% yield obtained as a result of aryl chloride coupling. Although perhaps not as significant an improvement in yield as one might have hoped for, the aryl bromide route still results in a 140% increase in the yield of desired product, and crucially, provides a reasonable amount of material to work with in subsequent syntheses. Consequently, due to improved yields of both the ligand precursor (**3**) and ligand (**4**), the aryl bromide route was selected as the preferred route.

2.5 Synthesis and characterisation of palladium, platinum and gold 3,3'-biisoquinoline complexes

2.5.1 $[\text{Pd}(i\text{-biq})_2](\text{BF}_4)_2$ (**7**)

Two bidentate 3,3'-biisoquinoline ligands were bound to a palladium metal centre following a ligand substitution reaction. Tetrakis(acetonitrile)palladium tetrafluoroborate was chosen as the starting palladium complex, whereby addition of

3,3-biisoquinoline in a 2:1 ratio results in the formation of the desired complex following overnight stirring in acetonitrile under an inert atmosphere (Figure 2.5.1-1).

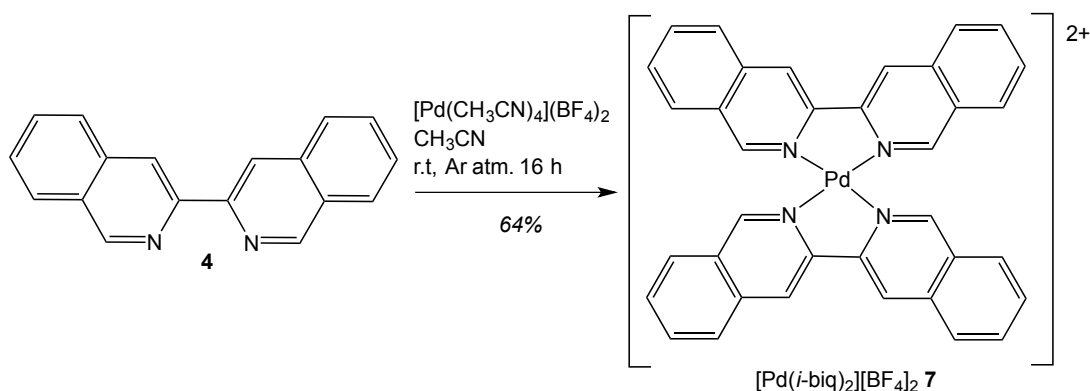


Figure 2.5.1-1 Synthesis of $[\text{Pd}(\text{i-biq})_2](\text{BF}_4)_2$.

The product was carefully washed in chloroform, methanol and diethyl ether to remove any unreacted starting materials before drying under vacuum to yield pure $[\text{Pd}(\text{i-biq})_2](\text{BF}_4)_2$ as pale yellow solid in 64% yield. The complex is soluble in both CH_3CN and DMSO. The ESI-MS spectrum shows peaks at m/z 309, 618 and 653 corresponding to $[\text{Pd}(\text{C}_{18}\text{H}_{12}\text{N}_2)_2]^{2+}$, $[\text{Pd}(\text{C}_{18}\text{H}_{12}\text{N}_2)_2]^+$ and $[\text{Pd}(\text{C}_{18}\text{H}_{12}\text{N}_2)_2\text{Cl}]^+$ respectively. The ^1H -NMR spectrum shows the same splitting pattern and number of proton peaks as those observed for the unbound ligand. Comparison of the two spectra shows a downfield shift of all signals due to the electron withdrawing effect of the palladium metal centre upon complex formation (Figure 2.5.1-2).

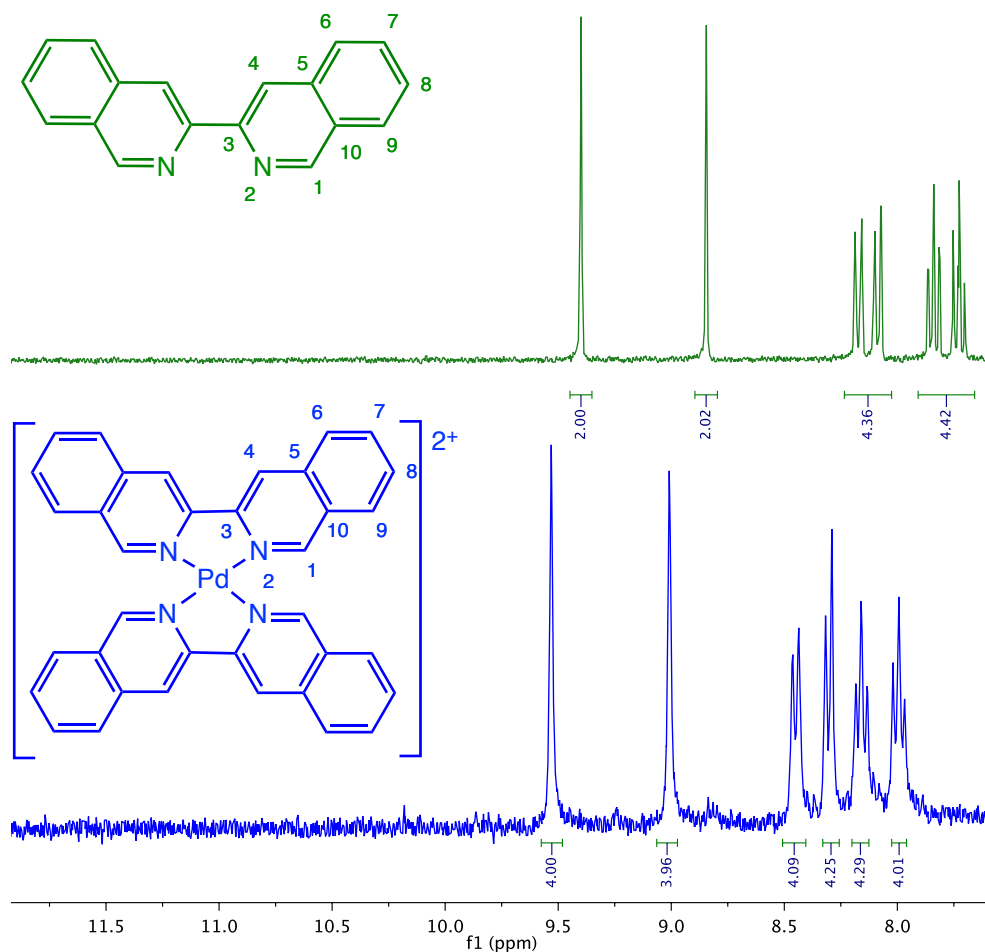


Figure 2.5.1-2 ¹H-NMR spectra overlay of 3,3-biisoquinoline (**4**) and [Pd(ibiq)₂](BF₄)₂ (**7**) (300 MHz, CD₃CN, 298 °K).

2.5.2 [Pt(*i*-biq)₂](PF₆)₂ (**8**)

In a similar manner to the approach used to form the palladium analogue, 3,3-biisoquinoline was reacted in a 2:1 ratio with a platinum complex capable of undergoing ligand substitution to form the desired product. Potassium tetrachloroplatinate was dissolved in water, before the addition of a suspension of 3,3-biisoquinoline in acetonitrile. The use of a 1:1 H₂O:CH₃CN solvent mixture aids dissolution of the biisoquinoline ligand.⁸ The mixture was heated under reflux overnight (Figure 2.5.2-1).

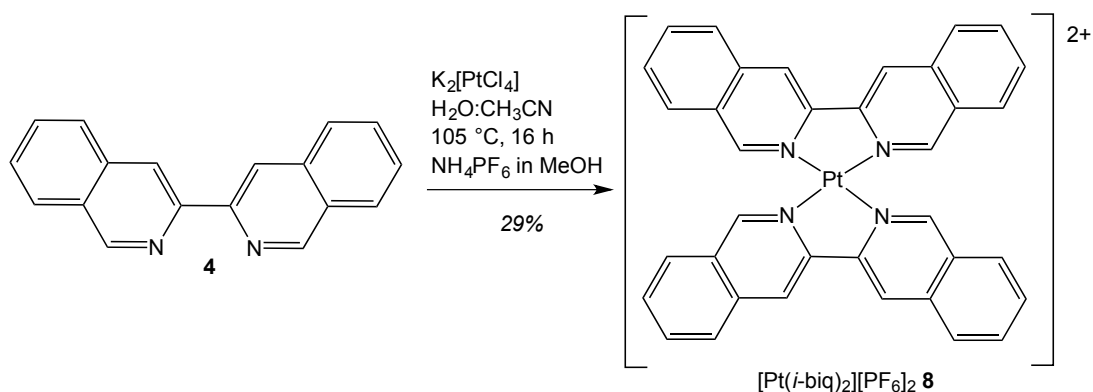


Figure 2.5.2-1 Synthesis of $[\text{Pt}(\text{i-biq})_2](\text{PF}_6)_2$.

The resulting solution was filtered to remove any unreacted ligand or $[\text{Pt}(\text{i-biq})\text{Cl}_2]$ that may have formed. A methanolic solution of ammonium hexafluorophosphate was added to cause the precipitation of the desired complex from solution. The product was carefully washed with chloroform, methanol and diethyl ether before drying under vacuum to yield pure $[\text{Pt}(\text{i-biq})_2](\text{PF}_6)_2$ as a very pale yellow solid in 29% yield. This is a poorer yield than that obtained when preparing the palladium analogue. This is most likely due to the rapid formation of some mono-substituted product $[\text{Pt}(\text{i-biq})\text{Cl}_2]$ (Figure 2.5.2-2), which has previously been reported to exhibit poor solubility in dimethyl sulphoxide, and is insoluble in all other common solvents.⁸ Consequently, the complex precipitates out of solution upon formation and is unable to react further to form the desired disubstituted complex.

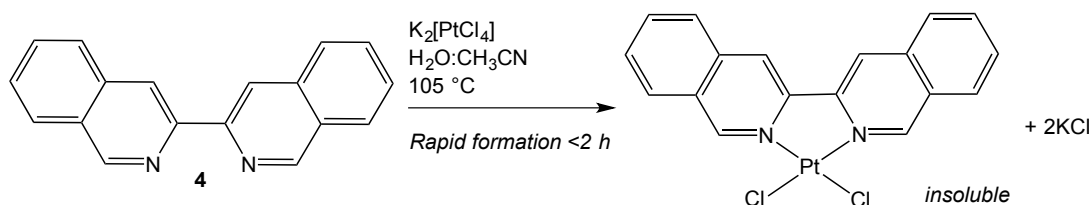


Figure 2.5.2-2 Rapid formation of mono-substituted $[\text{Pt}(\text{i-biq})\text{Cl}_2]$ during $[\text{Pt}(\text{i-biq})_2](\text{PF}_6)_2$ synthesis.

Similarly to palladium, the platinum complex is soluble in both acetonitrile and dimethyl sulphoxide. The ESI-MS spectrum showed peaks at m/z 353 and 743 corresponding to $[\text{Pt}(\text{C}_{18}\text{H}_{12}\text{N}_2)_2]^{2+}$, and $[\text{Pt}(\text{C}_{18}\text{H}_{12}\text{N}_2)_2\text{Cl} + \text{H}]^+$ respectively. The ^1H -NMR spectrum shows only the six proton signals attributed to 3,3-biisoquinoline, but with an observable downfield shift (compared to unbound ligand) arising from the removal of electron density from the aromatic system (Figure 2.5.2-3). This is evidence of complex formation, whereby the proximity of the platinum metal centre results in electron density withdrawal from the ring. Furthermore, ^{195}Pt - ^1H coupling satellites are clearly visible, confirming metal coordination of the ligand.

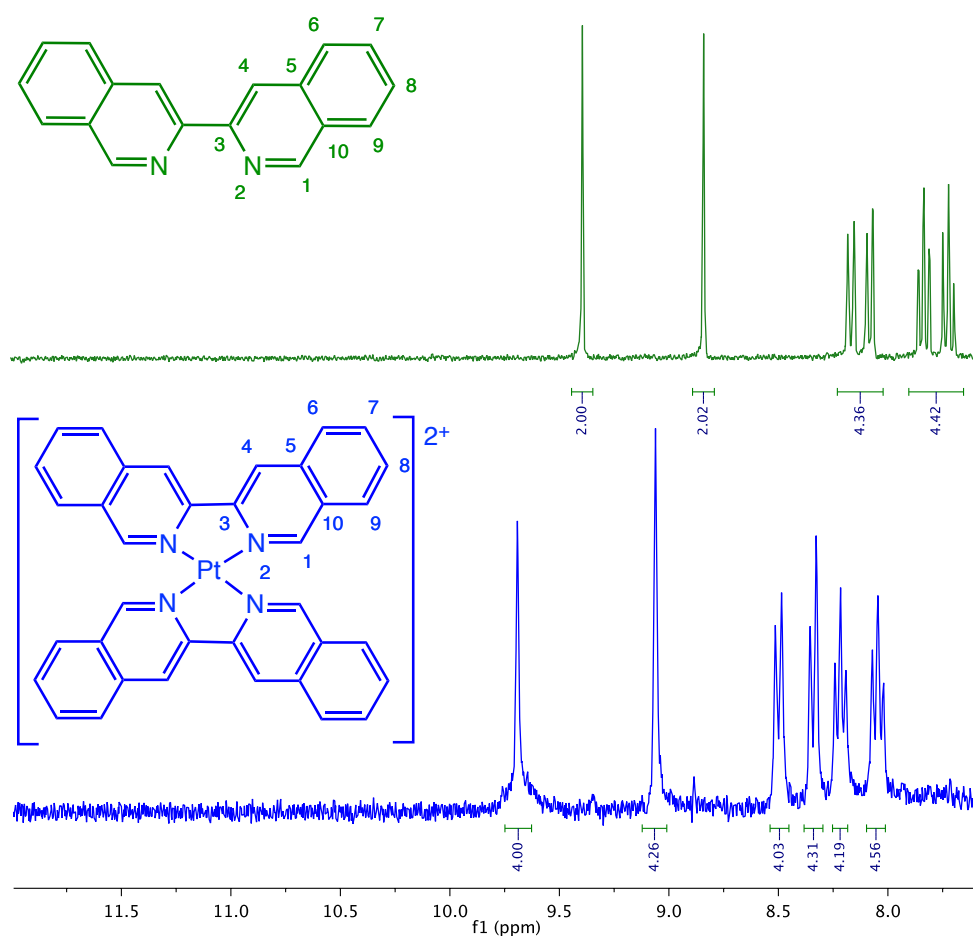


Figure 2.5.2-3 ^1H -NMR spectra overlay of 3,3-biisoquinoline (**4**) and $[\text{Pt}(\text{ibiq})_2](\text{PF}_6)_2$ (**8**) (300 MHz, CD_3CN , 298 °K).

2.5.3 Gold(III) complexes: an emerging new class of anticancer drugs

Gold(III) complexes were first considered as a possible alternative to platinum complexes due to the observation that they possess the same electronic configuration (d^8) as platinum(II) complexes, and thus exhibit the same preference towards square-planar complex formation. Following the discovery of the antiproliferative effects of cisplatin, there arose great interest in gold(III) complexes as a new family of anticancer drugs, with much attention devoted to the potential use of gold(III) as an alternative to platinum(II) in drugs.^{36,37} Unfortunately, the relatively poor chemical stability of gold(III) complexes in solution hindered any progress in this area for quite some time. Indeed, only a handful of reports describing the cytotoxic properties and antitumour effects of such complexes^{38–40} existed in the literature up until the mid-90's. Despite the small volume of research reported, gold(III) complexes had been reported to produce toxic effects.³⁶

From 2000 onwards, gold(III) compounds showing stability under physiologically relevant conditions were reported,^{41,42} with the stability attributed to an appropriate choice of ligands, in most cases bearing N atoms (Figure 2.5.3-1). These compounds have also been shown to manifest relevant antiproliferative properties against selected human tumour cell lines, prompting a renewed interest in the field.

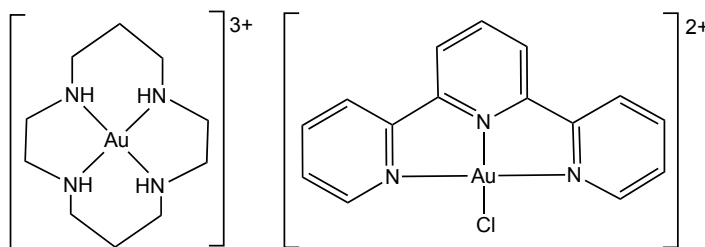


Figure 2.5.3-1 Two representative gold(III) complexes shown to be stable under physiological conditions and to manifest antiproliferative properties against human ovarian cells A2780, as reported by Messori et al.⁴³

Owing to their reported biological activity *in vitro*, gold(III) complexes remain a promising new class of anticancer agents. The ability to prepare a gold(III) analogue of the *i*-biq complexes was therefore a natural progression, as well as an attractive target. Bearing the required nitrogen atoms as donor groups, the *i*-biq ligand should promote the formation of a stable gold(III) complex, exhibiting the crucial square-planar geometry required for G-quadruplex binding.

2.5.4 [Au(*i*-biq)₂](3Cl) (9)

Synthesis of [Au(*i*-biq)₂](3Cl) was attempted several times, with varying degrees of success. The method employed to attach two biisoquinoline ligands around a single gold metal centre was similar to that used in preparing the palladium and platinum analogues. Sodium tetrachloroaurate(III) dihydrate and 3,3'-biisoquinoline were heated under reflux in methanol overnight (Figure 2.5.4-1). The resulting solution was hot filtered and concentrated *in vacuo* to afford a dark yellow solid.

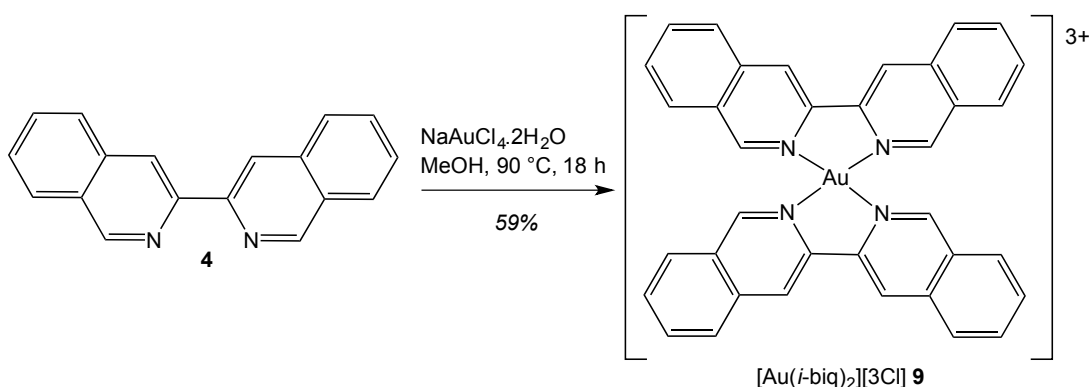


Figure 2.5.4-1 Synthesis of [Au(*i*-biq)₂](3Cl).

On the first attempt, the ¹H NMR spectrum of crude product showed a single product only when initially recorded in DCM. This proved to be the unbound ligand (by

comparison with a ligand spectrum recorded in DCM). A further spectrum of the crude product recorded in MeOD clearly showed two sets of signals, one of which was easily attributed to the free ligand, the other of which showed the same pattern of signals but with a downfield shift. It became evident that the free ligand could be removed from the crude product by washing and filtration, due to its solubility in DCM.

Following careful washing, the NMR spectrum (in MeOD) showed a single set of signals; ligand proton peaks having undergone a significant downfield shift (Figure 2.5.4-2). This is strong evidence towards the formation of the gold *i*-biq complex, since complex formation would result in removal of electron density from the aromatic ring system, resulting in the observed downfield shift in signals.

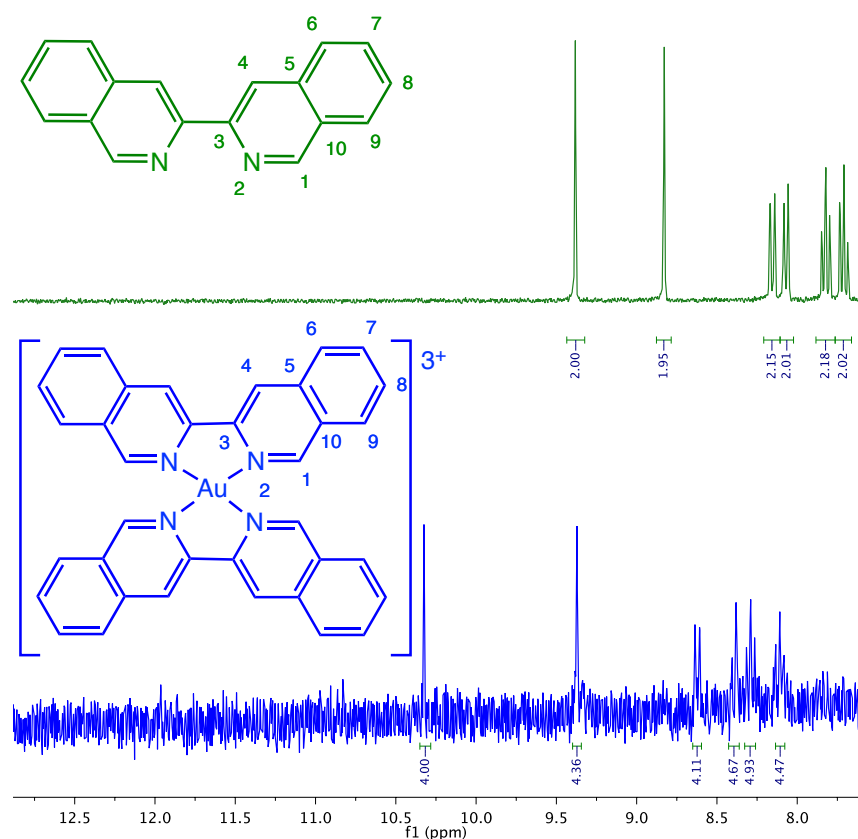


Figure 2.5.4-2 ^1H -NMR spectra overlay of 3,3-biisoquinoline (**4**) and $[\text{Au}(\text{ibiq})_2](3\text{Cl})$ (**9**) (300 MHz, MeOD, 298 °K).

The ESI-MS spectrum showed peaks at m/z 488 and 709 corresponding to $[(\text{Au}(\text{C}_{18}\text{H}_{12}\text{N}_2)(\text{OH})_2) + \text{H}]^+$ and $[\text{Au}(\text{C}_{18}\text{H}_{12}\text{N}_2)_2]^+$ respectively. Whilst there appears to be a peak corresponding to the desired product (m/z 709), its presence points towards a Au(I) metal complex, rather than the anticipated Au(III) central ion. Furthermore, there is a noticeable absence of peaks corresponding to a Au(III) metal centre (expected at m/z 236). Whilst the absence of this peak does not necessarily confirm that this species is not present in the sample, the presence of the m/z 709 peak is definitive evidence of the corresponding species' existence. These observations call into question whether or not the desired species (Au(III), 4 coordinate, square planar) has actually been prepared.

Subsequent attempts at synthesising the Au(III) complex yielded similar compounds producing identical NMR spectra. The ESI-MS spectra, however, showed some variation over a further two attempts; the peak at m/z 709 was not observed in one, whilst alternative peaks also arose, unfortunately none of which corresponded to the Au(III) target complex. Unfortunately, insufficient material was obtained for elemental CHN analysis to be carried out. Attempts to grow a crystal of the compound have so far been unsuccessful.

2.6 Binding of Pd(II) and Pt(II) complexes toward model nucleobases

2.6.1 ESI-MS binding studies

Previously, several biophysical techniques have been employed to probe the interaction between the palladium and platinum metal-biisoquinoline complexes and both duplex and G-quadruplex-forming DNA (summarised in 2.1.1). To better

understand the interaction between the complexes and DNA, electrospray ionisation mass spectrometry (ESI-MS) studies were carried out. The use of ESI-MS as a means by which to demonstrate complex-DNA binding is becoming increasingly common in the literature.⁴⁴ To identify the proposed binding of these complexes to guanine-rich regions of the DNA sequence (capable of forming G-quadruplex structures), preliminary studies with model nucleobase 9-ethyl guanine (9EG) were carried out to establish if either complex binds to guanine.

In order to assess the potential selectivity of these complexes for guanine, further studies were undertaken with model nucleobases 1-methylthymine, 9-methylguanine, 1-methylcytosine and 9-methyladenine. These studies were undertaken to assess the ability of each complex to bind alternative nucleobases, and determine if any preferences for a particular nucleobase exist in solution.

2.6.2 Preliminary ESI-MS studies with 9-ethylguanine

Solutions of 9EG and each complex were mixed in equal quantities and analysed by mass spectrometry. 9EG was solubilised in sodium cacodylate buffer whilst each complex was dissolved in DMSO to aid solubility. The spectrum for 9EG is shown in Figure 2.6.2-1, showing a peak at m/z 739 that can be attributed to G-quadruplex formation in solution (stabilised by a sodium cation). A full range of solvent controls were analysed alongside the experimental samples (data not shown) to enable accurate peak assignments to be made.

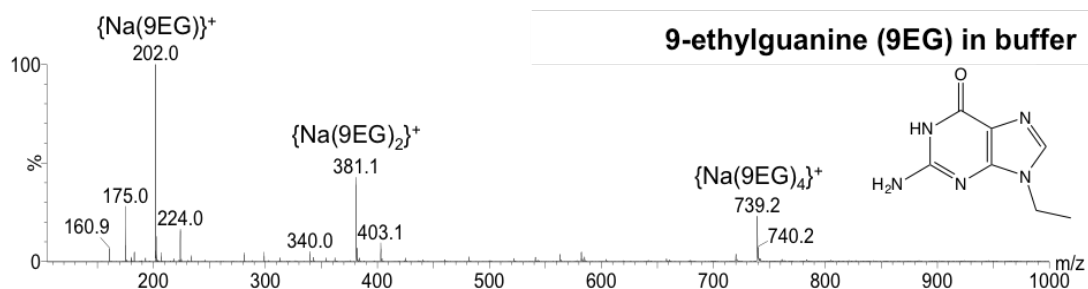


Figure 2.6.2-1 Mass spectrum of a 1 mM solution of 9EG in sodium cacodylate buffer. The peak at m/z 739.2 is due to G-quadruplex formation in solution.

Both complexes show binding to 9EG, as evidenced by the presence of new adducts in the spectra, corresponding to novel complex-base species. The palladium complex **(7)** spectra displayed in Figure 2.6.2-2 show the presence of new peaks at m/z 540, 575 and 1080 corresponding to $[\text{Pd}(i\text{-biq})(9\text{EG} - \text{H})]^+$, $[\text{Pd}(i\text{-biq})(9\text{EG})\text{Cl}]^+$ and $[\text{Pd}_2(i\text{-biq})_2(9\text{EG} - \text{H})_2]^+$, respectively. The platinum complex **(8)** spectra displayed in Figure 2.6.2-3 show the presence of new peaks at m/z 629 and 1257 corresponding to $[\text{Pt}(i\text{-biq})(9\text{EG} - \text{H})]^+$ and $[\text{Pd}_2(i\text{-biq})_2(9\text{EG} - \text{H})_2]^+$, respectively. The peak at m/z 1028 has not yet been assigned, however it appears in the complex only control spectrum and is therefore not due to complex-nucleobase binding.

Although in neither case do these new complex-nucleobase peaks constitute the major species, their presence alone is still encouraging evidence towards guanine interaction.

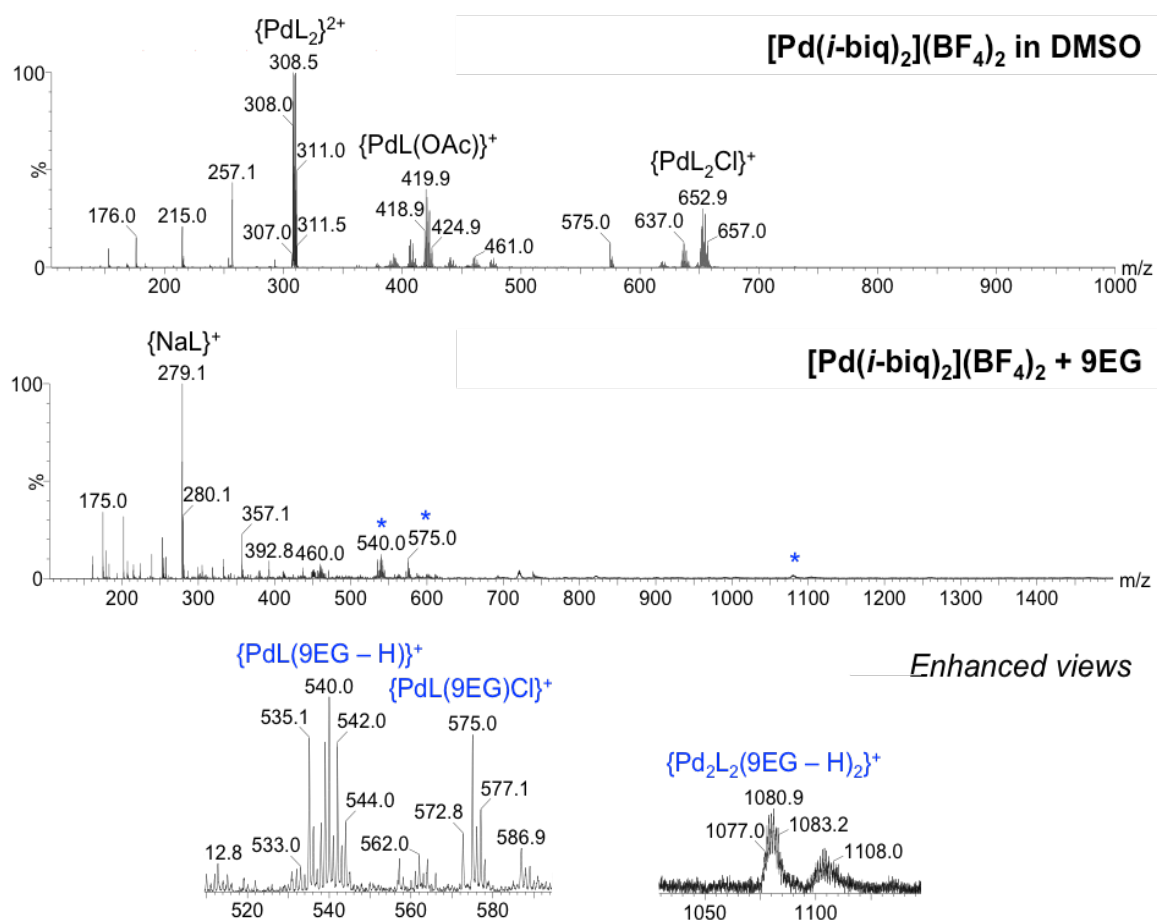


Figure 2.6.2-2 Mass spectra of [Pd(*i*-biq)₂(BF₄)₂] (**7**) in DMSO (top) and 1 mM [Pd(*i*-biq)₂(BF₄)₂] in DMSO + 1 mM 9EG in sodium cacodylate (bottom).

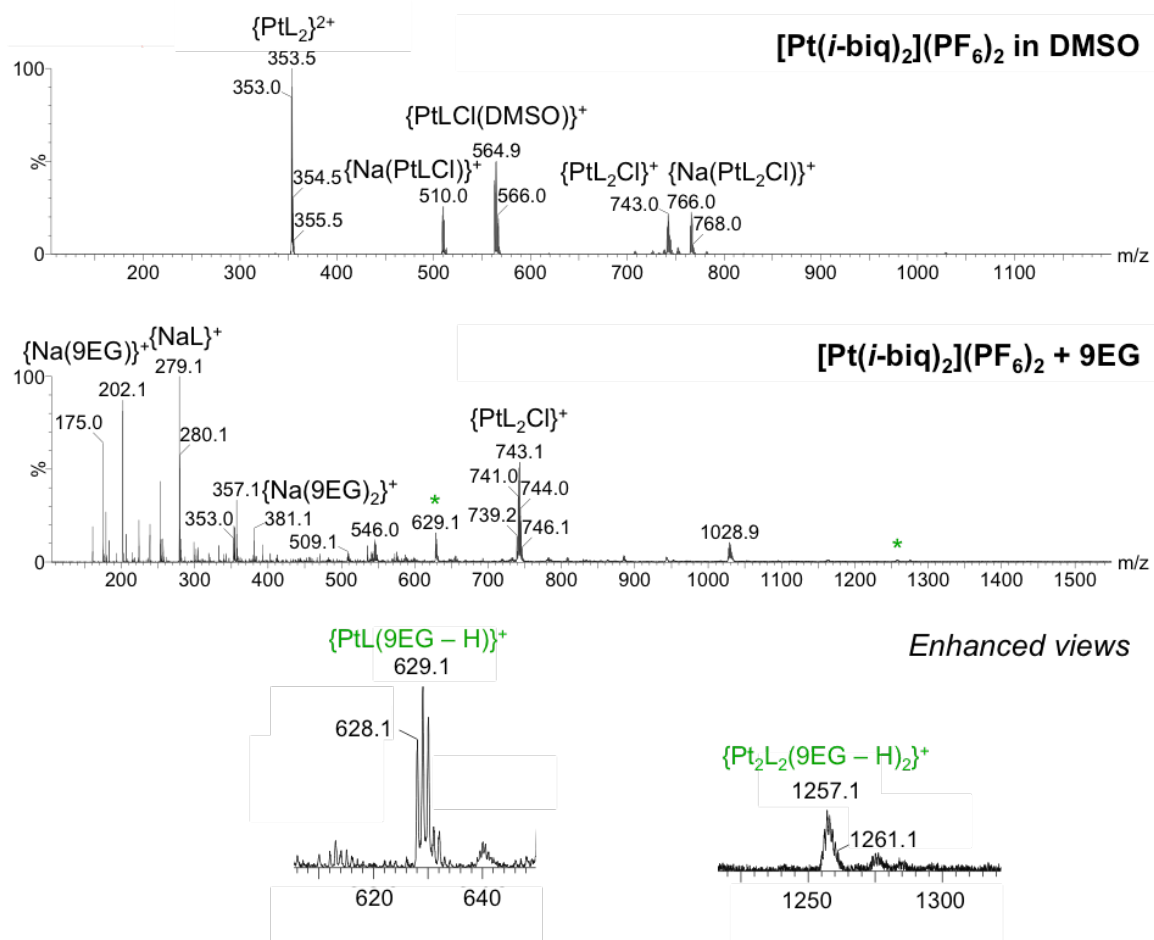


Figure 2.6.2-3 Mass spectra of [Pt(*i*-biq)₂](PF₆)₂ (**8**) in DMSO (top) and 1 mM [Pt(*i*-biq)₂](PF₆)₂ in DMSO + 1 mM 9EG in sodium cacodylate (bottom).

2.6.3 Further ESI-MS studies with 1-methylthymine, 9-methylguanine, 1-methylcytosine and 9-methyladenine.

Following preliminary studies that identified binding interactions between both complexes and 9-ethylguanine, each complex was tested with four further nucleobases (representative of A, C, T and G; 9-methyladenine, 1-methylcytosine, 1-methylthymine and 9-methylguanine, Figure 2.6.3-1) both individually and combined in solution.

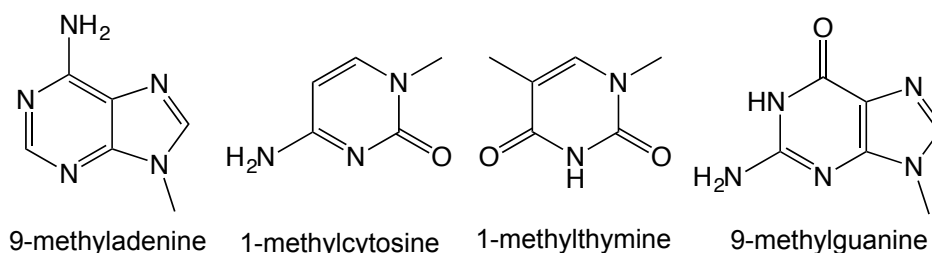


Figure 2.6.3-1 Structures of nucleobases.

Individual bases + complex

Solutions of each individual base and each complex were mixed in equal quantities and analysed by mass spectrometry. Owing to the complexity observed in previous spectra as a consequence of using sodium cacodylate buffer, the bases were solubilised in DMSO instead. Each complex was again dissolved in DMSO. The results, displayed in Table 2.6.3-1 show that the palladium complex (**7**) interacts with all four bases in solution, whilst the platinum complex (**8**) interacts with three out of four bases. There is no evidence of Pt-T binding in solution.

	9-methyl adenine (9MA)	1-methyl cytosine (1MC)	1-methyl thymine (1MT)	9-methyl guanine (9MG)
[Pd(<i>i</i> -biq) ₂](BF ₄) ₂	510 [PdL(9MA – H)] ⁺	488 [PdL(1MC – H)] ⁺	501 [PdL(1MT – H)] ⁺	526 [PdL(9MG – H)] ⁺
[Pt(<i>i</i> -biq) ₂](PF ₆) ₂	599 [PtL(9MA – H)] ⁺	575 [PtL(1MC – H)] ⁺	-	615 [PtL(9MG – H)] ⁺

Table 2.6.3-1 Mass spectra peaks observed upon mixing individual nucleobases (1 mM in DMSO) with 1 mM [Pd(*i*-biq)₂(BF₄)₂] (**7**) in DMSO and 1 mM [Pt(*i*-biq)₂(PF₆)₂] (**8**) in DMSO.

Given the interaction between both complexes and all four nucleobases in almost all cases (except between platinum complex and 1MT), further experiments were conducted to establish whether or not each complex displays a preference for one nucleobase over another.

Four base mix + complex

Creating a competitive environment, a solution containing all four bases in DMSO was mixed with each complex solution in equal quantities and analysed by mass spectrometry. With all four bases combined in solution, each complex may select its preferred binding partner, whereby the most dominant species observed in the spectrum gives an indication of this preference.

The results obtained are shown in Figure 2.6.3-2 with asterisks denoting significant complex-nucleobase peaks. Enhanced views of these peaks, showing their intensities relative to one another are shown in Figure 2.6.3-3.

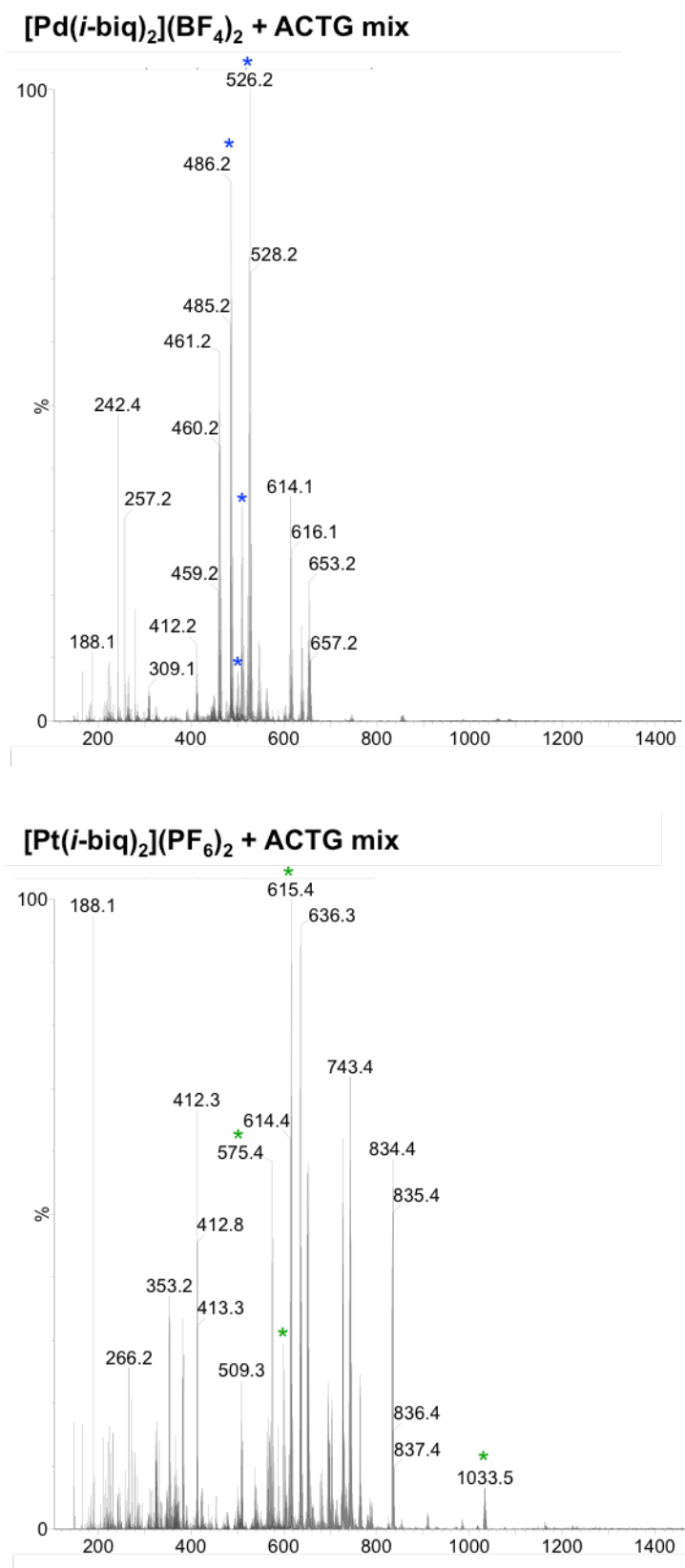


Figure 2.6.3-2 Mass spectra of 1 mM complex in DMSO + 1 mM ACTG mix in DMSO.

It is clear from both spectra that the species observed in the single base experiments are also present when all four bases are available in solution. Of particular note, is the presence of a new peak in the platinum complex spectrum. Located at m/z 1033, this peak could be attributed to $[\text{Pt}(i\text{-biq})_2(9\text{MG} - \text{H})_4\text{Na}]$ *i.e.* it may be due to the formation of G-quadruplex structures in solution, which are subsequently bound by the platinum species **(8)**. A comparable peak (G-quadruplex structure) does not appear in the spectrum for 9MG alone, possibly pointing towards the ability of the platinum species to induce G-quadruplex formation and then stabilise the structure in solution through binding interactions. It is also worth noting that the equivalent peak is not observed in the palladium spectrum.

Comparison of both spectra (see enhanced views in Figure 2.6.3-3) shows the same general pattern: the $[\text{ML}(\text{G} - \text{H})]^+$ guanine species dominate in both cases (followed by 1MC and 9MA). This is strongly supportive of preferential binding to guanine above alternative nucleobases; an extremely promising characteristic for complexes intended for G-quadruplex binding.

[Pd(*i*-biq)₂](BF₄)₂ + ACTG mix
Enhanced view of base adducts

[Pt(*i*-biq)₂](PF₆)₂ + ACTG mix
Enhanced view of base adducts

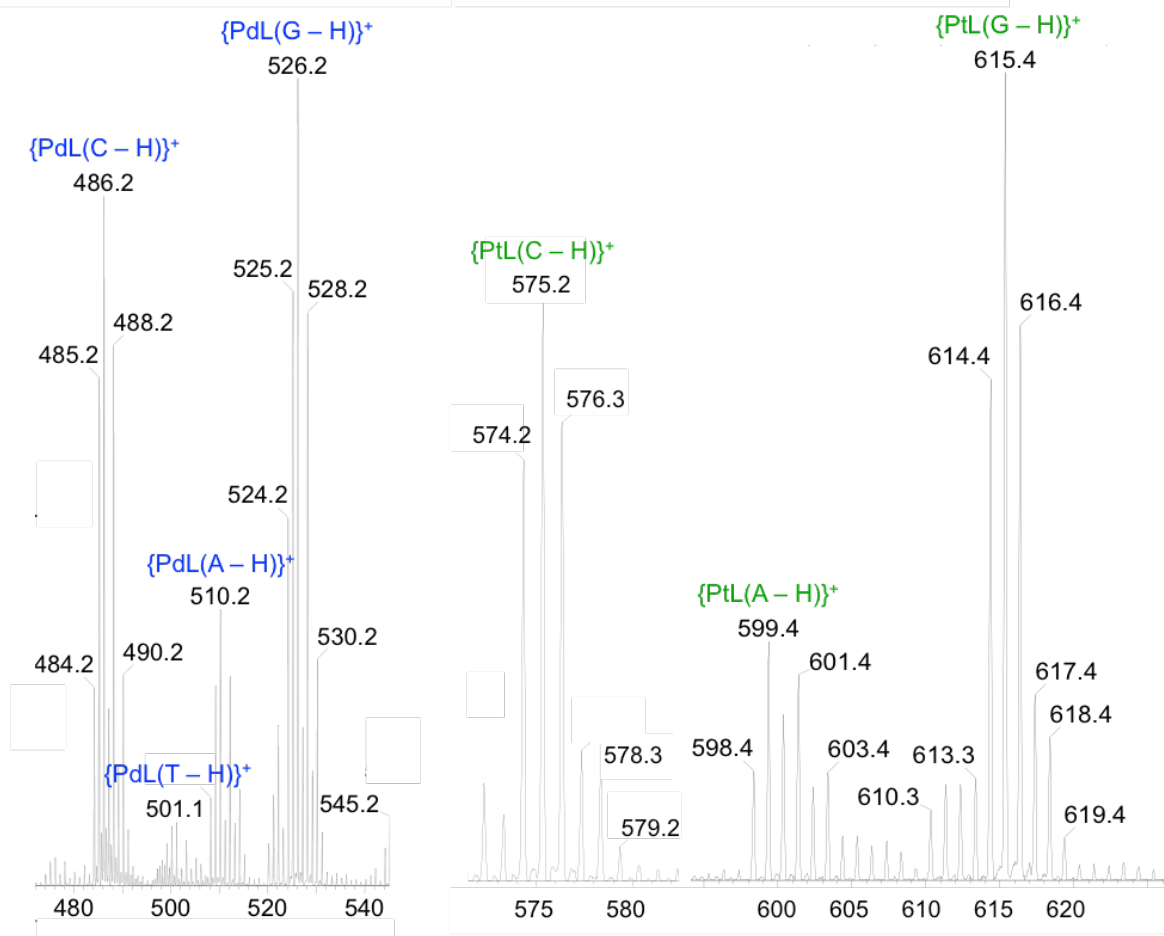


Figure 2.6.3-3 Enhanced views of the mass spectra obtained when 1 mM complex in DMSO is mixed with 1 mM ACTG mix in DMSO.

2.7 Part I: Conclusions

Both palladium and platinum 3,3-biisoquinoline complexes have been successfully synthesised, in addition to the attempted synthesis of a gold analogue. An alternative method was used to achieve selective removal of a single halide substituent at the C(1) position in the isoquinoline building block, resulting in a three-fold increase in

yield compared with the method previously used. Preparation of 3,3-biisoquinoline *via* nickel-catalysed homocoupling of an aryl bromide is described. Whilst more expensive, this route secured a higher yield of ligand and was a cleaner method. Suitable quantities of both the palladium and platinum complexes were obtained (several milligrams) to enable the biological studies discussed in Part II to be carried out. The successful preparation of the gold complex remains unconfirmed, for this reason biological studies were not pursued on this compound. ESI-MS binding studies have demonstrated the ability of both palladium and platinum species to interact with several model nucleobases to form new adducts. Preferential binding to guanine has been observed.

PART II: *IN VITRO* BIOLOGICAL ACTIVITY OF PALLADIUM AND PLATINUM

3,3-BIISOQUINOLINE COMPLEXES

2.8 Introduction

Since its approval in 1978, cisplatin continues to be one of the most effective anticancer drugs used in the treatment of solid tumours including testicular, ovarian, cervical and small-cell lung cancers.⁴⁵ Despite its widespread use, upon binding to double-stranded DNA cisplatin is known to be genotoxic and carcinogenic in mammalian cells, resulting in damage to healthy cells and an increased risk of inducing secondary malignancies.⁴⁶ Consequently, the ability to develop new complexes that demonstrate cytotoxic activity against cancer cells, without also inducing genotoxic or mutagenic damage to cells is an area of great interest.

The targeting of an alternative DNA structure in cells, such as the G-quadruplex, requires a different mode of binding and therefore an alternative mechanism of action which can be useful when circumventing cisplatin resistance. G-quadruplexes represent an ideal target since they are formed during active processes such as translation and replication; the frequencies of which are up-regulated in rapidly proliferating cells, such as cancer cells.⁴⁷

In order to demonstrate activity *in vitro*, compounds must be capable of entering cells to reach their desired target. In the case of targeting DNA, this would require the compound to cross both the cell and nuclear membranes.⁴⁸ Several pathways may gain the compound entry into the cell through the cell membrane, the

choice of which will affect the speed of complex uptake and subsequent distribution throughout the cell environment.⁴⁸

Several *in vitro* biological assays were carried out in order to investigate the biological activity of both the palladium and platinum complexes in cells.

2.8.1 Choice of cell line

In the past decade, a large proportion of the cell work carried out to assess the biological activity of novel compounds developed within the Hannon group, has been completed in the A2780 cell line. With established cell culture protocols in place, it is advantageous to continue working on this same cell line.

The A2780 cell line used in all the cellular studies discussed hereafter is a human ovarian carcinoma line originating from a human ovary. The line was established from tumour tissue obtained from an untreated patient.⁴⁹ Cells are adherent and grow as a monolayer in culture, with epithelial morphology (Figure 2.8.1-1).

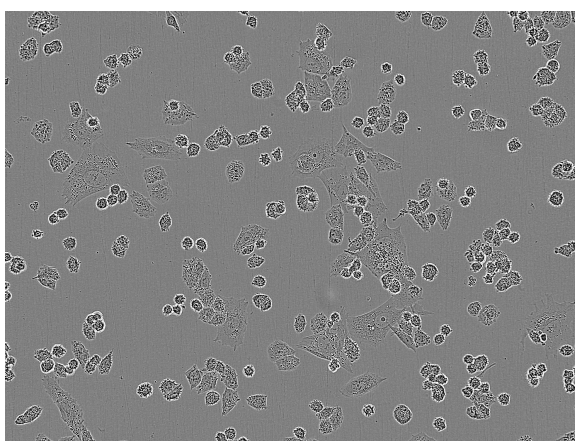


Figure 2.8.1-1 A2780 human ovarian carcinoma cell morphology

2.9 Cell viability

2.9.1 MTT assay

To study the cytotoxic activity, and therefore the potential chemotherapeutic properties of the palladium and platinum biisoquinoline compounds, the MTT assay was performed to yield half maximal inhibitory concentration (IC_{50}) values.⁵⁰ These values measure how effective a compound is, by assessing what concentration is required to inhibit a given biological process by half. In the case of an MTT assay, it is the biological activity of mitochondrial reductase enzymes that is being measured, following inhibition as a result of compound addition.

In metabolically active cells, the addition of a solution of yellow tetrazolium MTT (3-(4,5-dimethylthiazol-2-yl)-2,5-diphenyltetrazolium bromide) will result in its reduction to violet formazan crystals through electron transport processes involving mitochondrial reductase (Figure 2.9.1-1).⁵¹ The extent to which a colour change has occurred can be determined spectrophotometrically following dissolution of the violet crystals with dimethylsulfoxide. The intensity of the violet colour is an indicator of the proportion of functional mitochondria and consequently the proportion of viable cells.⁵²

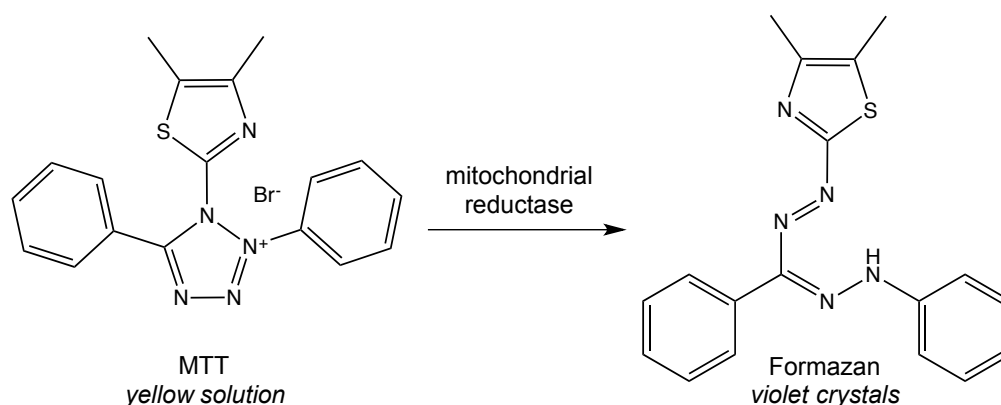


Figure 2.9.1-1 The reduction of MTT to formazan by mitochondrial reductase in living cells.

A range of concentrations per compound is tested, whereby a graph of concentration vs. absorbance can be plotted. The point at which the absorbance has decreased by 50% will correspond to the IC₅₀ concentration. The lower the IC₅₀ value, the more cytotoxic a compound is; since less is needed to reduce cell viability by 50%.

2.9.2 IC₅₀ results

A2780 cells were treated with eight different concentrations of [Pd(*i*-biq)₂](BF₄)₂ (**7**), [Pt(*i*-biq)₂](PF₆)₂ (**8**), 3,3-biisoquinoline (**4**) and cisplatin as a positive control to assess cell viability (mitochondrial MTT reduction). Cisplatin was tested as a well-studied comparison, whilst the unbound *i*-biq ligand (**4**) was tested to verify that the metal-bound complexes are still intact upon entry into the cell (as evidenced by a different IC₅₀ value), as well as to compare the activity of the ligand alone. The results of the assay are detailed in Table 2.9.2-1 and displayed in Figure 2.9.2-1, with the average IC₅₀ values of three independent runs reported in micromolar (μM). To confirm that cytotoxicity was not observed due to adverse solvent effects, vehicle controls of 2% DMSO/98% RPMI media were tested. No significant cytotoxic effects (assessed by MTT assay) were observed under these conditions (data not shown).

Compound	IC50 (μM)
[Pd(<i>i</i> -biq) ₂](BF ₄) ₂ (7)	2.47 ± 0.10
[Pt(<i>i</i> -biq) ₂](PF ₆) ₂ (8)	6.19 ± 0.20
<i>i</i> -biq (4)	17.4 ± 1.6
cisplatin	17.1 ± 0.8

Table 2.9.2-1 Evaluation of cytotoxic effects of treatment of [Pd(*i*-biq)₂](BF₄)₂, [Pt(*i*-biq)₂](PF₆)₂, 3,3-biisoquinoline (*i*-biq) and cisplatin using the MTT assay. A2780 cells were treated for 24 hours prior to obtaining IC₅₀ values. Values are mean ± S.E.M. for data from three independent experiments.

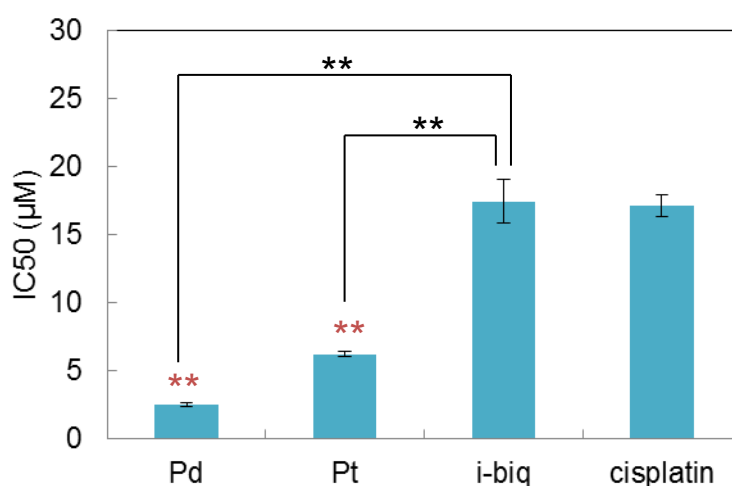


Figure 2.9.2-1 Evaluation of cytotoxic effects of treatment of [Pd(*i*-biq)₂](BF₄)₂, [Pt(*i*-biq)₂](PF₆)₂, 3,3-biisoquinoline (*i*-biq) and cisplatin using the MTT assay. A2780 cells were treated for 24 hours prior to obtaining IC₅₀ values. Values are mean ± S.E.M. for data from three independent experiments. Significant difference from cisplatin (*) and 3,3-biisoquinoline (*i*-biq) (*) ($p < 0.01$ **) (One-way ANOVA followed by Tukey test).

A statistically significant difference between the activity of both complexes and cisplatin can be immediately observed ($p < 0.01$). For the 24 hour treatment period studied, both complexes show cytotoxic activity exceeding that of cisplatin. The greatest difference in cytotoxicity is observed between cisplatin and the palladium

complex **(7)**, which exhibits approximately 6-fold greater cytotoxic activity than cisplatin on this cell line. In comparison, the platinum complex **(8)** shows approximately 3-fold greater activity than cisplatin, which, despite being less active than its palladium analogue, is still a notable improvement upon the activity of cisplatin.

The observed differences in activity between both complexes and cisplatin can likely be explained by differences in biological target, uptake and stability of these compounds. The mechanism of action of cisplatin has been widely researched and is well documented. Targeting both nuclear and mitochondrial DNA, cisplatin is hydrolysed upon entry into the cell and then binds to the N(7) position on guanines featured in double-stranded DNA. The resulting adduct initiates apoptotic pathways, leading to cell death. By contrast, complexes **(7)** and **(8)** are proposed to be interacting with G-quadruplex structures in addition to duplex DNA, as determined by previous spectrographic studies (on isolated DNA) (2.1.1). The combination of binding to both duplex and G-quadruplex cellular targets could account for the increased cytotoxicity observed for these compounds, due to their dual-mode ability to inhibit DNA replication.

Alternatively, the increased cytotoxicity observed may be less to do with the number of cellular targets bound and more to do with the type of target bound. Where both types of DNA are available in a single system, each complex has been shown to have a preference for G-quadruplex binding.⁹ The observed increase in cytotoxicity may therefore be due to the downstream effects of binding the more unusual G-quadruplex target structures over DNA, rather than as a cumulative result of binding to both targets.

Despite the comparatively low occurrence of G-quadruplex structures for interaction (compared to the availability of double stranded DNA), the lower IC₅₀ values obtained for the complexes targeting these structures leads to the suggestion that such a mode of binding produces a greater cytotoxic effect. This would account for the increased cell death observed at much lower treatment concentrations (*cf.* cisplatin), despite the limited availability of G-quadruplex binding sites. Further explanations for the observed differences in cytotoxicity between cisplatin and complexes **(7)** and **(8)** could be related to the uptake and localisation of the compounds, which will be investigated further.

In addition to differences between the activity of cisplatin and complexes **(7)** and **(8)**, there is a statistically significant difference between each complex and unbound *i*-biq ligand **(4)** ($p < 0.01$), whereby the unbound ligand is much less cytotoxic than both complexes formed upon its binding to a metal centre. This information supports the assertion that the complex is intact upon entry into the cell and has not undergone any degradation into free ligand and metal; either in solution or following uptake. Consequently, it is believed that the cytotoxic effect being observed is due to the biological activity of compounds **(7)** and **(8)** in their complex form.

Although the palladium complex **(7)** was more toxic than the platinum complex **(8)**, this was not statistically significant ($p = 0.07$). The cause of the observed difference in IC₅₀ values (the platinum complex requires a treatment concentration approximately 2.5-fold greater than the palladium complex in order to produce the same cytotoxic

effect) is unlikely due solely to G-quadruplex binding in cells, since it is the platinum complex that has been shown to bind more favourably to these regions.⁹

It is possible that the cell uptake and localisation mechanism for each complex varies, resulting in lower bioavailability of the platinum form, and consequently limited complex-DNA binding. This could explain why, despite a greater affinity for G4-interaction, the platinum complex is unable to reach its biological target as readily and thus requires a greater concentration of treatment to produce the same cytotoxic effect as the palladium compound. Exploration of cell uptake was thus prompted, with ICP-MS experiments completed in order to assess cell uptake and localisation (discussed in 2.12).

The literature reports a variety of G-quadruplex binding compounds that have been studied *in vitro* to assess their cytotoxicity across a range of cell lines (detailed in Figure 2.9.2-2). These include (a) metal-salphen complexes that bind to human telomeric DNA quadruplexes with antiproliferative activity,⁴ (b) 3,6,9-trisubstituted acridine complexes that bind to G-quadruplexes and display potent inhibitory activity against human telomerase,⁵⁴ (c) platinum Schiff base complexes that bind to G-quadruplexes located in cMyc gene promoter regions, thus inhibiting oncogene expression⁵⁵ and (d) copper terpyridine complexes that selectively bind and stabilise antiparallel G-quadruplex DNA, displaying greater cytotoxicity than cisplatin.⁵⁶

The IC₅₀ values obtained for both G-quadruplex binding compounds **(7)** and **(8)** are comparable to those reported in the literature, typically falling in the low micromolar range (broadly between 1-10 µM). The palladium *i*-biq compound **(8)** in particular has a similar IC₅₀ value (approximately 2.5 µM) to many of those quoted,

with the platinum *i*-biq compound (**7**) exhibiting a higher IC₅₀ value, though still demonstrating comparable cytotoxicity to several of the literature compounds.

Accounting also for their demonstrated increase in cytotoxicity compared to cisplatin, both the palladium and platinum *i*-biq compounds show great potential as anticancer agents. Subsequently, further investigation into the cell uptake and mode of action of these compounds was carried out.

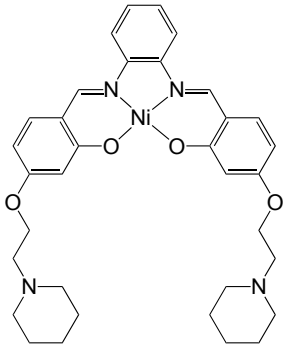
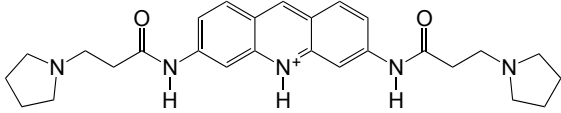
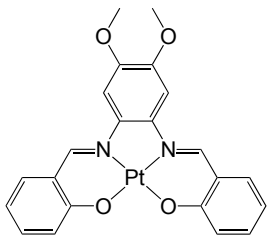
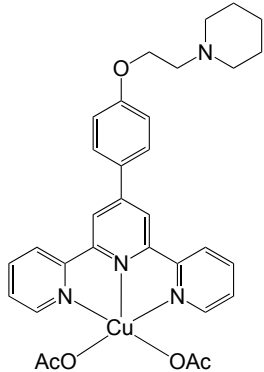
Compound	Cell line	IC50 (μM)
<p>a)⁴</p>  <p>SRB assay, 96 h</p>	<p>MCF-7 A549 RCC4 W138</p>	<p>2.3(14.5⁵⁶) 2.3(20.4⁵⁶) 2.3 2.4</p>
<p>b)⁵⁴</p>  <p>SRB assay, 96 h</p>	<p>A2780</p>	<p>2.7(1.58⁵⁷)</p>
<p>c)⁵⁵</p>  <p>MTT assay, 48 h</p>	<p>HeLa NC1-H460 CCD-19 Lu HepG2</p>	<p>1.3 (12.5) 4.8 (16.5) 46.1 (85.2) 1.1 (11.5)</p>
<p>d)⁵⁶</p>  <p>MTT assay, 48 h</p>	<p>Bel-7402 A549 HL-60 HeLa MCF-7</p>	<p>1.0 (8.1) 1.3 (20.4) 2.3 (2.9) 2.2 (20.3) 1.5 (14.5)</p>

Figure 2.9.2-2 G-quadruplex binding complexes reported in the literature and their determined IC50 values across a range of cell lines. Values in parentheses represent the IC50 values for cisplatin determined within the study, or (where available) in other work for comparison. Cancer cell lines: A2780 (ovarian), MCF-7 (breast), A549 (lung), RCC4 (renal), HeLa (cervical), HepG2 (hepatocellular), NC1-H460 (lung), Bel-7402 (hepatocellular), HL-60 (promyelocytic leukaemia). Normal cell lines: W138 (human fibroblast), CCD-19 Lu (lung fibroblast). Values taken from literature and quoted to 1 decimal place for comparison.

2.10 Genotoxicity

2.10.1 Comet assay for DNA double strand breaks

Human cells typically accumulate at least 10,000 DNA lesions daily,⁵⁸ with their efficient repair a mandatory biological process to avoid apoptosis. Failure to repair DNA damage can lead to an accumulation of genetic mutations causing genomic instability that may also result in the development of secondary tumours following the cessation of chemotherapeutic treatment.⁵⁹

Genotoxic chemicals exert their adverse effects through interaction with the DNA of cells. Such compounds have the potential to be carcinogens and/or mutagens, ultimately inducing cancer and/or heritable defects. Genotoxicity testing is carried out to identify compounds that are capable of inducing genetic damage directly or indirectly by various mechanisms of action.

First developed in 1984 by Ostling and Johanson,⁶⁰ the comet assay (also called the single cell gel electrophoresis (SCGE) assay) is a well-established, sensitive and relatively simple method for detecting DNA damage (specifically strand breaks) at the individual eukaryotic cell level.^{61,62} Requiring only small numbers of cells per sample, electrophoresis is performed on exposed cells that have been embedded in agarose gel. During the migration process the effect of DNA damage is detectable as DNA fragments that lag behind the intact, undamaged DNA, thus producing a comet tail effect when visualised under the microscope (Figure 2.10.1-1)

Analysis of each comet allows the amount of DNA present in the tail region to be calculated as a percentage of the total DNA present in both the tail and head regions combined, giving a percentage tail intensity value. A large percentage tail intensity value would be characteristic of a compound which is capable of causing

severe DNA strand breaks (*i.e* genotoxic), resulting in the majority of genetic material accumulating in the tail region.

Comparison of median percentage tail intensity values for different compounds enables the degree of genotoxicity to be determined. Furthermore, analysis of a single compound at varying concentrations can give an indication of the relationship between compound concentration and DNA damage induced.

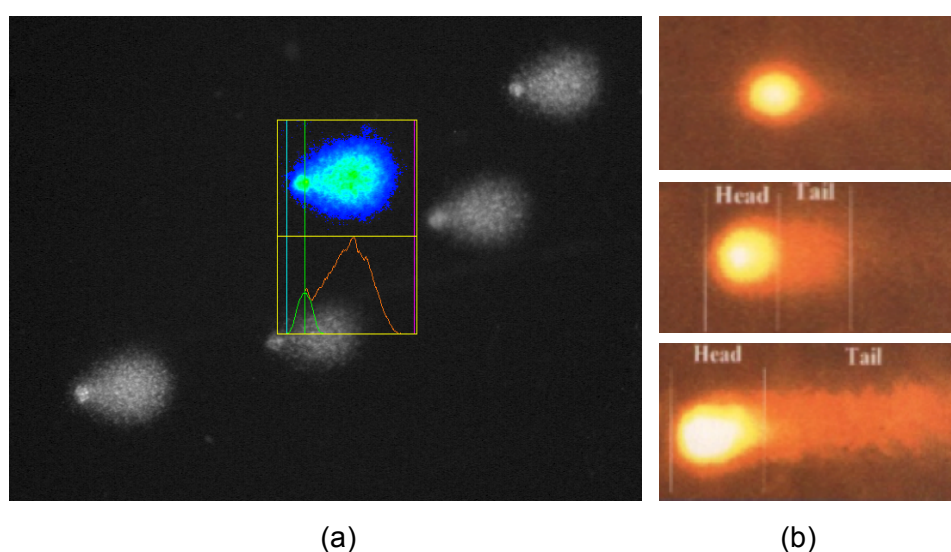


Figure 2.10.1-1 (a) Screenshot of the COMETIV user interface showing the graphical analysis of a selected comet. (b) Representative images demonstrating the increase in DNA occupying the tail region as a result of increasing severity of DNA damage.

The use of buffers with either neutral or alkaline pH results in two variations of the assay. The alkaline assay identifies both single (SSB) and double strand breaks (DSB), whilst the neutral assay is said to identify the occurrence of double strand breaks only.⁶³ There is, however, some discussion as to whether the use of a pH close to neutral is sufficient to specifically distinguish double-stranded breaks only.⁶⁴

2.10.2 DNA strand break results

The comet assay was performed under neutral conditions to enable detection of DNA double-strand breaks (DSB). Among the various types of damage experienced by a cell, DSBs represent the most lethal form and are frequently introduced by cellular processes such as stalled replication forks.^{58,65,66} Since stabilisation of G-quadruplex structures (as a result of complex binding) is proposed to interfere with cell replication, DSBs were deemed the most relevant type of damage expected to occur to cellular DNA following treatment with quadruplex-binding compounds **(7)** and **(8)**. The neutral assay was therefore chosen as the most appropriate method to analyse DNA damage following compound treatment.

Neutral comet assays were performed on A2780 cells following 24 hours incubation with either the palladium **(7)** or platinum **(8)** complex. Untreated control samples were also analysed. Three concentrations related to the IC_{50} of each compound were tested ($[IC_{50}]$, $[IC_{50}/2]$, $[IC_{50}/4]$) to determine if there is a concentration-response between the amount of compound administered and the severity of damage observed. Treatments at concentrations above the IC_{50} were excluded, since this would result in a large amount of cell death during the treatment period and thus limit the number of viable cells available for collection and examination. Treated cells were lysed and electrophoresed, after which time they were stained with SYBR gold to enable visualisation of the DNA under the microscope.

During the scoring process, one hundred cells were manually selected and analysed. Whilst this process is unbiased, there are some considerations when selecting a particular cell for analysis. When viewing the slides, there are regions of

non-cellular debris that have been stained, and could be mistaken for cells without closer inspection (Figure 2.10.2-1). Care must be taken to avoid selecting these regions. If mistakenly selected, it is clear that these regions are not representative of DNA, as there is no variation in the pixel intensity across the region, in which case, the erroneous selection must be deleted from the overall count. In addition to debris, cells which are too close in proximity to surrounding cells or debris on the slide are a poor choice, since the software is not able to distinguish the two objects as independent, and will therefore process the second cell (the neighbouring cell not selected) as the tail region of the first (Figure 2.10.2-1). Again, it is wise to avoid selecting these cells to ensure the median percentage tail intensity values generated from the software are representative and accurate.

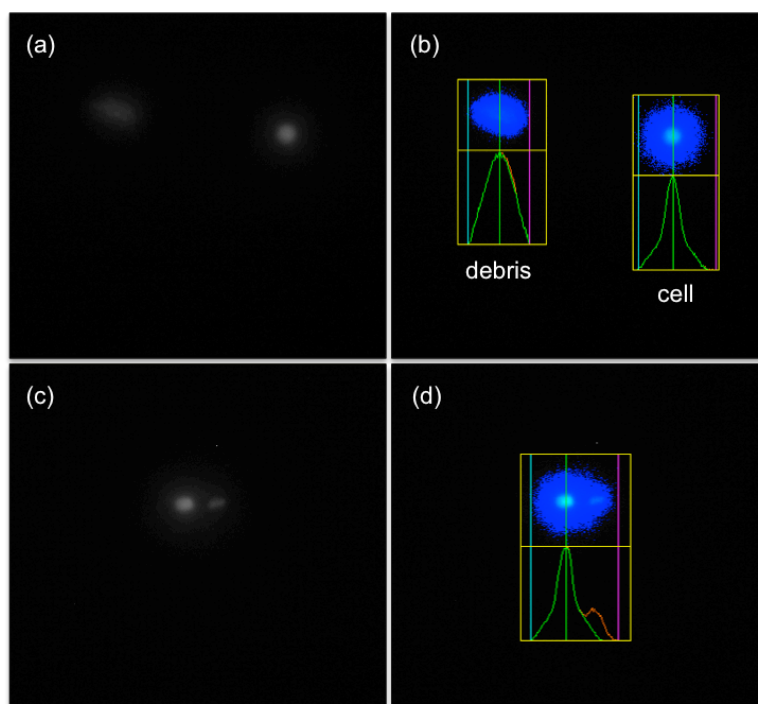


Figure 2.10.2-1 Screenshots of the COMETIV user interface showing (a) appearance of 'cells' pre-selection; (b) comparison of selection of debris vs. cell; (c) cell in close proximity to debris; (d) selection of such a cell produces inaccurate results due to the inclusion of the debris.

To assess the extent of DNA damage, the median percentage tail intensity was calculated as an average of three independent runs. The results of this assay are detailed in Table 2.10.2-1 and displayed in Figure 2.10.2-2. The measurement of percentage tail intensity was chosen because it is less dependent on electrophoresis voltage and run time, and has been shown to exhibit less inter-run variation due to this.⁶⁷ On account of its reliability, this parameter is also the most frequently quoted within the literature when presenting comet assay data.

Compound	Median (%) tail intensity		
	IC50/4	IC50/2	IC50
Control	-	1.25 ± 0.76	-
[Pd(<i>i</i> -biq) ₂](BF ₄) ₂ (7)	2.84 ± 0.24	5.42 ± 0.76	7.76 ± 1.03
[Pt(<i>i</i> -biq) ₂](PF ₆) ₂ (8)	3.56 ± 0.57	5.72 ± 0.85	6.26 ± 1.48
cisplatin	1.62 ± 0.38	1.92 ± 0.57	3.78 ± 0.51

*Table 2.10.2-1 Evaluation of genotoxic effects of treatment of [Pd(*i*-biq)₂](BF₄)₂, [Pt(*i*-biq)₂](PF₆)₂ and cisplatin using the neutral comet assay. A2780 cells were treated with three concentrations of compound for 24 hours prior to obtaining median % tail intensity values. Values are mean ± S.E.M. for data from three independent experiments.*

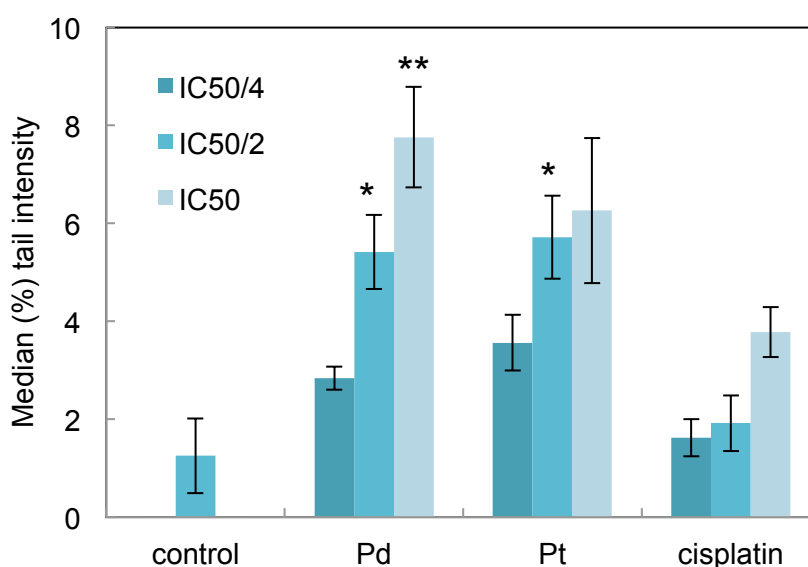


Figure 2.10.2-2 Evaluation of genotoxic effects of treatment of $[Pd(i-biq)_2](BF_4)_2$, $[Pt(i-biq)_2](PF_6)_2$ and cisplatin using the neutral comet assay. A2780 cells were treated with three concentrations of compound for 24 hours prior to obtaining median % tail intensity values. Values are mean \pm S.E.M. for data from three independent experiments. Significant difference from control ($p < 0.05$ *; $p < 0.01$ **) (One-way ANOVA followed by Tukey test).

The data shows that there is a statistically significant difference between the median percentage tail intensities of each complex and the untreated control cells ($p < 0.05$) at the IC50/2 and IC50 concentrations tested. No significant difference was observed at the IC50/4 concentration for either complex. This demonstrates that at concentrations exceeding the IC50/2 concentration, both the palladium and platinum complexes induce a greater number of DSBs compared to untreated control cells, indicating a degree of genotoxicity in their behaviour.

At each concentration tested, both complexes appear to cause comparable amounts of DNA damage. Since the treatment concentrations are related to the IC₅₀ value for each compound independently, this means that the same degree of damage is induced by different concentrations of each compound. This might be expected, as it reflects the difference in cytotoxicity of the two compounds. It is no

surprise therefore, to observe that treatment at the IC_{50} concentration induces a similar degree of damage, despite cells being exposed to an approximately 2.5-fold greater concentration of platinum complex versus palladium complex. Both complexes caused a concentration-dependent increase in DNA strand breaks that became statistically significant at concentrations greater than $IC_{50}/2$.

Compared to cisplatin, both complexes induce more DSBs, resulting in higher median % tail intensities at each concentration tested. Indeed, the differences in median % tail intensities observed for cisplatin are not statistically significant when compared to untreated control cells. The genotoxicity with respect to DSBs is therefore greater for both the palladium and platinum complex than for cisplatin. This is not entirely surprising given that cisplatin's genotoxicity is predominantly due to SSBs that occur as a result of DNA repair mechanisms attempting to remove the crosslinked adducts from the affected DNA regions.⁶⁸ Consequently, cisplatin alone would not be expected to exhibit significant tail moments when analysed under neutral assay conditions.

The genotoxicity displayed by both complexes is reasonably minimal, with less than 8% of the cell's DNA occupying the tail region upon treatment of either complex at its cytotoxic (IC_{50}) concentration. At this biologically relevant concentration, there is no statistically significant difference in tail intensities between the two complexes, indicating that their mechanisms of action may well be similar. The significance of the role that genotoxicity plays towards the overall cytotoxicity of both compounds is likely the same, since the occurrence of DSBs is the same at cytotoxic concentrations.

2.11 Cell cycle analysis

2.11.1 Cell cycle

Cells undergo a regular cycle of division separated by periods of cell growth, known as the cell cycle and defined by three stages; interphase, nuclear division and cell division (Figure 2.11.1-1).

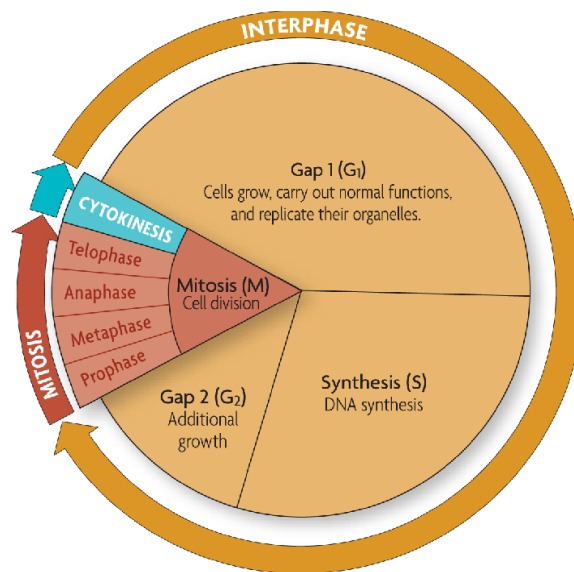


Figure 2.11.1-1 The cell cycle

Often termed the resting phase because no division takes place, interphase is divided into three stages. First gap phase (G₁) involves the production of proteins that are essential for the synthesis of cell organelles. Synthesis phase (S) involves the semi-conservative replication of DNA, in order that the resulting daughter cells may be genetically identical. Second gap phase (G₂) is a time when cell organelles grow and divide and energy stores are increased in preparation for nuclear and cell division.

Nuclear division can take place by either mitosis or meiosis to produce either two genetically identical daughter nuclei or four genetically distinct daughter nuclei,

respectively. The latter occurs exclusively in sexual reproduction. During mitosis, the nucleus divides into two identical daughter cells (clones). Cell division follows, whereby the whole cell divides into two in a process called cytokinesis.

Typically, a mammalian cell takes about 24 hours to complete a cell cycle, with approximately 90% of that time spent in interphase. To ensure cell division occurs correctly, control mechanisms known as cell cycle checkpoints exist. Typically consisting of a network of regulatory proteins, these checkpoints are used by the cell to monitor and regulate the progress of the cell cycle, preventing progression to the next phase until checkpoint requirements have been met. There are three main checkpoints (G1, G2, M) responsible for ensuring that incomplete or damaged DNA is not inherited by daughter cells.

2.11.2 Flow cytometry with propidium iodide staining

First described in 1969, cell cycle analysis by quantification of DNA content was one of the earliest applications of flow cytometry.⁶⁹ Staining of the DNA with propidium iodide (PI) allows cells to be categorized by phase, based on their fluorescence output.⁷⁰ This is based on the premise that PI binds stoichiometrically to DNA. Cells that are in S phase will have more DNA than cells in G1, taking up proportionally more dye and exhibiting a greater fluorescent output until they have doubled their DNA content. Cells in G2 will be approximately twice as bright as cells in G1.

This process allows the cell cycle to be probed, providing insight into the stage at which normal cell activity is interrupted, resulting in cell cycle arrest. The phase in which cell cycle arrest occurs in treated cells can be directly compared to control cells

(untreated, PI stained). Knowledge of the stage in which cell cycle arrest occurs following compound treatment provides information about the types of processes that may be experiencing interference. This information is invaluable in elucidating a possible mechanism of action of the drug.

2.11.3 Cell cycle arrest results

Cells were treated at two different concentrations of compound ([IC₅₀/10], [IC₅₀/2]) for a period of 24 hours prior to sample preparation. Cells were fixed in ethanol to ensure permeability of the cell membranes to ribonuclease A and propidium iodide for the following stages. Ribonuclease A was first added to the fixed cells to degrade RNA, resulting in only the remaining DNA being stained with propidium iodide. Following sample preparation, the passage of cells through the flow cytometer's laser generates a fluorescence pulse that correlates with the amount of PI and therefore the total amount of DNA in the cell. Plots of forward scatter (FS) vs. side scatter (SS) and pulse width vs. pulse area were recorded during sample analysis.

Following sample analysis, cell doublets were excluded from the data analysis. This is crucial, because a doublet of two cells in G₀/G₁ has the same total amount of DNA and thus the same fluorescence output as a single cell in G₂/M.⁷¹ These doublets would therefore create false positive results for G₂/M cells. The identified single cell population was manually gated (excluding debris), and the gate applied to a PI histogram displaying the distribution of cells. Application of a curve cell cycle fit to the histogram generated cell cycle statistics. This scheme of post-

processing, shown in Figure 2.11.3-1, enabled quantification of the percentage of cells per cell cycle phase (G0/G1, S phase, G2/M).

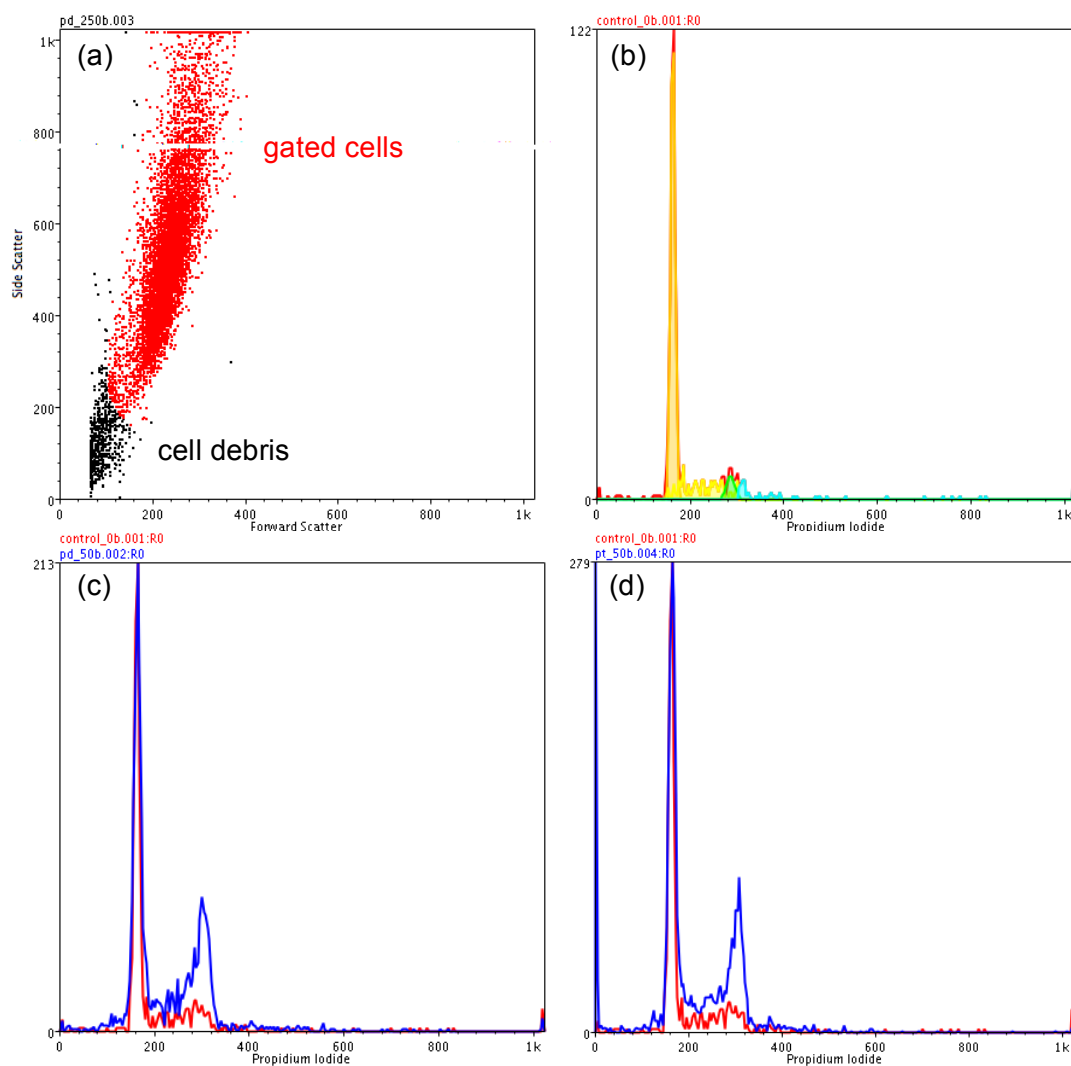


Figure 2.11.3-1 (a) Representative scatter plot of raw data showing gated region; (b) Histogram showing curve fitting to determine cell cycle stage proportions; (c-d) Overlay of histograms (control, complex [IC50/10]) showing the redistribution of cells following 24 hour treatment with (c) [Pd(i-biq)₂](BF₄)₂ (d) [Pt(i-biq)₂](PF₆)₂.

The percentage of cells per phase was calculated as an average of two or three independent experiments, with the results listed in Table 2.11.3-1, and displayed in Figure 2.11.3-2.

Compound	Cell cycle phase (%)		
	[IC50/10]		
	G0/G1	S	G2/M
Control	65.9 ± 5.7	27.8 ± 5.7	6.3 ± 1.2
[Pd(<i>i</i> -biq) ₂](BF ₄) ₂	45.4 ± 1.2	31.3 ± 0.9	23.4 ± 0.4
[Pt(<i>i</i> -biq) ₂](PF ₆) ₂	47.7 ± 1.2	29.0 ± 0.2	23.3 ± 1.0
cisplatin	29.8 ± 0.7	61.0 ± 2.6	8.5 ± 2.0
	[IC50/2]		
	G0/G1	S	G2/M
Control	-	-	-
[Pd(<i>i</i> -biq) ₂](BF ₄) ₂	53.1 ± 0.7	23.0 ± 2.1	24.0 ± 1.4
[Pt(<i>i</i> -biq) ₂](PF ₆) ₂	59.2 ± 1.1	22.9 ± 0.8	18.0 ± 1.8
cisplatin	30.6 ± 0.3	63.8 ± 0.7	5.6 ± 0.4

*Table 2.11.3-1 Evaluation of cell cycle arrest following treatment of [Pd(*i*-biq)₂](BF₄)₂, [Pt(*i*-biq)₂](PF₆)₂, and cisplatin using PI-stained flow cytometry. A2780 cells were treated with two concentrations of compound for 24 hours prior to obtaining percentage of cells per phase (indicating the phase at which cell cycle arrest has occurred). Values are mean ± S.E.M. for data from three (control, cisplatin) or two independent experiments (palladium, platinum).*

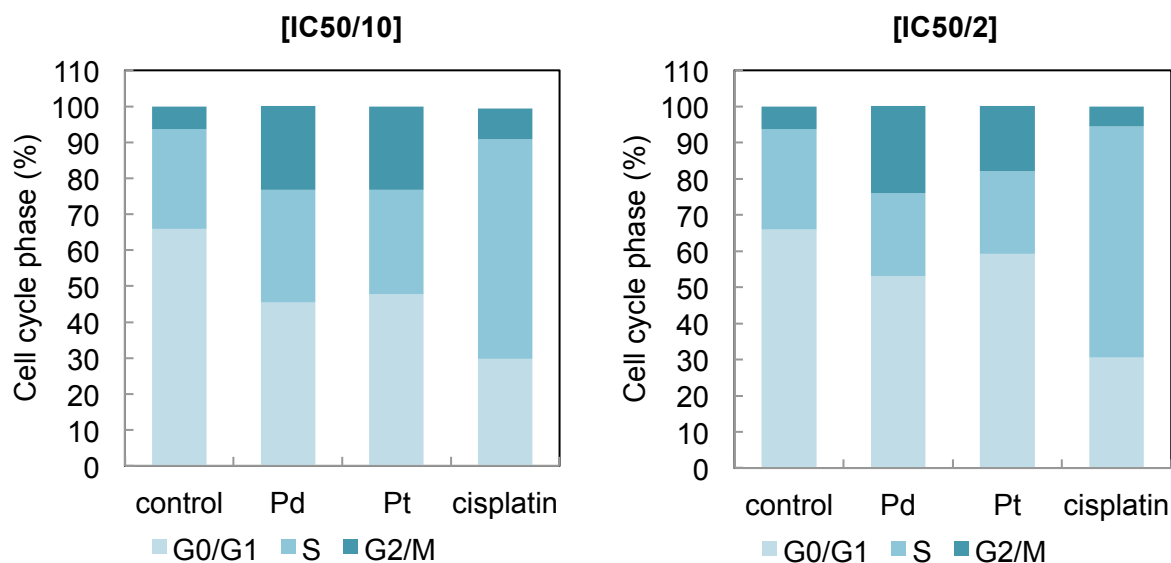


Figure 2.11.3-2 Evaluation of cell cycle arrest following treatment of $[Pd(i-biq)_2](BF_4)_2$, $[Pt(i-biq)_2](PF_6)_2$, and cisplatin using PI-stained flow cytometry. A2780 cells were treated with two concentrations of compound for 24 hours prior to obtaining percentage of cells per phase (indicating the phase at which cell cycle arrest has occurred). Values are mean for data from three (control, cisplatin) or two independent experiments (palladium, platinum).

The data shows a marked shift in the phase at which cell cycle arrest occurs when comparing control cells to treated cells. Control cells predominantly occupy the G0/G1 phase (~66%), with a reasonable number of cells in the S phase (~28%) and the remaining cells found in the G2/M phases (~6%).

The majority of cells treated with cisplatin accumulate in the S phase (~61%). Fewer cells are found in the G0/G1 phases compared to the control (~30%). In accordance with its reported activity, this demonstrates that cisplatin arrests cells during the S-phase of the cell cycle.⁷²

Treatment with either the palladium or platinum *i-biq* complex at the lower of the two concentrations tested ([IC50/10]) results in a noticeable change in cell phase

distribution, whereby the G0/G1 occupancy has decreased (~45-48%) alongside a significant increase in G2/M occupancy (~23%). The S phase occupancy is comparable to that seen in the control. These observations are indicative of G2/M phase arrest following complex treatment. The ability to observe such a striking shift at such low concentrations of either complex demonstrates the potent activity of these complexes *in vitro*. Indeed, at the higher concentration tested ([IC₅₀/2]), the distribution of cells is largely unaltered (compared to the lower concentration [IC₅₀/10]), indicating that the desired effect is achieved with minimal complex, and thus no further alteration in the distribution of cells occurs upon exposure to higher concentrations. Additional complex availability at high treatment concentrations appears to act as somewhat of an excess, with G2/M phase arrest already accomplished. The similarity between the two complexes is unsurprising, given that the concentrations were again related to their IC₅₀ concentrations, and that the results of the comet assay have already shown that their modes of action are very likely to be similar on account of their comparable genotoxicity.

G2/M cell phase arrest has previously been reported in G-quadruplex binding ligands including the cationic porphyrin TMPyP4.⁷³ Paralleled by telomerase inhibition, Hurley *et al.* noted the ability of TMPyP4 to inhibit telomerase activity at concentrations that do not have general toxic effects on the cells. This type of effect has been witnessed herein, with a dramatic shift in cell cycle arrest occurring at treatment concentrations far below those that induce cytotoxicity.

The arrest of the cell cycle at a different phase (compared to cisplatin) following treatment with these complexes likely indicates an alternative mode of action. The

arrest of cells is known to be regulated by complex pathways described as cell-cycle checkpoints,⁷⁴ the best known checkpoint being mediated by the tumour-suppressor protein p53.^{75,76} Arrest at different stages of the cell cycle may indicate the perturbation of different checkpoint processes, enabling comparison of the mechanisms of action.

Arrest in G2/M suggests that DNA replication is able to proceed as normal (since S phase is not arrested) however, once replicated, the cells may be unable to separate successfully during cytokinesis, therefore preventing cell cycle progression into G2/M. It may be that compound treatment inhibits some process involving the newly-replicated DNA, such as spindle formation or separation of the chromosomes during mitosis. One such example, is that of paclitaxel (Taxol), a chemotherapy drug used to treat various cancers including ovarian, breast and non-small cell lung carcinoma. Taxol-treated cells have defects in mitotic spindle disassembly, inhibiting chromosome segregation and cell division, ultimately triggering apoptosis or reversion to the G-phase without cell division.

2.12 Cell uptake and localisation

2.12.1 Inductively coupled plasma mass spectrometry

Inductively coupled plasma mass spectrometry (ICP-MS) is a highly sensitive analytical technique used for elemental determinations. Detection limits below parts per billion levels (sub-ppb) are routinely achieved for most elements. This technique can therefore be utilised to determine the cellular uptake of metal complexes *in vitro*.

Implementation of a suitable cell fractionation procedure prior to analysis can further enable cellular localisation to be determined.

2.12.2 Cell uptake results

To enable direct comparison between samples, cells were treated with a single concentration of compound for a single time period and the quantity of either platinum or palladium analysed by ICP-MS. A period of 3 hours incubation was chosen, since platinum compounds have been shown to enter the cell environment relatively quickly, in a couple of hours in some cases.⁷⁷ Cells were treated with 20 μ M compound. This concentration was selected because it was deemed high enough to ensure cell uptake took place in the 3 hour timeframe, whilst avoiding the premature cell death that would inevitably occur with higher concentrations and therefore prevent accurate analysis.

Following compound treatment, samples were processed to isolate nuclear and cytoplasmic fractions, with the uptake in these portions compared to whole cell uptake. Untreated control samples and cisplatin-treated samples were prepared for comparison. The elemental concentration in parts per billion for one set of samples is detailed in Table 2.12.2-1 and displayed in Figure 2.12.2-1.

Compound	Concentration (parts per billion)					
	Pt			Pd		
	whole cell	cytoplasmic fraction	nuclear fraction	whole cell	cytoplasmic fraction	nuclear fraction
Control	< 0.05	0.08	0.08	< 0.2	< 0.2	< 0.2
[Pd(<i>i</i> -biq) ₂](BF ₄) ₂	-	-	-	2.31	1.14	1.40
[Pt(<i>i</i> -biq) ₂](PF ₆) ₂	2.66	1.02	2.34	-	-	-
cisplatin	1.00	0.79	0.20	-	-	-

Table 2.12.2-1 Evaluation of cell uptake and localisation following treatment of [Pd(*i*-biq)₂](BF₄)₂, [Pt(*i*-biq)₂](PF₆)₂, and cisplatin using ICP-MS. A2780 cells were treated with 20 µM compound for 3 hours prior to obtaining palladium and platinum concentrations. Values are from one independent experiment.

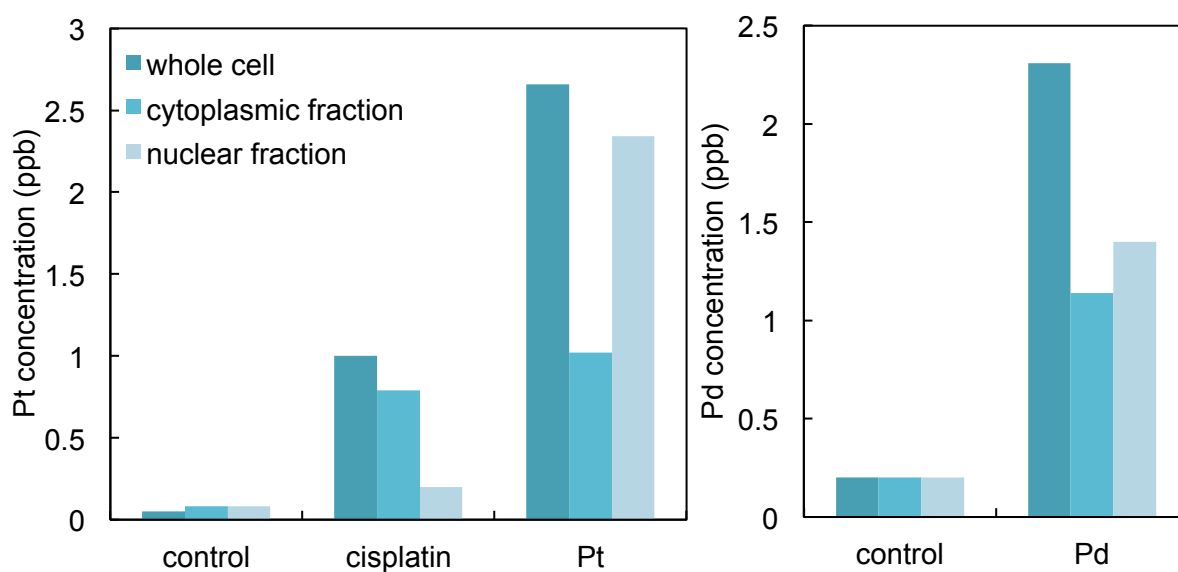


Figure 2.12.2-1 Evaluation of cell uptake and localisation following treatment of [Pd(*i*-biq)₂](BF₄)₂, [Pt(*i*-biq)₂](PF₆)₂, and cisplatin using ICP-MS. A2780 cells were treated with 20 µM compound for 3 hours prior to obtaining palladium and platinum concentrations. Values are from one independent experiment.

It is immediately evident that the concentration of both palladium and platinum present in treated cells is much greater than that present in untreated control cells. Regarding platinum, it is exciting to observe a greater concentration of platinum in cells following treatment with compound **(8)** compared to cisplatin. The ability to achieve cell uptake exceeding that of one of the most widely used and effective chemotherapeutic drugs is potentially very important and reflects the increased cytotoxicity observed for this compound (compared to cisplatin). In addition to exhibiting approximately 2.6-fold greater uptake across the whole cell, it is encouraging to examine the distribution. Whilst the majority of internalised cisplatin is located in the cytoplasmic fraction (~80%), with only a small proportion finding its way into the nucleus (~20%), platinum complex **(8)** shows a much higher localisation in the nuclear fraction demonstrating improved nuclear uptake. The palladium complex **(7)** shows greater uptake than the platinum complex (see Appendix B for data analysis quantifying the approximate concentration (μM) inside cells), with the majority of complex again localised in the nucleus. It is worth noting that this data was recorded at a relatively early time point (3 hours exposure) and that the distribution may change over time.

In light of the intended cellular target of these complexes, namely G-quadruplex forming regions of DNA, and their nuclear location within the cell environment, it is very promising to see increased overall cellular uptake coupled with improved nuclear uptake. These observations also account for the improved cytotoxicity (lower IC_{50} values) of these compounds compared to cisplatin (which also has non-nuclear DNA targets) (see 2.9.2), whereby their increased whole cell and nuclear localisation permits enhanced complex-DNA interaction.

In theory, the sum of the elemental concentration in the nuclear and cytoplasmic fractions should total the concentration observed in the whole cell portion. Whilst this is observed for both the palladium complex **(7)** and cisplatin, it is not the case for the platinum complex **(8)** analysed, where the two fractions combined exceed the concentration detected in the whole cell.

Since the overall and cytoplasmic uptake is comparable (within the same order of magnitude based on a single set of data) for both complexes, it is suggested that the recorded nuclear concentration of platinum is higher than the actual value, which is proposed to be similar to the nuclear concentration of palladium. Repeat measurements would enable mean and error values to be calculated, which would be highly beneficial in corroborating this theory, with the expectation that the concentration of platinum in the nuclear fraction would decrease to approximately the proportion of palladium observed in palladium-treated cells.

It is regrettable that only a single set of ICP-MS data was available for inclusion in this thesis. Disappointingly, due to the breakdown of the ICP-MS instrument, a further two sets of samples currently await analysis. Consequently, the initial conclusions discussed herein are preliminary in nature, with completion of the outstanding analysis certainly required before reliable conclusions can be drawn. Nevertheless, the early indication that substantial cellular uptake and nuclear localisation is occurring following treatment with either complex is very promising and supports the ongoing study of these exciting new compounds.

2.13 Part II: Conclusions

Both metal-biisoquinoline compounds have shown cytotoxicity exceeding that of cisplatin against A2780 cells, following a 24-hour incubation period. Demonstrating IC_{50} values in the low micromolar range, the palladium compound shows approximately 2.5-fold greater activity than the platinum complex in this cell line. Cell uptake studies demonstrated the ability of both complexes to successfully enter the cell, accumulating in the nucleus in approximately 7-fold greater concentration than that observed for cisplatin. This is highly likely to contribute to the improved cytotoxicity observed for these complexes. Furthermore, there is preliminary evidence of increased cell uptake and localisation of the palladium complex, which would account for its increased cytotoxicity, although this difference requires future validation and analysis for its significance through repeat experiments and statistical analysis.

Both compounds display some evidence of genotoxicity, as indicated by the occurrence of DNA double-strand breaks following treatment. Comparable levels of DSBs were observed for both complexes upon treatment at their respective IC_{50} concentrations. Further investigation into the incidence of single strand breaks would be beneficial. In contrast to the characteristic S phase cell cycle arrest induced as a result of cisplatin treatment, cells overwhelmingly undergo G2/M phase arrest upon exposure to very low concentrations of both complexes ($<1 \mu M$).

The observed similarities between the two complexes indicate a similar mechanism of action within cells, resulting in comparable outcomes.

2.14 Experimental materials and methods

2.14.1 General chemistry

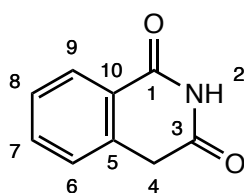
Reagents and solvents were obtained from Sigma Aldrich, Fisher Scientific, Scientific Lab Supplies, Acros Organics and VWR. All solvents were of standard grade and were used without purification. Unless otherwise stated, all reactions were carried out under standard conditions (298 °K, 1 atm pressure).

2.14.2 Analytical characterisation techniques

All characterisation techniques were conducted within the School of Chemistry at the University of Birmingham. Nuclear Magnetic Resonance (NMR) spectra were recorded in deuterated CDCl_3 , CD_3CN , CD_3OD and d_6 -DMSO. ^1H -NMR spectra were recorded on a Bruker AV(III)300 and AV(III)400 instruments, operating at 300 and 400 MHz respectively. ^{13}C -NMR spectra were recorded on a Bruker AV(III)400 instrument operating at 100 MHz. Electrospray Ionisation Mass Spectrometry (ESI-MS) spectra were carried out by Dr. Chi Tsang and Dr. Peter Ashton (Analytical Facility). Spectra were recorded on a Waters LCT Time of Flight Spectrometer. UV-Visible (UV-Vis) spectra were recorded on a Varian Cary 5000 spectrometer.

2.14.3 Chemical synthesis

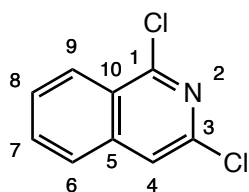
Isoquinoline-1,3-dione (1)



Homophthalic acid (15.0 g, 82.5 mmol) was dissolved in 1,2-dichlorobenzene (70 mL) by heating to 200 °C. Following the removal of the condenser, concentrated NH_4OH (10 mL) was added cautiously to the solution dropwise over a period of 1 h. The reaction was heated for a further 30 minutes, allowing some solvent to evaporate. Upon cooling to room temperature, MeOH (70 mL) was added and the mixture left to stand for 3 h. The precipitate was collected by filtration, washed with MeOH and dried under reduced pressure to afford **(1)** as peach shards (11.4 g, 86%).

^1H NMR (300 MHz, d_6 -DMSO): δ 11.32 (1H, s, $\text{NH}_{(2)}$), 8.02 (1H, d, $J = 6.0$, $\text{H}_{(9)}$), 7.64 (1H, t, $J = 6.0$, $\text{H}_{(7)}$), 7.45 (1H, t, $J = 6.0$, $\text{H}_{(8)}$), 7.38 (1H, d, $J = 6.0$, $\text{H}_{(6)}$), 4.03 (2H, s, $\text{H}_{(4)}$). ^{13}C NMR (100 MHz, d_6 -DMSO): δ 171.0, 165.3, 136.6, 133.5, 127.9, 127.4, 127.2, 124.9, 35.9. m/z (ESI +): 162 ($[\text{C}_9\text{H}_7\text{O}_2\text{N} + \text{H}]^+$).

1,3-dichloroisoquinoline (2)



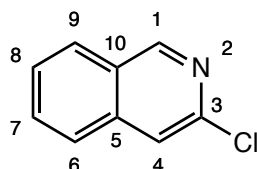
Phenylphosphonic dichloride (22.0 mL, 155 mmol) was added to **(1)** (11.0 g, 68.7 mmol) and the solution heated at 160 °C under reflux for 3 h. The reaction was left to cool to room temperature before leaving to stand for 3 h. The yellow solid which formed was dissolved in THF (345 mL) and water (105 mL) and the solution concentrated *in vacuo* to remove the THF. The remaining aqueous slurry was neutralized with concentrated NH_4OH before being extracted with EtOAc. The organic phases were combined, washed with water and brine, and dried over Na_2SO_4 .

before being concentrated *in vacuo* to afford **(2)** as yellow powdery solid (11.5 g, 85%).

^1H NMR (300 MHz, d_6 -DMSO): δ 8.27 (1H, d, J = 9.0, $\text{H}_{(9)}$), 8.13 (1H, s, $\text{H}_{(4)}$), 8.07 (1H, d, J = 8.7, $\text{H}_{(6)}$), 7.94 (1H, t, J = 8.9, $\text{H}_{(7)}$), 7.83 (1H, t, J = 8.9, $\text{H}_{(8)}$).

^{13}C NMR (100 MHz, d_6 -DMSO): δ 224.3, 149.6, 132.8, 129.8, 126.9, 125.7, 120.4, 100.5, 77.2. m/z (ESI +): 198 ($[\text{C}_9\text{H}_5\text{Cl}_2\text{N}]^+$).

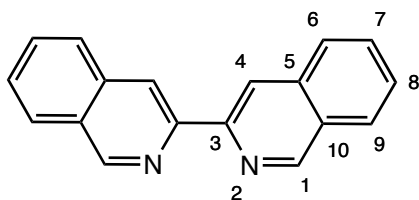
3-chloroisoquinoline (**3**)



A mixture containing **(2)** (10.0 g, 50.5 mmol), red phosphorus (3.44 g, 111 mmol) and a solution of hydriodic acid (21 mL) in acetic acid (50 mL) was heated at 125 °C under reflux for 24 h. The red-brown reaction mixture was cooled to room temperature and poured onto ice, and the resulting solution neutralised to pH 7 by the addition of conc. NaOH solution. The solution was extracted with DCM (2 \times 300 mL), and the organic phases combined and filtered before being dried over MgSO_4 and concentrated *in vacuo*. The residue was purified by column chromatography on silica gel, eluting with EtOAc:hexane (9:1) to afford **(3)** as yellow solid (2.54 g, 30%).

^1H NMR (300 MHz, d_6 -DMSO): δ 9.23 (1H, s, $\text{H}_{(1)}$), 8.19 (1H, d, J = 9.0, $\text{H}_{(9)}$), 8.06 (1H, s, $\text{H}_{(4)}$), 7.97 (1H, d, J = 9.0, $\text{H}_{(6)}$), 7.81 (1H, t, J = 9.0, $\text{H}_{(7)}$), 7.72 (1H, t, J = 9.0, $\text{H}_{(8)}$). ^{13}C NMR (100 MHz, d_6 -DMSO): δ 153.0, 144.5, 137.3, 131.7, 127.9, 127.7, 127.1, 125.8, 119.5. m/z (ESI +): 164 ($[\text{C}_9\text{H}_6\text{ClN} + \text{H}]^+$).

3,3-biisoquinoline (**4**)



Operating under an argon atmosphere $[\text{NiCl}_2 \cdot 6\text{H}_2\text{O}]$ (247 mg, 1.04 mmol), PPh_3 (1.09 g, 4.16 mmol) and zinc dust (washed in dilute HCl, dd. H_2O , EtOH, acetone and Et_2O ; 73.1 mg, 1.10 mmol) were added to a Schlenk tube. DMF (12 mL) was then added *via* syringe into the sealed vessel. The brick-red solution that formed upon heating to 70°C was left to stir for 1 h. Aryl halide (see *below*, 1.04 mmol) dissolved in DMF (6 mL) was then added and the mixture left to heat at 70°C for a further 4 h. After heating, and when the reaction returned to its original green colour, the mixture was cooled to room temperature and poured onto 7% NH_4OH (18 mL). A small amount of concentrated NH_4OH was added to ensure complete precipitation of the product. The product was extracted into 2:1 DCM: Et_2O (3×60 mL) before removal of the organic solvent *in vacuo*. The remaining yellow-orange oil was diluted with DCM (40 mL) and the solution washed with water (4×13 mL) and brine (26 mL) before drying over MgSO_4 and removing the solvent *in vacuo* to yield pale yellow solid. Purification was achieved by column chromatography on silica gel, eluting the impurities with DCM and the product with EtOAc to afford (**4**) as pale yellow solid.

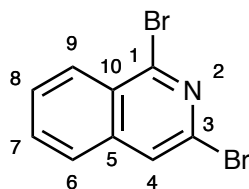
Ar-X: (**3**), 3-chloroisoquinoline (170 mg, 1.04 mmol): (38.7 mg, 15%).

Ar-X: (**6**), 3-bromoisoquinoline (215 mg, 1.04 mmol): (63.0 mg, 24%).

^1H NMR (300 MHz, d_4 -MeOD): δ 9.39 (2H, s, $\text{H}_{(1)}$), 8.84 (2H, s, $\text{H}_{(4)}$), 8.14 (2H, d, $J = 8.1$, $\text{H}_{(9)}$), 8.08 (2H, d, $J = 8.1$, $\text{H}_{(6)}$), 7.83 (2H, t, $J = 7.0$, $\text{H}_{(7)}$), 7.75 (2H, t, $J = 7.0$, $\text{H}_{(8)}$). ^{13}C NMR (100 MHz, d_4 -MeOD): δ 167.3, 164.0, 153.6, 138.2, 132.4, 129.2,

128.9, 128.6, 119.2. m/z (ESI +): 257 ($[C_{12}H_{18}N_2 + H]^+$).

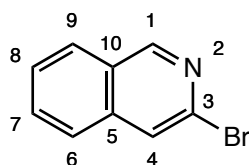
1,3-dibromoisquinoline (5)



Operating under an argon atmosphere, phosphorus oxybromide (11.6 g, 41.0 mmol) was dissolved in 1,4-dioxane (42 mL) at room temperature. **(1)** (3.00 g, 18.7 mmol) was added in small portions over 5 minutes under a strong flow of argon (no stirring during addition) and the solution then heated at 120 °C under reflux for 35 minutes. The reaction solution was cooled, dissolved in $CHCl_3$ (150 mL) and MeOH (25 mL) and the solvent removed *in vacuo* until solid formed. The resulting yellow crystals were collected by vacuum filtration, washed with 2-propanol, and dried at 50 °C to yield **(5)** as off-white solid (3.26 g, 61%).

1H NMR (300 MHz, $CDCl_3$): δ 8.26 (1H, d, J = 9.1, $H_{(9)}$), 7.87 (1H, s, $H_{(4)}$), 7.70-7.77 (3H, m, $H_{(6-8)}$). ^{13}C NMR (100 MHz, $CDCl_3$): δ 144.1, 138.9, 132.7, 132.1, 128.9, 127.9, 127.6, 126.2, 124.2. m/z (ESI +): 288 ($[C_9H_5Br_2N] + H]^+$).

3-bromoisquinoline (6)

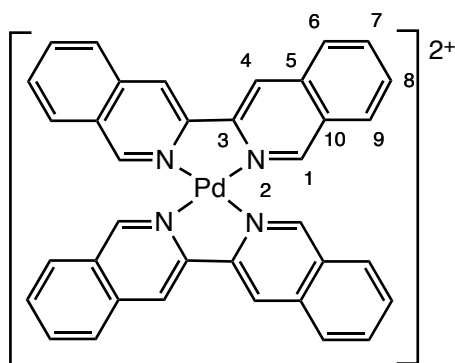


A mixture of **(5)** (5.91 g, 20.6 mmol), red phosphorus (1.40 g, 45.3 mmol) and a solution of hydriodic acid (6.50 mL) in acetic acid (25 mL) was heated at 125 °C under reflux for 24 h. The red-brown reaction mixture was cooled to room temperature and poured onto ice, and the resulting solution neutralised to pH 7 by the addition of conc. NaOH solution. The solution was extracted with DCM (2 × 300 mL), and the organic phases combined and filtered to remove insoluble material, before being dried over MgSO₄ and concentrated *in vacuo*. The red-brown residue was purified by column chromatography on silica gel, eluting with DCM:MeOH (9:1) to afford **(6)** as pale yellow solid (2.42 g, 57%).

¹H NMR (300 MHz, CDCl₃): δ 9.04 (1H, s, H₍₁₎), 7.97 (1H, d, *J* = 9.0, H₍₉₎), 7.91 (1H, s, H₍₄₎), 7.75 (2H, d, *J* = 9.1, H₍₆₎), 7.72 (2H, t, *J* = 9.3, H₍₇₎), 7.63 (1H, t, *J* = 9.4, H₍₈₎).

¹³C NMR (100 MHz, CDCl₃): δ 152.7, 137.8, 135.8, 131.3, 127.7, 127.6, 127.5, 125.6, 123.7. *m/z* (ESI +): 208 ([C₉H₆BrN + H]⁺).

[Pd(*i*-biq)₂](BF₄)₂ (**7**)

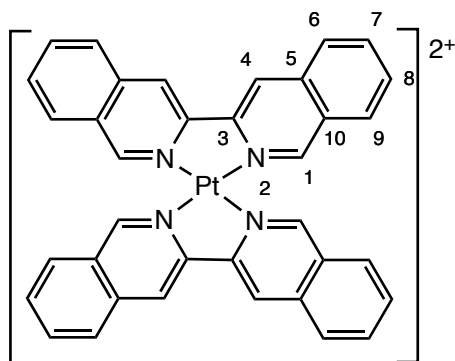


Under an argon atmosphere, *i*-biq **(4)** (5.00 mg, 19.0 μmol) was dissolved in dry acetonitrile (3 mL). Tetrakis(acetonitrile)palladium(II) tetrafluoroborate (4.50 mg, 10.0 μmol) was then added under a strong flow of argon and the solution stirred overnight

at room temperature. The solution was filtered through a fine filter membrane and the filtrate concentrated *in vacuo* to form a yellow solid. The solid was washed with chloroform (2 mL), acetone (2 mL) and diethyl ether (2 mL) and left to dry under vacuum to yield $[\text{Pd}(i\text{-biq})_2](\text{BF}_4)_2$ as bright yellow solid (5.00 mg, 64%).

^1H NMR (300 MHz, CD_3CN): δ 9.56 (4H, s, $\text{H}_{(1)}$), 9.07 (4H, s, $\text{H}_{(4)}$), 8.50 (4H, d, J = 8.0, $\text{H}_{(9)}$), 8.36 (4H, d, J = 8.0, $\text{H}_{(6)}$), 8.21 (4H, t, J = 7.0, $\text{H}_{(7)}$), 8.05 (t, 4H, J = 7.1, $\text{H}_{(8)}$). m/z (ESI $+$): 309 ($[\text{Pd}(\text{C}_{18}\text{H}_{12}\text{N}_2)_2]^{2+}$), 618 ($[\text{Pd}(\text{C}_{18}\text{H}_{12}\text{N}_2)_2]^+$), 637 ($[\text{Pd}(\text{C}_{18}\text{H}_{12}\text{N}_2)_2\text{F}]^+$), 653 ($[\text{Pd}(\text{C}_{18}\text{H}_{12}\text{N}_2)_2\text{Cl}]^+$). UV-Vis (15 % DMSO:85 % milliQ water): λ_{max} (nm) ($\epsilon_{\text{max}}/\text{dm}^3\text{mol}^{-1}\text{cm}^{-1}$): 251 (95600), 305 (31600), 328 (27500), 370 (16400).

$[\text{Pt}(i\text{-biq})_2][\text{PF}_6]_2$ (**8**)

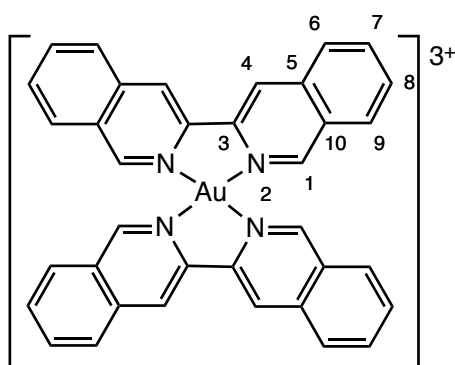


Potassium tetrachloroplatinate (4.50 mg, 10.0 μmol) was dissolved in water (5 mL) before the addition of a suspension of *i*-biq (**4**) (5.50 mg, 20.0 μmol) in acetonitrile (5 mL). The mixture was heated under reflux (105 $^\circ\text{C}$) overnight, resulting in a yellow solution which was hot filtered through a fine membrane. A methanolic solution of NH_4PF_6 (slight excess 0.15 mmol) was then added to the filtrate, resulting in the immediate precipitation of an off-white solid. The product was collected by filtration

and carefully washed with chloroform (2 mL), methanol (2 mL) and diethyl ether (2 mL) before drying under vacuum to afford $[\text{Pt}(i\text{-biq})_2][\text{PF}_6]_2$ as pale cream solid (2.80 mg, 29%).

^1H -NMR (300 MHz, CD_3CN): δ 9.56 (4H, s, $\text{H}_{(1)}$), 9.07 (4H, s, $\text{H}_{(4)}$), 8.50 (4H, d, J = 8.1, $\text{H}_{(9)}$), 8.36 (4H, d, J = 8.2, $\text{H}_{(6)}$), 8.21 (4H, t, J = 7.4, $\text{H}_{(7)}$), 8.05 (4H, t, J = 7.2, $\text{H}_{(8)}$). m/z (ESI +): 353 ($[\text{Pt}(\text{C}_{18}\text{H}_{12}\text{N}_2)_2]^{2+}$), 743 ($[\text{Pt}(\text{C}_{18}\text{H}_{12}\text{N}_2)_2\text{Cl} + \text{H}]^+$). UV-Vis (15 % DMSO:85 % milliQ water): λ_{max} (nm) ($\epsilon_{\text{max}}/\text{dm}^3\text{mol}^{-1}\text{cm}^{-1}$): 262 (72400), 335 (19300), 382 (13000).

$[\text{Au}(i\text{-biq})_2](3\text{Cl})$ (**9**)



A mixture of sodium tetrachloroaurate(III) dihydrate (3.90 mg, 9.70 μmol) and *i*-biq (**4**) (5.00 mg, 19.5 μmol) in MeOH (10 mL) was heated under reflux (90 $^\circ\text{C}$) overnight. The resulting yellow solution was hot filtered through a fine membrane and reduced *in vacuo* to yield dark yellow-orange solid. Following careful washing with DCM and drying under vacuum, tan solid remained (4.70 mg, 59%).

^1H -NMR (300 MHz, MeOD): δ 10.32 (4H, s, $\text{H}_{(1)}$), 9.37 (4H, s, $\text{H}_{(4)}$), 8.63 (4H, d, J = 8.4, $\text{H}_{(9)}$), 8.38 (4H, d, J = 8.2, $\text{H}_{(6)}$), 8.28 (4H, t, J = 7.8, $\text{H}_{(7)}$), 8.11 (4H, t, J = 7.5, $\text{H}_{(8)}$). m/z (ESI +): 488 ($[\text{Au}(\text{C}_{18}\text{H}_{12}\text{N}_2)(\text{OH})_2 + \text{H}]^+$), 709 ($[\text{Au}(\text{C}_{18}\text{H}_{12}\text{N}_2)_2]^+$).

2.14.4 ESI-MS nucleotide binding studies

9-ethylguanine (9EG) was stored at 4 °C in a dessicator and freshly dissolved in sodium cacodylate buffer (1 mM, pH 6.8) before each experiment. 9-methyladenine (9MA), 1-methylcytosine (1MC), 1-methylthymine (1MT) and 9-methylguanine (9MG) were stored at 4 °C in a dessicator and freshly dissolved in DMSO (1 mM) before each experiment. A solution of all four bases was prepared in DMSO (1 mM). Stock solutions of both palladium (**7**) and platinum (**8**) complexes in DMSO were prepared. Equal volumes of nucleobase and complex solutions were added together, to mix complex and nucleobase(s) in 1:1 ratio. The solutions were incubated at 37 °C in the dark for 72 h. ESI-MS spectra were recorded periodically. ESI-MS spectra of solvent control samples (buffer, buffer + DMSO, buffer + base, buffer + base + DMSO) were also recorded, to account for peaks arising from solvent effects.

2.14.5 General cell culture

Preparation of complete media

Cells were cultured in GIBCO® Roswell Park Memorial Institute (RPMI-1640) media supplemented with foetal bovine serum, FBS (10% v/v), penicillin (100 U/mL), streptomycin (100 ug/mL) and L-glutamine (2 mM), along with antimetabolic solution (1 % v/v, 1×). Complete media was stored at 4 °C and warmed to 37 °C in a water bath before use.

Cell line thawing and initiation

The A2780 human ovarian carcinoma cell line was obtained from ECACC (European Collection of Cell Cultures). Cryovials containing cells were removed from liquid nitrogen storage and quickly thawed in a water bath (37 °C) before immediate transfer of the contents to a 75 cm³ tissue culture flask (T₇₅, Corning Costar) containing warm complete media (20 mL). Cultures were incubated at 37 °C in 5% CO₂, 95% air (Sanyo, MCO-17A) for 6 hours to allow cell adhesion. Due to the presence of DMSO in the media from the cryopreservation process, a media change must be carried out as soon as adhesion has occurred.

Cell passage

Upon reaching 80% confluency, cells were passaged (approximately twice weekly). Complete RPMI-1640 media, phosphate buffered saline (PBS, 0.01 M) and trypsin-EDTA (1×) were warmed to 37 °C in a water bath. Media was removed from the T₇₅ flask and PBS added (10 mL). The flask was tilted back and forth to ensure the entire surface was thoroughly washed to remove dead cells and cell debris. The PBS was removed and trypsin-EDTA (3 mL) added, followed by incubation at 37 °C for 5 minutes. To ensure cell detachment, flasks were gently tapped and checked under the microscope to confirm detachment of the cell monolayer before proceeding. Fresh media (10 mL) was then added to inhibit the trypsin-EDTA. Following thorough rinsing of the flask surface, the cell suspension was transferred to a 15 mL falcon tube. Cells were collected by centrifugation (Rotofix 32, Hettich Zentrifugen, Germany) at 1500 rpm for 5 minutes at room temperature. The supernatant was discarded, with the cell pellet resuspended in 1 mL complete media, before aliquoting

into new T₇₅ flasks.

Cell counting

To enable accurate and uniform cell seeding across wells, cells were counted using a Neubauer haemocytometer. Following resuspension of the cell pellet in 1 mL fresh media, 10 µL of this cell suspension was added to 90 µL PBS in an eppendorf (1:10 dilution). 10 µL of this mixture was pipetted underneath each side of the coverslip placed onto the haemocytometer slide. Viewed under a microscope (10× objective lens), cells present in two of the grids on each end of the haemocytometer were counted and averaged (Note. Cells positioned along the top and left hand edges were included in the count, with cells falling along the bottom and right edges excluded). The number of cells per millilitre was calculated using the following equation:

$$\text{Cell density (cells/mL)} = \text{Average number of cells counted} \times \text{dilution factor (10)} \times 10^4$$

Multiplication of this value by both the desired number of cells per well and the number of wells to be seeded gives a required volume (mL), allowing a media-cell suspension to be made up. This mixture can then be equally aliquoted out between all wells to ensure an even distribution of cells.

Cryopreservation of cell line

To ensure a stock of viable cells was maintained for future use, low passage confluent cultures were cryopreserved. Cells were collected and the cell pellet resuspended in freezing medium (3 mL, 10% v/v DMSO in FBS) and 1 mL aliquots

transferred to cryovials (Nunc). Following overnight storage in a freezer (-80 °C), cryovials were transferred to vapour phase liquid nitrogen for long term storage.

2.14.6 MTT assay for cell viability

Thiazolyl blue tetrazolium bromide (MTT) and Hybriderm-DMSO were obtained from Sigma, UK. Cells were seeded into 96 well microtiter plates (Corning Costar) at 4,000 cells per well, with a total volume of 100 μ L complete media cell suspension in each well. The plates were incubated for 24 hours before treatment to allow cell adhesion to the well base. The two bisisoquinoline complexes required DMSO to aid solubility. The volume of DMSO per well did not exceed 2 % v/v. Cisplatin was dissolved in complete media alone. Eight different concentrations were tested for each compound. Compound treatments were made up into 100 μ L total volume (at twice the desired treatment concentration to account for the dilution) before addition to the 100 μ L cell solution already in the wells. Two control lanes (B and K) were prepared by treating with complete media alone (B5-8 and K5-8) or 2 % DMSO/98 % complete media as a vehicle control (B1-4 and K1-4). Each test was run in quadruplicate and repeated three times. The treated plates were returned to the incubator for 24 hours. The cell viability was determined by adding 20 μ L of a 5 mg/mL MTT solution in PBS to each well (final concentration 0.5 mg/mL), excluding one set of control wells (K1-8), followed by a further 2 hours incubation. The medium was carefully removed by aspiration from all wells, before washing with PBS (200 μ L) followed by the addition of 200 μ L DMSO to all wells to dissolve the purple formazan crystal product. The plates were rocked for 2 hours before the absorbance was measured at 590 nm using a microplate reader (BioRad). Plotting the absorbance values measured versus

the concentration of treatment allows the IC₅₀ to be determined.

2.14.7 Neutral comet assay for DNA double strand breaks

Cells were seeded into a 12 well plate (Corning Costar) at 80,000 cells per well, with a total volume of 800 µL complete media cell suspension in each well. The plates were incubated for 24 hours before treatment to allow cell adhesion to the well base. Both biisoquinoline complexes required DMSO to aid solubility. The volume of DMSO per well did not exceed 2% total. Cisplatin was directly dissolved in complete media and further diluted. Three different concentrations were tested for each compound. Compound treatments were made up into 800 µL total volume in media, which was added fresh into wells following removal of the seeding media and a single wash with PBS (500 µL). Control wells received fresh complete media. Treated plates were returned to the incubator for 24 hours. Following removal of media, cells were washed with 1 ml PBS and collected by scraping into 300 µL PBS before transferring into eppendorfs and centrifuging at 13000 rpm for 5 minutes. Cell pellets were resuspended in 80 µL PBS. An aliquot of resuspended cells (15 µL) was placed into a sterile tube containing 150 µL low melting point agarose (0.5% w/v LMPA warmed for 1 minute in the microwave, 600 W) and aspirated to aid mixing. A portion of this cell suspension (150 µL) was then transferred to coat a glass microscope slide (VWR International), precoated with normal melting point agarose (0.5% w/v NMPA). Glass coverslips were added to the slides before placing them on a metal tray over ice for 20 minutes to solidify. Coverslips were removed (horizontal sliding away from the gel surface) and the slides incubated at 4 °C for 1 hour in a Coplin jar containing lysis buffer (146 mM NaCl, 30 mM Na₂EDTA, 1 mM Tris-HCl, 1% sodium N-lauryl

sarcosinate, pH 9). Following lysis, slides were transferred to a horizontal electrophoresis tank containing cold electrophoresis buffer (0.4 M Tris base, pH 8.3) for 20 minutes in the dark to allow DNA unwinding to occur. DNA was then subjected to electrophoresis (32 V) for a further 20 minutes. Slides were removed from the tank and washed three times (5 minutes) with neutralisation buffer (0.4 M Tris base, adjusted to pH 7.5 with HCl) and once with dH₂O. Slides were subsequently stained with 75 µL/slide SYBR Gold solution (Invitrogen 1 µL/mL in dH₂O) before addition of a coverslip and overnight incubation at 4 °C in a moist box in the dark. The slides were examined on a Zeiss Axiovert 10 inverted fluorescence microscope (Zeiss Ltd, Gottingen, Germany) fitted with a 515-560 nm excitation filter and a 590 nm barrier filter. A USB digital camera (Merlin, Allied Vision Technologies) received the images, which were analysed using a computer-based image analysis system, Comet Assay IV (Perceptive Instruments). One hundred randomly selected nuclei were scored and analysed per slide. Median percentage tail intensity was the parameter chosen for assessing the extent of DNA damage. For each condition tested, median values were obtained from three independent experiments and analysed.

2.14.8 Flow cytometry (inc. PI staining) for cell cycle analysis

Cells were seeded into a 6 well plate (Corning Costar) at 300,000 cells per well, with a total volume of 2 mL complete media cell suspension in each well. The plates were incubated for 24 hours before treatment to allow cell adhesion to the well base. Both bisoquinoline complexes required DMSO to aid solubility. The volume of DMSO per well did not exceed 2% v/v. Cisplatin was dissolved in complete media. Two different concentrations were tested for each compound. Compound treatments were made

up into 2000 μ L total volume in media, which was added fresh into wells following removal of the seeding media. Two control wells received fresh media alone. Each test was repeated two or three times. The treated plates were returned to the incubator for 24 hours. Each well was washed with 2 mL PBS following removal of media. Cells were collected following the standard trypsin-EDTA protocol and the cell pellet washed with 2 mL PBS. The cell pellet was vortexed gently to prevent aggregation, as 3 mL ice cold 70% ethanol was carefully added dropwise. The sample was then placed on ice for 30 min. Fixed cells were stored at 4 °C overnight. Cells were centrifuged at 1500 rpm for 5 mins (ensuring a visible pellet is observed). Following careful aspiration of the supernatant, the pellets were washed with 3 mL PBS before being resuspended in 500 μ L PBS. Samples were treated with RNase A solution

(50 μ L, 1 mg/mL) and propidium iodide (10 μ L, 1 mg/mL) and incubated at room temperature for 30 min in the dark. Samples were mixed (vortex mixer) for 10 seconds before analysis. Propidium iodide has a maximum emission of 605 nm.

2.14.9 Inductively coupled plasma mass spectrometry for cell uptake

Cells were seeded into 25 cm³ flasks, T₂₅ (Corning Costar) at 2,000,000 cells per well, with a total volume of 3 mL complete media cell suspension in each. Flasks were incubated for 24 hours before treatment to allow cell adhesion to the flask surface. Both biisoquinoline complexes required DMSO to aid solubility. The volume of DMSO per well must not exceed 2% v/v total. Cisplatin was dissolved in complete media. A single concentration was tested for each compound, for a single time period. Compound treatments were made up into 3 mL media and administered to

flasks following the removal of the seeding media and washing with PBS. The control flask received fresh media alone. Flasks were returned to the incubator for 3 hours, after which time the media was removed and the flask washed three times with PBS (5 mL) to remove any excess compound not taken up into cells. Cells were collected following the standard trypsin-EDTA protocol and the cell pellet isolated following removal of the supernatant. Following resuspension in 1 mL media, the pellet was split into two 500 µL aliquots, each containing approximately 1 million cells. The first aliquot was pelleted and washed twice with PBS (200 µL), before resuspension in 200 µL PBS ready for whole cell digestion. The second aliquot was processed to enable separation and isolation of the nuclear and cytoplasmic fractions. This was achieved using a Nuclear/Cytosol Fractionation Kit (BioVision Inc, Catalog K266-25), following the protocol accompanying the kit (Appendix: A). Upon collecting the three fractions (whole cell, nuclear and cytoplasmic), concentrated (69%) nitric acid (200 µL) was added to all samples except those containing palladium, to which aqua regia (3:1 HCl (32%):HNO₃ (69%), 42% acid total, 200 µL) was added as an alternative. Samples were transferred to vials¹ (3 mL screw-top V-Vials® with solid-top cap, Sigma) and left overnight to digest at 80 °C in an oven. Each sample was diluted with an appropriate volume of milliQwater to bring the final acid concentration down to 2%.² Samples were stored in plastic falcon tubes at 4 °C before analysis.

¹ The use of V-vials® ensures there is no loss of acid due to evaporation during the

² The ICP-MS instrument cannot withstand higher concentrations of acid in the system

2.14.10 Statistical analysis of data

Completed by Dr. N. Hodges

Statistical analysis of data was carried out where possible ($n \geq 3$) using SPSS statistics 20. Parametric statistics were used for normally distributed data showing homogeneity of variances (One-way ANOVA with Post-hoc: Tukey test).

2.15 References

- 1 E. Largy, F. Hamon, F. Rosu, V. Gabelica, E. De Pauw, A. Guédin, J. Mergny and M. Teulade-Fichou, *Chem. - A Eur. J.*, 2011, **17**, 13274–13283.
- 2 J. C. Peberdy, J. Malina, S. Khalid, M. J. Hannon and A. Rodger, *J. Inorg. Biochem.*, 2007, **101**, 1937–45.
- 3 S. Khalid, M. J. Hannon, A. Rodger and P. M. Rodger, *J. Mol. Graph. Model.*, 2007, **25**, 794–800.
- 4 N. H. Campbell, N. H. A. Karim, G. N. Parkinson, M. Gunaratnam, V. Petrucci, A. K. Todd, R. Vilar and S. Neidle, *J. Med. Chem.*, 2012, **55**, 209–22.
- 5 L. Wang, Y. Wen, J. Liu, J. Zhou, C. Li and C. Wei, *Org. Biomol. Chem.*, 2011, **9**, 2648–2653.
- 6 Y. Ma, T.-M. Ou, J.-H. Tan, J.-Q. Hou, S.-L. Huang, L.-Q. Gu and Z.-S. Huang, *Bioorg. Med. Chem. Lett.*, 2009, **19**, 3414–3417.
- 7 C. Bazzicalupi, M. Ferraroni, A. R. Bilia, F. Scheggi and P. Gratteri, *Nucleic Acids Res.*, 2013, **41**, 632–638.
- 8 M. Kato, K. Sasano, C. Kosuge, M. Yamazaki, S. Yano and M. Kimura, *Inorg. Chem.*, 1996, **35**, 116–123.
- 9 H. L. Pritchard, Thesis, University of Birmingham, 2015.
- 10 Abbott Laboratories, US 7335678 B2, 2004.
- 11 J. Clayden Greeves, N., Warren, S., Wothers, P., *Organic Chemistry*, Oxford University Press, 2001.
- 12 M. M. Robison, *J. Am. Chem. Soc.*, 1958, **80**, 5481–5483.
- 13 T. Kametani, K. Fukumoto and G. Grethe, in *Synthetic and Natural Sources of the Isoquinoline Nucleus*, John Wiley and Sons, 1981.
- 14 H. F. Skinner, *Forensic Sci. Int.*, 1990, **48**, 123–134.
- 15 M. Fieser and L. Fieser, *Reagents for Organic Synthesis*, Wiley and Sons, 1967.
- 16 C. Buehler and D. Pearson, *Survey of Organic Synthesis*, Wiley and Sons,

- 1970.
- 17 S. Menor, *A Comprehensive Treatise on Inorganic and Theoretical Chemistry*, Longsman, 1922.
 - 18 P. J. Durrant and B. Durrant, *Introduction to advanced inorganic chemistry*, Longmans Green and Co, 1962.
 - 19 D. Albouy, G. Etemad-Moghadam, M. Vinatoru and M. Koenig, *J. Organomet. Chem.*, 1997, **529**, 295–299.
 - 20 F. Monnier and M. Taillefer, *Angew. Chemie Int. Ed.*, 2009, **48**, 6954–6971.
 - 21 E. Sperotto, G. P. M. van Klink, G. van Koten and J. G. de Vries, *Dalton. Trans.*, 2010, **39**, 10338–10351.
 - 22 D. D. Hennings, T. Iwama and V. H. Rawal, *Org. Lett.*, 1999, **1**, 1205–1208.
 - 23 A. V Aksenov and V. I. Goncharov, *Chem. Heterocycl. Compd.*, 2008, **44**, 1491–1492.
 - 24 J. Hassan, V. Penalva, L. Lavenot, C. Gozzi and M. Lemaire, *Tetrahedron*, 1998, **54**, 13793–13804.
 - 25 US 4263466 A, 1981.
 - 26 B. M. Rosen, K. W. Quasdorf, D. A. Wilson, N. Zhang, A.-M. Resmerita, N. K. Garg and V. Percec, *Chem. Rev.*, 2011, **111**, 1346–416.
 - 27 X. Tao, W. Zhou, Y. Zhang, C. Dai, D. Shen and M. Huang, *Chinese J. Chem.*, 2006, **24**, 939–942.
 - 28 M. Iyoda, H. Otsuka, K. Sato, N. Nisato and M. Oda, *Bull. Chem. Soc. Jpn.*, 1990, **63**, 80–87.
 - 29 O. S. Wolfbeis, I. Trummer and A. Knierzinger, *Liebigs Ann. der chemie*, 1981, **5**, 811–818.
 - 30 M. N. Gitlitz and M. K. Moran, *Tin compounds*, 1983.
 - 31 C. R. Smith, *Synlett*, 2009, **2009**, 1522–1523.
 - 32 M. Sugiura, M. and Nakajima, *Encyclopedia of Reagents for Organic Synthesis, Triphenylphosphine Oxide*, John Wiley & Sons, 2010.
 - 33 Y. Yamamoto and A. Yanagi, *Chem. Pharm. Bull.*, 1982, **30**, 2003–2010.

- 34 J. Hashim and C. O. Kappe, *Adv. Synth. Catal.*, 2007, **349**, 2353–2360.
- 35 Sigma-Aldrich, *Product Specification, Phosphorus(V) oxybromide*, 2001.
- 36 B. Bruni, A. Guerri, G. Marcon, L. Messori and P. Orioli, *Croat. Chem. Acta*, 1999, **72**, 221–229.
- 37 L. Messori, F. Abbate, G. Marcon, P. Orioli, M. Fontani, E. Mini, T. Mazzei, S. Carotti, T. O'Connell and P. Zanello, *J. Med. Chem.*, 2000, **43**, 3541–3548.
- 38 F. Abbate, P. Orioli, B. Bruni, G. Marcon and L. Messori, *Inorganica Chim. Acta*, 2000, **311**, 1–5.
- 39 G. Marcon, T. O. Connell, P. Orioli, L. Messori, U. Florence and G. Capponi, *Met. Based. Drugs*, 2000, **7**, 253–256.
- 40 G. Marcon, S. Carotti, M. Coronello, L. Messori, E. Mini, P. Orioli, T. Mazzei, M. A. Cinellu and G. Minghetti, *J. Med. Chem.*, 2002, **45**, 1672–1677.
- 41 L. Messori, P. Orioli, C. Tempi and G. Marcon, *Biochem. Biophys. Res. Commun.*, 2001, **281**, 352–60.
- 42 M. Coronello, G. Marcon, S. Carotti, B. Caciagli, E. Mini, T. Mazzei, P. Orioli and L. Messori, *Oncol. Res.*, 2000, **12**, 361–70.
- 43 L. Messori, G. Marcon and P. Orioli, *Bioinorg. Chem. Appl.*, 2003, **1**, 177–87.
- 44 S. A. Hofstadler and K. A. Sannes-Lowery, *Nat. Rev. Drug Discov.*, 2006, **5**, 585–595.
- 45 A. Basu and S. Krishnamurthy, *J. Nucleic Acids*, 2010, **2010**, 1–16.
- 46 C. Marzano, F. Bettio, F. Baccichetti, A. Trevisan, L. Giovagnini and D. Fregona, *Chem. Biol. Interact.*, 2004, **148**, 37–48.
- 47 T. Ou, Y. Lu, J. Tan, Z. Huang, K. Wong and L. Gu, *ChemMedChem*, 2008, **3**, 690–713.
- 48 C. A. Puckett, R. J. Ernst and J. K. Barton, *Dalton Trans.*, 2010, **39**, 1159–70.
- 49 ECACC Public Health England, *Cell Collection Detail: A2780*, European Collection of Authenticated Cell Cultures.
- 50 T. Mosmann, *J. Immunol. Methods*, 1983, **65**, 55–63.
- 51 F. Freimoser, C. Jakob, M. Aebi and U. Tuor, *Appl. Env. Microbiol.*, 1999, **65**,

3727–3729.

- 52 J. van Meerloo, G. J. L. Kaspers and J. Cloos, *Methods Mol. Biol.*, 2011, **731**, 237–45.
- 53 D. Wang and S. J. Lippard, *Nat. Rev. Drug Discov.*, 2005, **4**, 307–20.
- 54 M. Read, R. J. Harrison, B. Romagnoli, F. A. Tanious, S. H. Gowan, A. P. Reszka, W. D. Wilson, L. R. Kelland and S. Neidle, *Proc. Natl. Acad. Sci. U. S. A.*, 2001, **98**, 4844–9.
- 55 P. Wu, D. Ma, C. Leung, S. Yan, N. Zhu, R. Abagyan and C. Che, *Chem. Eur. J.*, 2009, **15**, 13008–13021.
- 56 W. Chu, Y. Wang, S. Liu, X. Yang, S. Wang, S. Li, G. Zhou, X. Qin, C. Zhou and J. Zhang, *Bioorg. Med. Chem. Lett.*, 2013, **23**, 5187–91.
- 57 K. Pestell, S. Hobbs, J. Titley and L. Kelland, *Mol. Pharmacol.*, 2000, **57**, 503–511.
- 58 T. Ohnishi, E. Mori and A. Takahashi, *Mutat. Res.*, 2009, **669**, 8–12.
- 59 Y. Jung and S. J. Lippard, *Chem. Rev.*, 2007, **107**, 1387–1407.
- 60 O. Ostling and K. J. Johanson, *Biochem. Biophys. Res. Commun.*, 1984, **123**, 291–8.
- 61 N. P. Singh, M. T. McCoy, R. R. Tice and E. L. Schneider, *Exp. Cell Res.*, 1988, **175**, 184–91.
- 62 W. Liao, M. a McNutt and W. Zhu, *Methods*, 2009, **48**, 46–53.
- 63 E. Peycheva, M. Georgieva and G. Miloshev, *Biotechnol. Biotechnol. Equip.*, 2014, **23**, 1090–1092.
- 64 A. R. Collins, A. A. Osoz, G. Brunborg, I. Gaivão, L. Giovannelli, M. Kruszewski, C. C. Smith and R. Štětina, *Mutagenesis*, 2008, **23**, 143–151.
- 65 L. F. Povirk, *DNA Repair*, 2006, **5**, 1199–212.
- 66 T. Helleday, J. Lo, D. C. van Gent and B. P. Engelward, *DNA Repair*, 2007, **6**, 923–35.
- 67 P. L. Olive and R. E. Durand, *Cytom. Part A*, 2005, **66**, 1–8.
- 68 P. L. Olive and J. P. Banáth, *Cytom. Part B Clin. Cytom.*, 2009, **76**, 79–90.

- 69 M. A. Van Dilla, T. T. Truiullo, P. F. Mullaney and J. R. Coulter, *Science*, 1969, **163**, 1213–1214.
- 70 A. Krishan, *J. Cell Biol.*, 1975, **66**, 188–193.
- 71 R. P. Wersto, F. J. Chrest, J. F. Leary, C. Morris, M. A. Stetler-Stevenson and E. Gabrielson, *Cytometry*, 2001, **46**, 296–306.
- 72 B. Lippert, *Cisplatin: Chemistry and Biochemistry of a Leading Anticancer Drug*, John Wiley & Sons, 1999.
- 73 E. Izbicka, R. T. Wheelhouse, E. Raymond, K. K. Davidson, R. A. Lawrence, D. Sun, B. E. Windle, L. H. Hurley and D. D. Von Hoff, *Cancer Res.*, 1999, **59**, 639–44.
- 74 L. Hartwell and T. Weinert, *Science*, 1989, **246**, 629–634.
- 75 L. Hartwell and M. Kastan, *Science*, 1994, **266**, 1821–1828.
- 76 M. B. Kastan, O. Onyekwere, D. Sidransky, B. Vogelstein and R. W. Craig, *Cancer Res.*, 1991, **51**, 6304–6311.
- 77 S. R. McWhinney, R. M. Goldberg and H. L. McLeod, *Mol. Cancer Ther.*, 2009, **8**, 10–6.

Chapter III

III. DEVELOPING A TERPYRIDINE PLATFORM FOR METAL-TERPYRIDINE G-QUADRUPLEX BINDING COMPLEXES

3.1 Introduction

2,2':6',2''-terpyridine (tpy) was selected as the basis for the development of novel palladium and platinum complexes capable of quadruplex binding. Terpyridine is a widely used scaffold in inorganic synthesis, due to the availability of ligands from facile, high yielding syntheses.^{1,2}

Metal complexes containing metal ions with low oxidation states (the majority of transition metal complexes feature +2 or +3 metal ions) are characterised by an excess of electron density at the metal atom. Stabilisation of the metal centre is best achieved by the use of electron-withdrawing ligands possessing low-lying vacant orbitals of appropriate symmetry for overlap with the filled metal orbitals.³ Terpyridine is ideally suited to this role, since it possesses a LUMO of suitable energy for interactions with metal *d* orbitals,⁴ enabling the transfer of electron density from metal to ligand (back-bonding). The geometries of complexes containing the terpyridine ligand are predominantly determined by the configuration of the ligand, where the planarity of the aromatic surface must be compromised with the optimum geometry for the metal ion. Therefore, palladium and platinum complexes incorporating terpyridine frequently adopt four-coordinate square planar geometry.

The features of terpyridine itself, along with those it imparts upon complex formation explain its widespread success as a ligand in general. In particular, its large aromatic surface and planar geometry would indicate its suitability as the basis for a metal complex capable of binding to G-quadruplex DNA. However, despite

showing a good affinity for G-quadruplexes, terpyridine metal complexes are not designed to maximise G-quartet coverage, resulting in π -stacking opportunities being missed. It may, therefore, seem an unusual strategy to select terpyridine-based complexes for the purpose of quadruplex binding. The reason for doing so lies in the ability to tailor the properties of terpyridine-based complexes by utilising appended substituent groups.⁵ This crucial property allows us to move beyond the point of binding which is dependent largely upon the ligand surface itself (as observed in 3,3-biisoquinoline), and towards binding that can be directly influenced by added functionality, such as that demonstrated by Pt-MPQ (Chapter I, 1.7)

This chapter focuses on the methodology explored whilst designing and synthesising a suitable terpyridine ligand platform, capable of future modification to enable dual modality binding. Initial exploration of metal complexes incorporating the established tpy ligand will also be carried out, in order to assess the G-quadruplex binding abilities of these complexes.

3.2 Overview of synthetic methodology

3.2.1 Molecular design of G-quadruplex end-stacking terpyridine complexes

2,2':6',2''-terpyridine will be modified to incorporate a methylsulphinyl group at the C(4') position of the ligand. It is intended that this substituent will be used in the future to add to the complex specific functionality targeted to the G-quadruplex structure being probed. This would be achieved *via* coupling of the appended sulfoxide with various types of Grignard reagent (Figure 3.2.1-1), to yield a variety of products dependent on the Grignard reagents used. This particular coupling method has been effectively demonstrated by Oae *et al.*,^{6,7} where in the case of

coupling arylsulphonyl groups, the new carbon-carbon bond is formed with retention of the configuration.⁸

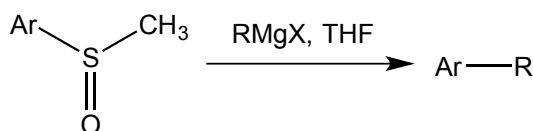


Figure 3.2.1-1 Grignard coupling of methylsulphonylarene, as demonstrated by Oae et al.

The methylsulphonyl-substituted terpyridine ‘base unit’ could therefore be modified to include any one of a range of substituents that would offer the ‘best match’ to the G-quadruplex loop region sequences in close proximity. Thus, binding interactions between the complex and DNA target would be maximised, leading to an increased binding affinity between the two.

In an effort to establish this functionalisable terpyridine platform, initial exploration involves the successful synthesis of the methylsulphonyl-substituted terpyridine ligand, followed by complex formation with both palladium and platinum (Figure 3.2.1-2).

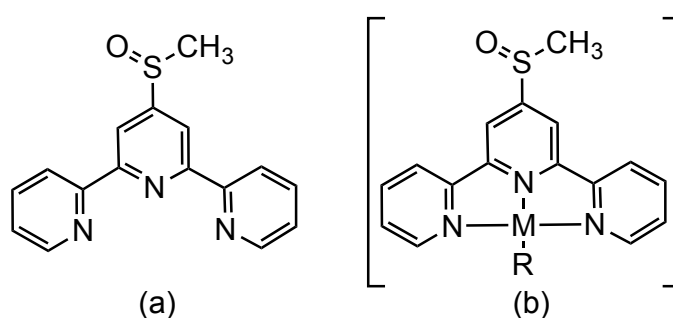


Figure 3.2.1-2 (a) Structure of target ligand (b) Representative structure of target complexes.

The resulting complexes possess similar features to the 3,3-biisoquinoline compounds previously synthesised including a large aromatic surface (albeit not

optimised for π -stacking interactions with the G-quartet) along with a central metal ion displaying square planar geometry. They will therefore be investigated to determine their ability to bind to G-quadruplex regions of DNA before any further modification has taken place. This information will allow for comparison between the two ligand systems investigated (3,3-biisoquinoline and 2,2':6',2''-terpyridine), as well as serving as somewhat of a baseline for future complexes to be compared against (specifically those derived from the terpyridine complex with targeted functionality added).

3.2.2 Routes towards 2,2':6',2''-terpyridines

Two general methodologies exist in the synthesis of 2,2':6',2''-terpyridines, involving either the construction of the central ring *in situ*, or alternatively the coupling of three existing pyridine rings, *via* oxidative coupling of pyridines, or Ullman coupling of bromopyridines (Figure 3.2.2-1). Synthetically, several methods have been utilised to prepare this system, some examples of which include condensation methodology, Tohda methodology, metal-mediated coupling and cycloaddition (Sauer methodology).

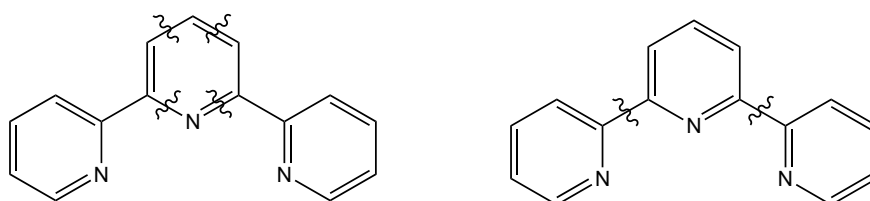


Figure 3.2.2-1 Synthetic routes towards 2,2':6',2''-terpyridine; *in situ* central ring construction or coupling of existing pyridine rings.

Perhaps the most efficient methodology to optimise the preparation of 2,2':6',2''-terpyridine was reported by Jameson and Guise⁹ (Figure 3.2.2-2). Reaction of 2-acetylpyridine with N,N-dimethylformamide dimethyl acetate yields the key intermediate enaminone. Condensation of the potassium enolate of 2-acetylpyridine with this intermediate results in the loss of dimethyl amine. *In situ* ring closure of the resulting 1,5-enedione with ammonium acetate yields the terpyridine directly.

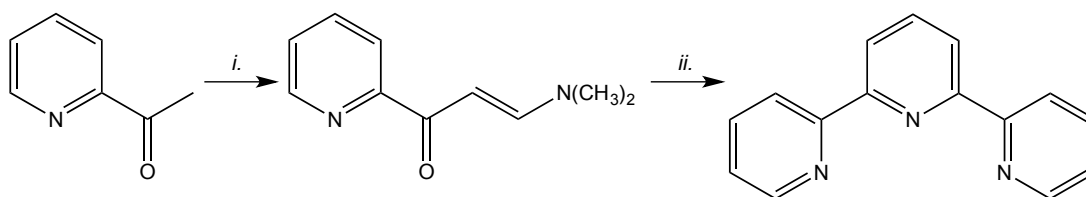


Figure 3.2.2-2 Preparation of 2,2':6',2''-terpyridine as reported by Jameson and Guise under the following conditions: i. DMF dimethyl acetate; ii. *t*-BuOK, 2-acetylpyridine / NH₄OAc, HOAc.

This route was based upon a strategy previously reported by Potts *et al.*, which features an α -oxoketene dithioacetal as the key synthetic intermediate in the preparation of 2,2':6',2''-terpyridine.^{10,11} Potts and co-workers first described the basis for this strategy in earlier work; reporting a new and versatile synthesis of 1,5-enediones to enable a variety of 2,6-disubstituted pyridines to be readily produced following efficient ring closure of the unsaturated intermediate (Figure 3.2.2-3).¹² This procedure has found widespread application, particularly in the preparation of oligopyridines with a thioalkyl group substituted at C(4').^{13,14}

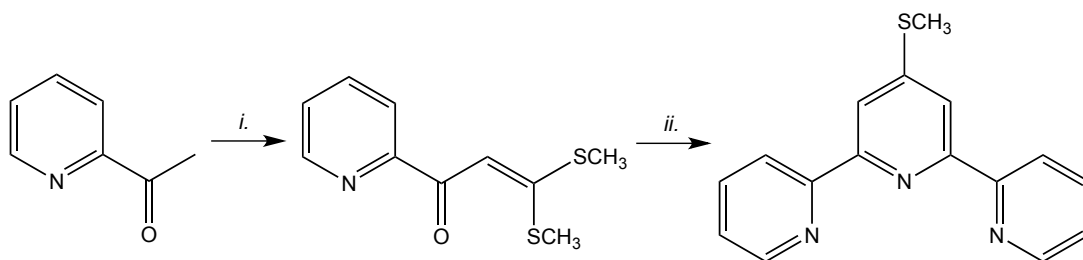


Figure 3.2.2-3 Preparation of substituted pyridines from the corresponding 1,5-dione and hydroxylamine as reported by Potts *et al.* under the following conditions: i. NaH, CS₂, CH₃I; ii. *t*-BuOK, 2-acetylpyridine / NH₄OAc, HOAc.

Since we desired a substituted terpyridine ligand, the earlier work of Potts *et al.* formed the basis of the synthetic strategy employed herein.

3.2.3 Preparation of methylsulphonyl-substituted terpyridines

The desired terdentate binding ligand can be successfully synthesised in high yield in a three-step procedure starting with 2-acetylpyridine (Figure 3.2.3-1). This is a readily available and relatively inexpensive starting reagent, enabling large-scale synthesis to be completed with ease.

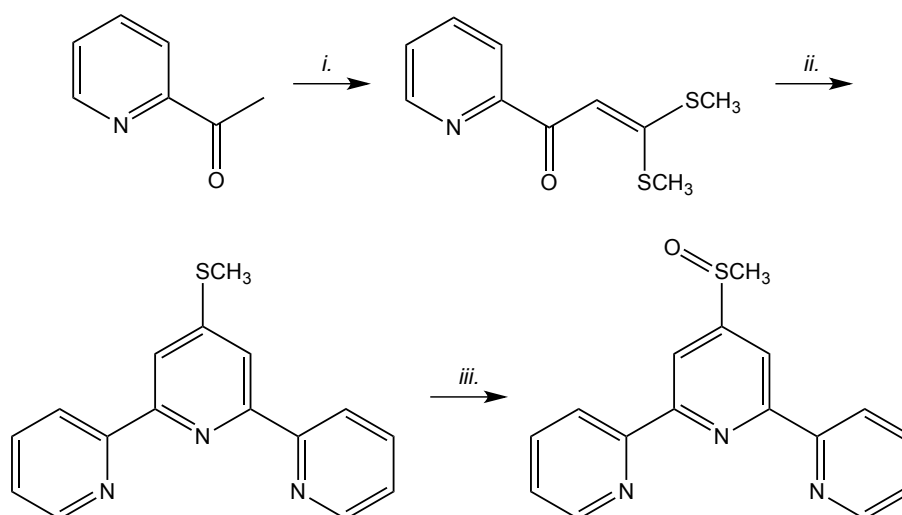


Figure 3.2.3-1 Synthesis of 4'-(methylsulfinyl)-2,2':6',2''-terpyridine under the following conditions: i. Method 1: NaH, CS₂, CH₃I, Method 2: *t*-BuOK, CS₂, CH₃I; ii. *t*-BuOK, 2-acetylpyridine, NH₄OAc, HOAc; iii. H₂O₂/HOAc.

Step i. The first stage towards the desired ligand was preparation of an α -oxoketene dithioacetal *via* the reaction of 2-acetylpyridine with carbon disulphide in the presence of a base followed by alkylation.¹⁵ The mechanism for this transformation is shown in Figure 3.2.3-2. The enolate derived from 2-acetylpyridine reacts with CS₂ to give an intermediate that is deprotonated to give an unsaturated monothiolate anion.¹⁶ S-alkylation with the halohydrocarbon results in the desired α -oxoketene S,S-acetal product. Several bases can be utilised,^{17–19} however sodium hydride has been shown to be very effective in securing high yields.¹⁹

Step ii. The synthesis of a substituted pyridine from the α -oxoketene dithioacetal prepared in the first stage is achieved by further reaction with the potassium enolate of 2-acetylpyridine (Figure 3.2.3-2). α -oxoketene dithioacetals undergo 1,4-addition with ketone enolates followed by elimination of methanethiolate to yield 1,5-enedione intermediates.^{12,20} *In situ* ring closure is then achieved with the addition of ammonium acetate in glacial acetic acid at reflux. This method is particularly advantageous in that it enables both symmetric and asymmetrical terpyridine ligands to be synthesised in good yields.²¹

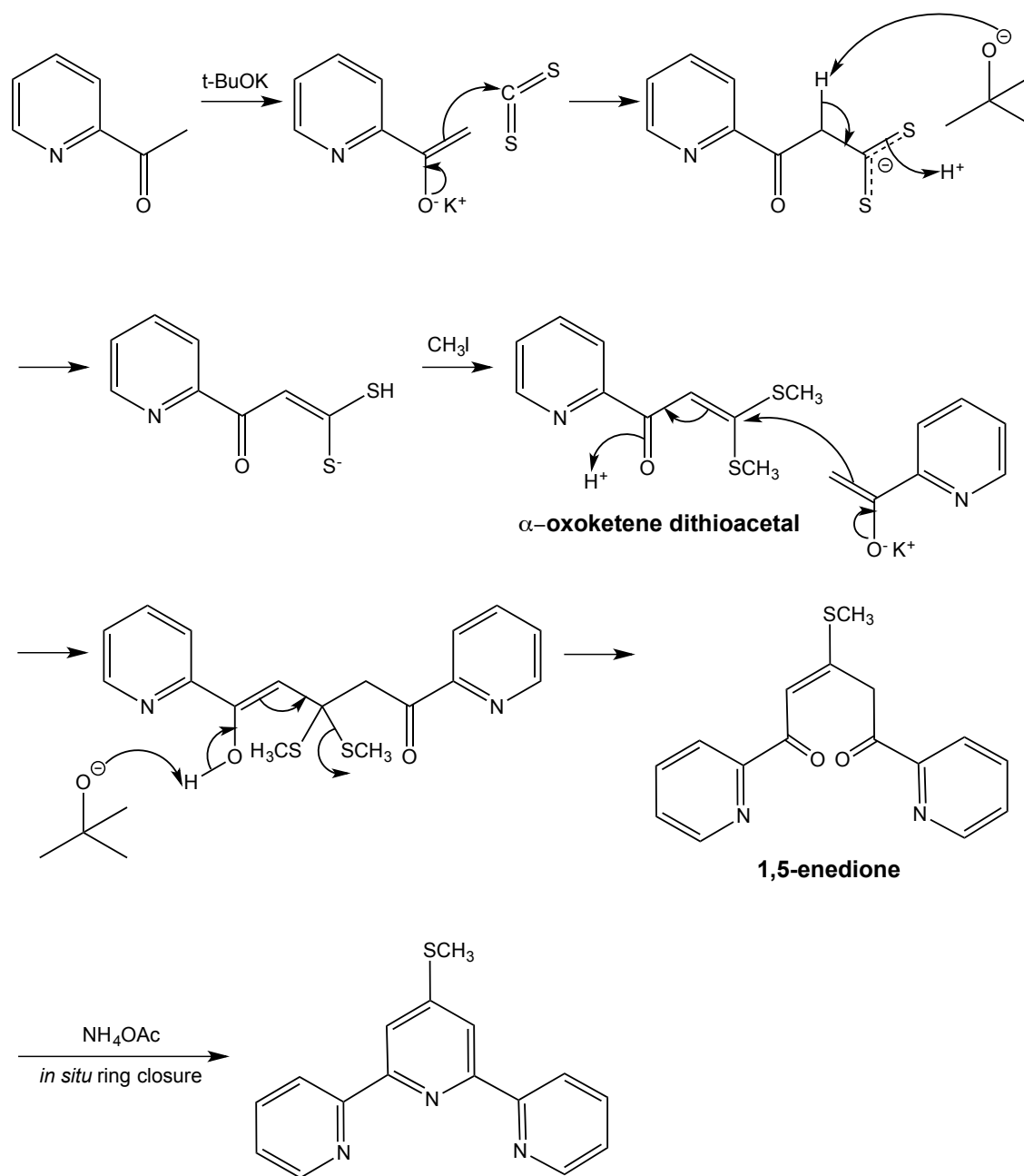


Figure 3.2.3-2 Mechanism of 4'-(methylsulfinyl)-2,2':6,2''-terpyridine formation via an α -oxoketene dithioacetal (step i.) and 1,5-enedione (step ii.)

Step iii. Thioethers can be readily oxidised to sulfoxides (R-S(=O)-R) and sulfones ($\text{R-S(=O)}_2\text{-R}$) using a variety of oxidizing agents,^{22–26} such as hydrogen peroxide,^{27,28} nitric acid²⁹ or sodium periodate.³⁰ The sulphide is either fully oxidised to the sulfone or transformed into a sulfoxide. The choice of oxidizing agent determines the

products of the reaction, which in the case of hydrogen peroxide will be the desired sulfoxide and water. The mechanism for this partial oxidation is shown in Figure 3.2.3-3. The sulphur atom first attacks the terminal oxygen of the peroxide group, causing breakage of the peroxide bond. The resulting alkoxy anion and protonated sulfoxide undergo proton exchange to yield the sulfoxide and water.^{26,31}

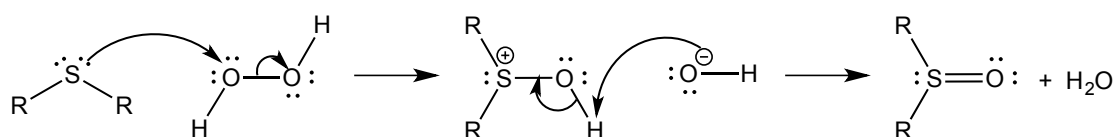


Figure 3.2.3-3 Mechanism of oxidation of sulphide to sulfoxide using hydrogen peroxide.

3.3 4'-(methylsulphinyl)-2,2':6',2''-terpyridine synthesis and characterisation

3.3.1 3,3-bis(methylthio)-1-(pyridine-2-yl)prop-2-en-1-one (10)

Preparation of compound **(10)** was first attempted using an early method described by Potts *et al.*,¹² with the preferred choice of base, NaH (Figure 3.3.1-1; Method a). NaH was added to anhydrous DMSO, followed by the dropwise addition of 2-acetylpyridine, CS₂ and CH₃I to the vigorously stirred solution. After 12 hours at room temperature, iced water was cautiously added to consume any unreacted NaH, which otherwise presents a fire hazard due to its violent reactivity with water. Analysis of the crude solid following collection and washing showed a combination of starting materials to be present, indicating that the reaction had been unsuccessful.

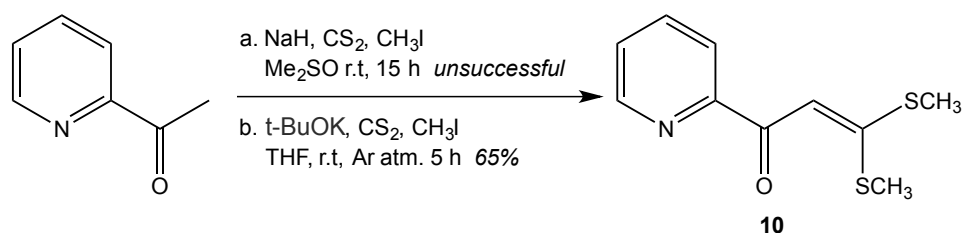


Figure 3.3.1-1 Synthesis of 3,3-bis(methylthio)-1-(pyridine-2-yl)prop-2-en-1-one by two alternative methods.

A search of the literature provided an alternative procedure for the preparation of the α -oxoketene dithioacetal. Reported by Han *et al.*, this method was itself based on procedures described by Potts and coworkers,^{10,12} however THF was now the solvent of choice, and potassium tert-butoxide was used as a source of strong base (rather than NaH) (Figure 3.3.1-1; Method b).³² The ratio of reagents used was mostly unchanged. As before, operating under an argon atmosphere, 2-acetylpyridine, CS₂ and CH₃I were added dropwise with caution to a vigorously stirred suspension of base in solvent. Following stirring at room temperature for approximately half the time period required previously (5 h *cf.* 12 h), the reaction was poured onto ice water and allowed to stand overnight. The precipitate was washed to successfully yield compound (**10**) as dark yellow solid in good yield. Electrospray ionisation mass spectrometry and nuclear magnetic resonance data were in accordance with those reported in the literature (Figure 3.3.1-2).

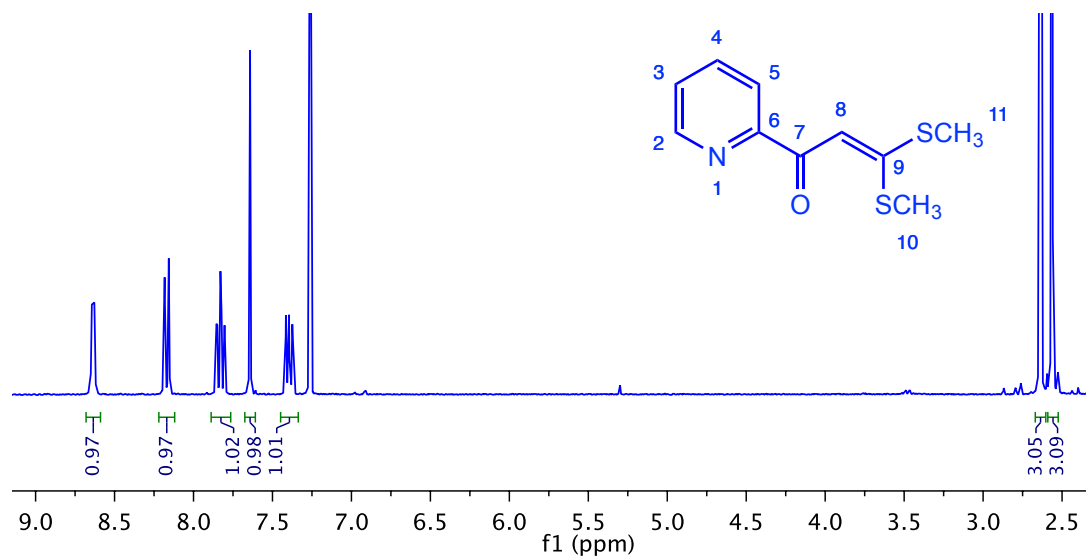


Figure 3.3.1-2 ^1H -NMR spectrum of 3,3-bis(methylthio)-1-(pyridine-2-yl)prop-2-en-1-one (**10**) (300 MHz, CDCl_3 , 298 °K).

The use of potassium tert-butoxide in the second method allows successful formation of the potassium enolate of 2-acetylpyridine, which is perhaps more reactive than the sodium enolate that would be formed under the former method. Additionally, it is possible that the NaH utilised in the first attempt (stored as oil dispersion) was not sufficiently dry to enable formation of the enolate on that occasion. The only remaining variable between the two methods was the solvent choice. Despite the relatively unusual solvent choice in the first route (DMSO), this method reports widespread success; therefore any failure associated with the solvent is expected to be due to issues arising from its dryness. Despite every effort to ensure the conditions remained anhydrous throughout, there was no evidence of success in the crude analysis. The alternative procedure adapted by Han *et al.* resulted in first-time success.

3.3.2 4'-(methylthio)-2,2':6',2''-terpyridine (**11**)

Reaction of the prepared α -oxoketene dithioacetal (**10**) with a further equivalent of the potassium enolate of 2-acetyl pyridine followed by ring closure with NH_4OAc yields the desired terpyridine product (Figure 3.3.2-1).

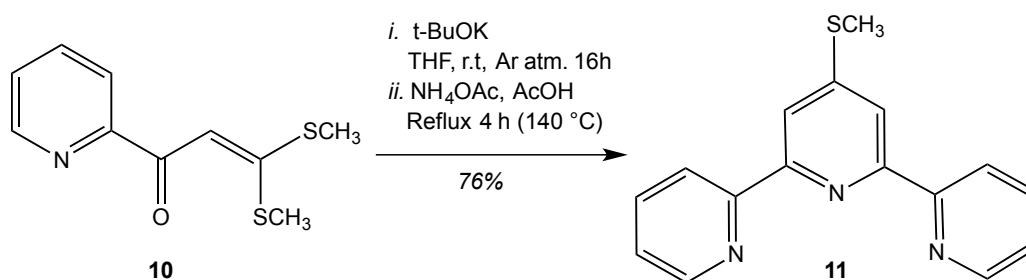


Figure 3.3.2-1 Synthesis of 4'-(methylthio)-2,2':6',2''-terpyridine via 1,5-enedione.

Following the successful synthesis of compound (**10**) using a method described by Han *et al.*, compound (**11**) was prepared following a similar method also described by Han and coworkers.³² The reaction proceeded well. Isolation and purification of the crude product was achieved by cooling, precipitation and filtration, as described by Potts and coworkers.¹² The product was obtained in good yield as brown solid. Despite its alternative physical appearance (it has been previously reported as yellow solid), characterisation of the product by ESI-MS and ^1H NMR was in full accordance with the literature.³³

3.3.3 4'-(methylsulphinyl)-2,2':6',2''-terpyridine (**12**)

The desired methylsulphinyl-substituted terpyridine was prepared by oxidising the existing methylthio-substituted terpyridine. This was achieved using hydrogen peroxide in glacial acetic acid, as demonstrated by Oae *et al.*³⁴ (Figure 3.3.3-1).

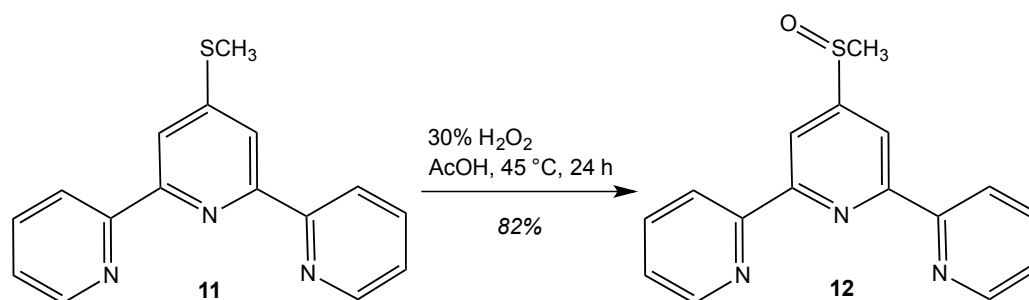


Figure 3.3.3-1 Synthesis of 4'-(methylsulphonyl)-2,2':6',2''-terpyridine

The addition of just one equivalent of 30% H_2O_2 causes only a single oxidation to occur. This ensures that the methylsulphonyl group is retained (i.e. it cannot undergo further oxidation to the sulfone, $\text{S}(=\text{O})_2\text{CH}_3$), potentially allowing functionality to be later added to the terpyridine scaffold at the C(4') position through Grignard coupling routes (see 3.2.1).

The reaction proceeded well under acidic conditions. Neutralisation followed by extraction of the product into chloroform produced a pale brown solid in good yield. The ^1H NMR spectrum shows a downfield shift in the $\text{H}_{3'/5'}$ peak, on account of the close proximity of these protons to the sulphonyl oxygen atom following successful oxidation. Previously appearing at 8.30 ppm, the peak now resides at 8.63 ppm. Similarly, the thiomethyl peak shifts downfield from 2.66 ppm ($\text{R-S}(\text{CH}_3)$) to 2.83 ppm ($\text{R-S}(=\text{O})(\text{CH}_3)$) (Figure 3.3.3-2). The ESI-MS spectrum showed peaks at m/z 296 corresponding to $[\text{M} + \text{H}]^+$.

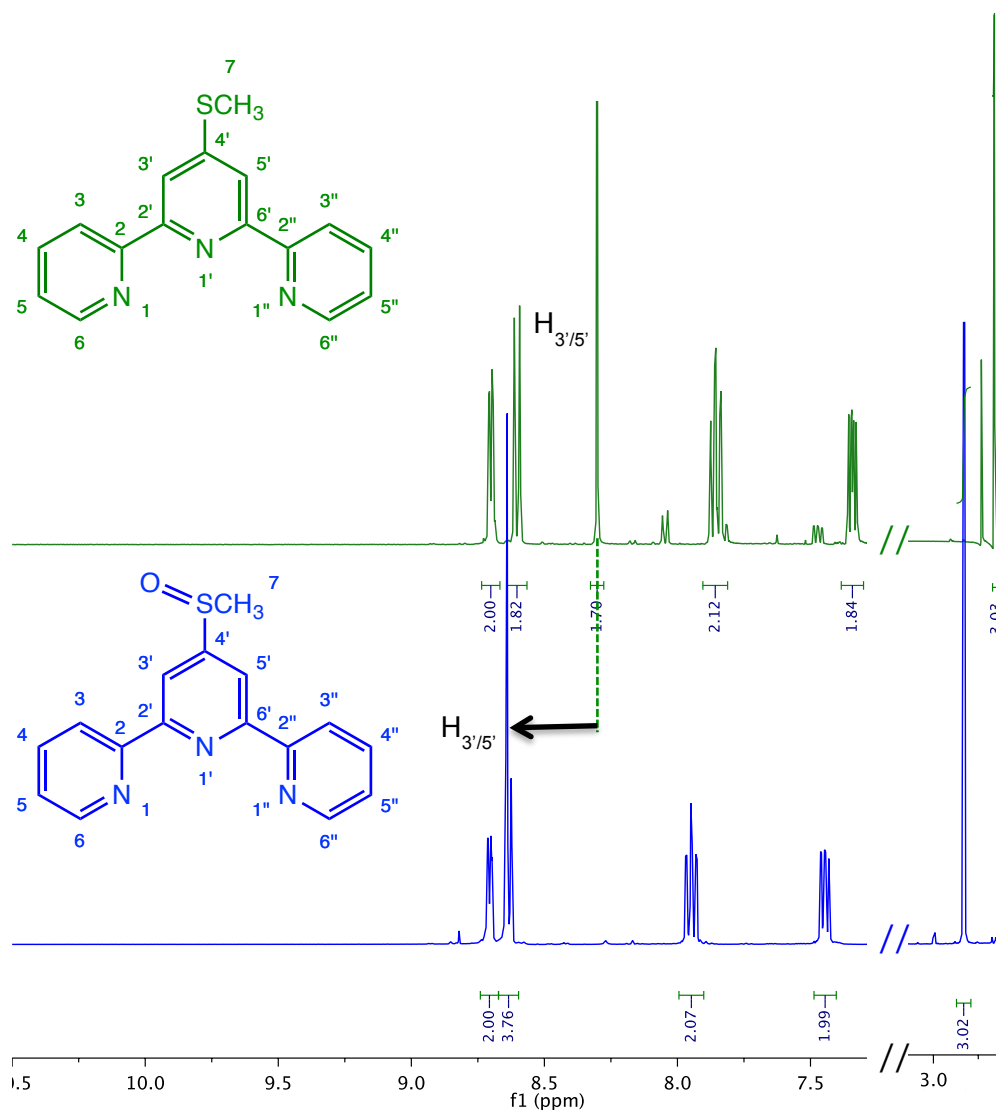


Figure 3.3.3-2 ^1H NMR spectra overlay of 4'-(methylthio)-2,2':6',2''-terpyridine (**11**) and 4'-(methylsulphonyl)-2,2':6',2''-terpyridine (**12**) (300 MHz, CD_3CN , 298 °K).

3.3.4 Synthesis and characterisation of palladium and platinum complexes incorporating 4'-(methylsulphonyl)-2,2':6',2''-terpyridine (**12**)

3.3.5 $[\text{Pd}(\text{12})(\text{CH}_3\text{CN})](\text{BF}_4)_2$ (**13**)

A single terpyridine ligand was bound to a palladium metal centre following a ligand substitution reaction. Replicating the conditions used to prepare the palladium 3,3-biisoquinoline compound, tetrakis(acetonitrile)palladium tetrafluoroborate was

reacted with the ligand, this time in a 1:1 ratio, to form the desired complex (Figure 3.3.5-1).

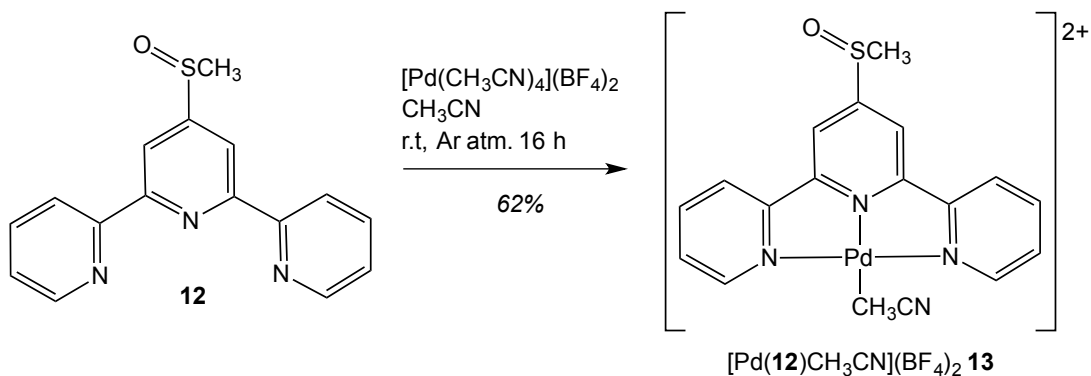


Figure 3.3.5-1 Synthesis of $[\text{Pd}(\mathbf{12})(\text{CH}_3\text{CN})](\text{BF}_4)_2$

The crude product was washed with chloroform, methanol and diethyl ether before drying under vacuum to yield pure $[\text{Pd}(\mathbf{12})\text{CH}_3\text{CN}](\text{BF}_4)_2$ as a pale beige solid in 62% yield. The complex shows good solubility in acetonitrile. The ESI-MS spectrum showed a peak at m/z 442 corresponding to $[\text{Pd}(\mathbf{12})(\text{CH}_3\text{CN})]$. The ^1H -NMR spectrum shows both the same splitting pattern and number of peaks as those observed for the unbound ligand. Upon comparison of these two spectra, noticeable shifts can be observed in the complex spectrum. This is due to the electron withdrawing effect of the palladium metal centre, and is most evident when comparing the positions of the peaks attributed to protons $\text{H}_{(4/4'')}$ and $\text{H}_{(5/5'')}$, as shown in Figure 3.3.5-2.

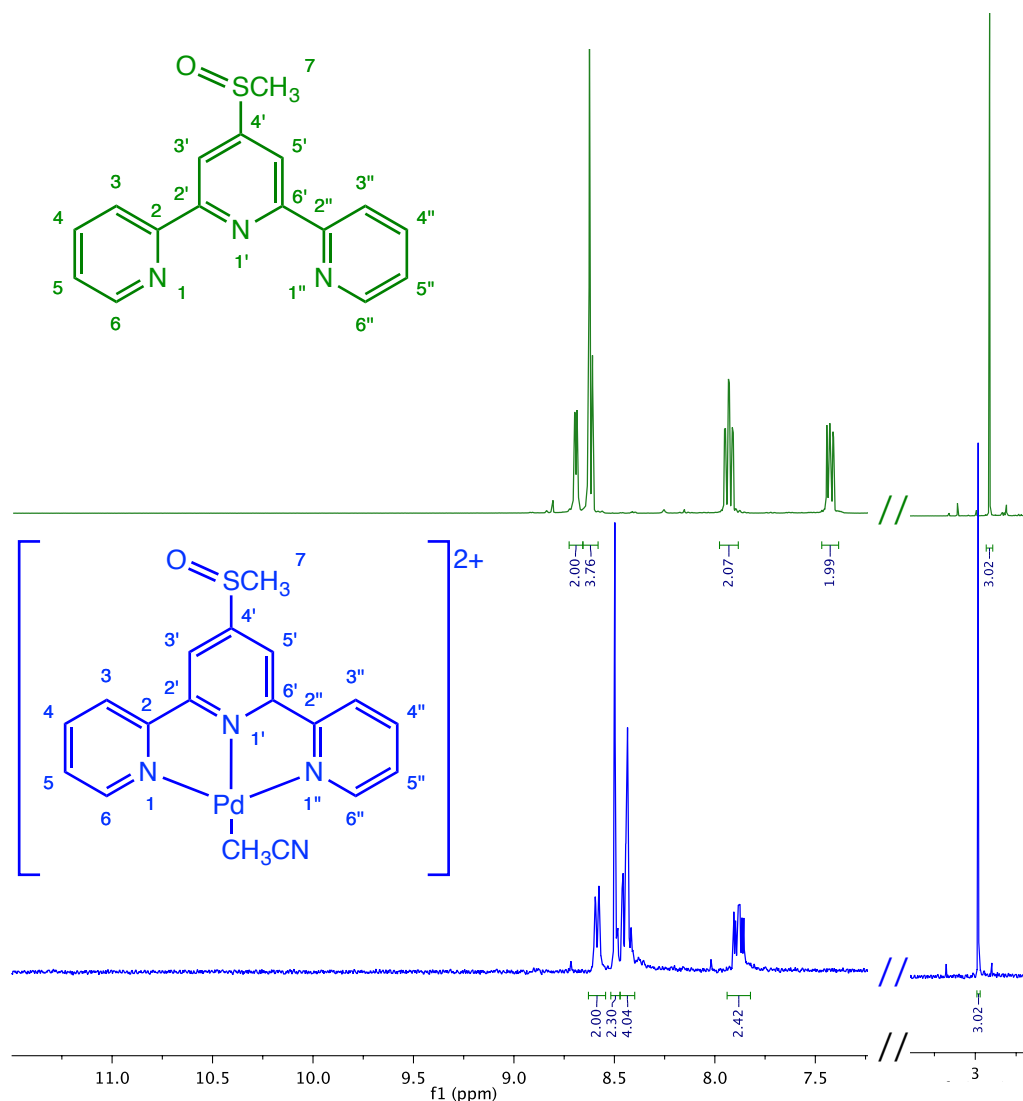


Figure 3.3.5-2 ¹H NMR spectra overlay of 4'-(methylsulphonyl)-2,2':6',2''-terpyridine (**12**) and $\text{Pd}(\mathbf{12})(\text{CH}_3\text{CN})](\text{BF}_4)_2$ (**13**) (300 MHz, CD_3CN , 298 °K).

3.3.6 $[\text{Pt}(\mathbf{12})\text{Cl}](\text{PF}_6)$ (**14**)

Referring back to the method used to prepare the platinum 3,3-biisoquinoline compound and owing to the similar solubilities of the ligands, the same solvent and reaction conditions were employed to produce the platinum tpy complex (Figure 3.3.6-1). One minor exception was the 1:1 ratio in which the ligand was reacted with

the potassium tetrachloroplatinate starting compound; a direct result of its terdentate binding mode, thus accommodating only one ligand per metal centre.

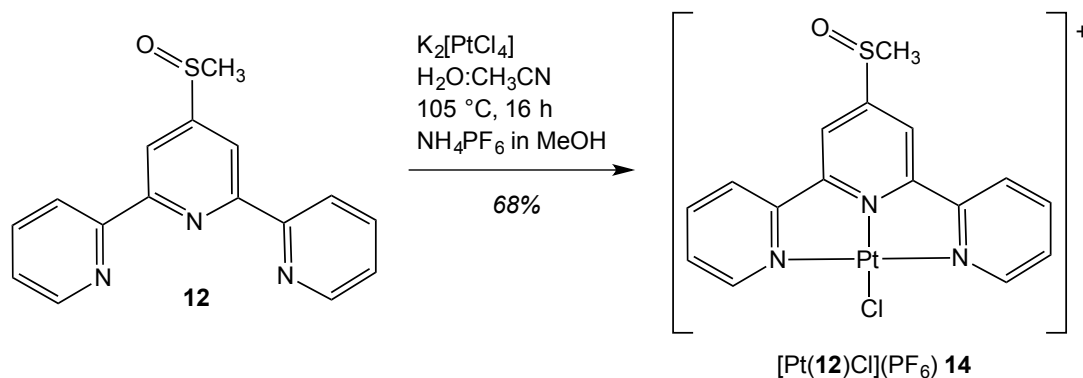


Figure 3.3.6-1 Synthesis of $[\text{Pt}(\mathbf{12})\text{Cl}](\text{PF}_6)$

Following heating under reflux overnight, the solution was hot filtered and a methanolic solution of ammonium hexafluorophosphate added. The desired product immediately precipitated from solution as a vibrant raspberry purple solid. Careful washing with chloroform, methanol and diethyl ether yielded the title compound as purple solid in 68% yield. The compound shows good solubility in acetonitrile.

The ESI-MS spectrum showed a peak at m/z 525 corresponding to $[\text{Pt}(\text{C}_{16}\text{H}_{13}\text{N}_3\text{SO})\text{Cl}]$. In a similar pattern to that observed for the palladium analogue, comparison of the ^1H -NMR spectra of the unbound ligand and complex shows some prominent downfield signal shifts, owing to the withdrawal of electron density from the terpyridine ring system upon complex formation (Figure 3.3.6-2). The presence of ^{195}Pt - ^1H coupling satellites confirms metal coordination of the ligand.

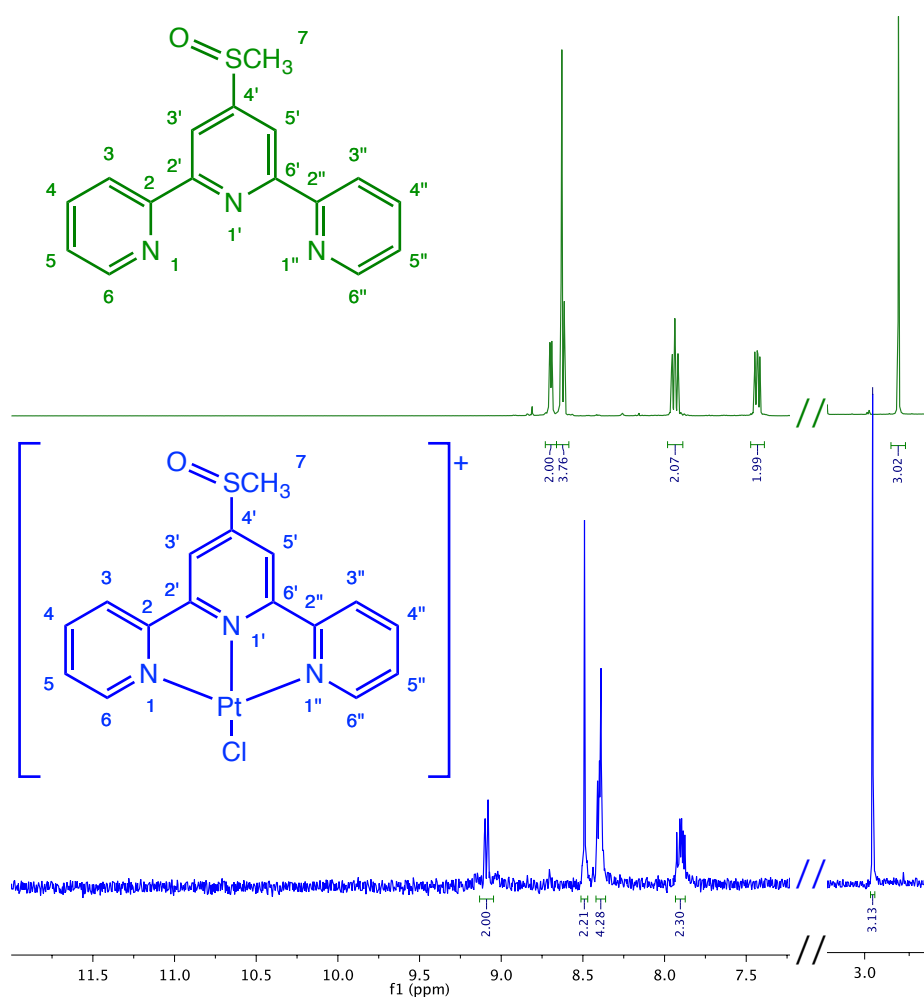


Figure 3.3.6-2 ^1H -NMR spectra overlay of 4'-(methylsulphonyl)-2,2':6',2''-terpyridine (**12**) and $[\text{Pt}(\text{12})\text{Cl}](\text{PF}_6)$ (**14**) (300 MHz, CD_3CN , 298 °K).

3.4 UV-Visible spectroscopy studies

3.4.1 Absorbance characteristics

Unbound tpy ligand (**12**) and both palladium and platinum complexes (**13**) and (**14**) were characterised by UV/Vis spectroscopy. Solutions of each were prepared in acetonitrile. The absorbance spectrum of 4'-(methylsulphonyl)-2,2':6',2''-terpyridine (**12**) shows strong π - π^* ligand transitions in the UV region at 251 and 277 nm. These

transitions are also observed in the spectra recorded for both complexes, appearing between 241-283 nm (Figure 3.4.1-1).

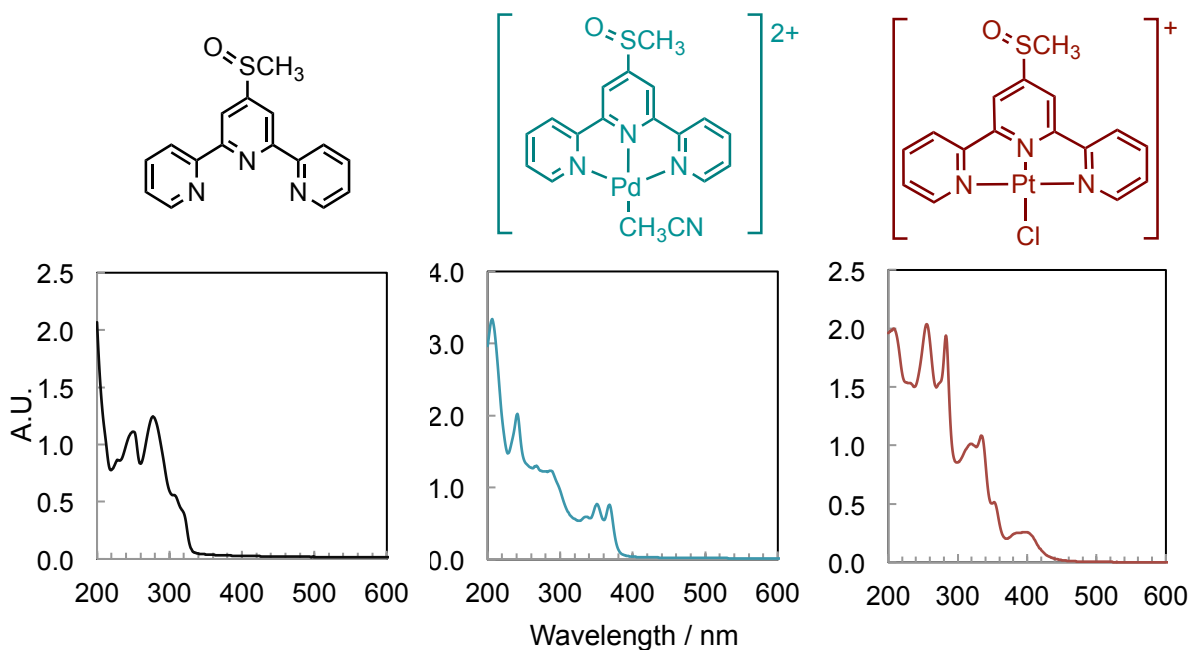


Figure 3.4.1-1 UV-Vis absorption spectra for 4'-(methylsulphonyl)-2,2':6',2''-terpyridine (**12**), $[Pd(12)CH_3CN]^{2+}$ (**13**) and $[Pt(12)Cl]^+$ (**14**) in acetonitrile.

Further charge transfer bands are observed between 319-398 nm in the metal complexes containing the ligand. These bands do not appear in the spectrum for the unbound ligand and are therefore due to interactions between the metal centre and the terpyridine ligand. The bands at 351 and 368 nm in the palladium complex and 334 and 398 nm in the platinum complex originate from spin-allowed MLCT (metal to ligand charge transfer) transitions. These occur due to the overlap of orbitals of appropriate symmetry, allowing electron density to be donated from metal $d\pi$ orbitals to vacant low-lying π^* ligand orbitals. The presence of these MLCT bands is evidence for coordination of the terpyridine moiety. Furthermore, the MLCT bands observed for

these two complexes are comparable to those reported for similar complexes containing tpy ligands, such as [Pt(tpy)Cl]Cl³⁵ and [Pd(tpy)Cl]PF₆.³⁶

Table 3.4.1-1 shows the UV-Vis absorption data obtained for ligand **(12)** and complexes **(13)** and **(14)**. The UV-Vis transitions reported in the literature for both [Pt(tpy)Cl]Cl and [Pd(tpy)Cl]PF₆ are included for comparison.

Compound	$\pi - \pi^* \lambda_{\max}$ (nm)	MLCT λ_{\max} (nm)
4'-(methylsulphanyl)-tpy (12) ^a	251 (21800) 277 (24500)	
[Pd(12)(CH ₃ CN)](BF ₄) ₂ (13) ^a	241 (26900) 267 (17200)	335 (7700) 351 (10100) 368 (10100)
[Pt(12)Cl](PF ₆) (14) ^a	255 (26300) 283 (25200)	319 (12500) 334 (14000) 398 (3200)
[Pd(tpy)Cl]PF ₆ ^b	205 (57500) 246 (25800) 279 (23900)	328 (8670) 345 (9050) 362 (8180)
[Pt(tpy)Cl]Cl ^c	284 (23000)	334 (13400) 404 (1600)

Table 3.4.1-1 UV-Vis absorption data for synthesised compounds **(12)**-**(14)** and two literature compounds for comparison. ^aCH₃CN, ^bCH₃CN, 3 × 10⁻⁵ M, data taken from ³⁶; ^cMeOH:EtOH (4:1), 2 × 10⁻⁵ M, data taken from ³⁵. Extinction coefficients ($\epsilon / M^{-1} \text{ cm}^{-1}$) are given in parenthesis.

3.4.2 Stability in solution

Before proceeding with DNA binding experiments, the stability of each complex in solution was assessed using UV-Vis spectroscopy. Observing the change in absorbance over time, complex instability is typically characterised by a decrease in the intensity of the λ_{max} signal, with stable complexes exhibiting no change in their λ_{max} over time. Solutions of both complexes in acetonitrile were analysed periodically over 24 hours. Figure 3.4.2-1 shows the spectra obtained.

It is immediately evident that the palladium complex (**13**) is extremely stable, showing no loss in signal intensity after 24 hours in solution. By contrast, the platinum complex (**14**) shows a 6% loss of intensity over the same time period. It is interesting to note that the signal loss occurs over the first hour in solution, and that no further decrease in signal is observed over the remaining 23 hours. The cause of complex instability is therefore likely to be a process that occurs rapidly in solution, resulting in no further instability over time. Exchange of the chloride ligand with acetonitrile (from the solvent) would account for this. The stability observed for the palladium complex further supports this conclusion, since the palladium analogue already possesses an acetonitrile ligand and would therefore not be expected to undergo such ligand exchange with the solvent.

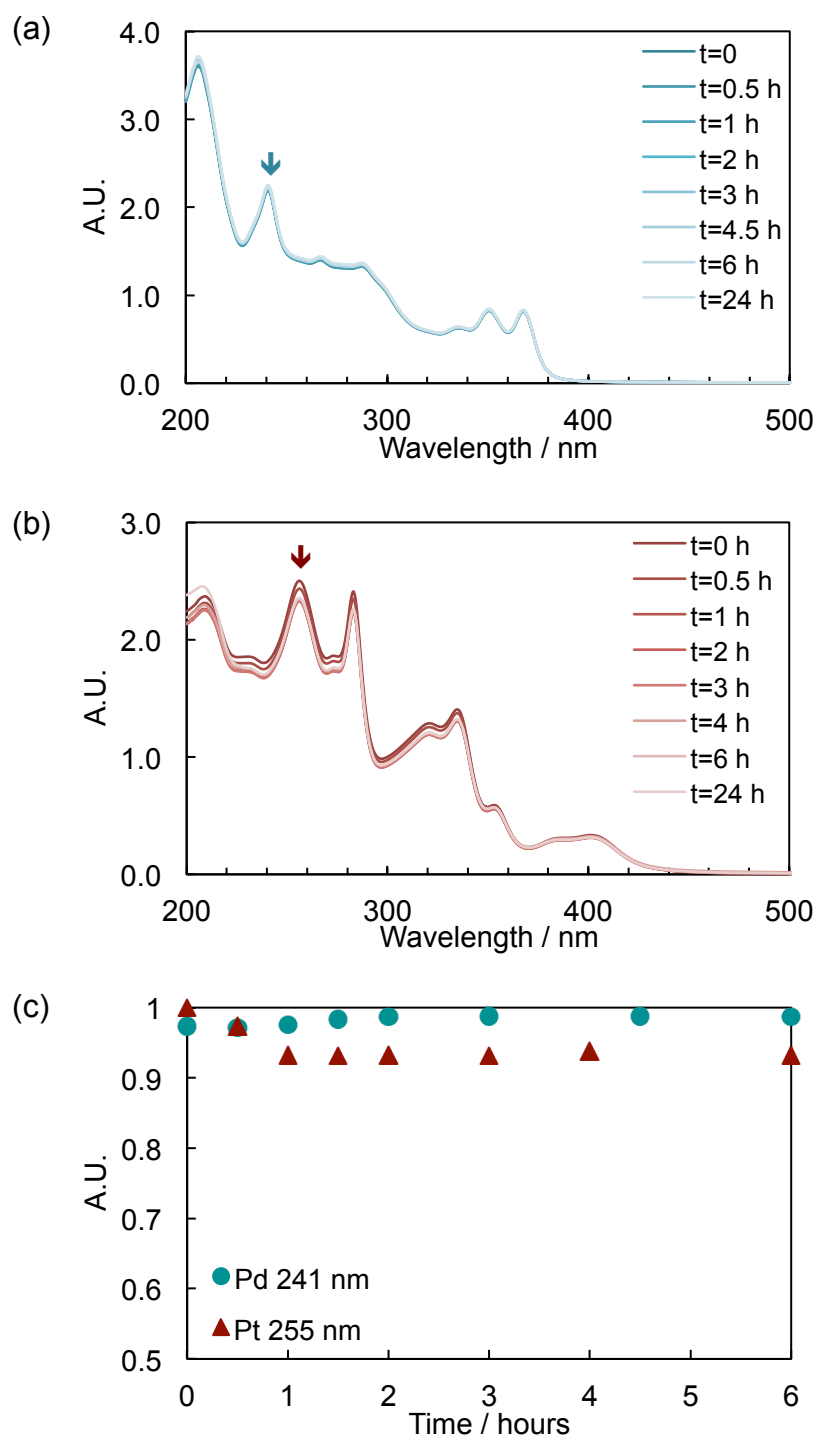


Figure 3.4.2-1 UV-Vis absorption spectra of complex solutions (CH_3CN) recorded over a 24 hour period. (a) $[Pd(12)CH_3CN]^{2+}$ (13); (b) $[Pt(12)Cl]^{+}$ (14); (c) Loss in signal intensity of λ_{max} peak over 6 hours.

3.5 Circular dichroism DNA binding studies

To qualify as a good G-quadruplex binder, a complex must show specificity for G-quadruplex sequences over the more commonly occurring duplex form of DNA. To begin to determine if this is the case with these complexes, circular dichroism (CD) can be used to study the binding (if any) to both types of structure, where a comparison between the two types of DNA will inform on the affinity of the complexes towards each type of DNA. A stronger interaction observed for G-quadruplex types of DNA (compared to duplex DNA) would be the first indication of preferential binding. This would provide the impetus to continue studying these compounds as potentially selective G-quadruplex binders.

3.5.1 Circular dichroism (CD)

Circular dichroism is a spectroscopic technique that can be used to probe the conformation of different types of DNA. A spectrum is generated by measuring the difference in absorbance between left (A_l) and right (A_r) circularly polarised light, producing a signal known as ellipticity θ (expressed in degrees).³⁷ The circularly polarised light utilised in this technique arises from superposition of oscillating vertical and horizontal polarised light. The size of electric field vector remains constant, however it rotates about the propagation direction in the form of either a left or right handed helix, resulting in the production of left or right circularly polarised light (Figure 3.5.1-1). At any point in time and space the magnitude vector will be perpendicular to the electric field.³⁸

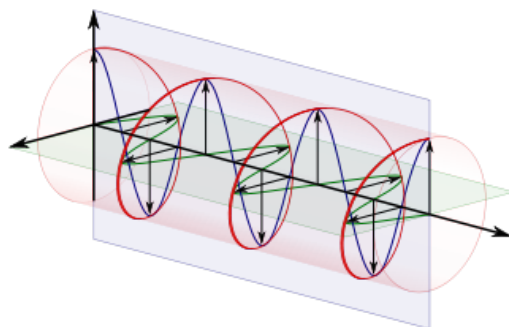


Figure 3.5.1-1 Left-handed or counter-clockwise circularly polarized light as defined from the point of view of the receiver.

Only molecules displaying chirality can produce a CD spectrum. Chiral molecules interact differently with right and left circularly polarised light due to their non-superimposable mirror images with no plane of reflection. Each type of light will have different extinction coefficients, which may be plotted against wavelength to produce a CD spectrum.³⁸ Non-chiral molecules can only be observed by CD when they interact with a chiral molecule. Chirality may then be induced in the non-chiral molecule by the environment, causing new bands to appear in the spectrum, the effect of which is called induced circular dichroism (ICD).

The phosphate-sugar DNA backbone comprises chiral sugar units that impart chirality into the structure and enable it to be studied by CD. Each sequence of DNA has a characteristic spectrum that may display alterations as a result of binding with a non-chiral molecule. CD is a highly sensitive method allowing conformational transitions between complex nucleic acid arrangements to be monitored over time.

3.5.2 Types of DNA investigated

DNA binding was determined using three types of DNA in the CD experiments. Two of these - Htelo and cMyc - represent quadruplex-forming regions of DNA. The other,

ct-DNA, is representative of duplex DNA.

Calf-thymus (ct-DNA)

ct-DNA consists of predominantly double, but also single stranded regions of DNA, composed of a variety of DNA sequences containing all four bases. Consequently, strand concentration cannot be calculated and the concentration is measured in bases, as determined by UV-Vis spectroscopy. This form of DNA is representative of genomic duplex DNA and allows the interaction between complexes and double stranded DNA to be assessed. The characteristic CD spectrum for ct-DNA shows relatively weak bands between 200-300 nm (Figure 3.5.2-1). These signals arise from the transitions of purine and pyrimidine bases that experience a weakly chiral environment due to the base pairs sitting perpendicular to the double helix.³⁷ Any changes observed in this region may indicate conformational changes in the DNA. Binding of the complexes to DNA may induce chirality, resulting in the appearance of new bands in the spectrum (ICD bands).

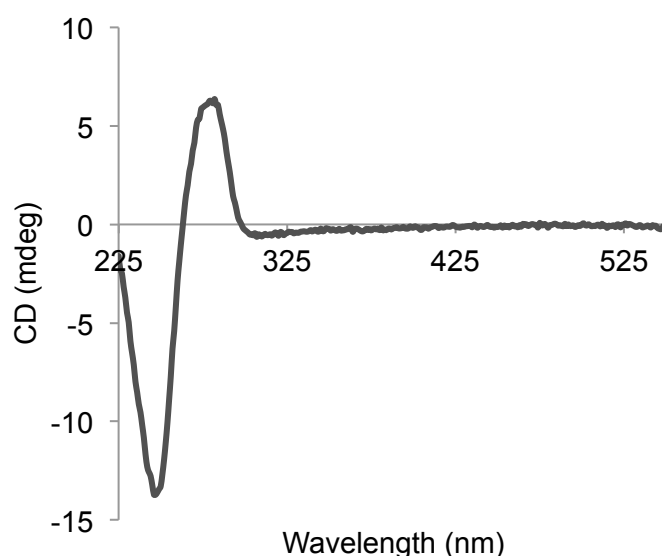


Figure 3.5.2-1 Characteristic CD spectrum of ct-DNA

Human telomeric (Htelo) DNA

Htelo DNA comprises a guanine-rich repeating base sequence of TTA-GGG which is capable of forming G-quadruplex structures;



The 22-base sequence mimics the sequence of DNA located at the telomeric ends, and is therefore used to assess telomeric quadruplex DNA binding. Prior to measuring the CD response of this strand, the DNA must be annealed and slowly cooled to room temperature before placing in a fridge overnight. This protocol allows the most thermodynamically stable conformation to form during the cooling process, with no overnight deterioration. Any conformation adopted by the strand during the CD experiment is therefore as a result of the specific experimental conditions only.

The various different conformations adopted by telomeric DNA are the result of the salt conditions of the buffer, which determine the type of cation present in solution. Held in place by electrostatic interactions with eight O(6) atoms lining the two planes of G-tetrads, both potassium and sodium cations are the correct size to occupy the space between the G-tetrads.³⁹ In general, sodium cations sit in the central cavity of the quartet, with potassium cations sitting between the quartet layers.⁴⁰

In potassium-rich solution an antiparallel hybrid conformation forms. This is characterised by a major peak at 295 nm originating from antiparallel character, in addition to a smaller peak at 265 nm representing its parallel nature. A further peak at 253 nm is usually observed due to a small amount of unfolded DNA.

It has been reported that due to the relative energies of hydration, the potassium cation is preferred for G-quadruplex stabilisation.⁴¹ Under cellular

conditions, the telomeric DNA is therefore most likely to adopt the conformation observed in potassium-rich solution, and this buffer system provides the best environment to mimic cell conditions. Consequently, a Tris-HCl/KCl buffer system was chosen for these binding experiments; providing the necessary potassium-rich environment that favours the antiparallel hybrid conformation. A characteristic CD spectrum of Htelo DNA under these conditions is shown in Figure 3.5.2-2.

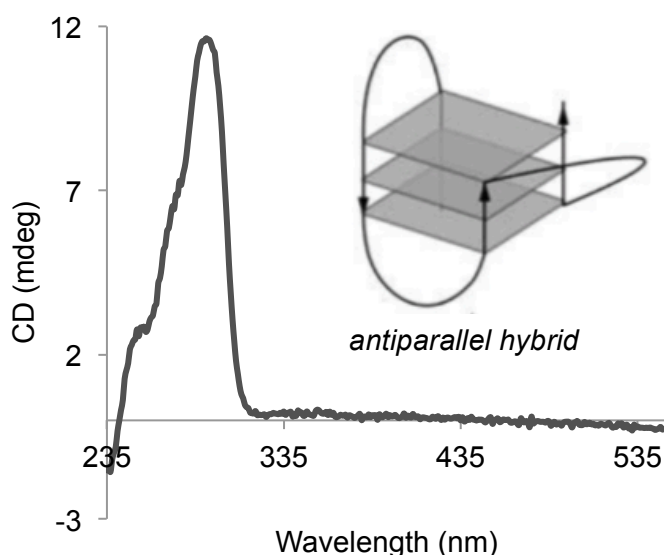


Figure 3.5.2-2 Characteristic CD spectrum of Htelo DNA in K^+ rich buffer conditions, forming antiparallel hybrid G-quadruplex.

In sodium-rich solution a purely antiparallel conformation forms, characterised by a single peak at 295 nm. The guanine bases are arranged in both *syn* and *anti* positions about the glycosidic bond. In the absence of both potassium and sodium ions in solution, G-quadruplex formation is less successful, with a defined peak at 253 nm originating from unfolded DNA. Despite the lack of stabilising cation in solution, there is still evidence of some degree of folding to form a G-quadruplex,

characterised by a peak at 295 nm which is indicative of antiparallel G-quadruplex formation.

The conformational arrangement of the Htelo strand can be sensitively monitored using circular dichroism. Observed changes in the CD spectra of the sequence following complex addition are indicative of a binding interaction between the DNA and complex. This may constitute stabilisation of the structure, or an alteration in its structure altogether; which would be evident from induced peaks corresponding to another conformation.

cMyc DNA

cMyc DNA consists of a guanine-rich base sequence that is therefore capable of forming G-quadruplex structures;



The 22-base sequence forms part of an oncogene promoter region and is used to assess promotor region quadruplex DNA binding. Oncogenic regions of DNA are commonly found to contain guanine-rich sequences that have the potential to form G-quadruplexes, and are therefore of much interest experimentally. The cMyc sequence consistently forms parallel G-quadruplex structures, regardless of the salt conditions used. The characteristic CD spectrum of cMyc DNA shows a peak at 265 nm originating from its parallel nature (Figure 3.5.2-3). In this conformation all of the guanine bases are in an *anti* position about the glycosidic bond. Once again, any change in the CD spectra of the sequence indicates a binding event has occurred.

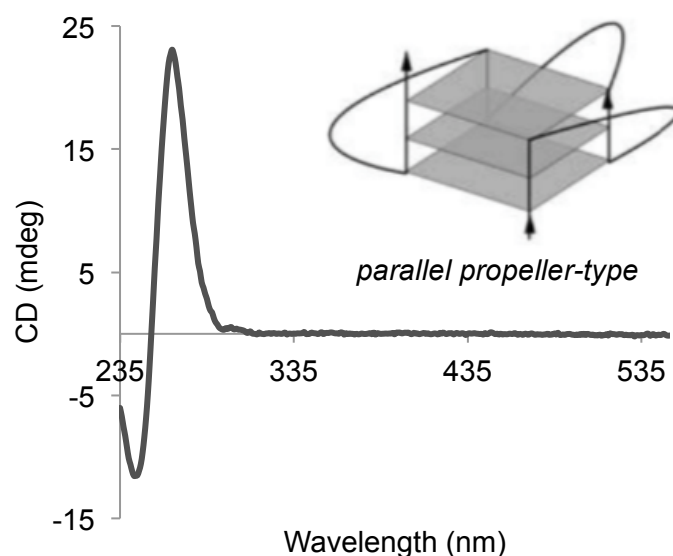


Figure 3.5.2-3 Characteristic CD spectrum of cMyc DNA, forming parallel G-quadruplex.

Since each quadruplex-forming strand adopts a different conformation, the complexes may show a preference for interaction with one sequence over the other. This would be most likely due to the variation in the loop regions between the two structures, where the exposure of bases for binding is different for each sequence. Any selectivity for one type of structure would provide information about the possible modes of interaction.

3.5.3 Circular dichroism binding results

Binding experiments were carried out using complex solutions that were prepared in 15% acetonitrile: 85% milliQwater to aid solubility. A solution of each complex was titrated into a solution of each type of DNA whilst monitoring and recording a CD spectrum after each addition. Following the addition of the final titre to the experimental solution, the overall percentage of CH₃CN did not exceed 3%. Solvent control experiments were conducted to verify that the final percentage of non-

aqueous solvent did not cause any alterations in the observed spectrum (data not shown).

ct-DNA

Both the platinum and palladium complexes generate ICD bands in the MLCT region of the ct-DNA spectra at 350 nm and 375 nm respectively, indicating that binding is occurring between the two species (Figure 3.5.3-1). The degree to which the CD spectrum responds to DNA binding differs between the two species, with a more intense ICD peak emerging for the platinum species.

The peak at 275 nm corresponding to the B-DNA configuration undergoes two transitions during platinum complex (**14**) addition; initially increasing in intensity at low concentrations, the peak then decreases at concentrations above 15 μM . By contrast, palladium complex (**13**) addition results in an initial decrease in intensity, followed by an increase at concentrations above 30 μM .

The intensity of the peak at 253 nm (unfolded DNA) decreases substantially in both cases, indicating that complex addition causes the DNA to adopt a more defined conformation, most likely as a result of complex-DNA interactions.

ct-DNA

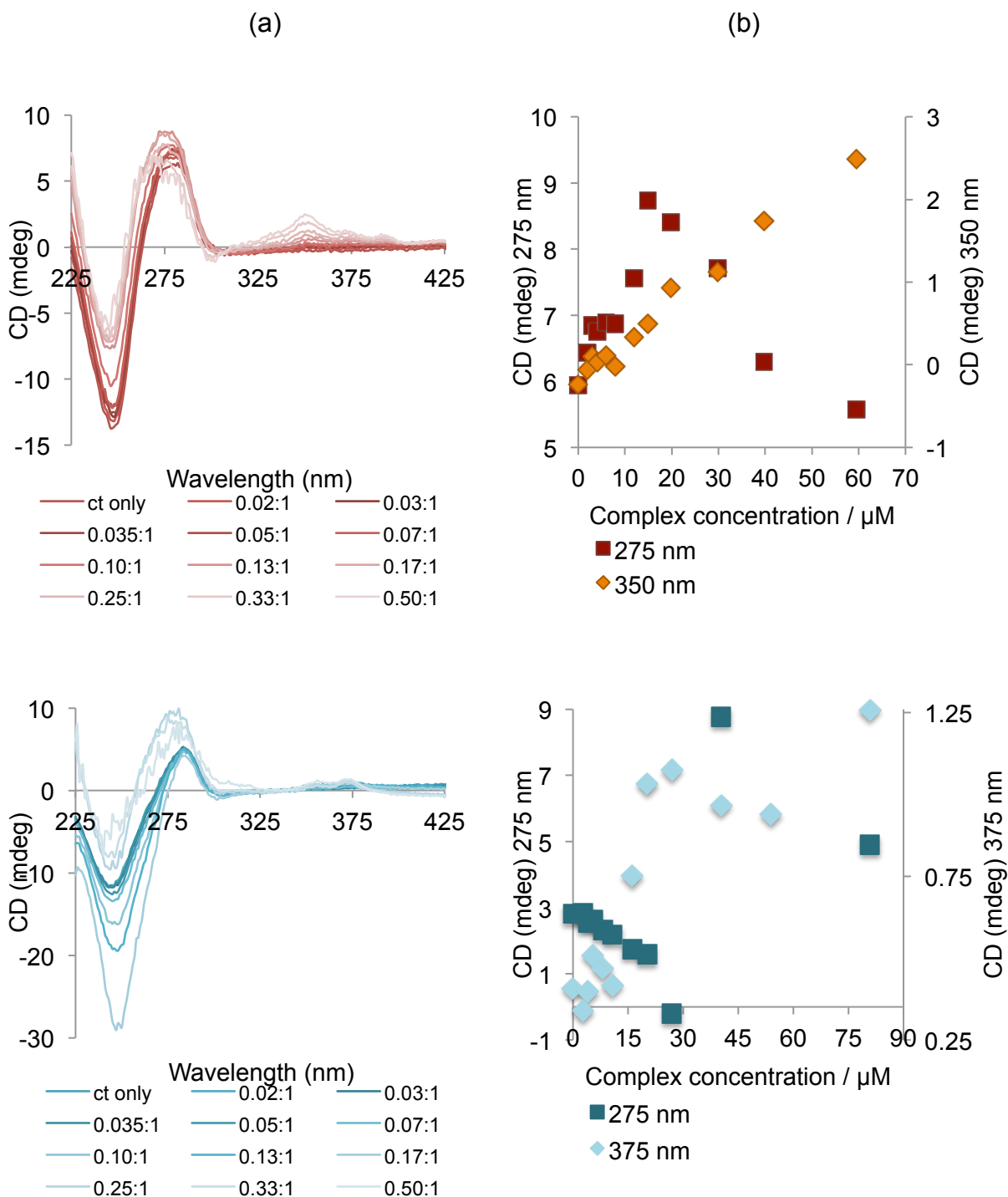


Figure 3.5.3-1 (a) CD spectrum showing the titration of $[\text{Pt}(\mathbf{12})\text{Cl}](\text{PF}_6)$ (top) and $[\text{Pd}(\mathbf{12})\text{CH}_3\text{CN}](\text{BF}_4)_2$ (bottom) in increasing concentrations to ct-DNA (150 μM , 20 mM NaCl, 1 mM $\text{Na}(\text{CH}_2)_2\text{AsO}_2 \cdot 3\text{H}_2\text{O}$, pH 6.8). Ratio of complex:DNA shown in the legend beneath each plot. (b) Peak intensity versus complex concentration for $[\text{Pt}(\mathbf{12})\text{Cl}](\text{PF}_6)$ (top) and $[\text{Pd}(\mathbf{12})\text{CH}_3\text{CN}](\text{BF}_4)_2$ (bottom) at λ_{max} 275 and 350 (Pt)/375 nm (Pd).

Htelo DNA

Addition of the platinum complex **(14)** to telomeric DNA alters the intensity of both characteristic Htelo peaks. The peak at 295 nm increases, indicating that complex addition causes stabilisation of the antiparallel G-quadruplex structure (Figure 3.5.3-2). The observed increase in this peak levels off at approximately 12 μM , indicating a 2:1 complex:DNA binding ratio. Binding of the complex at both faces (top and bottom) of the G-quartet stack would account for such a ratio. The peak at 253 nm decreases in intensity, demonstrating the ability of the complex to induce further G-quadruplex formation amongst any previously unfolded regions of DNA. Despite the lack of ICD peaks at longer wavelengths, it is evident that the platinum species interacts with the Htelo DNA, both to stabilise existing G4 structures and induce further folding.

Interestingly, similar alterations are not observed in the spectra upon addition of the palladium complex **(13)** to telomeric DNA. Comparable stabilisation of G-quadruplex structures is not observed, rather, an increase in the intensity of the 253 nm peak indicates unfolding of the DNA. The peak at 295 nm fluctuates a little, but shows no consistent pattern of increasing or decreasing signal. The interaction of the palladium complex is evidently weaker than its platinum analogue.

Htelo DNA

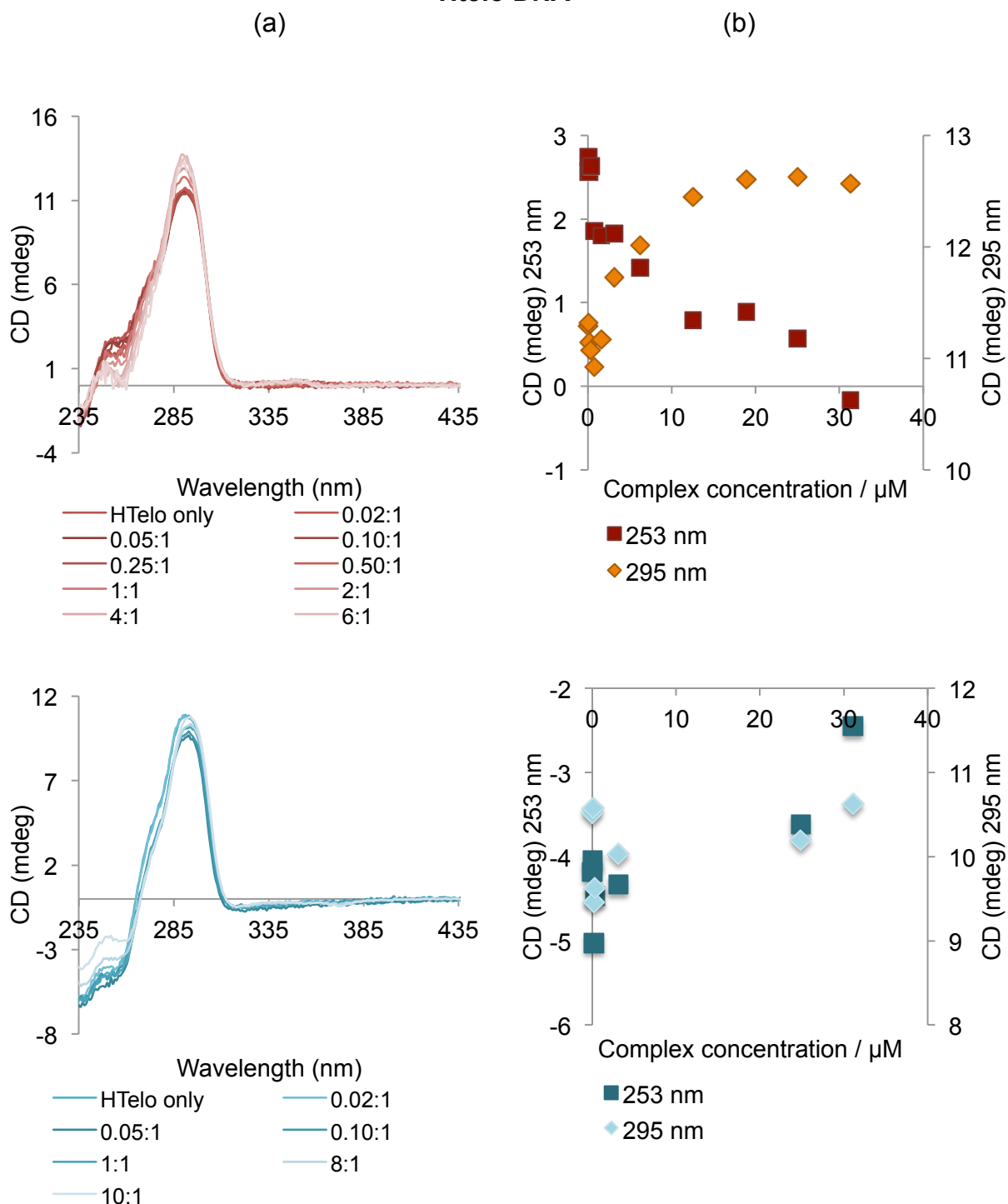


Figure 3.5.3-2 (a) CD spectrum showing the titration of $[\text{Pt}(\mathbf{12})\text{Cl}](\text{PF}_6)$ (top) and $[\text{Pd}(\mathbf{12})\text{CH}_3\text{CN}](\text{BF}_4)_2$ (bottom) in increasing concentrations to Htelo (3 μM per strand, 100 mM KCl, 10 mM Tris/HCl, pH 7.4). Ratio of complex:DNA shown in the legend beneath each plot. (b) Peak intensity versus complex concentration for $[\text{Pt}(\mathbf{12})\text{Cl}](\text{PF}_6)$ (top) and $[\text{Pd}(\mathbf{12})\text{CH}_3\text{CN}](\text{BF}_4)_2$ (bottom) at λ_{max} 253 and 295 nm.

cMyc DNA

Addition of the platinum complex **(14)** to promoter regions cMyc DNA causes an ICD peak to emerge at 295 nm (Figure 3.5.3-3). This new peak plateaus in intensity at approximately 12 μ M, indicating a 2:1 complex:DNA binding mode, in a similar fashion to that observed between the platinum complex and Htelo DNA. The appearance of this ICD peak is paired with a decrease in the peak at 265 nm (characteristic of the parallel G4 structure adopted by cMyc). These combined observations confirm that interaction is occurring, resulting in a change in G-quadruplex conformation from parallel to antiparallel.

The palladium complex **(13)** also induces ICD formation at 295 nm. However, the peak at 265 nm does not simply decrease as witnessed for the platinum complex. Rather, the peak initially decreases, before increasing at higher concentrations. The structural transitions responsible for these observed alterations appear more complex, but it seems possible that the G4 structures that begin with parallel conformation are transitioning to structures with some antiparallel nature, possibly hybrid structures.

cMyc DNA

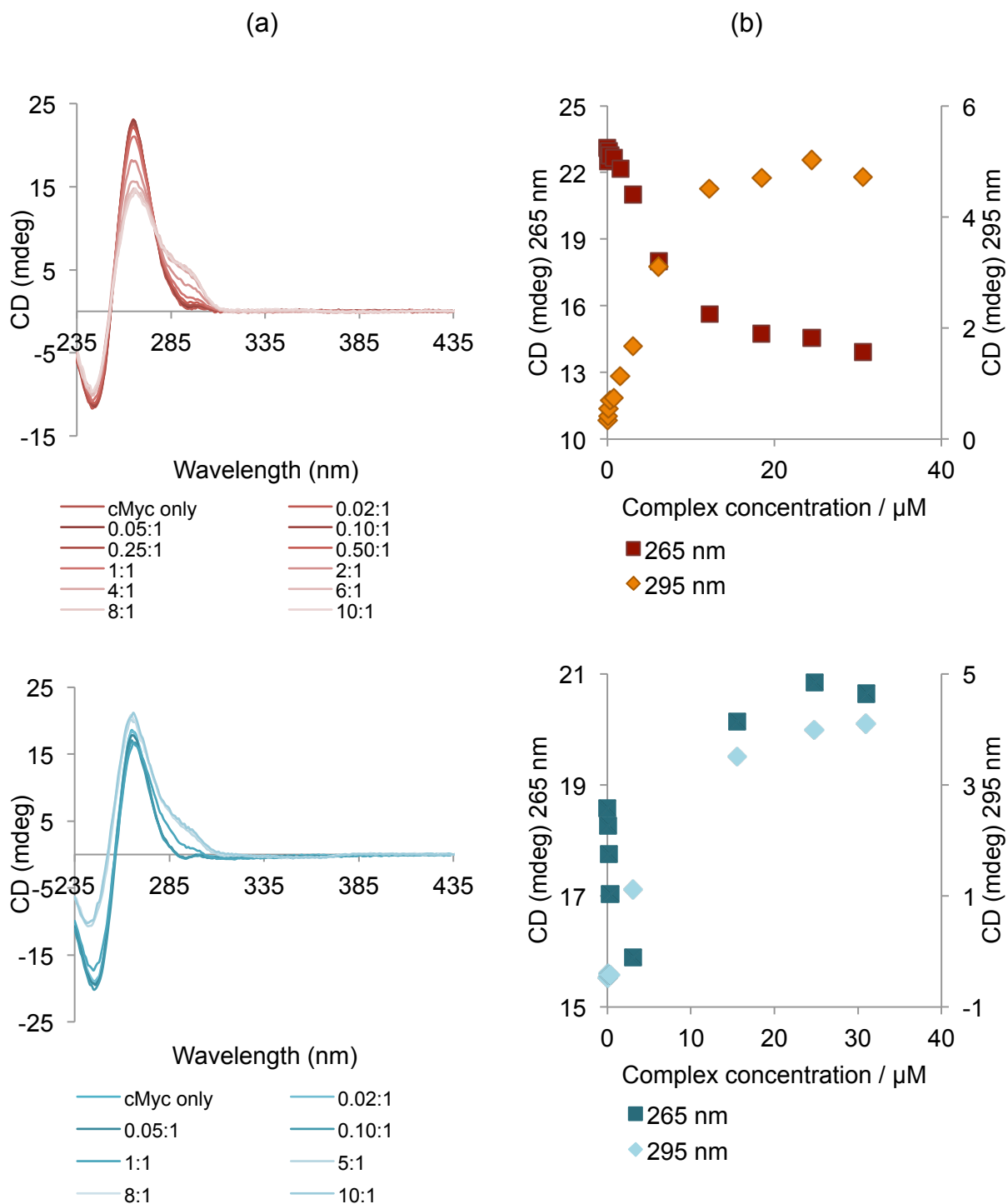


Figure 3.5.3-3 (a) CD spectrum showing the titration of $[\text{Pt}(\mathbf{12})\text{Cl}](\text{PF}_6)$ (top) and $[\text{Pd}(\mathbf{12})\text{CH}_3\text{CN}](\text{BF}_4)_2$ (bottom) in increasing concentrations to cMyc ($3 \mu\text{M}$ per strand, 100 mM KCl , 10 mM Tris/HCl , $\text{pH } 7.4$). Ratio of complex:DNA shown in the legend beneath each plot. (b) Peak intensity versus complex concentration for $[\text{Pt}(\mathbf{12})\text{Cl}](\text{PF}_6)$ (top) and $[\text{Pd}(\mathbf{12})\text{CH}_3\text{CN}](\text{BF}_4)_2$ (bottom) at λ_{max} 265 and 295 nm.

Overall, the results of these CD studies demonstrate the presence of binding interactions between both complexes and each type of DNA, though the exact nature of these interactions is not yet fully understood. Both complexes interact with ct-DNA in similar manners, resulting in the presence of ICD peaks. When titrated into Htelo and cMyc DNA sequences, it is evident that there are some differences between the two complexes, whereby the platinum complex (**14**) induces more defined changes in both DNA spectra indicating its potentially preferential binding.

To further elucidate the binding interactions occurring between each complex and these DNA structures, gel electrophoresis was employed.

3.6 Gel electrophoresis DNA binding studies

Owing to the negatively charged sugar-phosphate backbone, DNA molecules will migrate through a gel matrix towards a positively charged electrode during gel electrophoresis. Depending upon their size, DNA fragments migrate at varying speeds, with smaller fragments moving more rapidly through the gel than larger fragments.⁴² Movement of the DNA fragments through the gel may also be affected by overall charge and conformation.

3.6.1 Polyacrylamide gel electrophoresis (PAGE)

Due to the small pore size created by the gel forming process⁴³ polyacrylamide gel electrophoresis (PAGE) is commonly used for small DNA sequences (typically tens of bases), offering improved resolution of the DNA (compared to alternative gel methods such as agarose), but with a limited range of separation.

3.6.2 PAGE results

Visualisation of DNA bands can be achieved using a variety of techniques including the use of radiolabelled fragments that can be recorded by an autoradiogram,⁴⁴ fluorescently labelled DNA strands that can be easily and sensitively detected,^{45,46} and UV-Visible spectroscopy of the gel. In these experiments, DNA bands were visualised following staining of the gel with SyBr gold, which exhibits a 10,000-fold increase in fluorescence upon binding to DNA. The use of SyBr gold (as opposed to more commonly used ethidium bromide) means that extremely small volumes of DNA can be detected, saving both materials (particularly DNA) and limiting the electrophoresis run-time, which saves both time and money.⁴⁷

The quadruplex-forming DNA strands (Htelo and cMyc) used in the PAGE experiments were annealed in a potassium-rich buffer before use, ensuring that the G-quadruplex structure has pre-formed in solution and the test conditions represent binding of the complexes to existing G-quadruplexes. Each complex was incubated with the DNA for one hour prior to loading the wells on the gel. Control samples - DNA alone, DNA + solvent (10% CH₃CN) - were loaded alongside the DNA:complex samples. Once loaded, application of an electric field causes the DNA to migrate towards the positive electrode.

cMyc and Htelo DNA

The results of the PAGE experiments with cMyc and Htelo DNA are shown in Figure 3.6.2-1. On first glance, the results seem somewhat disappointing, with few striking observations. On closer inspection, there appear to be some new bands appearing, although these are rather faint.

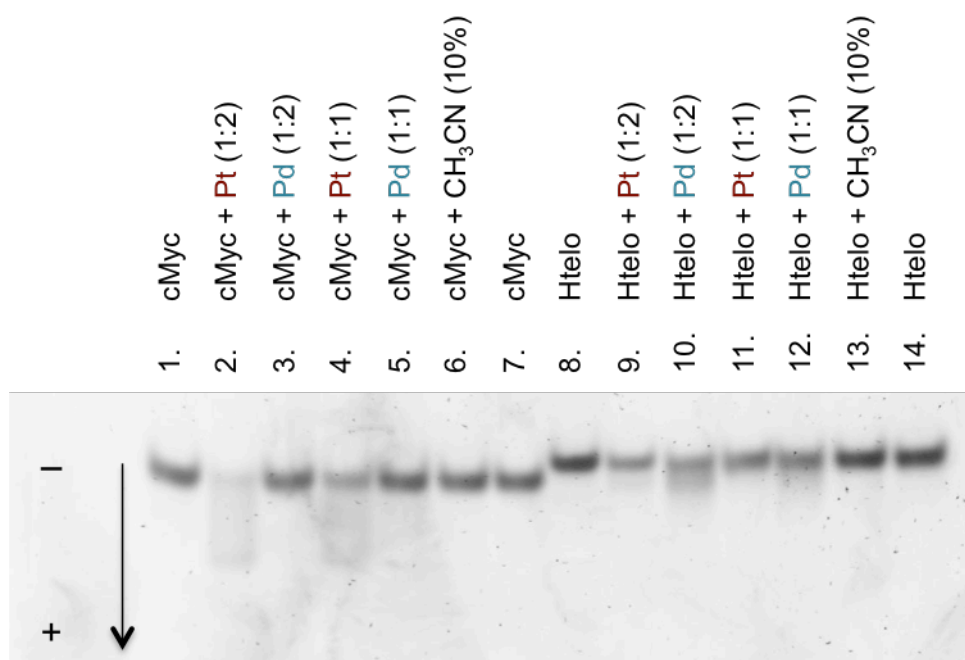


Figure 3.6.2-1 PAGE (15%) showing the migration of cMyc (lanes 1-7) and Htelo (lanes 8-14) DNA when an electric potential is applied. Samples were left at room temperature for 1 hour before loading and electrophoresis of the gel.

cMyc DNA appears to interact more strongly with the platinum complex (**14**), as evidenced by the presence of new bands in lanes 2 and 4. There is no significant difference between these two lanes, with a single new species observed in both cases, indicating a 1:1 binding mode. No effect is seen with the palladium species.

By contrast, Htelo DNA appears to interact more strongly with the palladium complex (**13**), as evidenced by the presence of new bands in lanes 10 and 12. The effect here is certainly less pronounced than that seen between cMyc and the

platinum species, possibly indicating a weaker binding interaction between Htelo and the palladium species. Again, little difference is observed between lanes 10 and 12, indicating a 1:1 binding mode. There doesn't appear to be any interaction with the platinum species.

Comparison of these results with the CD data appears to show some disparity. Although confusing, this highlights the importance of employing a combination of methods to study quadruplex-ligand interactions, in order to build a complete picture of the interactions taking place. The CD data shows that the platinum complex (**14**) interacts with both G-quadruplex forming sequences, despite it only appearing to interact with cMyc in the gel studies. The palladium complex (**13**) induced less pronounced changes in the CD spectra, but did indicate some interaction with both DNA sequences, appearing to induce conformational changes in G-quadruplex structures rather than stabilisation. The weak interaction observed between the palladium complex and Htelo in these gel studies is in agreement with the CD data, however the cMyc data is currently inconsistent, since there is no comparable interaction observed in the gel in support of the CD data.

ds26 DNA

ds26 is a reverse complementary 42 base DNA sequence that forms double-stranded DNA when two strands base pair (head-to-tail) with one another;

5'-CCT-TCA-CGC-GAA-CGT-AAT-CCT-AGG-ATT-ACG-TTC-GCG-TGA-AGG-3'

ds26 can be used in gel electrophoresis experiments as representative duplex DNA, since ct-DNA cannot be used due to the variable lengths of DNA sequences it contains. The result of the PAGE experiment with ds26 is shown in Figure 3.6.2-2.

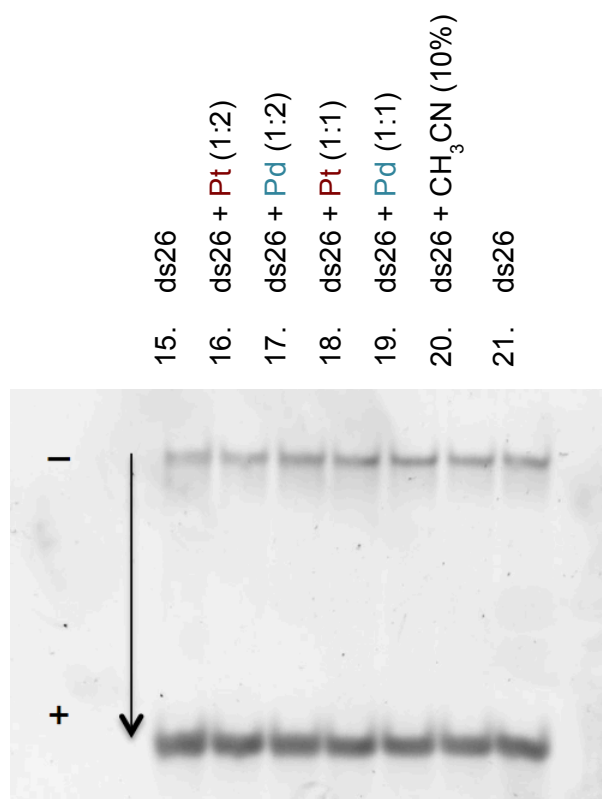


Figure 3.6.2-2 PAGE (15%) showing the migration of ds26 DNA when an electric potential is applied. Samples were left at room temperature for 1 hour before loading and electrophoresis of the gel.

There is no observable interaction between either complex and ds26, as evidenced by the absence of any new bands in the gel. It is somewhat unusual to see no interaction with duplex DNA, particularly in light of the induced peaks observed in the CD studies with ct-DNA, which indicated the presence of some interaction for both complexes. It is possible that the interaction observed in the CD studies was due to each complex interacting with non-duplex components in the ct-DNA (which is predominantly but not solely duplex), however this seems unlikely given the response observed. The absence of any evidence suggesting binding of either complex to ds26 is therefore questionable and requires repeat experiments for validation.

3.7 Conclusions

The incorporation of the terpyridine moiety into novel metal complexes fulfils the requirements for G-quadruplex binding compounds to possess both a planar aromatic surface for π -stacking interactions, along with a central metal atom to withdraw electron density from the aromatic ligands, thus providing electrostatic interactions.

Preparation of the desired tpy-based ligand was achieved using a combination of methods centred on the highly successful work of Potts *et al.*, whereby the central tpy ring was constructed *in situ*. The selected methods enabled the desired methylsulphonyl-substituted tpy ligand to be prepared in good yield. The syntheses of platinum and palladium complexes incorporating this ligand have been described.

Both complexes show good stability in solution, along with some early indications that they are capable of interacting with both duplex and G-quadruplex forming regions of DNA. On account of the discrepancies between the CD and PAGE data, repeat studies are required to determine the binding interactions taking place. To supplement this, it would be beneficial to conduct UV-Vis spectroscopy titration experiments with both complexes and each type of DNA to compare with the existing CD data.

3.8 Experimental materials and methods

3.8.1 General chemistry

Reagents and solvents were obtained from Sigma Aldrich, Fisher Scientific, Scientific Lab Supplies, Acros Organics and VWR. All solvents were of standard grade and were used without purification. Unless otherwise stated, all reactions were carried out

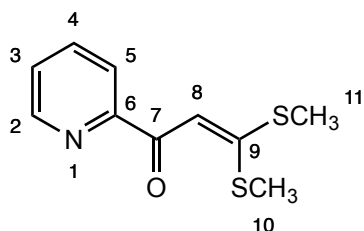
under standard conditions (298 °K, 1 atm pressure).

3.8.2 Analytical characterisation techniques

All characterisation techniques were conducted within the School of Chemistry at the University of Birmingham. Nuclear Magnetic Resonance (NMR) spectra were recorded in deuterated CDCl_3 and CD_3CN . ^1H -NMR spectra were recorded on a Bruker AV(III)300 and AV(III)400 instruments, operating at 300 and 400 MHz respectively. ^{13}C -NMR spectra were recorded on a Bruker AV(III)400 instrument operating at 100 MHz. Electrospray Ionisation Mass Spectrometry (ESI-MS) spectra were carried out by Dr. Chi Tsang and Dr. Peter Ashton (Analytical Facility). Spectra were recorded on a Waters LCT Time of Flight Spectrometer. Elemental CHN Analysis was carried out Dr. Lianne Hill (Analytical Facility) on a CE Instrument EA1110. UV-Visible (UV-Vis) spectra were recorded on a Varian Cary 5000 spectrometer. CD spectra were recorded between 200–800 nm on a ChirascanTM circular dichroism spectrometer (Applied Photophysics).

3.8.3 Chemical synthesis

3,3-bis(methylthio)-1-(pyridine-2-yl)prop-2-en-1-one (10)



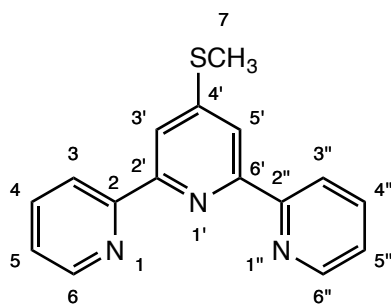
Method a. NaH (1.73 g, 60% oil dispersion, 72.0 mmol) was added in small portions at a steady rate to anhydrous DMSO (20 mL), so as to prevent frothing. Whilst

stirring vigorously, the solution was treated dropwise with 2-acetylpyridine (2.50 g, 21.0 mmol) over 15 min, followed by dropwise addition of carbon disulphide (1.65 g, 21.7 mmol) before the final dropwise addition of methyl iodide (5.71 g, 40.0 mmol). The resulting dark green mixture was stirred at room temperature for 15 h after which the mixture was cautiously quenched by the addition of iced water (10 mL). The dark solid was collected and washed with water and ice-cold ethanol until the washings were colourless. Crude analysis was carried out on the dried solid. ^1H NMR (300 MHz, CDCl_3) spectrum showed no peaks corresponding to the desired product.

Method b. Operating under an argon atmosphere, a suspension of potassium tert-butoxide (4.85 g, 43.2 mmol) in anhydrous THF (115 mL) was vigorously stirred at room temperature. A solution of 2-acetylpyridine (2.50 g, 20.7 mmol) in anhydrous THF (15 mL) was added dropwise and with caution over 5 minutes, followed by the addition of carbon disulphide (1.65 g, 21.7 mmol) over 20 minutes, resulting in a viscous, heterogeneous orange mixture. Methyl iodide (6.15 g, 43.4 mmol) was added over 1 h and the reaction mixture left stirring at room temperature for 5 h. The tan reaction mixture was poured into cold water (500 mL) and left to stand overnight. The resulting precipitate was collected by vacuum filtration and air dried to afford the title compound as brown solid (3.02 g, 65%).

^1H NMR (300 MHz, CDCl_3): δ 8.64 (1H, d, $J = 4.5$, $\text{H}_{(2)}$), 8.16 (1H, d, $J = 7.5$, $\text{H}_{(5)}$), 7.83 (1H, t, $J = 7.4$, $\text{H}_{(3)}$), 7.64 (1H, s, $\text{H}_{(8)}$), 7.40 (1H, t, $J = 6.0$, $\text{H}_{(4)}$), 2.64 (3H, s, $\text{H}_{(10)}$), 2.56 (3H, s, $\text{H}_{(11)}$). ^{13}C NMR (100 MHz, CDCl_3): δ 180.0, 161.7, 148.5, 148.2, 137.0, 135.9, 125.9, 122.7, 108.8, 17.5, 15.1. m/z (ESI +): 226 ($[\text{C}_{10}\text{H}_{11}\text{NOS}_2 + \text{H}]^+$).

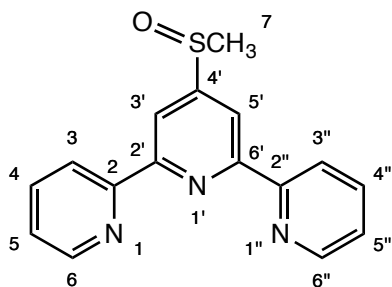
4'-(methylthio)-2-2':6'2''-terpyridine (11)



Operating under an argon atmosphere at room temperature, a suspension of potassium tert-butoxide (2.50 g, 22.0 mmol) in anhydrous THF (70 mL) was vigorously stirred. The addition of 2-acetylpyridine (1.15 mL, 10.2 mmol) resulted in the reaction mixture taking on a deep orange complexion, after which 3,3-bis(methylthio)-1-(2-pyridinyl)-2-propen-1-one (2.32 g, 10.2 mmol) was added. Following 16 h stirring at room temperature, ammonium acetate (7.93 g, 0.10 M) and glacial acetic acid (20 mL) were added before heating under reflux for a further 4 h with continuous removal of THF. The solution was cooled to 15 °C, diluted with ice and allowed to stand for 3 h. Water was then added, and the resulting precipitate collected by filtration and air dried to afford the title compound as a brown solid (2.16 g, 76%).

^1H NMR (300 MHz, CDCl_3): δ 8.71 (2H, d, $J = 7.4$, $\text{H}_{(3/3'')}$), 8.60 (2H, d, $J = 7.2$, $\text{H}_{(6/6'')}$), 8.30 (2H, s, $\text{H}_{(3'/5')}$), 7.85 (2H, t, $J = 7.6$, $\text{H}_{(4/4'')}$), 7.34 (2H, t, $J = 6.9$, $\text{H}_{(5/5'')}$), 2.66 (3H, s, $\text{H}_{(7)}$). ^{13}C NMR (100 MHz, CDCl_3): δ 155.9, 154.8, 153.6 149.0, 136.9, 123.9, 121.7, 117.0, 14.0. m/z (ESI +): 280 ($[\text{C}_{16}\text{H}_{13}\text{N}_3\text{S} + \text{H}]^+$).

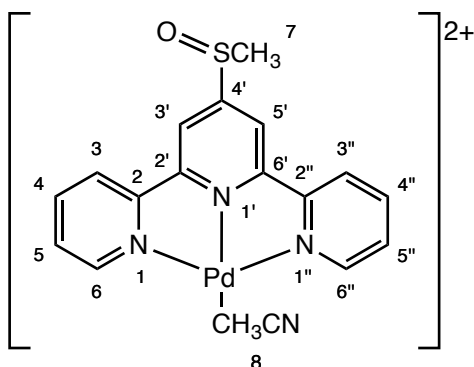
4'-(methylsulfinyl)-2-2':6'2''-terpyridine (12)



4'-(methylthio)-2-2':6'2''-terpyridine (1.60 g, 5.73 mmol) was added to a solution of glacial acetic acid (10 mL) and 30% H₂O₂ solution (2 mL) and heated at 45 °C for 18 h. Following the addition of CHCl₃ (5 mL), the solution was basified to pH 8 by the addition of 30% NH₃ solution. The solution was extracted with CHCl₃ and the organic phases combined and dried over MgSO₄. Removal of the solvent under reduced pressure yielded the product as brown solid (1.38 g, 82%).

¹H NMR (300 MHz, CD₃CN): δ 8.71 (2H, d, *J* = 7.4, H_(3/3'')), 8.63 (2H, s, H_(3'/5')), 8.62 (2H, d, *J* = 7.2, H_(6/6'')), 7.95 (2H, t, *J* = 7.5, H_(4/4'')), 7.45 (2H, t, *J* = 7.0, H_(5/5'')), 2.83 (3H, s, H₍₇₎). ¹³C NMR (100 MHz, CD₃CN): δ 160.1, 156.9, 155.3, 150.0, 137.9, 125.3, 121.7, 117.9, 115.3, 43.3. *m/z* (ESI +): 296 ([C₁₆H₁₃N₃SO + H]⁺). UV-Vis (CH₃CN) λ_{max} / nm (ε_{max} dm³mol⁻¹cm⁻¹): 251 (21800), 277 (24500).

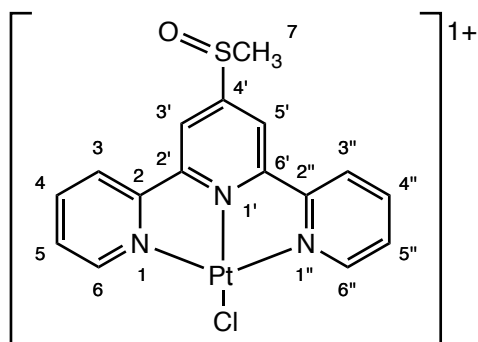
[Pd(12**)CH₃CN](BF₄)₂ (**13**)**



Operating under an argon atmosphere 4'-(methylsulfinyl)-2-2':6'2''-terpyridine (6.60 mg, 23.0 μ mol) was dissolved in dry acetonitrile (15 mL). Tetrakis(acetonitrile)palladium(II) tetrafluoroborate (10.0 mg, 23.0 μ mol) was added under a strong flow of argon and the solution stirred for 18 h at room temperature. The solution was filtered through a fine filter membrane and the filtrate concentrated *in vacuo* to form a brown solid. The solid was washed with chloroform (2 mL), methanol (2 mL) and diethyl ether (2 mL) and left to dry under vacuum to yield [Pd(**12**)CH₃CN](BF₄)₂ as a beige solid (8.70 mg, 62%).

¹H NMR (300 MHz, CD₃CN): δ 8.59 (2H, d, J = 7.4, H_(3/3'')), 8.50 (2H, s, H_(3'/5')), 8.45 (4H, overlapping m, H_{(6/6'')/(4/4'')}), 7.88 (2H, t, J = 6.9, H_(5/5'')), 2.97 (3H, s, H₍₇₎). m/z (ESI +): 442 ([Pd(C₁₆H₁₃N₃SO)(CH₃CN)]). UV-Vis (CH₃CN) λ_{max} / nm (ϵ_{max} dm³mol⁻¹cm⁻¹): 241 (26900), 267 (17200), 335 (7700), 351(10100), 368 (10100). Elemental analysis: Calculated for [Pd(C₁₆H₁₃N₃SO)(CH₃CN)](BF₄)₂ 1/3 Et₂O: C, 36.21; N, 8.74; H, 3.04. Found: C, 36.40; N, 8.33; H, 2.39.

[Pt(12)Cl](PF₆) (14)



A solution of 4'-(methylsulfinyl)-2,2':6,6''-terpyridine (7.10 mg, 25.0 μ mol) in acetonitrile was added to a solution of potassium tetrachloroplatinate (10.0 mg, 25.0 μ mol) in water. The mixture was heated under reflux at 105 °C for 18 h. Following hot filtration through a fine membrane, a methanolic solution of ammonium hexafluorophosphate (slight excess) was added to the orange filtrate. Raspberry pink precipitate immediately formed and was collected by filtration and washed carefully with CHCl₃, MeOH and Et₂O, before drying under vacuum to yield [Pt(12)Cl](PF₆) as raspberry purple solid (11.4 mg, 68%).

¹H NMR (300 MHz, CD₃CN): δ 9.08 (2H, d, J = 7.4, H_(3/3'')), 8.49 (2H, s, H_(3'/5')), 8.40 (4H, overlapping m, H_{(6/6'')/(4/4'')}), 7.90 (2H, t, J = 6.9, H_(5/5'')), 2.96 (3H, s, H₍₇₎). m/z (ESI +): 525 ([Pt(C₁₆H₁₃N₃SO)Cl]). UV-Vis (CH₃CN) λ_{max} / nm (ϵ_{max} dm³mol⁻¹cm⁻¹): 255 (26300), 283 (25200), 319 (12500), 334 (14000), 398 (3200). Elemental analysis: Calculated for [Pt(C₁₆H₁₃N₃SO)Cl](PF₆) 1/4 CHCl₃: C, 27.85; N, 6.00; H, 1.91. Found: C, 27.78; N, 5.89; H, 2.01.

3.8.4 Circular dichroism (CD)

Calf-thymus DNA (ct-DNA) was purchased from Sigma Aldrich. Htelo and cMyc DNA sequences were purchased from Eurofins. DNA stock solutions were made up in ultrapure water (18.2 MΩ). Solutions were contained within a quartz cuvette with a 1 cm pathlength. Solutions A-C (see below) were prepared for each experiment. A CD spectrum of solution A was initially recorded, before equal volumes of solutions B and C were added. Following each addition, a new CD spectrum was recorded. The addition of solution B ensures the DNA concentration remains constant over the duration of the experiment, whilst increasing the complex concentration accordingly.

ct-DNA was stored in a 3000 μM frozen stock solution. DNA solutions were analysed by UV-Vis to determine an accurate DNA concentration ($\epsilon_{258} = 6600 \text{ mol}^{-1}\text{dm}^3\text{cm}^{-1}$ calculated per base).

- A. 150 μM DNA in 20 mM NaCl, 1 mM sodium cacodylate
- B. 300 μM DNA in 40 mM NaCl, 2 mM sodium cacodylate
- C. 250 μM complex solution

Htelo DNA was stored in a 200 μM frozen stock solution. DNA solutions were analysed by UV-Vis to determine an accurate DNA concentration ($\epsilon_{252} = 228000 \text{ mol}^{-1}\text{dm}^3\text{cm}^{-1}$ calculated per strand).

- A. 3 μM DNA in 10 mM tris-HCl, 100 mM KCl
- B. 6 μM DNA in 20 mM tris-HCl, 200 mM KCl
- C. 150 μM complex solution

n.b. Htelo DNA sequences were annealed at 95 °C for 5 minutes prior to overnight storage in the fridge in preparation for use the following day.

cMyc DNA was stored in a 100 μM frozen stock solution. DNA solutions were analysed by UV-Vis to determine an accurate DNA concentration ($\epsilon_{250} = 231000 \text{ mol}^{-1}\text{dm}^3\text{cm}^{-1}$ calculated per strand).

A. 3 μM DNA in 10 mM tris-HCl, 100 mM KCl

B. 6 μM DNA in 20 mM tris-HCl, 200 mM KCl

C. 150 μM complex solution

n.b. cMyc DNA sequences were annealed at 95 $^{\circ}\text{C}$ for 5 minutes prior to overnight storage in the fridge in preparation for use the following day.

3.8.5 Polyacrylamide gel electrophoresis (PAGE)

Sample preparation completed by L. Bright. Electrophoresis completed by P. Cail.

Gel Preparation. 15% native polyacrylamide gel solution containing 2x TB buffer (1x: 890 mM tris(hydroxymethyl)amino methane, 890 mM boric acid, 25 mL, pH 8.3), 40% acrylamide (29:1, 18.75 mL) and dd H_2O (6.25 mL) was mixed before the addition of 10% (w/v) ammonium persulfate solution (234 μL) and TEMED (25 μL). The solution was poured between a set of glass electrophoresis plates (20 cm x 20 cm) and a 14 well comb inserted into the top. The gel was left for 45 minutes to polymerise before removal of the comb and thorough washing of each well with running buffer (1x TB buffer). The gel slab was mounted into an electrophoresis unit (Bio-rad) and pre-run at 300 V for 10 minutes.

Electrophoresis. Samples were prepared in eppendorfs (1.5 mL) containing the components of interest (DNA, tris HCl-KCl buffer, complex) and incubated at room temperature for 1 h. 30% glycerol solution (5 μL) was added to each sample to help the sample sink into the gel wells whilst in buffer. The samples were then loaded into

separate lanes on the gel. DNA loading dye (5x gelPilot™, QIAGEN) was loaded into the first well to monitor the progress of the experiment. The gel was run at a constant 10 V/cm for 5 h. The gel was then removed from the glass plates and immersed in a 1x SyBr Gold DNA staining solution (ThermoFisher) for 40 minutes. The gel was imaged and photographed directly in a photo illuminator (UviPro).

3.9 References

- 1 E. C. Constable and J. Lewis, *Polyhedron*, 1982, **1**, 303–306.
- 2 E. C. Constable, F. K. Khan, J. Lewis, M. C. Liptrot and P. R. Raithby, *J. Chem. Soc., Dalt. Trans.*, 1985, 333–335.
- 3 E. C. Constable, *Adv. Inorg. Chem.*, 1986, **30**, 69–121.
- 4 I. Novak and L. Klasinc, *Zeitschrift für Naturforsch. A*, 1978, **33**, 247–248.
- 5 A. M. W. Cargill Thompson, *Coord. Chem. Rev.*, 1997, **160**, 1–52.
- 6 S. Oae, *Croat. Chem. Acta*, 1986, **59**, 129.
- 7 S. Oae, *Phosphorus Sulfur Relat. Elem.*, 1986, **27**, 13–29.
- 8 S. Oae, T. Kawai and N. Furukawa, *Tetrahedron Lett.*, 1984, **25**, 69–72.
- 9 D. L. Jameson and L. E. Guise, *Tetrahedron Lett.*, 1991, **32**, 1999–2002.
- 10 K. T. Potts and P. A. Winslow, *J. Org. Chem.*, 1985, **50**, 5405–5409.
- 11 K. T. Potts, D. A. Usifer, A. Guadalupe and H. D. Abruna, *J. Am. Chem. Soc.*, 1987, **109**, 3961–3967.
- 12 K. T. Potts, M. J. Cipullo, P. Ralli and G. Theodoridis, *J. Org. Chem.*, 1982, **47**, 3027–3038.
- 13 G. R. Newkome, D. C. Hager and G. E. Kiefer, *J. Org. Chem.*, 1986, **51**, 850–853.
- 14 V. Hegde, Y. Jahng and R. P. Thummel, *Tetrahedron Lett.*, 1987, **28**, 4023–4026.
- 15 S. Mashhood and S. Tanimoto, *Bull. Inst. Chem. Res. Kyoto Univ.*, 1990, **68**, 199–207.
- 16 P. Yu, Y. Zu, Y. Fu and T. Efferth, *Molecules*, 2011, **16**, 4500–4510.
- 17 E. J. Corey and R. H. K. Chen, *Tetrahedron Lett.*, 1973, **14**, 3817–3820.

- 18 S. M. S. Chauhan and H. Junjappa, *Tetrahedron*, 1976, **32**, 1779–1787.
- 19 I. Shahak and Y. Sasson, *Tetrahedron Lett.*, 1973, **14**, 4207–4210.
- 20 W. Leslie, Thesis, Durham University, 2003.
- 21 K. T. Potts, *Bull. des Sociétés Chim. Belges*, 1990, **99**, 741–768.
- 22 M. Hudlicky, *Oxidations in Organic Chemistry*, American Chemical Society, 1990.
- 23 S. Patai, Z. Rappoport and C. Stirling, *The chemistry of sulphones and sulphoxides*, John Wiley and Sons, 1988.
- 24 S. Oae, *The Organic Chemistry of Sulfur*, Springer US, 1977.
- 25 M. Madesclaire, *Tetrahedron*, 1986, **42**, 5459–5495.
- 26 M. B. Smith and J. March, *March's Advanced Organic Chemistry: Reactions, Mechanisms, and Structure (6th Edition)*, Wiley-Interscience, 2007.
- 27 K. Kaczorowska, Z. Kolarska, K. Mitka and P. Kowalski, *Tetrahedron*, 2005, **61**, 8315–8327.
- 28 K. Sato, M. Hyodo, M. Aoki, X.-Q. Zheng and R. Noyori, *Tetrahedron*, 2001, **57**, 2469–2476.
- 29 D. Goheen and C. Bennett, *J. Org. Chem.*, 1961, **26**, 1331–1333.
- 30 N. J. Leonard and C. R. Johnson, *J. Org. Chem.*, 1962, **27**, 282–284.
- 31 R. Cremllyn, *An introduction to organosulfur chemistry*, John Wiley & Sons, 1996.
- 32 J. S. Choi, C. W. Kang, K. Jung, J. W. Yang, Y.-G. Kim and H. Han, *J. Am. Chem. Soc.*, 2004, **126**, 8606–8607.
- 33 J. R. Jeitler, M. M. Turnbull and J. L. Wikaira, *Inorganica Chim. Acta*, 2003, **351**, 331–344.
- 34 S. Oae, T. Kawai and N. Furukawa, *Phosphorous Sulfur Relat. Elem.*, 1987,

- 34**, 123–132.
- 35 G. Arena, G. Calogero, S. Campagna, L. Monsù Scolaro, V. Ricevuto and R. Romeo, *Inorg. Chem.*, 1998, **37**, 2763–2769.
- 36 W. Zhang, C. Bensimon and R. J. Crutchley, *Inorg. Chem.*, 1993, **32**, 5808–5812.
- 37 J. Kypr, I. Kejnovská, D. Renciuik and M. Vorlícková, *Nucleic Acids Res.*, 2009, **37**, 1713–25.
- 38 B. M. Bulheller, A. Rodger and J. D. Hirst, *Phys. Chem. Chem. Phys.*, 2007, **9**, 2020–35.
- 39 T. Ou, Y. Lu, J. Tan, Z. Huang, K. Wong and L. Gu, *ChemMedChem*, 2008, **3**, 690–713.
- 40 N. V Hud, F. W. Smith, F. A. L. Anet and J. Feigon, *Biochemistry*, 1996, **35**, 15383–15390.
- 41 J. Gu and J. Leszczynski, *J. Phys. Chem. A*, 2002, **106**, 529–532.
- 42 M. Yilmaz, C. Ozic and İ. Gok, *Principles of Nucleic Acid Separation by Agarose Gel Electrophoresis*, InTech, 2012.
- 43 N. C. Stellwagen, *Electrophoresis*, 2009, **30**, S188–S195.
- 44 J. Malina, M. J. Hannon and V. Brabec, *Chem. - A Eur. J.*, 2007, **13**, 3871–3877.
- 45 D. M. Engelhard, R. Pievo and G. H. Clever, *Angew. Chemie Int. Ed.*, 2013, **52**, 12843–12847.
- 46 H. Yu, X. Wang, M. Fu, J. Ren and X. Qu, *Nucleic Acids Res.*, 2008, **36**, 5695–5703.
- 47 S. Wang and E. T. Kool, *Nucleic Acids Res.*, 1994, **22**, 2326–2333.

Chapter IV

IV. EXPLORING ROUTES TO ALTERNATIVE LIGANDS

4.1 Introduction

This chapter details the synthetic methodology employed whilst exploring several routes towards alternative G-quadruplex binding ligands. Attempted with varying degrees of success, they are presented herein for the purposes of completeness, and in order to demonstrate their feasibility for future work. These routes include the design and synthesis of unsymmetrical ligand systems, the exploration of N⁺C coordination points and the incorporation of 'click'-capable functionalities. Several coupling methodologies are explored, including Suzuki, Stille, Grignard and Sonogashira.

4.2 Incorporating isoquinoline into an unsymmetrical ligand

4.2.1 Target compound 1: 3-(pyridine-2-yl)isoquinoline

On account of its demonstrated ability to achieve G-quadruplex binding interactions, incorporation of the isoquinoline motif into unsymmetrical ligands was explored. Chosen due to its structural simplicity, the first synthetic target was 3-(pyridine-2-yl)isoquinoline (Figure 4.2.1-1). Unsymmetrical ligands such as this have the potential to bind to a metal atom in the same bidentate fashion as 3,3-biisoquinoline to yield novel metal complexes. Such complexes may contain two unsymmetrical ligands, or a combination of unsymmetrical and symmetrical ligands in a mixed system.

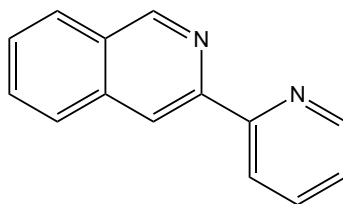


Figure 4.2.1-1 Synthetic target: 3-(pyridine-2-yl)isoquinoline

4.2.2 Palladium-catalysed α -arylation of ketones with aryl halides

Originally reported by Palucki and Buchwald,¹ Hamann and Hartwig² and Miura and coworkers,³ the palladium-catalyzed α -arylation of ketone enolates represents a powerful reaction in synthetic chemistry.⁴ Utilising a disconnection approach, Donohoe *et al.* recently reported that *pseudo*-1,5-dicarbonyl intermediates can be accessed *via* the Pd-catalyzed α -arylation of ketones with aryl halides possessing a protected ketone or aldehyde in the *ortho* position.^{5,6} Subsequent treatment with an acidic ammonium source results in acetal deprotection and aromatization to yield the corresponding isoquinoline (Figure 4.2.2-1). This route represents an entirely different approach towards isoquinoline formation than that previously employed in Chapter II. Requiring commercially available or readily-prepared precursors, it also offers an attractive method for regioselective substitution of isoquinoline in a single step.

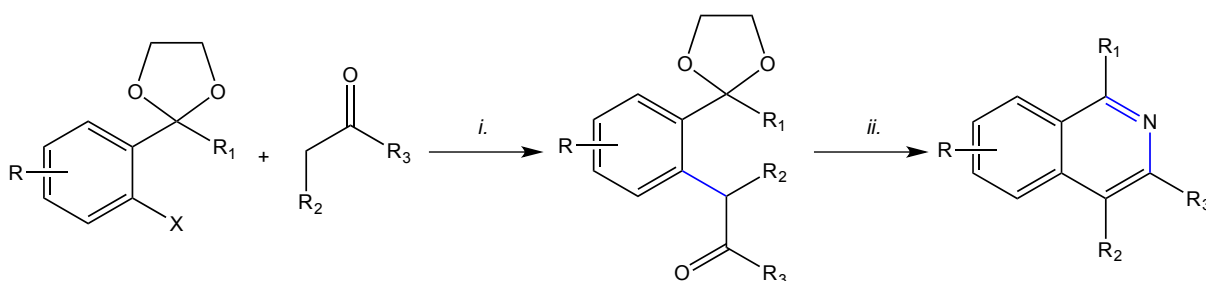


Figure 4.2.2-1 Preparation of substituted isoquinolines utilizing *i.* palladium-catalysed α -arylation of ketones followed by *ii.* ammonium chloride mediated deprotection and cyclization, as reported by Donohoe and coworkers.⁶

4.2.3 3-(pyridine-2-yl)isoquinoline (15)

Utilising the one-pot procedure reported by Donohoe *et al.* for sequential arylation and cyclisation, preparation of 3-(pyridine-2-yl)isoquinoline was attempted (Figure 4.2.3-1).

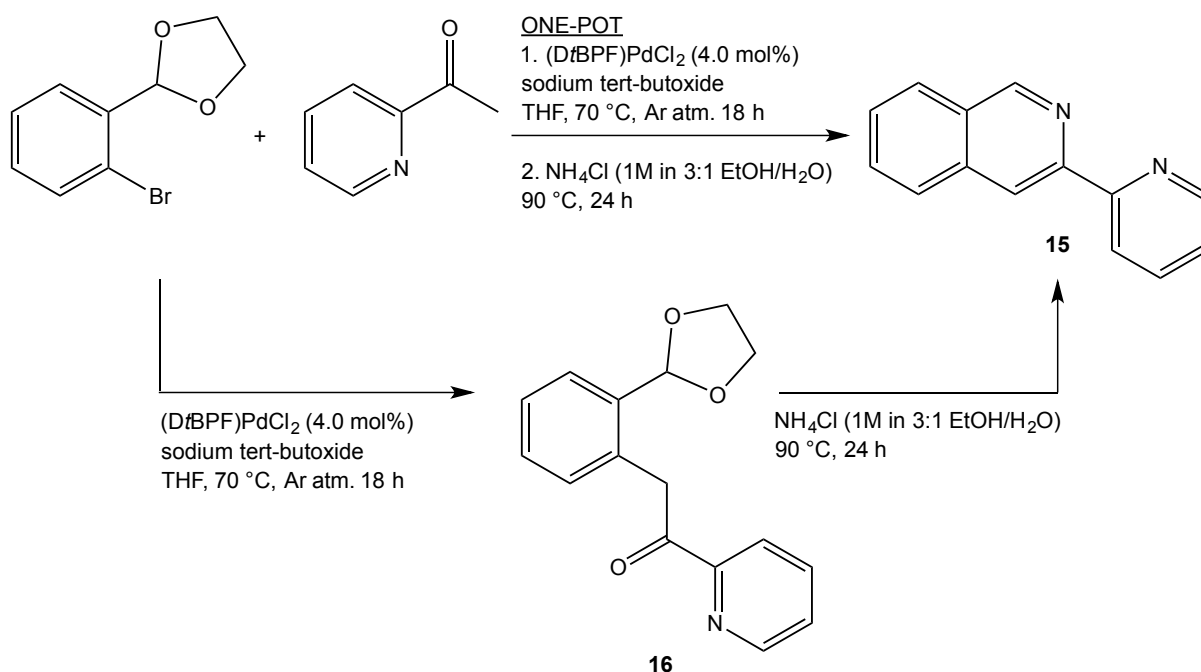


Figure 4.2.3-1 Synthesis of 3-(pyridine-2-yl)isoquinoline.

Catalyst loading of 4.0 mol % was used during the initial α -arylation of 2-acetylpyridine with aryl bromide. Following overnight heating, the cooled solution was acidified to pH 5 to enable acetal hydrolysis. Subsequent heating of the intermediate (not isolated) in a solution of ammonium chloride failed to yield the desired product, with the reaction unfortunately proving unsuccessful.

The possible cause for the reaction failure was unclear. Donohoe and coworkers have reported the successful preparation of structurally similar 3-phenylisoquinoline in 74% yield using the one-pot method. Evidently, the use of 2-

acetylpyridine instead of acetophenone to achieve the pyridine-substituted isoquinoline (**15**) instead of the phenyl-substituted isoquinoline creates a problem.

Unclear whether or not the failure was as a result of unsuccessful α -arylation in the first instance, or problems arising from the base-mediated deprotection and cyclisation that follows, the reaction was repeated. On this attempt, the transformation was carried out in two discrete synthetic steps rather than the one-pot procedure previously employed.

Disappointingly, preparation of the intermediate product, 2-(2-(1,3-dioxolan-2-yl)phenyl)-1-(pyridine-2-yl)ethanone (**16**) was unsuccessful, indicating an apparent inability of 2-acetylpyridine to undergo α -arylation. Following multiple attempts with no success, a discussion with the Donohoe group confirmed that preparation of the desired pyridine-substituted isoquinoline (**15**) can not be achieved *via* this route. Indeed, they had attempted such transformations themselves and determined the nitrogen atom from the pyridine ring to interfere with the catalytic cycle, thus preventing isoquinoline formation. This particular route towards an unsymmetrical bidentate N-donor ligand was consequently abandoned.

4.3 Incorporating isoquinoline into an unsymmetrical N[^]C-coordinating ligand with “click” capable functionality

4.3.1 Target compound 2: 3-(4-ethynylphenyl)isoquinoline

Maintaining the intention to synthesise unsymmetrical ligands incorporating the isoquinoline unit, the next synthetic target incorporated two additional features; an

alkyne group for the purpose of introducing future functionality *via* “click chemistry” and a modified N⁺C metal binding system (Figure 4.3.1-1).

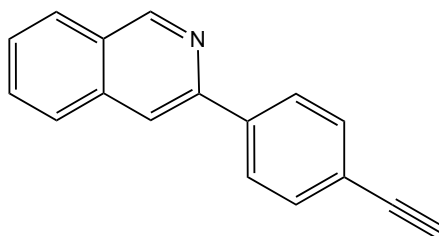


Figure 4.3.1-1 Synthetic target: 3-(4-ethynylphenyl)isoquinoline

4.3.2 “Click chemistry”

Introduced by K. Barry Sharpless in 2001, the term "click chemistry" denotes the development of a set of reactions that are highly reliable and selective, enabling the rapid synthesis of useful novel compounds through heteroatom links.⁷ These reactions are described as high-yielding, wide in scope, stereospecific, simple to perform, and can be conducted in easily removable solvents with by-products that can be easily removed without chromatography.

Click chemistry is demonstrated well for many cycloaddition reactions, especially 1,3-dipolar cycloadditions that bring together two unsaturated reactants to provide a variety of five- and six-membered heterocycles.^{8,9} The Huisgen 1,3-dipolar cycloaddition of azides and terminal alkynes to give 1,2,3-triazoles is a powerful click reaction, regarded as the ‘cream of the crop’.^{7,10} This concerted, Cu(I)-catalyzed reaction is effective in producing 1,4-regioisomers of 1,2,3-triazoles as the single products (Figure 4.3.2-1).¹¹

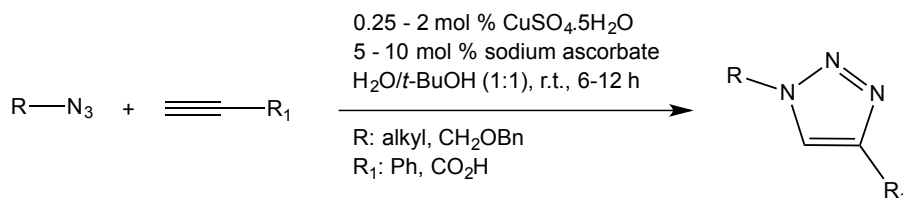


Figure 4.3.2-1 Azide-alkyne cycloaddition to produce 1,2,3-triazoles.

The addition of alkyne functionality to the target ligand facilitates future functionalization of the ligand with a wide variety of components such as a cationic side-chain capable of promoting G-quadruplex interactions *via* binding duality. There is also the potential to attach a fluorophore at this site for the purposes of imaging. Click chemistry finds widespread application for this very purpose, with an excellent selection of azide functionalised molecular probes commercially available. The *para* position is an ideal site for such modifications to be made; avoiding future hindrance to complex formation that may occur as a result of bulky substituents occupying either the *ortho* or *meta* positions. Furthermore, there is good availability of *para* substituted alkyne reagents for synthesis.

Incorporating such functionality into the target ligand enables it to serve as a ‘base unit’ which can undergo several modifications to generate a panel of novel ligands, each tailored towards maximising G-quadruplex binding interactions.

4.3.3 N⁺C coordination

Square planar complexes possessing simple bipyridine or terpyridine ligands are typically non-emissive at room temperature, due to their metal-centred *d-d* states being subject to efficient non-radiative deactivation, providing a decay pathway for the emissive state.^{12,13} The incorporation of a cyclometallated carbon raises the

energy of the metal-centred excited states due to the strong ligand field influence of the aromatic carbon atom, therefore limiting non-radiative decay.¹⁴

Several examples of cyclometallated organometallic platinum complexes based on N[^]C aromatic chelates have been reported in the literature, including homoleptic complexes (N[^]C)₂,¹⁵ heteroleptic complexes (N[^]C)(N'[^]C),¹⁶ and complexes containing a single cyclometallating ligand (N[^]C) and a non-cyclometallating ancillary ligand (LX).^{17,18} Many of these cyclometallated complexes are strongly emissive and exhibit long luminescent lifetimes (microseconds) in solution, indicative of emission from the triplet excited state.

Consequently, the incorporation of a cyclometallated carbon represents an alternative route to luminescent complexes suitable for *in vitro* imaging, possibly negating the need for molecular probe attachment at all. The wide variety of complexes reported to date, reinforce the desire to develop mixed-ligand complexes incorporating 3,3-biisoquinoline, which will very likely exhibit varying photophysical properties to the homoleptic complexes.

4.3.4 Palladium-catalysed Suzuki-coupling of organoboranes with organohalides

First published by Akira Suzuki in 1979, the Suzuki reaction is a palladium-catalysed coupling reaction between an organoborane and an organohalide.^{19–21} A carbon-carbon bond is formed between the coupling partners, using a Pd-catalyst and base (Figure 4.3.4-1).

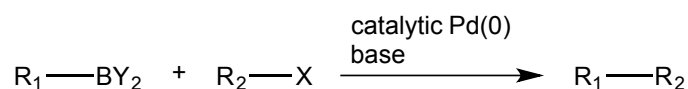


Figure 4.3.4-1 Suzuki cross-coupling between an organoborane and organohalide.

Oxidative addition of the organohalide to palladium(0) to form an organopalladium(II) species is followed by its reaction with base. Transmetalation with a boronate complex (produced by reaction of the boronic acid with base) then occurs.²² The desired coupled product is generated through reductive elimination of the palladium(II) species, regenerating the palladium(0) reagent and completing the catalytic cycle (Figure 4.3.4-2).

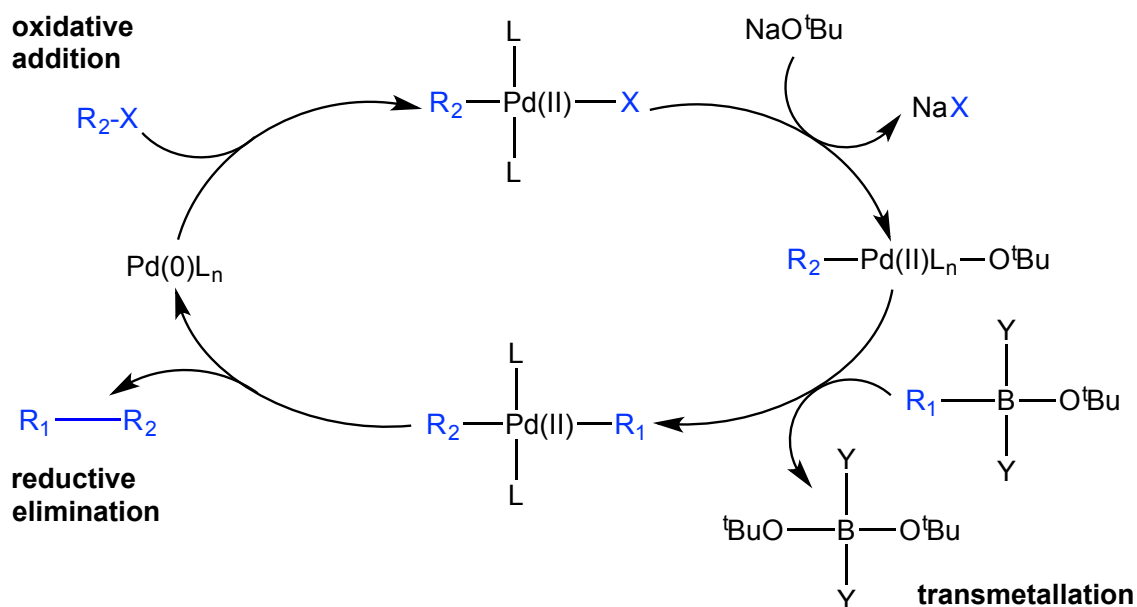


Figure 4.3.4-2 Mechanism for palladium catalysed Suzuki cross-coupling via oxidative addition, transmetalation and reductive elimination.

This route was chosen due to the availability of common boronic acids, their lower toxicity (compared to organostannane or organozinc compounds), mild reaction conditions and the convenience of already having prepared suitable halide-

substituted isoquinolines in good yields (compounds **(3)** and **(6)**, Chapter II).

4.3.5 3-(4-ethynylphenyl)isoquinoline (**17**)

The first attempt to prepare this compound involved the coupling of 3-chloroisoquinoline (**3**) and 4-ethynylphenylboronic acid pinacol ester. Using a method described by Yamashita *et al.*,²³ tetrakis(triphenylphosphine)palladium(0) and aqueous sodium carbonate solution were added to the coupling partners in anhydrous 1,4-dioxane and heated under an argon atmosphere overnight (Figure 4.3.5-1, Method a). Following cooling and filtration, analysis of the crude product showed the reaction had been unsuccessful, with no evidence of compound formation (analysed by ¹H NMR, ESI-MS, TLC). On reflection, the use of an aqueous solution of base, within a procedure that requires air sensitivity seemed somewhat counterproductive. For this reason, an alternative method was selected for a second attempt.

Utilising more common Suzuki coupling reagents, 4-(dihydroxyborophenyl)acetylene and compound (**3**) were added to tetrakis(triphenylphosphine) palladium(0) and potassium carbonate in anhydrous DMF and heated under an argon atmosphere overnight (Figure 4.3.5-1, Method b).²⁴ Rather disappointingly, following an identical work-up, this method also proved to be unsuccessful. Analysis showed the clear presence of unreacted isoquinoline-halide.

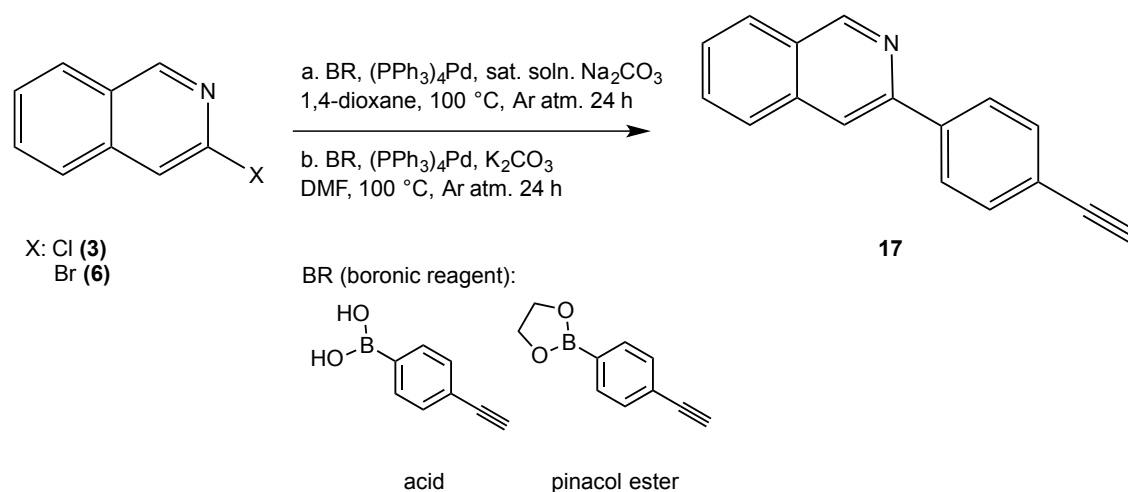


Figure 4.3.5-1 Synthesis of 3-(4-ethynylphenyl)isoquinoline by two alternative palladium-catalysed Suzuki coupling routes.

Owing to the demonstrated ability of bromine to improve reaction success by acting as a better leaving group than chlorine, the reaction was attempted using 3-bromoisoquinoline (**6**), to no avail.

Following several further unsuccessful attempts utilising both isoquinoline-halides (**3/6**) and both organoborane reagents, method (b) was trialled for a similar transformation available in the literature (Figure 4.3.5-2).²⁴

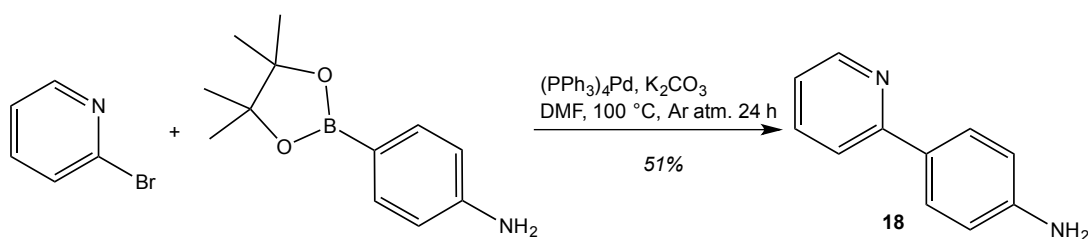


Figure 4.3.5-2 Synthesis of 4-(pyridine-2-yl)aniline

A solution of 2-bromopyridine, 4-aminophenylboronic acid pinacol ester, tetrakis(triphenylphosphine) palladium(0) and potassium carbonate in anhydrous DMF was heated under an argon atmosphere overnight. The reaction mixture was cooled, filtered, extracted into EtOAc and purified by column chromatography to yield an orange liquid which analysis confirmed to be the desired product, 4-(pyridine-2-yl)aniline (**18**) albeit in poorer yield than that reported (51% vs. 79%).

Clearly, the method being employed is a suitable method for the successful coupling of organoboranes and organohalides. Consequently, the failure of this method to achieve the target ligand is most likely due to the specific coupling reagents involved in this route. There are many examples of Suzuki couplings involving isoquinolines in the literature, therefore it is unlikely to be due to this reagent. It is proposed that the presence of the alkyne moiety on the borane reagent is causing some interference with the catalytic cycle. Formation of a metal alkyne complex in solution may prevent oxidative addition of the organohalide to the palladium catalyst, halting the catalytic cycle. This would account for the repeated presence of unchanged organohalide peaks in ^1H NMR and ESI-MS analysis of the crude product.

Owing to the repeated failure of several routes towards the desired N⁴C, click-capable ligand, and the proposed interference of the alkyne moiety, coupling reactions involving an *in situ* alkyne were no longer pursued.

4.4 An alternative route to an unsymmetrical N[^]C-coordinating isoquinoline ligand: coupling in the absence of an alkyne

4.4.1 Target ligand 3: 3-(4-chlorophenyl)isoquinoline

Following the repeated failure of Suzuki coupling routes towards the desired ligand, a new method was selected. In addition to employing an alternative coupling procedure, it was also decided to attempt coupling with a halide-substituted aromatic, rather than an alkyne-substituted aromatic. Any possible interference or hindrance experienced by the presence of the alkyne moiety is therefore avoided during the coupling process. The alkyne may then be added to the already coupled product, *via* palladium catalysed Sonogashira cross-coupling of a terminal alkyne and the existing halide. The target ligand still possesses the desired N[^]C coordination, differing only in the presence of a halide in place in of the alkyne (Figure 4.4.1-1).

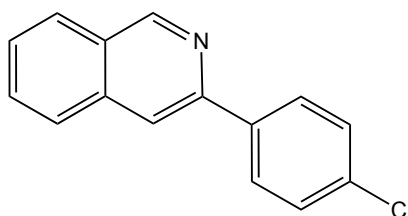
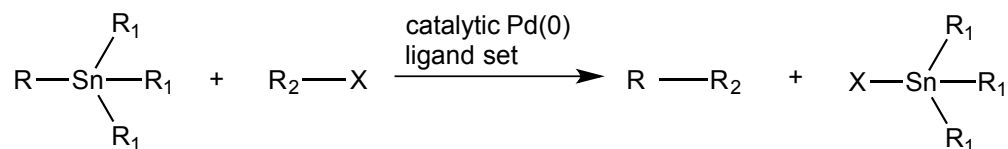


Figure 4.4.1-1 Synthetic target: 3-(4-chlorophenyl)isoquinoline

4.4.2 Palladium-catalysed Stille-coupling of organostannanes with halides

Developed by John Stille in 1978, the Stille reaction is a palladium-catalysed coupling reaction between an organotin compound and an organic electrophile (Figure 4.4.2-1).^{25,26}



X: halide (Cl, Br, I), pseudohalide (OTf, OSO₂CF₃, OPO(OR)₂)

R, R₂: typically sp² hybridised carbon (aryl, alkenyl, allyl)

R₁: alkyl

Figure 4.4.2-1 Stille cross-coupling between an organostannane and organohalide.

Oxidative addition of the halide to palladium(0) to form an organopalladium(II) species is followed by transmetalation with an organotin reagent. Reductive elimination of the palladium(II) species yields the coupled product and the regenerated palladium(0) catalyst (Figure 4.4.2-2).²⁷ Organnostannane reagents are both air and moisture stable, with many reagents commercially available or readily synthesised.²⁸

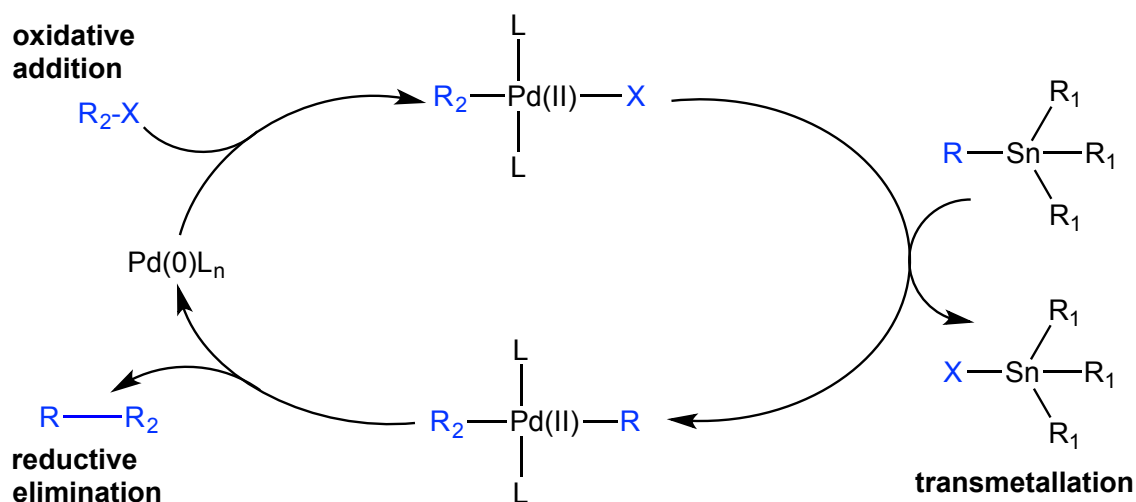


Figure 4.4.2-2 Mechanism for palladium-catalysed Stille cross-coupling via oxidative addition, transmetalation and reductive elimination.

4.4.3 3-(4-chlorophenyl)isoquinoline (19)

Based on a method described by Buchwald *et al.*,²⁹ utilising a biarylphosphine-based catalyst system, 3-bromoisoquinoline (**6**) was coupled with tributyl(4-chloro)phenylstannane (Figure 4.4.3-1).

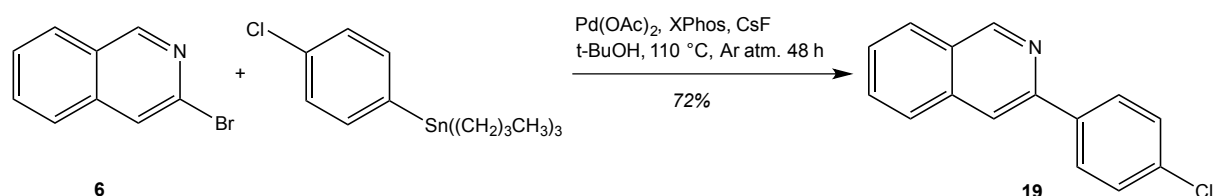


Figure 4.4.3-1 Synthesis of 3-(4-chlorophenyl)isoquinoline by palladium-catalysed Stille coupling

Reduction of the palladium(II) source ($\text{Pd}(\text{OAc})_2$), by added phosphine ligands (XPhos) generates the active palladium(0) catalyst. Fluoride ions have been found to have two useful effects on the catalytic cycle in their ability to increase rates of reactions of organotriflates, and act as scavengers for tin by-products, therefore making them easier to remove by filtration.³⁰ For these reasons, caesium fluoride is a common additive to the Stille reaction and was used herein.

Under an argon atmosphere, the reaction was heated for 48 hours and monitored by TLC. The reaction proceeded well. Purification of the crude solid by column chromatography yielded the desired product in good yield. Electrospray ionisation mass spectrometry and nuclear magnetic resonance data were in accordance with those reported in the literature.

The Stille reaction has proved to be an effective and successful method for the preparation of this compound. Previously prepared *via* silver-catalysed cyclization of

2-alkynyl benzyl azides,³¹ the Stille method represents a novel route towards this compound, securing a higher yield than that previously reported (72% vs. 56%).

Following the successful synthesis of this N[^]C coordinating ligand, future work would include attachment of an alkyne moiety *via* Sonogashira coupling at the halide site. The formation of metal complexes with various metal centres including Pt, Pd and Au could then be attempted.

4.5 Incorporating N[^]C-coordination into a terdentate ligand system

Whilst exploring the aforementioned modifications to the bidentate ligand system utilised in Chapter II, namely the incorporation of N[^]C coordination and the ability to introduce further functionality *via* a suitably located organohalide, it was a natural progression to determine if these features could also be introduced into terpyridine-based systems such as those described in Chapter III.

4.5.1 Target ligand 4: 5-chloro-1,3-di(2-pyridyl)benzene

In addition to complexes with bidentate N[^]C coordination (see 4.3.3), three classes of tridentate cyclometallating ligands have been investigated, comprising N[^]N[^]C,³² C[^]N[^]C³³ and N[^]C[^]N³⁴ coordination modes. Most notably, Williams and co-workers have reported a class of cyclometallated Pt(II) complexes of the N[^]C[^]N-coordinating ligand 1,3-di(2-pyridyl)benzene, which exhibit remarkably high luminescence quantum yields.³⁵ They have further demonstrated the ability to fine-tune the emission energy of this class of platinum complexes, enabling the emission spectra to be shifted to a shorter or longer wavelength with the use of electron-withdrawing or

electron-donating aryl substituents at the 5-position of the phenyl ring. Modification *via* the *para* substituent on the phenyl ring leaves the quantum yields and luminescent lifetimes largely unaffected.³⁶

The target ligand is a 5-substituted derivative of 1,3-di(2-pyridyl)benzene (Figure 4.5.1-1). This N^{^C^}N-coordinating ligand possesses a chloride substituent at the *para* position on the phenyl ring, ideally positioned for further modification to the chelate. This positioning (on the opposite side to the N^{^C^}N-coordination sites), ensures that any appendages will extend away from the complex centre, thus avoiding steric hindrance. In the event of enhancing G-quartet interaction, the interacting moiety is not shackled to the complex core (which will likely sit above or below the G-quadruplex stack, aligned with the core), rather it extends freely out towards the quadruplex backbone, facilitating loop/groove region interaction or intercalation between G-quartets (dependent on the linker length). A halide was chosen due to its versatility to engage in several coupling routes (including Sonogashira, Suzuki, Stille, Grignard), enabling a wide variety of modifications to be made.

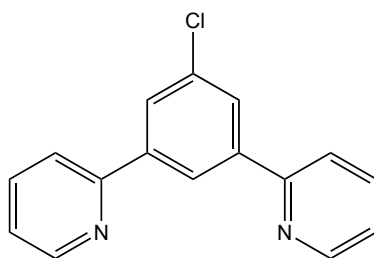


Figure 4.5.1-1 Synthetic target: 5-chloro-1,3-di(2-pyridyl)benzene

4.5.2 5-chloro-1,3-di(2-pyridyl)benzene (20)

Utilising the approach demonstrated by Williams *et al.*,³⁷ the desired N[^]C[^]N ligand was prepared by palladium-catalysed Stille cross-coupling (Figure 4.5.2-1). A mixture of 1,3-dibromo-5-chlorobenzene, 2-tributylstannylpyridine, LiCl and bis(triphenylphosphine)palladium chloride in toluene was degassed *via* five freeze-pump-thaw cycles and then heated at reflux under an inert atmosphere for 3 days. A solution of potassium chloride was added, and the mixture stirred for 30 minutes. Purification of the crude product by column chromatography yielded the desired product as colourless solid in reasonable yield.

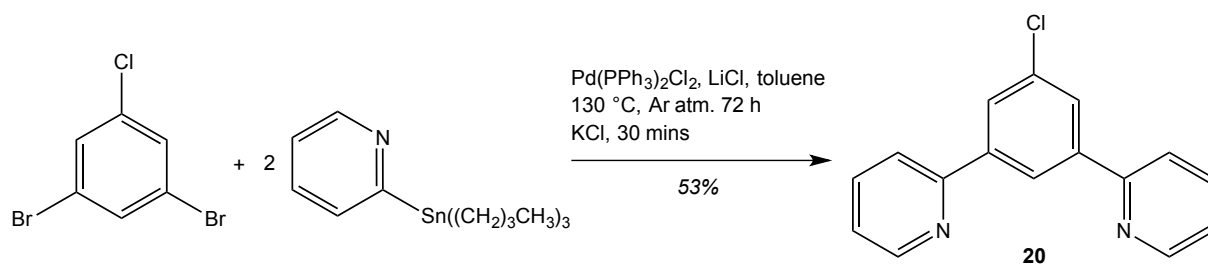


Figure 4.5.2-1 Synthesis of 5-chloro-1,3-di(2-pyridyl)benzene by palladium-catalysed Stille coupling.

Future studies with this ligand would focus on modification of the base unit to explore the full scope of functionalities that can be added to the tpy unit *via* several of the coupling methods mentioned thus far. Determining what conditions can be tolerated by the ligand is key to establishing the most effective strategy towards G-quadruplex specific ligands.

4.6 Exploring an alternative coupling route towards 3,3-biisoquinoline

4.6.1 Grignard-mediated homocoupling of sulfoxide ligands

In addition to cross-coupling reactions of sulfoxides with Grignard reagents (as described in Chapter III, *Fig. 3.2.1-1*), Oae *et al.* have also demonstrated a convenient method for ligand coupling between two methylsulphinylarenes using Grignard reagent (*Figure 4.6.1-1*).³⁸ This represents an alternative route towards 3,3-biisoquinoline; potentially circumventing the issues relating to poor yield, currently arising from the zinc-catalysed Colon-coupling route.

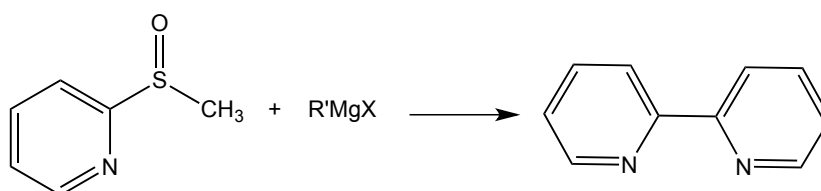


Figure 4.6.1-1 Ligand coupling between two heteroaryl groups using a Grignard reagent

4.6.2 Method trial: 5,5'-dibromo-2,2'-bipyridine synthesis

Implementation of the Grignard coupling method was first tested on a known system, in order to establish the procedure (*Figure 4.6.2-1*).

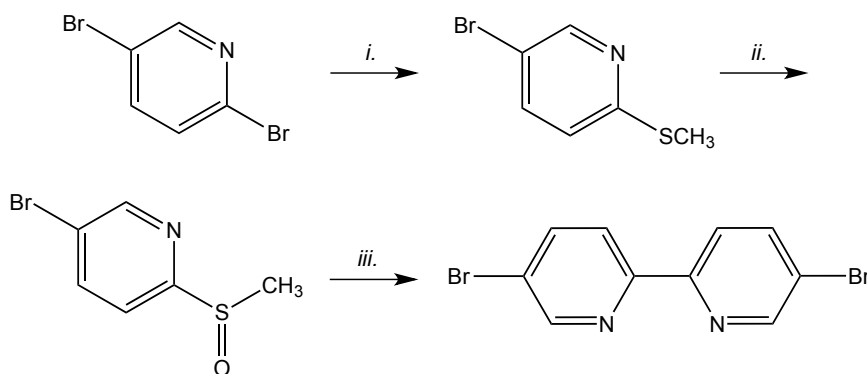


Figure 4.6.2-1 Synthesis of 5,5'-dibromo-2,2'-bipyridine under the following conditions: i. NaSMe; ii. H₂O₂/HOAc iii. EtMgBr.

Step i. The first step involves the reaction of a halogenopyridine with sodium alkanethiolate to form the methylthio-substituted pyridine. This nucleophilic aromatic substitution reaction proceeds *via* the bimolecular displacement mechanism S_NAr .^{39,40} Rate-determining addition of $^-SCH_3$ is followed by elimination to yield the methylthio-substituted pyridine.

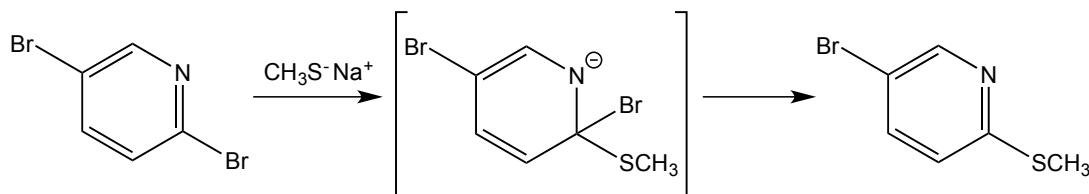


Figure 4.6.2-2 Nucleophilic aromatic substitution (step i.) *via* S_NAr mechanism.

Step ii. Partial oxidation of the sulphide to sulfoxide using hydrogen peroxide occurs in the same manner as that described previously (Chapter III, Fig. 3.2.3-3).

Step iii. Ligand coupling between two heteroaryl groups proceeds *via* an σ -sulfurane intermediate as shown in Figure 4.6.2-3. The initial step of the reaction involves ligand exchange between the (2-pyridyl group) methylsulphinyl substituent and Grignard reagent. The 2-pyridyl magnesium bromide formed immediately attacks the sulphinyl sulphur atom of the starting sulfoxide to form the crucial σ -sulfurane intermediate. Orbital overlap of the two ligands within this intermediate, results in biaryl formation.⁴¹ Grignard reagents inherently have poor functional group tolerance requiring low-temperature syntheses.

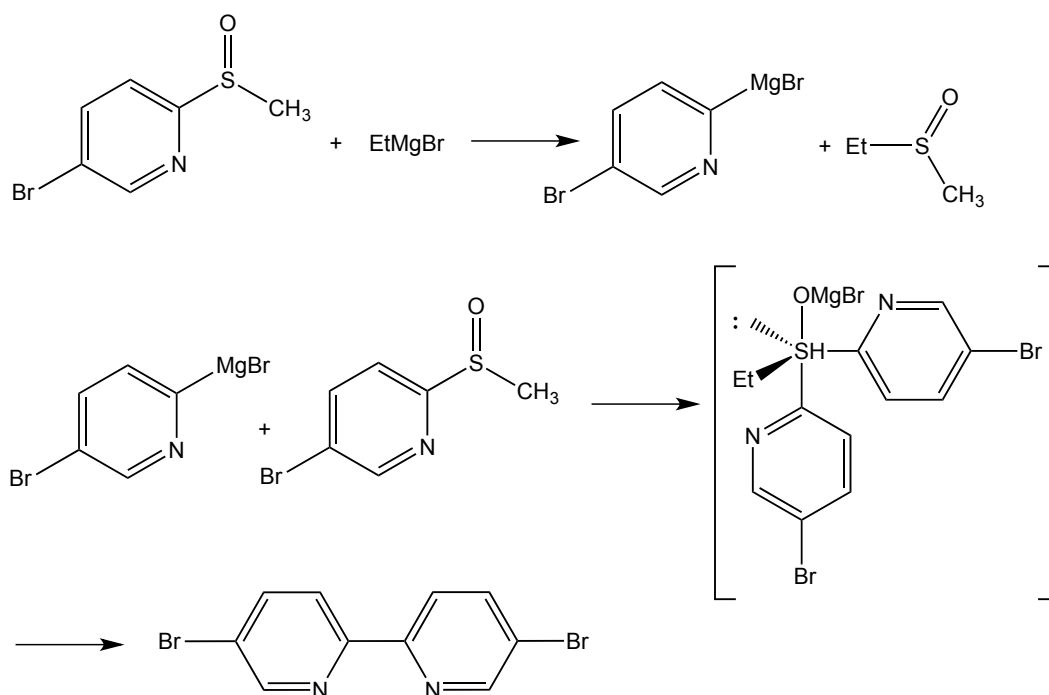


Figure 4.6.2-3 Mechanism for ligand coupling (step iii.) through an σ -sulfurane intermediate, following treatment of sulfoxides with Grignard reagent.

Specific details relating to each step of the synthesis are now briefly described, and summarised in Figure 4.6.2-4.

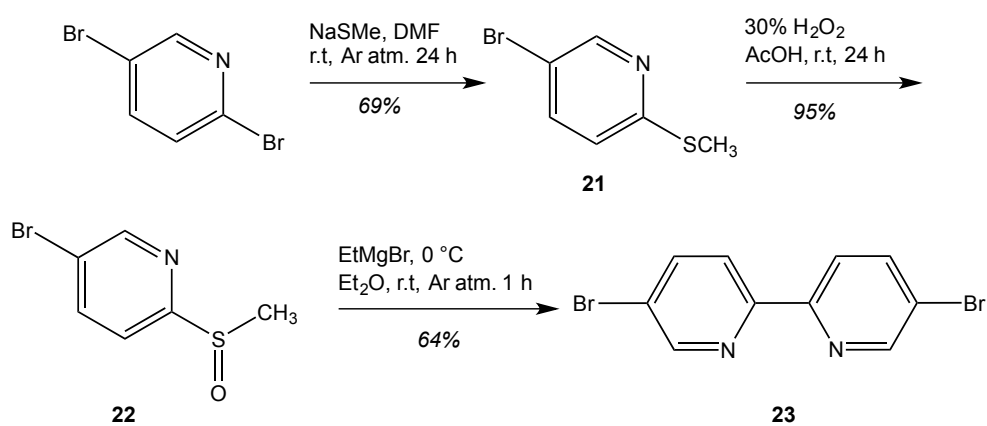


Figure 4.6.2-4 Three-step synthesis of 5,5'-dibromo-2,2'-bipyridine.

Step i. 5-bromo-2-(methylthio)pyridine (21)

Preparation of compound **(21)** was completed using a method described by Testaferri *et al.*⁴² A solution of 2,5-dibromopyridine and NaSMe in DMF was stirred under an inert atmosphere and monitored by TLC. The reaction proceeded well. Isolation of the crude product after 24 hours yielded yellow crystalline solid in good yield, and requiring no further purification. Electrospray ionisation mass spectrometry and nuclear magnetic resonance data were in accordance with those reported in the literature.

Step ii. 5-bromo-2-(methylsulphinyl)pyridine (22)

Owing to prior success in achieving partial oxidation of the sulphide to sulfoxide (see Chapter III, 3.2.3-3), the method described by Oae *et al.* was once again employed.⁴³ A solution of **(21)** in 30% H₂O₂ and glacial acetic acid was stirred for 24 hours. Following extraction of the crude product and overnight drying over P₂O₅ in a dessicator, the desired product was afforded as a yellow solid in very high yield. Electrospray ionisation mass spectrometry and nuclear magnetic resonance data were in accordance with those reported in the literature.

Step iii. 5,5'-dibromo-2,2'-bipyridine (23)

In accordance with the standard method reported by Oae *et al.*,³⁸ EtMgBr was added to an ice-cold solution of **(22)** in Et₂O. The resulting suspension was stirred at room temperature for 1 hour. Addition of water, followed by extraction with toluene isolated crude solid that was recrystallized with EtOAc to afford the desired product as gold-

brown crystals in good yield. Electrospray ionisation mass spectrometry and nuclear magnetic resonance data were in accordance with those reported in the literature.

4.6.3 Synthesis of 3,3-biisoquinoline *via* Grignard-mediated homocoupling

Having successfully trialled Grignard-mediated ligand coupling, the method was applied to the formation of 3,3-biisoquinoline (Figure 4.6.3-1). Utilising the same three-step procedure as that demonstrated above, conversion of isoquinoline-halide is followed by partial oxidation of the resulting sulphide to sulfoxide. Ligand coupling through an σ -sulfurane intermediate produces the coupled biisoquinoline product.

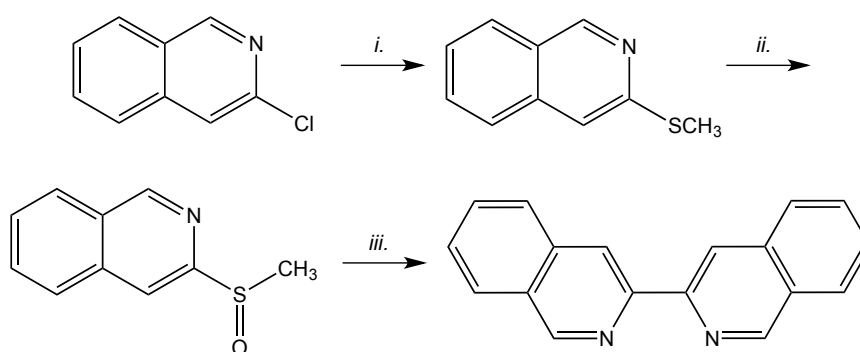


Figure 4.6.3-1 Synthesis of 3,3-biisoquinoline under the following conditions: i. NaSMe; ii. H₂O₂/HOAc iii. EtMgBr.

3-(methylthio)isoquinoline (**24**)

In accordance with Testaferri *et al.*,⁴² a solution of 3-chloroisoquinoline (**3**) and NaSMe in DMF was stirred under an inert atmosphere overnight (Figure 4.6.3-2).

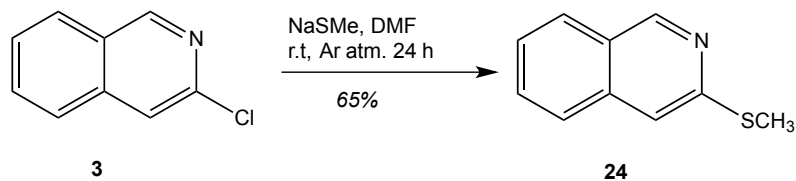


Figure 4.6.3-2 Synthesis of 3-(methylthio)isoquinoline

An identical work-up to that previously employed yielded a yellow solid in good yield. Electrospray ionisation mass spectrometry and nuclear magnetic resonance data were in accordance with those reported in the literature.

3-(methylsulphonyl)isoquinoline (25)

Oxidation of the existing methylthio-substituted isoquinoline to the desired methylsulphonyl-substituted isoquinoline was achieved using hydrogen peroxide in glacial acetic acid as described by Oae *et al.*⁴³ (Figure 4.6.3-3).

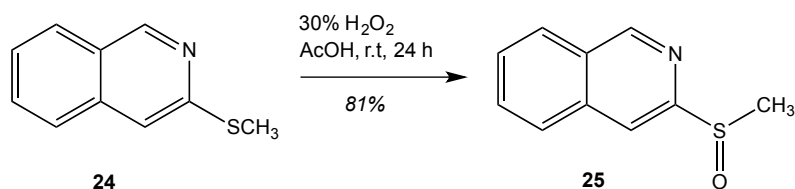


Figure 4.6.3-3 Synthesis of 3-(methylsulphonyl)isoquinoline

The reaction proceeded well under acidic conditions, producing a dark yellow solid in good yield. Electrospray ionisation mass spectrometry and nuclear magnetic resonance data were in accordance with those reported in the literature. Partial oxidation of the sulphide is confirmed by an observable downfield shift in all peaks (Figure 4.6.3-4). In particular, the thiomethyl peak from 2.63 ppm (R-S(CH₃)) to 3.29 ppm (R-S(=O)(CH₃)), and the aromatic proton in closest proximity and thus that which

experiences the greatest degree of deshielding due to the nearby oxygen atom from 7.43 ppm to 8.55 ppm.

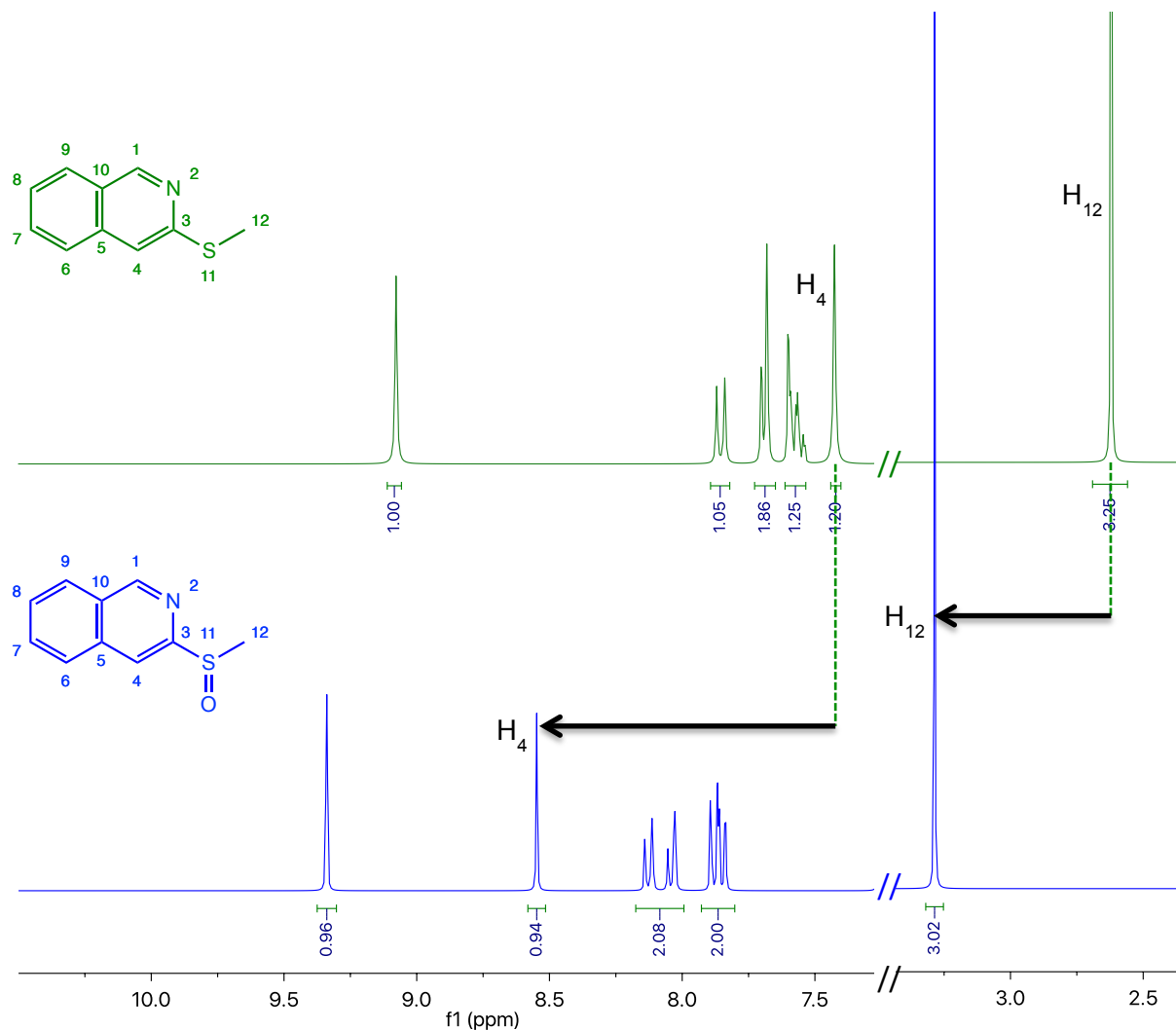


Figure 4.6.3-4 ¹H-NMR spectra overlay of 3-(methylthio)isoquinoline (**24**) and 3-(methylsulphonyl)isoquinoline (**25**) (300 MHz, CDCl₃, 298°K)

3,3-biisoquinoline (**26**)

In accordance with Oae *et al.*,³⁸ EtMgBr was added to a cold solution of 3-(methylsulphonyl)isoquinoline (**25**) in THF and stirred under an inert atmosphere at room temperature (Figure 4.6.3-5).

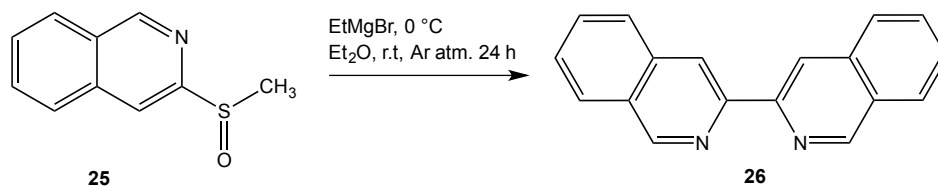


Figure 4.6.3-5 Synthesis of 3,3'-biisoquinoline

White cloudy suspension formed upon addition of the Grignard to the yellow solution. Monitoring of the reaction by TLC saw no change, even after 24 hours (Oae *et al.* report ligand coupling typically achieved in under one hour).³⁸ At this point, the reaction was 'worked up', with analysis unfortunately confirming the reaction to be unsuccessful. The ^1H NMR spectrum showed the clear presence of unreacted starting material.

Further attempts were made, with no noticeable developments or success. Following the repeated failure of this method, it was proposed that the solvent may have some effect, since the trial coupling to prepare (**23**) was completed in diethyl ether, whilst the attempted synthesis of 3,3'-biisoquinoline had been carried out in tetrahydrofuran due to insolubility of the ligand in Et_2O .

To assess this hypothesis, preparation of trial compound (**23**) was revisited, and upon confirming solubility of the methylsulphonylpyridine (**22**) in THF, the reaction was repeated under otherwise identical conditions. The reaction was surprisingly unsuccessful, with evidence of only the starting material in crude analysis. Despite THF being both a common and widely used solvent for reactions involving Grignard reagents, the success of this particular transformation was shown to be solvent-dependent.

Assuming that the use of THF hinders 3,3-biisoquinoline formation in a similar way to that observed for the trial reaction, attempting the coupling in Et₂O would likely be more successful. Unfortunately, 3-(methylsulphinyl)isoquinoline (**25**) is insoluble in Et₂O, which currently limits the reaction from proceeding *via* this route. Future attempts would benefit from the exploration of mixed-solvent systems that could mediate the Grignard coupling, whilst assisting solubility.

4.7 Incorporating alkyne functionality

Whilst exploring alternative syntheses not included within this thesis, Sonogashira cross-coupling was one method employed. Since this method is implicated in the further development/modification of the ligands discussed herein, the successful implementation of this method is now described, by way of demonstration of its suitability and scope.

4.7.1 Palladium- and copper-catalysed Sonogashira-coupling of terminal alkynes with halides

First reported by Kenkichi Sonogashira and coworkers in 1975, the sonogashira reaction is a palladium and copper catalysed coupling reaction between a terminal alkyne and halide (Figure 4.7.1-1).⁴⁴ Simultaneous catalyst use increases the rate of reaction, rendering the Sonogashira cross-coupling reaction highly useful, particularly in the alkynylation of aryl and alkenyl halides.⁴⁵

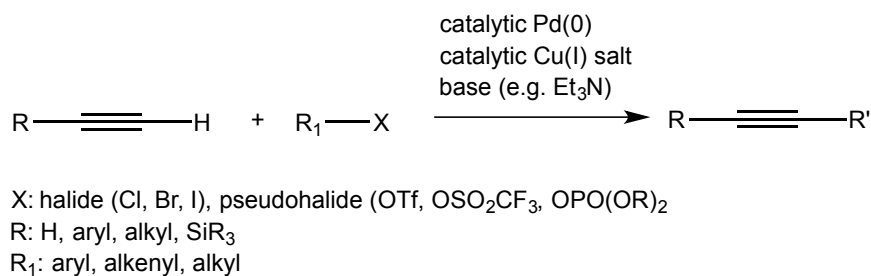


Figure 4.7.1-1 Sonogashira cross-coupling between a terminal alkyne and halide

The mechanism of the catalytic cycles involved is not clearly understood, particularly with regards to the copper co-catalyst.⁴⁶ Oxidative addition of the halide to the active palladium(0) species produces an organopalladium(II) species. Transmetalation of this species with a copper(I) acetylide species (produced in the copper cycle) expels the copper halide. Reductive elimination yields the coupled alkyne product, alongside regeneration of the palladium(0) catalyst, completing the cycle (Figure 4.7.1-2).

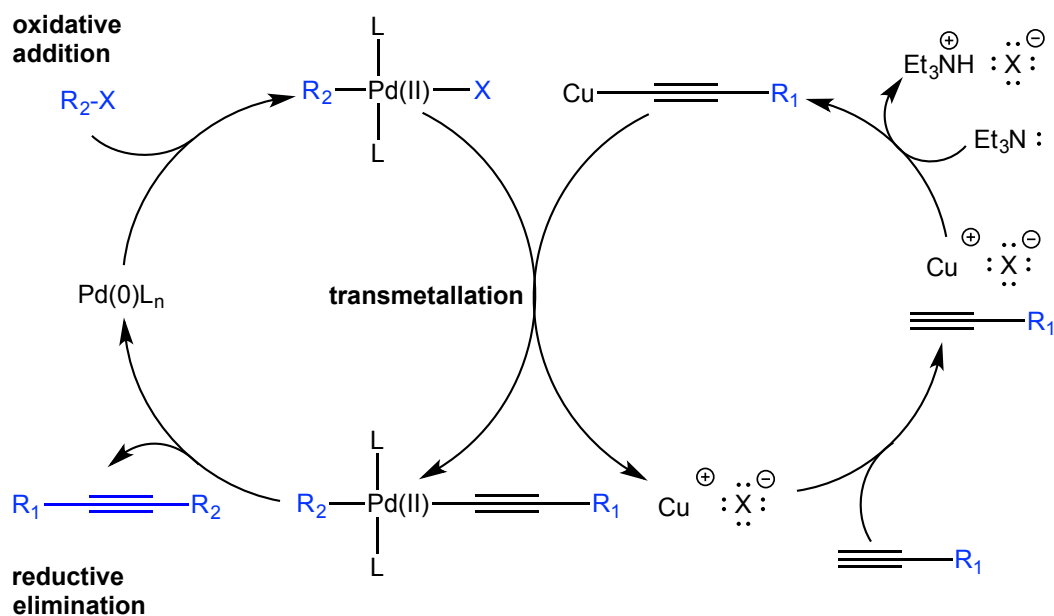


Figure 4.7.1-2 Mechanism for palladium and copper catalysed Sonogashira cross-coupling via oxidative addition, transmetalation and reductive elimination of the palladium catalyst, alongside a less-understood copper cycle.

4.7.2 6-(2-trimethylsilyl)ethynyl-3-chloroisoquinoline (27)

A solution of 6-bromo-3-chloroisoquinoline, ethynyltrimethylsilane, $\text{PdCl}_2(\text{PPh}_3)_2$ and copper iodide in triethylamine was heated under an inert atmosphere for 4 hours, whilst monitoring with TLC (Figure 4.7.2-1).

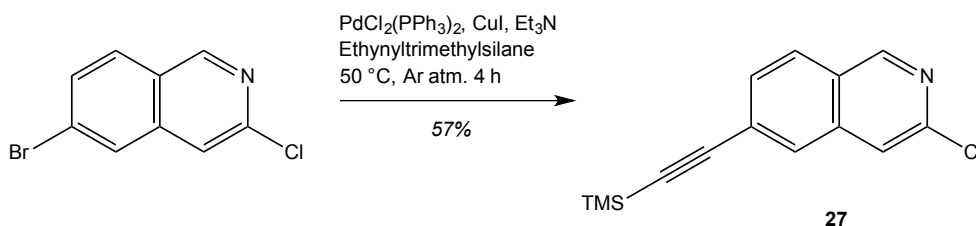


Figure 4.7.2-1 Synthesis of 6-(2-trimethylsilyl)ethynyl-3-chloroisoquinoline by palladium and copper catalysed Sonogashira coupling.

Triethylamine acts as both the base and solvent. The reaction medium must be basic to facilitate deprotonation of the terminal alkyne to form the corresponding alkyne anion, which is then able to bind to the oxidised copper.⁴⁷ Removal of the solvent and column chromatography purification of the crude solid yielded the desired product in reasonable yield. The success of the coupling reaction is evidenced by the presence of a new peak attributed to $\text{Si}(\text{CH}_3)_3$ (Figure 4.7.2-2). Furthermore, the alkynyl substituent has a greater shielding effect than the halide atom it replaces, resulting in an upfield shift in the peaks attributed to the neighbouring protons ($\text{H}_{(6)}$: 8.15 ppm to 8.02 ppm; $\text{H}_{(8)}$: 7.78 ppm to 7.65 ppm).

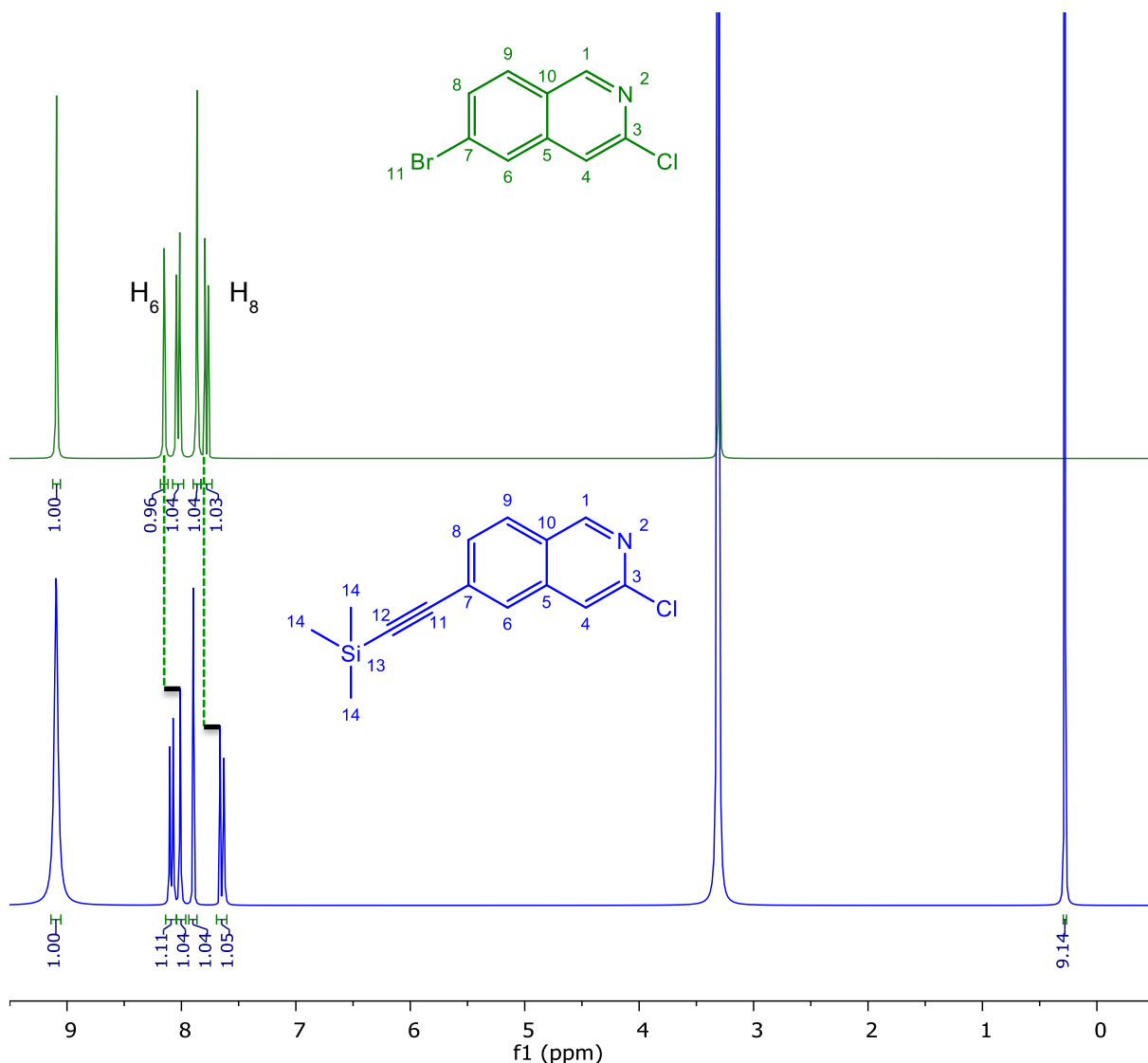


Figure 4.7.2-2 ^1H -NMR spectra overlay of 6-bromo-3-chloroisoquinoline and 6-(2-trimethylsilyl)ethynyl-3-chloroisoquinoline (**26**) (300 MHz, MeOD, 298 °K)

Preparation of this product (**26**) has demonstrated the feasibility of the Sonogashira cross-coupling method for coupling alkynes to isoquinolines. Despite its original role in an alternative synthetic scheme, this target still represents a very useful building block in the preparation of novel ligands incorporating isoquinoline. The additional halide group facilitates further modification through a variety of coupling routes, several of which have been explored within this chapter.

4.8 Conclusions

This chapter demonstrates synthetic success and failure in equal measure. Initial attempts to prepare an unsymmetrical ligand *via* α -arylation were hindered due to the presence of an additional nitrogen during the catalytic cycle. Attempts to utilise an N[^]C coordination system alongside an alkyne moiety also failed, on account of the interference of the unprotected alkyne. The preparation of an unsymmetrical ligand with N[^]C coordination, prepared *via* Stille coupling in the absence of an alkyne were successful. This ligand possesses a halide substituent that can be exploited to introduce alkyne functionality *via* Sonogashira cross-coupling. Alternatively, the halide serves as a versatile coupling partner for a variety of methodologies, should alternative functionalities be desired. The incorporation of N[^]C coordination into a terdentate system also proved successful. Grignard homocoupling routes have been explored, so far proving unsuccessful for the preparation of 3,3-biisoquinoline due to solubility. Mixed solvent-systems are anticipated to resolve this issue in the future.

4.9 Experimental materials and methods

4.9.1 General chemistry

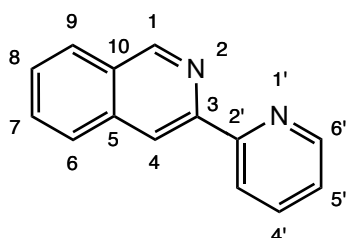
Reagents and solvents were obtained from Sigma Aldrich, Fisher Scientific, Scientific Lab Supplies, Acros Organics and VWR. All solvents were of standard grade and were used without purification. Unless otherwise stated, all reactions were carried out under standard conditions (298 °K, 1 atm pressure).

4.9.2 Analytical characterisation techniques

All characterisation techniques were conducted within the School of Chemistry at the University of Birmingham. Nuclear Magnetic Resonance (NMR) spectra were recorded in deuterated CDCl_3 , CD_3CN , CD_3OD and d_6 -DMSO. ^1H -NMR spectra were recorded on a Bruker AV(III)300 and AV(III)400 instruments, operating at 300 and 400 MHz respectively. ^{13}C -NMR spectra were recorded on a Bruker AV(III)400 instrument operating at 100 MHz. Electrospray Ionisation Mass Spectrometry (ESI-MS) spectra were carried out by Dr. Chi Tsang and Dr. Peter Ashton (Analytical Facility). Spectra were recorded on a Waters LCT Time of Flight Spectrometer.

4.9.3 Chemical synthesis

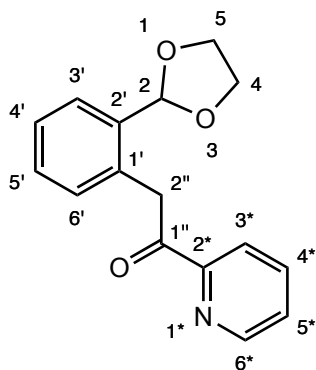
3-(pyridine-2-yl)isoquinoline (15)



A resealable reaction tube was sealed with a rubber septum and flame dried under a flow of argon. $(\text{DtBPF})\text{PdCl}_2$ (4.0 mol%, 3.80 mg, 5.82 μM) and sodium *tert*-butoxide (69.9 mg, 728 μM) were added to the tube. The aryl halide (66.7 mg, 291 μM) was dissolved in dry THF (5 mL) and the resulting solution was added *via* syringe to the tube. The ketone (42.0 mg, 349 μM) was then added *via* syringe to the tube. The rubber septum was replaced with a screw cap and the tube heated at 70 $^\circ\text{C}$ for 18 h. Upon cooling to room temperature, the reaction was acidified to pH 5 by the addition of aqueous HCl (1.0 M). A solution of NH_4Cl (10 eq., 1.0 M in 3:1 EtOH/ H_2O) was

then added and the tube resealed and heated at 90 °C for 24 h. The reaction was cooled to room temperature and quenched by the addition of saturated aqueous NaHCO₃ (10 mL). The aqueous layer was extracted with Et₂O and the combined organics were dried over Na₂SO₄, filtered and the solvent removed *in vacuo*. Analysis of crude ¹H NMR showed the presence of starting materials and deprotected aryl halide only.

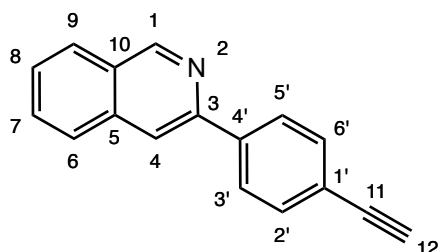
2-(2-(1,3-dioxolan-2-yl)phenyl)-1-(pyridine-2-yl)ethanone (16)



A resealable reaction tube was sealed with a rubber septum and flame dried under a flow of argon. (DfBPF)PdCl₂ (4.0 mol%, 3.80 mg, 5.82 μM) and sodium *tert*-butoxide (69.9 mg, 728 μM) were added to the tube. The aryl halide (66.7 mg, 291 μM) was dissolved in dry THF (5 mL) and the resulting solution was added *via* syringe to the tube. The ketone (42.0 mg, 349 μM) was then added *via* syringe to the tube. The rubber septum was replaced with a screw cap and the tube heated at 70 °C for 18 h. The reaction was then cooled to room temperature and quenched by the addition of H₂O (25 mL). The aqueous layer was extracted with Et₂O and the combined organics were dried over Na₂SO₄, filtered and the solvent removed *in vacuo* to give crude

product. Analysis of crude ^1H NMR showed the presence of starting materials only.

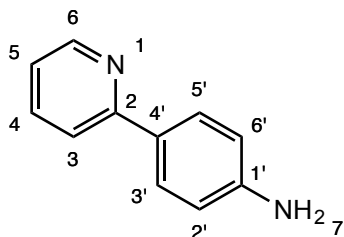
3-(4-ethynylphenyl)isoquinoline (17)



Method a. A mixture of 3-chloroisoquinoline (**3**) (93.4 mg, 0.57 mmol), 4-ethynylphenylboronic acid pinacol ester (156 mg, 0.68 mmol), tetrakis(triphenylphosphine)palladium(0) (32.8 mg, 0.03 mmol), 2M Na_2CO_3 aqueous solution (1 mL) and 1,4-dioxane (3 mL) was degassed and heated at 100 °C for 18 h. Upon cooling to room temperature, the reaction mixture was filtered through celite, which was rinsed with EtOAc. The filtrate was concentrated *in vacuo* and dried under reduced pressure. Purification of the remaining brown, oily residue was attempted by flash column chromatography on silica gel, eluting with EtOAc:hexane (1:1). No product was obtained.

Method b. A mixture of 3-chloroisoquinoline (**3**) (93.4 mg, 0.57 mmol), 4-(dihydroxyborophenyl)acetylene (92.0 mg, 0.63 mmol), K_2CO_3 (237 mg, 1.72 mmol), tetrakis(triphenylphosphine)palladium(0) (19.5 mg, 17.0 μmol) and anhydrous DMF (20 mL) was degassed and heated at 100 °C for 18 h. Remainder of method as stated above (method a). No product was obtained.

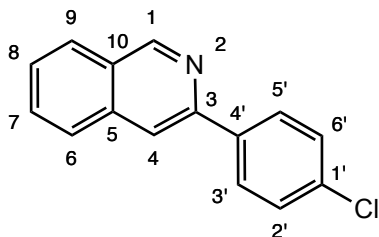
4-(pyridine-2-yl)aniline (18)



2-bromopyridine (144 mg, 0.91 mmol) and 4-aminophenylboronic acid pinacol ester (300 mg, 1.37 mmol) were dissolved in anhydrous DMF (30 mL). To the solution were added tetrakis triphenylphosphine palladium (73.7 mg, 0.06 mmol) and K_2CO_3 (629 mg, 4.56 mmol) and the mixture was stirred under an inert atmosphere for 2 h at 100 °C. The reactant was poured into water and filtered, and the filtrate was extracted with ethyl acetate. The organic layer was washed with water and brine, and dried over $MgSO_4$. The solvent was removed under reduced pressure and the residue purified by column chromatography on silica gel, eluting with EtOAc/Hexanes (3:7) to afford the desired product as orange liquid (79.0 mg, 51%).

1H NMR (300 MHz, d_6 -DMSO): δ 8.51 (1H, dt, J = 8.5, $H_{(6)}$), 7.79 (2H, d, J = 7.8, $H_{(5'/3')}$), 7.75-7.72 (2H, m, $H_{(4/3)}$), 7.14 (1H, td, J = 7.1, $H_{(5)}$), 6.63 (2H, d, J = 8.0, $H_{(6'/2')}$), 5.44 (s, 2H, $H_{(7)}$). ^{13}C NMR (MHz, d_6 -DMSO): δ 154.6, 149.2, 144.2, 137.2, 129.0, 128.4, 123.6, 120.5, 115.1. m/z (ESI+): 171.1 [$C_{11}H_{10}N_2 + H$] $^+$

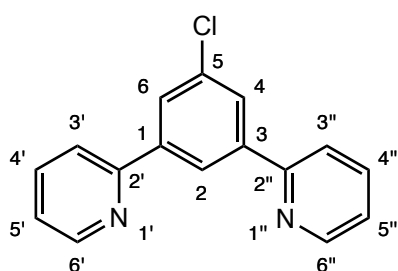
3-(4-chlorophenyl)isoquinoline (19)



An oven-dried Schlenk tube was charged with palladium(II) acetate (2 mol%), 3-bromoisoquinoline (**6**) (100 mg, 0.48 mmol), caesium fluoride (161 mg, 1.06 mmol), and XPhos (4 mol%). The vessel was evacuated and backfilled with argon three times before the addition of tributyl(4-chloro)phenylstannane (0.20 mL, 0.58 mmol) and t-BuOH (2 mL) *via* syringe. The solution was heated to 110 °C for 48 h. Upon cooling to room temperature, the reaction mixture was filtered through a plug of silica (eluting with EtOAc) and concentrated *in vacuo*. Purification by column chromatography on silica gel eluting with DCM:MeOH (grading from 100:0 to 95:5) yielded the desired product as white solid (82.6 mg, 72%)

^1H NMR (300 MHz, CDCl_3): δ 9.33 (1H, s, $\text{H}_{(1)}$), 8.11-8.04 (3H, m, $\text{H}_{(5'/3'/4)}$), 8.00 (1H, d, $J = 7.9$, $\text{H}_{(9)}$), 7.88 (1H, d, $J = 8.0$, $\text{H}_{(6)}$), 7.72 (1H, ddd, $\text{H}_{(8)}$), 7.61 (1H, ddd, $\text{H}_{(7)}$), 7.41 (2H, m, $\text{H}_{(2'/6')}$). ^{13}C NMR (MHz, CDCl_3): δ 152.2, 149.9, 137.7, 136.6, 134.9, 130.5, 128.8, 128.0, 127.7, 127.1, 126.8, 116.5. m/z (ESI+): 240.2 [$\text{C}_{15}\text{H}_{10}\text{ClN} + \text{H}$] $^+$

5-chloro-1,3-di(2-pyridyl)benzene (**20**)

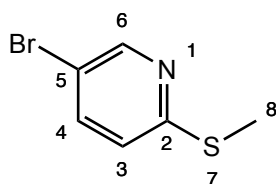


A mixture of 1,3-dibromo-5-chlorobenzene (149 mg, 549 μmol), 2-tributylstannylpyridine (500 mg, 1.36 mmol), lithium chloride (37.0 mg, 828 μmol) and bis(triphenylphosphine)palladium(II) chloride (102 mg, 144 μmol) in anhydrous toluene was degassed *via* three freeze-pump-thaw cycles and heated at reflux (130

°C) under an inert atmosphere for 3 days. Upon cooling to room temperature, a saturated aqueous solution of potassium chloride (10 mL) was added, and the mixture stirred for 30 min. The insoluble residue was removed by filtration and washed with toluene. The filtrate was concentrated *in vacuo* and taken into DCM, before washing with aqueous NaHCO₃ (2 × 30 mL). The organic phased was dried over Na₂SO₄ and concentrated under reduced pressure. Purification of the crude solid by column chromatography on silica gel, eluting with EtOAc:hexanes (grading from 10:90 to 50:50) yielded the desired product as white solid (77.6 mg, 53%).

¹H NMR (300 MHz, d₆-DMSO): δ 8.78 (1H, s, H₍₂₎), 8.73 (2H, ddd, *J* = 4.8, 1.8, 1, H_(6'/6'')), 8.21-8.15 (4H, m, H_(6/4/3'/3'')), 7.95 (2H, m, H_(4'/4'')), 7.44 (2H, ddd, *J* = 6.8, 4.8, 1.6, H_(5'/5'')). ¹³C NMR (MHz, d₆-DMSO): δ 150.2, 149.7, 138.1, 137.9, 127.0, 124.7, 123.6, 121.3, 120.9 *m/z* (ESI+): 267.2 [C₁₇H₁₁ClN₂ + H]⁺, 289.1 [C₁₇H₁₁ClN₂ + Na]⁺

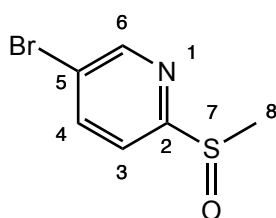
5-bromo-2-(methylthio)pyridine (21)



2,5-dibromopyridine (2.51 g, 10.6 mmol) and NaSMe (0.74 g, 10.6 mmol) were dissolved in anhydrous DMF (40 mL) and the solution stirred under an inert atmosphere at room temperature for 24 h. The solution was poured onto water (200 mL) and extracted with EtOAc. The organic phases were combined, dried over MgSO₄ and concentrated *in vacuo* to yield the desired product as yellow solid (1.50 g, 69%).

^1H NMR (300 MHz, CDCl_3): δ 8.47 (1H, s, $\text{H}_{(6)}$), 7.56 (1H, dd, $J = 8.5, 2.4$, $\text{H}_{(4)}$), 7.06 (1H, d, $J = 8.5$, $\text{H}_{(3)}$), 2.53 (3H, s, $\text{H}_{(8)}$). ^{13}C NMR (100 MHz, CDCl_3): δ 158.7, 150.2, 138.3, 122.6, 115.7, 13.4. m/z (ESI $^+$): 203.9 [$\text{C}_6\text{H}_6\text{BrNS} + \text{H}$] $^+$

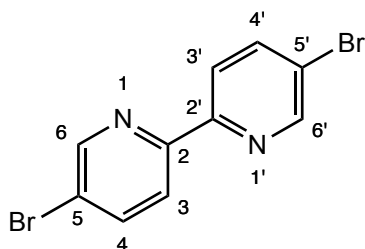
5-bromo-2-(methylsulphonyl)pyridine (**22**)



5-bromo-2-(methylthio)pyridine (**21**) (1.50 g, 7.30 mmol) was dissolved in glacial acetic acid (10 mL) and 30% H_2O_2 (1 mL) added. The solution was stirred at room temperature for 24 h. Following the addition of chloroform (10 mL), the solution was basified to pH 8 with 30% NH_3 solution. The solution was extracted with chloroform (2×20 mL) and DCM (2×20 mL) and the combined organics washed with water, dried over MgSO_4 and concentrated *in vacuo*. Overnight drying of the resulting white liquid in a dessicator with P_2O_5 yielded the desired product as yellow solid (1.53 g, 95%).

^1H NMR (300 MHz, CDCl_3): δ 8.67 (1H, s, $\text{H}_{(6)}$), 8.07 (1H, dd, $J = 8.3, 2.2$, $\text{H}_{(4)}$), 8.02 (1H, d, $J = 8.3$, $\text{H}_{(3)}$), 2.84 (3H, s, $\text{H}_{(8)}$). ^{13}C NMR (100 MHz, CDCl_3): δ 163.5, 149.6, 139.7, 121.1, 119.8, 40.3. m/z (ESI $^+$): 219.9 [$\text{C}_6\text{H}_6\text{BrNOS} + \text{H}$] $^+$

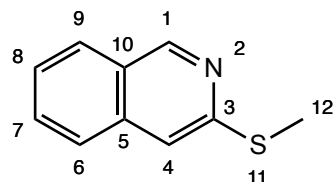
5,5'-dibromo-2,2'-bipyridine (**23**)



5-bromo-2-(methylsulphanyl)pyridine (**22**) (740 mg, 3.36 mmol) was dissolved in anhydrous Et₂O (30 mL) and the solution cooled in an ice bath to 0 °C. EtMgBr (0.9 M in Et₂O, 2.46 mL, 2.22 mmol) was added *via* syringe and the solution warmed to room temperature before stirring for 1 h. Following the addition of water (5 mL), the resulting suspension was extracted with toluene and the organic fractions combined and dried over MgSO₄, before reducing under reduced pressure. Recrystallisation of the crude product with hot EtOAc yielded the desired product as golden-brown crystals. (337 mg, 64%).

¹H NMR (300 MHz, CDCl₃): δ 8.69 (2H, s, H₍₆₎), 8.28 (2H, d, *J* = 8.4, H₍₃₎), 7.92 (2H, d, *J* = 8.2, H₍₄₎). *m/z* (ESI⁺): 314.9 [C₁₀H₆Br₂N₂ + H]⁺

3-(methylthio)isoquinoline (**24**)

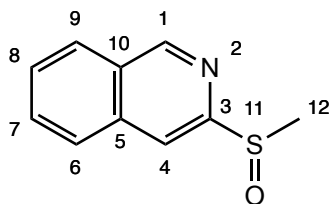


Operating under an argon atmosphere, 3-chloroisoquinoline (**3**) (2.50 g, 15.3 mmol) and sodium thiomethane (1.07 g, 15.3 mmol) were dissolved in anhydrous DMF (45 mL) and the solution stirred at room temperature for 2 days. The solution was poured

into water (250 mL) and the resulting milky solution extracted with Et₂O (3 × 100 mL). The organic phases were combined, dried over MgSO₄ and the solvent concentrated *in vacuo*. Purification of the remaining orange-brown, oily residue was carried out *via* flash column chromatography on silica gel, eluting with DCM:MeOH (19:1). The desired product was obtained as yellow solid (1.74 g, 65%).

¹H NMR (300 MHz, CDCl₃): δ 9.08 (1H, s, H₍₁₎), 7.86 (1H, d, *J* = 6.0, H₍₉₎), 7.71-7.68 (2H, m, H_(6/7)), 7.60-7.55 (1H, m, H₍₈₎), 7.43 (1H, s, H₍₄₎), 2.63 (3H, s, H₍₁₂₎). ¹³C NMR (400 MHz, CDCl₃): δ 152.6, 136.6, 130.8, 127.7, 127.4, 126.6, 125.8, 125.4, 119.7, 115.6. *m/z* (ESI⁺): 176.2 [C₁₀H₉NS + H]⁺

3-(methylsulphonyl)isoquinoline (25)

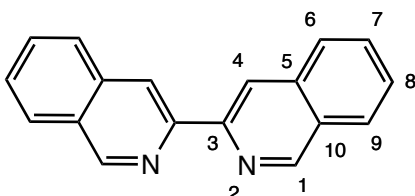


3-(methylthio)isoquinoline (**24**) (1.00 g, 5.71 mmol) was added to glacial acetic acid (3 mL) and 30% H₂O₂ solution (1 mL) and heated at 45 °C. After 2 days, CHCl₃ (5 mL) was added and the solution basified to pH 8 by the addition of 30% NH₃ solution. The solution was extracted with CHCl₃ (3 × 10 mL) and the organic phases combined and dried over MgSO₄. Removal of the solvent *in vacuo* yielded orange oil that was purified by column chromatography on silica gel, eluting with DCM:MeOH (3.5%) to afford the desired product as pale yellow solid (0.88 g, 81%).

¹H NMR (300 MHz, CDCl₃): δ 9.33 (1H, s, H₍₁₎), 8.55 (1H, s, H₍₄₎), 8.13 (1H, d, *J* = 6.0, H₍₉₎), 8.04 (1H, d, *J* = 6.0, H₍₆₎), 7.90-7.83 (2H, m, H_(7/8)), 3.29 (3H, s, H₍₁₂₎). ¹³C NMR

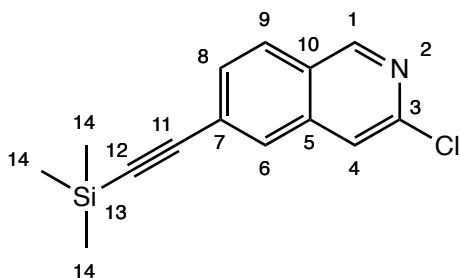
(400 MHz, CDCl₃): δ 153.5, 151.3, 135.3, 132.2, 130.4, 129.8, 128.3, 128.0, 120.4, 40.6. m/z (ESI⁺): 230.1 [C₁₀H₉NOS + K]⁺

3,3-biisoquinoline (26)



3-(methylsulphinyloxy)isoquinoline (**25**) (122 mg, 0.63 mmol) was dissolved in anhydrous THF (10 mL) and the solution cooled in an ice bath to 0 °C. MeMgBr (1.0 M in THF, 0.50 mL, 0.42 mmol) was added *via* syringe and the solution warmed to room temperature before stirring for 1 h. Following the addition of water (5 mL), the resulting suspension was extracted with toluene and the organic fractions combined and dried over MgSO₄, before reducing under reduced pressure. Crude analysis confirmed the reaction to be unsuccessful. No product was obtained.

6-(2-trimethylsilyl)ethynyl-3-chloroisoquinoline (27)



Under an argon atmosphere, an oven-dried Schlenk tube was charged with 6-bromo-3-chloroisoquinoline (380 mg, 1.57 mmol), PdCl₂(PPh₃)₂ (66.0 mg, 0.09 mmol) and copper iodide (52.0 mg, 0.28 mmol). Triethylamine (10 mL) was thoroughly de-

gassed before addition to the vessel. Ethynyltrimethylsilane (0.50 mL) was then added *via* syringe before heating the solution to 50 °C for 1 h. The solvent was then removed *in vacuo* and the residue purified by flash column chromatography on silica gel, eluting with hexane/EtOAc (9:1), to afford the desired product as pale cream solid (231 mg, 57%).

^1H NMR (300 MHz, MeOD): δ 9.11 (1H, s, $\text{H}_{(1)}$), 8.12-8.07 (1H, d, $J = 15.0$, $\text{H}_{(9)}$), 8.02 (1H, s, $\text{H}_{(6)}$), 7.91 (1H, s, $\text{H}_{(4)}$), 7.68-7.63 (1H, d, $J = 15.0$, $\text{H}_{(8)}$), 0.3 (9H, s, $\text{H}_{(14)}$).

^{13}C NMR (100 MHz, MeOD): δ 153.9, 141.5, 133.3, 131.7, 130.7, 129.4, 128.1, 121.8, 121.0, 98.6, 71.3. m/z (ESI+): 260.1 [$\text{C}_{14}\text{H}_{14}\text{ClNSi} + \text{H}$] $^+$

4.10 References

- 1 M. Palucki and S. L. Buchwald, *J. Am. Chem. Soc.*, 1997, **119**, 11108–11109.
- 2 B. C. Hamann and J. F. Hartwig, *J. Am. Chem. Soc.*, 1997, **119**, 12382–12383.
- 3 T. Satoh, Y. Kawamura, M. Miura and M. Nomura, *Angew. Chemie Int. Ed.*, 1997, **36**, 1740–1742.
- 4 P. Novak and R. Martin, *Curr. Org. Chem.*, 2011, **15**, 3233–3262.
- 5 J. M. Fox, X. Huang, A. Chieffi and S. L. Buchwald, *J. Am. Chem. Soc.*, 2000, **122**, 1360–1370.
- 6 T. J. Donohoe, B. S. Pilgrim, G. R. Jones and J. A. Bassuto, *Proc. Natl. Acad. Sci. U. S. A.*, 2012, **109**, 11605–11608.
- 7 H. C. Kolb, M. G. Finn and K. B. Sharpless, *Angew. Chemie Int. Ed.*, 2001, **40**, 2004–2021.
- 8 V. V. Rostovtsev, L. G. Green, V. V. Fokin and K. B. Sharpless, *Angew. Chemie*, 2002, **114**, 2708–2711.
- 9 W. Q. Fan and A. R. Katritzky, *Comprehensive Heterocyclic Chemistry II*, Oxford University Press, 1996.
- 10 R. Huisgen, *Pure Appl. Chem.*, 1989, **61**, 613–628.
- 11 F. Himo, T. Lovell, R. Hilgraf, V. V. Rostovtsev, L. Noodleman, K. B. Sharpless and V. V. Fokin, *J. Am. Chem. Soc.*, 2005, **127**, 210–216.
- 12 T. Aldridge, E. Stacy and D. McMillin, *Inorg. Chem.*, 1994, **33**, 722–727.
- 13 V. Miskowski, V. Houlding and C. Che, *Inorg. Chem.*, 1993, **32**, 2518–2524.
- 14 P. Kvam, M. Puzyk and K. Balashev, *Acta Chem.*, 1995, **49**, 335–343.
- 15 L. Chassot, E. Mueller and A. Von Zelewsky, *Inorg. Chem.*, 1984, **23**, 4249–4253.
- 16 C. Deuschel-Cornioley and R. Löönd, *Helv. Chim. Acta*, 1989, **72**, 377–382.
- 17 K. Balashev, M. Puzyk and V. Kotlyar, *Coord. Chem. Rev.*, 1997, **159**, 109–120.
- 18 J. Brooks, Y. Babayan, S. Lamansky, P. I. Djurovich, I. Tsyba, R. Bau and M.

- E. Thompson, *Inorg. Chem.*, 2002, **41**, 3055–3066.
- 19 N. Miyaura, K. Yamada and A. Suzuki, *Tetrahedron Lett.*, 1979, **20**, 3437–3440.
- 20 N. Miyaura and A. Suzuki, *J. Chem. Soc. Chem. Commun.*, 1979, 866–867.
- 21 N. Miyaura and A. Suzuki, *Chem. Rev.*, 1995, **95**, 2457–2483.
- 22 K. Matos and J. A. Soderquist, *J. Org. Chem.*, 1998, **63**, 461–470.
- 23 2005.
- 24 Siemens Medical Solutions USA Inc., US 8491869 B2, 2010.
- 25 V. Farina, V. Krishnamurthy and W. J. Scott, *The Stille Reaction*, John Wiley and Sons, 1997.
- 26 J. Stille, *Angew. Chemie Int. Ed.*, 1986, **25**, 508–524.
- 27 R. Crabtree, *The organometallic chemistry of the transition metals*, John Wiley and Sons, 2009.
- 28 T. Mitchell, *Synthesis*, 1992, **9**, 803–815.
- 29 J. R. Naber, B. P. Fors, X. Wu, J. Gunn and S. L. Buchwald, *Heterocycles*, 2010, **80**, 1215–1226.
- 30 S. Mee, V. Lee and J. Baldwin, *Angew. Chemie Int. Ed.*, 2004, **43**, 1132–1136.
- 31 Y.-N. Niu, Z.-Y. Yan, G.-L. Gao, H.-L. Wang, X.-Z. Shu, K.-G. Ji and Y.-M. Liang, *J. Org. Chem.*, 2009, **74**, 2893–2896.
- 32 S.-W. Lai, M. C.-W. Chan, T.-C. Cheung, S.-M. Peng and C.-M. Che, *Inorg. Chem*, 1999, **38**, 4046–4055.
- 33 V. Yam, R. Tang and K. Wong, *Chem. Eur. J.*, 2002, **8**, 4066–4076.
- 34 Z. Wang, E. Turner, V. Mahoney, S. Madakuni, T. Groy and J. Li, *Inorg. Chem*, 2010, **49**, 11276–11286.
- 35 J. A. G. Williams, A. Beeby, E. S. Davies, J. A. Weinstein and C. Wilson, *Inorg. Chem. Commun.*, 2003, **42**, 8609–8611.
- 36 S. J. Farley, D. L. Rochester, A. L. Thompson, J. A. K. Howard and J. A. G. Williams, *Inorg. Chem.*, 2005, **44**, 9690–9703.
- 37 W. Mróz, C. Botta, U. Giovanella, E. Rossi, A. Colombo, C. Dragonetti, D.

- Roberto, R. Ugo, A. Valore and J. A. G. Williams, *J. Mater. Chem.*, 2011, **21**, 8653–8661.
- 38 T. Kawai, N. Furukawa and S. Oae, *Tetrahedron Lett.*, 1984, **25**, 2549–2552.
- 39 P. Cogolli, F. Maiolo, L. Testaferri, M. Tingoli and M. Tiecco, *J. Org. Chem.*, 1979, **44**, 2642–2646.
- 40 J. F. Bunnett, *Q. Rev. Chem. Soc.*, 1958, **12**, 1–16.
- 41 S. Oae, T. Kawai and N. Furukawa, *Tetrahedron Lett.*, 1984, **25**, 69–72.
- 42 L. Testaferri, M. Tiecco, M. Tingoli and D. Bartoli, *Tetrahedron*, 1985, **41**, 1373–1384.
- 43 S. Oae, T. Kawai and N. Furukawa, *Phosphorous Sulfur Relat. Elem.*, 1987, **34**, 123–132.
- 44 K. Sonogashira, Y. Tohda and N. Hagihara, *Tetrahedron Lett.*, 1975, **16**, 4467–4470.
- 45 R. Chinchilla and C. Nájera, *Chem. Soc. Rev.*, 2011, **40**, 5084.
- 46 R. Chinchilla and C. Nájera, *Chem. Rev.*, 2007, **107**, 879–922.
- 47 R. A. D. Arancon, C. Sze Ki Lin and C. Vargas, *Org. Biomol. Chem.*, 2014, **12**, 10–35.

Chapter V

V. CONCLUSIONS AND FUTURE WORK

The aim of this work was to develop ligands and complexes capable of interacting with G-quadruplex DNA structures. Utilising 3,3-biisoquinoline, the synthetic route towards two pre-existing palladium and platinum complexes incorporating this ligand has been modified to secure higher yields through more facile routes. The interaction of both complexes with model nucleobases has been investigated, with each complex demonstrating a preference for binding to guanine. A range of *in vitro* studies have been conducted, all providing further information about the mechanism of action of these compounds. Both compounds have been shown to exhibit cytotoxicity in the low micromolar range and exceeding that of cisplatin. The palladium complex was shown to be more cytotoxic, although this difference was not significant. It has been demonstrated that treatment with either complex induces a small degree of double-strand breaks in cells, alongside G2/M phase cell cycle arrest. Both cells have demonstrated excellent cell uptake and nuclear localisation, again exceeding that of cisplatin.

The precise cause of the increased cytotoxicity displayed by the palladium complex remains to be established. ICP-MS data has so far shown the cellular concentration of each complex to be within the same order of magnitude following 3 hours incubation. There may, however, be changes in the cellular concentration of each complex over a longer period of time. Such changes may account for the differences observed in the MTT cytotoxicity assay, which was conducted over a 24 hour timeframe. To investigate this hypothesis further, it would be beneficial to carry

out further ICP-MS studies in the future, at multiple timepoints between 3 and 24 hours. The potential role of any influx or efflux mechanisms may then be probed.

These compounds continue to show great promise as G-quadruplex binders. It would be highly beneficial to carry out the telomerase repeat amplification assay (TRAP assay) with both compounds, in order to assess their ability to inhibit telomerase. Determining the potential contribution of telomerase inhibition to the overall cytotoxicity of these compounds would enable their mechanism of action to be further elucidated. In addition to the further biological exploration of the palladium and platinum bisisoquinoline compounds, attempted synthesis of the gold analogue needs revisiting in order to ascertain the success of this preparation and make any necessary changes to the procedure to isolate this compound. The full range of biophysical and biological testing so far carried out on the palladium and platinum species would then be repeated with this novel analogue for comparison.

A terpyridine platform capable of further modification *via* an appended methylsulphonyl group has been successfully prepared and incorporated into two novel complexes. UV-Vis spectroscopy studies on these palladium and platinum compounds have demonstrated them to be stable in solution (acetonitrile) over a period of 24 hours. Initial DNA binding studies have proved quite complex, with some discrepancies between the CD and PAGE data obtained thus far.

Future studies will endeavour to determine the exact nature of these proposed DNA binding interactions. To aid this, it would be beneficial to conduct UV-Visible spectroscopy titration studies with the same DNA sequences investigated in the CD and PAGE studies. Fluorescent intercalator displacement studies would also help to

elucidate any binding preference for G-quadruplex forming regions of DNA. Despite the seemingly inferior G-quadruplex binding activity displayed by these terpyridine complexes so far (compared to their palladium and platinum biisoquinoline counterparts), terpyridine itself is a far easier ligand platform to work with synthetically, affording higher yields from simpler syntheses. It is anticipated that the introduction of further functionality to the terpyridine platform will be achieved with greater ease than previous attempts with 3,3-biisoquinoline (work not included herein). For these reasons, and on account of the huge potential for further functionality to be added at the methylsulphonyl site, the terpyridine ligand still represents a viable ligand target for G-quadruplex binding. Moving forward, the focus with this system should undoubtedly rest on the incorporation of moieties capable of enhancing G-quadruplex binding interaction, appended *via* Grignard coupling routes at the methylsulphonyl site. Complexes containing such ligands would then be analysed in a similar manner to that described within this work, to compare their activity to that of the compounds herein.

A variety of alternative synthetic methodologies have been explored, each with the intention of securing novel ligands with desirable features such as alkyne or N[^]C coordination. The most promising route involved the use of Stille-coupling to generate an unsymmetrical N[^]C coordinating ligand that is poised for further modification due to the presence of a halide substituent in the *para* position. Incorporation of an alkyne moiety at this site *via* Sonogashira cross-coupling is the natural progression with this ligand. Complex formation with the resulting alkyne-N[^]C

ligand will produce novel compounds that can be tested for G-quadruplex binding potential (as assessed by CD, FID, UV-Vis, PAGE and ESI-MS).

A terpyridine-based N^CN ligand has also been successfully prepared. Again incorporating a halide atom, further functionalization of this ligand is anticipated. The incorporation of a linked appendage that is capable of imparting dual-modality binding (such as that seen in Pt-MPQ) into any future complexes is the end goal.

Appendix

Nuclear/Cytosol Fractionation Kit

[Click to view datasheet online](#)

Cell fraction	A _r of metal	concentration (ppb)	sample mass (g)	mass in sample (g)	moles/sample (pmol/10 ⁶ cells)	moles/cell	molecules/cell	concentration inside cells (μmol/10 ⁶ cells)
Whole cell								
[Pt(<i>i</i> -biq) ₂][PF ₆] ₂	195	2.66	4.20	1.12E-08	57.3	5.73E-17	3.45E+07	14.3
cisplatin	195	1.00	4.20	4.20E-09	21.5	2.15E-17	1.30E+07	5.83
[Pd(<i>i</i> -biq) ₂][BF ₄] ₂	106	2.31	6.90	1.59E-08	150	1.50E-16	9.05E+07	37.6
Cytoplasmic								
[Pt(<i>i</i> -biq) ₂][PF ₆] ₂	195	1.02	4.20	4.28E-09	22.0	2.20E-17	1.32E+07	5.49
cisplatin	195	0.79	4.20	3.32E-09	17.0	1.70E-17	1.02E+07	4.25
[Pd(<i>i</i> -biq) ₂][BF ₄] ₂	106	1.14	6.90	7.87E-09	74.2	7.42E-17	4.47E+07	18.6
Nuclear								
[Pt(<i>i</i> -biq) ₂][PF ₆] ₂	195	2.34	4.20	9.83E-09	50.4	5.04E-17	3.03E+07	12.6
cisplatin	195	0.20	4.20	8.40E-10	4.31	4.31E-18	2.59E+06	1.08
[Pd(<i>i</i> -biq) ₂][BF ₄] ₂	106	1.40	6.90	9.66E-09	91.1	9.11E-17	5.49E+07	22.8